Faculty of Agricultural Sciences

Institute of Agricultural Sciences in the Tropics (Hans-Ruthenberg-Institute)
Agronomy in the Tropics and Subtropics
University of Hohenheim

Prof. Dr. Georg Cadisch (Supervisor)

UNIVERSITY OF HOHENHEIM

Mid-infrared spectroscopy and enzyme activity temperature sensitivities as experimental proxies to reduce parameter uncertainty of soil carbon models

Dissertation
Submitted in fulfilment of the requirement for the degree
"Doktor der Agrarwissenschaften"
(Dr.sc.agr./Ph.D. in Agricultural Sciences)

to the
Faculty of Agricultural Sciences
Presented by
Moritz Laub
Stuttgart, Germany
2021

This thesis was accepted as doctoral dissertation in fulfilment of the requirements for the degree "Doktor der Agrarwissenschaften" (Dr.sc. Agr./PhD in Agricultural Sciences) by the Faculty of Agricultural Sciences at University of Hohenheim on July 15, 2020

Date of oral examination: Janurary 15, 2021

Examination Committee

Chairperson of the oral examination	Prof. Dr. Thilo Streck
Supervisor and Reviewer	Prof. Dr. Georg Cadisch
Co-Reviewer	Prof. Dr. Claas Nendel
Additional Examiner	Prof. Dr. Hans-Peter Piepho

Acknowledgements

The time as a PhD candidate was a time of tremendous learning for me. It had its heights and depths with each challenge presenting a new learning opportunity. Getting into the world of scientific thinking is a growing phase, where one learns to rely on ones' own judgement, but this is only possible through the guidance of those who are already further on the path. I am grateful that I could share this time of development with an inspiring mix of colleagues and under good supervision. Without these people, I would not be where I am, today.

I first want to thank Prof. Dr. Georg Cadisch for the opportunity to conduct my PhD at his institute. His clear, hypothesis driven thinking and his ability to maintain a system understanding while simultaneously diving into the details, have been a great inspiration to me. The challenging discussions have been a constant source of new insights and helped to push the articles to the next level. I am equally grateful to Dr. Sergey Blagodatskiy who, next to Georg, closely supervised me during the PhD time. His door was always open for discussions and professional advice. This opportunity for quick, informal and professional exchange helped tremendously in developing core ideas of this thesis and was also a lot of fun. I want to express my special gratitude to Georg, Sergey and other colleagues from the institute for their moral support during one especially tough time in my PhD. I am certainly not the only PhD candidate who thought about quitting but the right support at the "tipping point" was crucial for me.

I furthermore want to thank Dr. Michael Scott Demyan for introducing me to DRIFTS and modelling, laying the foundation for this thesis and Yvonne Funkuin Nkwain for the joint work within the project and discussions about spectroscopy. Further thanks to Dr. Rana Shahbaz Ali and Dr. Christian Poll for their collaboration throughout and the interesting discussions during the development of the joint paper. Also, a thanks to Dr. Christian Troost, Dr. Arne Poyda and Dr. Pascal Kremer for the interesting time spent in the field and when working to combine our different models. A further thanks to Prof. Dr. Petra Högy, Dr. Joachim Ingwersen, Prof. Dr. Ellen Kandeler and Prof. Dr. Thomas Kätterer for the constructive joint working experience. I want to address a special thanks to Prof. Dr. Hans-Peter Piepho for his kind support and high responsiveness for detailed statistical questions and for the deep insights he gave in the PhD students' statistics seminar.

In addition, I want to acknowledge the DFG for providing the funding for my PhD through the FOR 1695 project. I am grateful for living in a system, which provides free education and thus the basis for objective science. The importance of this act of solidarity in a society has never been more evident to me than in the global COVID-19 pandemic that occurred during the time of finalizing this thesis.

I also want to express my gratitude to the friends and colleagues from the institute. The shared experiences, lunches, institute excursions and “Staffelläufe” throughout the years made this time enjoyable and much more than just work or higher education. Special thanks with this regard to Lisa Pataczek, Sahrah Fischer, Catherine Meyer, Lang Rong, Konrad Egenolf, Dr. Hannes Karwat and Dr. Christian Brandt for many interesting discussions and the good times spent inside and outside university. Further thanks to the colleagues Isaac Balume, Birhanu Endalew, Eric Koomson, Xueqing Yang, Hongxi Liu, Krittiya Tongkoom, Ruj Kasetsuwan, Nuttapon Khongdee, Dr. Carsten Marohn, Dr. Thomas Hilger and PD. Dr. Frank Rasche and to all the other great people in the Hans Ruthenberg and other institutes.

A big thanks to Gaby Kircher, who was the glue, keeping the institute together through all her supportive actions behind the scenes, making sure that everyone, especially our foreign guests, are taken care of and helping with all official documents. Thanks also to Carolin Stahl for the daily efforts in keeping the lab and all people working there together. Also thanks to Xiaomin Yu, for her part in the lab work for the first paper.

I also want to address a special thanks to Prof. Dr. Patma Vityakon, Wimonsiri Pingthaisong, Ratanapon Poosathit and Dr. Benjapon Kunlanit for the fruitful collaboration, enabling me the enriching exchange to Khon Kaen and their kindness during my stay in Thailand. I am looking forward for the fruits of this once the thesis is submitted. I enjoyed a lot our time spent together in Stuttgart and Khon Kaen.

Finally, I want to thank my family and especially my parents for the unconditional moral support throughout my life, laying the foundation for me to even attempt a PhD. Last but not least, I want to thank Caro, who enriches my life since many years, helped to maintain my balance throughout the PhD and patiently went through all ups and downs while always morally supporting me.

Table of Contents

List of Figures

List of Tables

List of Abbreviations

AIC	Aikaike information criterion
AOM	Added organic matter
AOM_f/s	Fast/slow added organic matter pools
bare_soil_inc_BC	Bayesian calibration of the laboratory bare soil incubation experiment 5 alone
combined _BC	Bayesian calibration combining all experiments
DRIFTS	Diffuse reflectance mid infrared Fourier transform spectroscopy
DSI	DRIFTS stability index
DSI	DRIFTS stability index
EF	Modelling efficiency
EW	Equal weight
field_BC	Bayesian calibration combining field experiments 1,2 and 3
LC	Lack of correlation
litter_inc_BC	Bayesian calibration of the crop-litter incubation experiment 4 alone
NU	Nonunitiy slope
OW	Original weight
PA	Peak area
SB	Squared bias
(R)MSD	(Root) mean squared deviation
SMB	Soil microbial biomass
SMB_f/s	Fast/slow soil microbial biomass pools
SME	Squared model error
SOC	Soil organic carbon
SOM	Soil organic matter
SOM_f/s	Fast/slow soil organic matter pools
SWSME	Sum of weighted squared model errors
TS	Temperature sensitivity

Summary

Models that simulate the dynamics of soil organic carbon (SOC) are crucial to understand the global carbon cycle and to predict how this cycle could be affected by changes in climatic conditions. For the prediction of the potential effects of climate change, current generation models are subject to major uncertainties due to two model shortcomings. Firstly, their different carbon pools are not connected to measurable SOC fractions. Secondly, there is uncertainty about the response of the different carbon pools to temperature. This means that the more temperature will deviate from the long-term mean, the higher will be the uncertainty about changes in SOC stocks.

The aim of this thesis was to contribute towards solving these shortcomings by linking the SOC model pools of the Daisy model to measurable proxies for SOC quality and pool specific temperature sensitivity. In the first study, the drying temperature for soil samples assessed by diffuse reflectance mid infrared Fourier transform spectroscopy (DRIFTS) was optimized to assure optimal representativeness of aliphatic and aromatic-carboxylate absorption bands as proxies for fast- and slow-cycling SOC pools. Their ratio was termed the DRIFTS stability index (DSI). In the second study, the DSI was used to distinguish fast- and slow-cycling SOC model pools at model initialization. The suitability of the approach was tested by analysis of the model performance and the reduction of model parameter uncertainty. In the third study, model initialization using DSI was performed to infer pool specific temperature sensitivities for the different Daisy carbon pools. Furthermore, it was tested whether the measured temperature sensitivities of different extracellular soil enzymes could be used as proxies for pool specific temperature sensitivity.

Using a global collection of soil samples revealed that the absorption of all studied DRIFTS absorption bands increased significantly ($p < 0.0001$) with increasing drying temperature from 32°C to 105°C. This effect was disproportionally strong for the aliphatic absorption band. Due to the strong interference of the residual soil sample moisture content with the aliphatic absorption band, drying at 105°C and storage in a dessiccator prior to measurement would be necessary for representative spectra. This improved method would lead to a representative ratio of aliphatic and aromatic-carboxylate absorption bands in the the DSI and thus be best for for model pool intialization.

In the following, a combination of medium to long-term bare-fallow experiments from Ultuna in Sweden (50 years) and the German sites of Bad Lauchstädt (25 years), the Kraichgau and the Swabian Jura (both 7 years) was used, to test the utility of the DSI for SOC pool initialization. It could be shown that pool partitioning by the DSI was superior to using a fixed pool partitioning under the assumption that SOC was at steady state. The DSI contained robust information on SOC quality across sites. Therefore, in the majority of cases, the application of the DSI led to significantly lower model errors than the steady state assumption. This suggested that the soils SOC stocks, although under long-term

agricultural use, were not necessarily at a steady state. Furthermore, the application of the DSI in Bayesian calibration led to a reduced parameter uncertainty for the turnover of the slow-cycling SOC pool and the humification efficiency. The 95% credibility interval of the slow-cycling SOM pools' half-life between 278 and 1095 years suggested faster SOC turnover than earlier studies. The robustness of the inferred parameters was corroborated by similar results of the SOC turnover as reported in other recent Bayesian calibration studies.

The DSI used for SOC model pool initialization was then combined with the lignin-to-nitrogen ratio for litter pool initialization to infer pool specific temperature sensitivities. The simulations of five field studies and laboratory incubations with fallow soil and crop-litter inputs were combined. Based on a clear pool definition, pool specific temperature sensitivities could be inferred by Bayesian calibration. However, differences in temperature sensitivities of the same pools between experiments suggested that carbon stability was not the main driver of temperature sensitivities. Instead, the main difference was found between the laboratory incubations (higher Q_{10} values up to 3) and the field (lower Q_{10} values centered around 2). In a second approach, the measured Q_{10} value of phenoloxidase (1.35) was used as Q_{10} value of the temperature function of both SOM pools and the slow crop-litter pool while ß-glucosidase (1.82) was used for the fast crop-litter pool. This improved field simulations by 3 to 10% compared to assuming a standard Q_{10} of 2 for all pools. Also, measured field Q_{10} and Bayesian-calibration-inferred Q_{10} were in a similar range. Thus, site specific Q_{10} of different soil enzymes showed potential as proxy for site and pool specific temperature sensitivities. The derived conceptual model divided the main drivers of temperature sensitivity into fluctuating state variables and constant soil properties. Important state variables that explain the observed Q_{10} value differences between experiments were identified as physical protection of SOC, substrate availability and environmental stress for microorganisms due to fluctuating state variables in the field.

In conclusion, the usefulness of the DSI as an indicator of SOC stability and proxy for pool initialization was demonstrated for several soils in central Europe. In addition, it was shown that pool partitioning proxies can help to infer pool specific temperature sensitivity by Bayesian calibration. However, temperature sensitivity was not mainly a function of carbon stability. In the face of the difficulty to uniquely delineate controlling factors, measured enzyme temperature sensitivities proved a suitable proxy for field SOC mineralization temperature sensitivity. In combination, the presented results show that measurable proxies for different pools in SOC models are not only important for the assessment of SOC stability but are also needed to reduce the high uncertainty linked to the temperature functions of SOC models. The confidence in future climate predictions up to global scales is therefore intimately linked to understanding SOC stabilization mechanisms.

Zusammenfassung

Modelle, welche die Flüsse des organischen Bodenkohlenstoffes (OBK) simulieren, sind entscheidend, um den globalen Kohlenstoffkreislauf zu verstehen und um vorherzusagen, wie dieser Kreislauf durch Veränderungen der klimatischen Bedingungen beeinflusst werden könnte. Bei der Vorhersage der potenziellen Auswirkungen des Klimawandels sind die Modelle der heutigen Generation aufgrund von zwei Hauptschwächen mit großen Unsicherheiten behaftet. Zum einen sind die unterschiedlichen Kohlenstoffpools nicht mit messbaren OBK Fraktionen verknüpft. Zum anderen besteht Unsicherheit darüber, wie die verschiedenen Kohlenstoffpools auf die Temperatur reagieren. Infolgedessen nimmt die Unsicherheit in Bezug auf Veränderungen der OBK Bestände zu, je weiter sich die Temperatur vom langjährigen Mittel entfernt.

Das Ziel dieser Arbeit war es, einen Beitrag zur Reduzierung dieser Schwächen zu leisten, indem die OBK Pools des Daisy Modelles mit messbaren Proxies für Kohlenstoffqualität und poolspezifische Temperatursensitivitäten verknüpft werden. In der ersten Studie wurde die Vorbehandlung von Bodenproben zur Messung mit diffuser Reflexions-Fourier-Transformations-Infrarotspektroskopie (DRIFTS) optimiert. Die Trocknungstemperatur der Vorbehandlung wurde angepasst, um die Repräsentativität von aliphatischen sowie aromatisch-carboxylischen Absorptionsbändern zu verbessern. Diese Bänder wurden respektive als Proxies für sich schnell und langsam umsetzende OBK Pools, verwendet. Ihr Verhältnis wurde als DRIFTS Stabilitätsindex (DSI) bezeichnet. In der zweiten Studie wurde der DSI genutzt, um sich schnell und langsam umsetzende OBK Modellpools bei der Modellinitialisierung zu unterteilen. Die Eignung dieses Ansatzes wurde durch Analysen der Modellperformance sowie der Reduktion von Parameterunsicherheit verifiziert. In der dritten Studie wurde die entwickelte Modellinitialisierung mittels des DSI eingesetzt, um poolspezifische Temperatursensitivitäten für unterschiedliche Daisy Kohlenstoffpools abzuleiten. Darüber hinaus wurde untersucht, ob die gemessene Temperatursensitivitäten unterschiedlicher extrazellulärer Bodenenzyme als Proxies für poolspezifische Temperatursensitivitäten geeignet sind.

Unter Verwendung einer globalen Sammlung von Bodenproben wurde festgestellt, dass die Absorption der untersuchten DRIFTS Absorptionsbänder mit der Trocknungstemperatur zwischen 32°C und 105°C signifikant zunahm ($p < 0.0001$). Auf Grund der starken Interferenz der Restfeuchte von Bodenproben mit dem aliphatischen Absorptionsband ist daher die Trocknung bei 105°C und die Aufbewahrung im Exsikkator vor der Messung notwendig, um repräsentative Spektren zu erhalten. Die Anwendung dieser verbesserten Methode sollte daher zu einem möglichst repräsentativen Verhältnis von aliphatischen und aromatisch-carboxylischen Absorptionsbändern im DSI führen und ist daher für die Modellinitialisierung zu bevorzugen.

Im Folgenden wurde in einer Kombination aus Mittel- bis Langzeitversuchen mit Bodenbrache, bestehend aus Proben aus Ultuna (Schweden; 50 Jahre) sowie aus Bad Lauchstädt (Deutschland; 25 Jahre), dem Kraichgau und dem Schwäbischen Jura (Deutschland; je 7 Jahre), verwendet, um die Nützlichkeit des DSI für die OBK Poolinitialisierung zu testen. Es konnte gezeigt werden, dass die Poolaufteilung durch den DSI einer fixen Poolaufteilung, unter der Annahme eines Gleichgewichtszustandes des OBK, überlegen war. Der DSI enthielt über mehrere Standorte hinweg belastbare Informationen zur OBK Qualität. Folglich führte die Anwendung des DSI in der Mehrzahl der Fälle zu einem signifikant niedrigeren Modellfehler als die Annahme eines Gleichgewichtszustandes der OBK. Dies legte nahe, dass sich die Bodenbestände an OBK trotz langjähriger landwirtschaftlicher Nutzung nicht zwangsläufig im Gleichgewichtszustand befanden. Darüber hinaus führte die Anwendung des DSI bei der Bayes'schen Kalibrierung zu einer reduzierten Parameterunsicherheit für die Umsatzrate des sich langsam umsetzenden OBK Pools sowie der Humifizierungseffizienz. Das 95% Glaubwürdigkeitsintervall der Halbwertszeit des sich langsam umsetzenden OBK Pools betrug 278 bis 1095 Jahre und deutete, im Vergleich zu früheren Studien, auf schnellere OBK Umsatzraten hin. Die Zuverlässigkeit der abgeleiteten Parameter wurde durch ähnliche Umsatzraten des OBK in anderen Studien bestätigt, welche allesamt Bayes'sche Kalibrierung anwendeten.

Im Anschluss daran wurde die Verwendung des DSI für OBK Poolinitialisierung mit der Verwendung des Lignin-zu-Stickstoff Verhältnisses für die Poolinitialisierung der Pflanzenstreu-Pools kombiniert, um nachfolgend Pool spezifische Temperatursensitivitäten abzuleiten. Hierbei wurden die Simulationen von fünf Versuchen, bestehend aus Feldstudien und Laborinkubationen mit Brachflächen sowie Streueinarbeitung, kombiniert. Auf Grundlage der klaren Pooldefinitionen konnten poolspezifische Temperatursensitivitäten durch Bayes'sche Kalibrierung abgeleitet werden. Unterschiedliche Temperatursensitivitäten derselben Pools in verschiedenen Experimenten deuteten jedoch darauf hin, dass Kohlenstoffstabilität nicht die Hauptursache der beobachteten Temperatursensitivitäten war. Stattdessen bestand der Hauptunterschied zwischen den Laborinkubationen (höhere Q_{10} Werte bis zu 3) und den Feldversuchen (niedrigere Q_{10} Werte um 2 zentriert). In einem zweiten Ansatz wurden die gemessenen Q_{10} Werte der Phenoloxidase (1.35) als Q_{10} Wert der Temperaturfunktion der beiden OBK-Pools und des langsamen Pflanzenstreu-Pools verwendet, während ß-Glucosidase (1.82) für den schnellen Pflanzenstreu-Pool verwendet wurde. Dies verbesserte die Simulationen der Feldversuche um 3 bis 10% im Vergleich zur Verwendung des Standard-Q_{10} von 2 für alle Pools. Zusätzlich lagen die die gemessenen Feld-Q_{10} Werte und die durch Bayes'sche Kalibrierung abgeleiteten Q_{10} Werte in einem ähnlichen Bereich. Standortspezifische Q_{10} Werte verschiedener Bodenenzyme bewiesen somit das Potenzial, als Proxies für standort- und poolspezifische Temperatursensitivitäten verwendet zu werden. Das anschließend entwickelte konzeptionelle Modell unterteilte die wichtigsten Einflussfaktoren, die die Temperatursensitivität

beeinflussen, in die sich ständig ändernden Zustandsvariablen und die konstanten Bodeneigenschaften ein. Als wichtige Zustandsvariablen zur Erklärung der beobachteten Q_{10} Wert-Unterschiede zwischen den Experimenten wurden der physikalischer Schutz von OBK, die Substratverfügbarkeit und der Umweltstress für Mikroorganismen infolge der sich ständig ändernden Zustandsvariablen im Feld identifiziert.

Zusammenfassend konnte in dieser Arbeit der Mehrwert des DSI als Indikator der OBK Stabilität und als Proxy für die Poolinitialisierung für eine Reihe von Böden in Mitteleuropa demonstriert werden. Darüber hinaus konnte gezeigt werden, dass Poolpartitionierungs-Proxies helfen können, die poolspezifische Temperatursensitivität durch Bayes'sche Kalibrierung abzuleiten. Die Temperatursensitivität konnte jedoch nicht primär durch die Kohlenstoffstabilität erklärt werden. Angesichts der Schwierigkeit, die Einflussfaktoren eindeutig abzugrenzen, erwiesen sich die gemessenen Enzym-Temperatursensitivitäten als hilfreicher Proxy für die Temperatursensitivität der Mineralisierung von OBK in den Feldversuchen. Insgesamt zeigten die vorgestellten Ergebnisse, dass messbare Proxies für verschiedene Pools in OBK-Modellen nicht nur für die Bewertung der OBK-Stabilität wichtig sind, sondern auch benötigt werden, um die mit den Temperaturfunktionen von OBK-Modellen verbundene hohe Unsicherheit zu reduzieren. Die Verlässlichkeit zukünftiger Klimaprognosen bis hin zu globalen Skalen ist daher eng mit dem Verständnis der OBK-Stabilisierungsmechanismen verbunden.

1 General Introduction

With an estimated total of about 2500 * 10^{15} g C, the global soil organic carbon (SOC) stocks contain more carbon than atmosphere and plants together (Lal, 2004). The expected rise of global temperatures, resulting from climate change, poses a risk for this important carbon reservoir. A global loss of SOC stocks would threaten soil fertility and bear the risk that CO_2 emissions from soils further accelerate the climate change. Mathematical process models are used to simulate SOC dynamics to better understand the SOC mineralization process. However, with regards to simulating the potential change of SOC stocks under climate change, their accuracy is limited by three main shortcomings: Firstly, their simulated SOC model pools are not linked to measurable SOC fractions. Secondly, the different SOC pools do not have distinct different reactions to temperature increase, though experimental evidence suggest that they should. Thirdly, most SOC models fail to display the uncertainty of model parameters and outputs. These weaknesses undermine the potential of SOC models to estimate the potential impact of climate change on SOC stocks and to determine the potential of countermeasures.

The aim of this thesis was to study these three aspects in detail and improve their representation in SOC models. The SOC model pools were to be connected to a measurable proxy of SOC complexity by diffuse reflectance Fourier transform mid-infrared spectroscopy (DRIFTS). Following this, pool specific temperature functions for clearly defined SOC pools by DRIFTS should be derived. To display the uncertainty of the model parameters and temperature sensitivity, the probabilistic Bayesian calibration framework was used. Thus, the overall goal was to reduce model uncertainty by connecting SOC models to novel measurable proxies for SOC complexity and temperature sensitivity.

1.1 The importance of SOC in the global carbon cycle

About 58% of the soil organic matter (SOM) consists of carbon (Nelson and Sommers, 1996), the rest consists mostly of oxygen, hydrogen and nitrogen. This results in a close link between SOC and plant nutrients (such as nitrogen and phosphorus) making buildup and mineralization of SOC important for the provision of nutrients to plants. In natural ecosystems, low input systems or organic farming systems, for example, mineralization of SOM is the predominant process for providing nitrogen to plants (Nendel et al., 2019). Other important ecosystem services of soils are directly correlated with soil organic matter content. For example, the capacity of storing nutrients and water for plants, being well aerated and easy to penetrate by roots (Amelung et al., 2018, pp. 64-65). At the global scale, SOC could be an important source or sink of CO_2, with the potential to offset major portions of manmade CO_2 emissions (Minasny et al., 2017). Despite the benefits of high SOC stocks, the current trend is that global SOC stocks decrease due to globally increasing agricultural production, deforestation and rising

temperatures. This leads to the risk of a positive feedback loop, where higher CO_2 concentrations increase air temperature, leading to increased SOC mineralization and hence, again increased CO_2 from soils. The potential of this feedback will largely depend on the reaction of SOC decomposition to increased temperature and other factors of the changing climate. Additionally, it will be influenced by changes in input quality and quantity of carbon sources into the soil.

As agricultural systems are the main driving force behind SOC stock loss (Lal, 2004), agricultural management schemes should be optimized towards maintaining or increasing SOC stocks. The ability to maintain or increase the SOC stocks of agricultural systems by management, is based on a thorough understanding of the processes that control the SOC cycle. Those can be roughly divided into processes that regulate inputs and losses, hence, the stabilization of plant material (such as roots and harvest residues) into SOC and the mineralization of present SOC (Wiesmeier et al., 2019). Inputs of carbon into SOC and SOC loss flow through the soil microbiome (Cotrufo et al., 2013). These flows are controlled by the environmental factors moisture and temperature, and their interactions (Sierra et al., 2015b). Further relevant processes are the influence of substrate quality on carbon use efficiency, priming effects, internal recycling of SOC through microbes, protection mechanisms such as aggregate formation and effects of agricultural management, leading to a highly complex system. An example of these interactions is the exponential increase of microbial activity and SOC turnover with temperature which interacts with the roughly binary activity function of soil moisture. As a result, the activity and even the temperature response is drastically reduced under conditions of suboptimal soil moisture (Sierra et al., 2015b). As an example for the input side, a lower quality of substrate is associated with lower microbial carbon use efficiency, meaning less growth per amount of carbon absorbed. However, this efficiency for low quality substrate is further reduced by higher temperatures (Frey et al., 2013).

The mechanics of these processes, their relative importance and their interactions need to be better understood to determine what measures help to maintain SOC. Due to the vast number of possible interactions, a thorough understanding cannot be derived by manipulation experiments alone. Simultaneous modeling of the many processes therefore presents the most holistic and comprehensive way to combine and systematize the understanding of the soil system. By this method they can further be related to other modeled processes, for example, plant growth and climate models. With such models of SOC dynamics, the current theories and understanding about the interactions of different carbon altering processes in the soil can be tested against real measured data and potential adaptions to future climates tested (Nendel et al., 2014). In this respect, modeling is first and foremost a learning tool. From the amount of processes involved, it becomes clear that simultaneously modeling all processes is a complex mathematical problem of high dimensionality. However, it has been shown that process models are able to match the quality of interpolation based CO_2 emissions from measurements and thus can be used to estimate carbon fluxes in agroecosystems and net ecosystem

CO_2 exchange (Specka et al., 2016). Furthermore, process models are the only way one can attempt to make predictions for altered conditions such as climate change, because they attempt to simulate causalities, not only correlations. It is therefore crucial to ensure that the processes to simulate (e.g., reactions to higher temperatures in the future) are well represented in the model structure. To better understand the current model structures, the next subchapter will present the history of SOC models and challenges arising from current model structures.

1.2 History of common modeling concepts to represent SOC dynamics

Since the early modeling concepts, differential equations were used to describe the decay of SOC and plant material in soils through microorganisms, mostly using 1st order kinetics (eg. Van Veen et al., 1984). The 1st order kinetic models originate from chemical reaction models, where the reaction speed is proportional to the amount of substrate, and they serve well to describe decomposition of carbon in soils, most easily observable for plant litter (e.g., Spaccini et al., 2001). To address increasing levels of humification, on its way from plant material to SOC, a series of pools of increasing complexity were introduced where carbon passes through. Each pool is still subject to 1st order decomposition. In a next step of increasing model complexity, the SOC models were linked to the surrounding abiotic factors such as soil temperature, moisture and texture, which alter the decomposition speed. Through this, site comparisons were possible, and the models became more mechanistic, not just a mathematical fitting exercise. Having two or more pools for SOC and plant material provided flexibility and a better fit to field observations in most cases. It also fit to the theoretical concept of carbon of different qualities and different stabilization mechanisms, where the slowest cycling SOC pool is either interpreted as intrinsically recalcitrant SOC or physically stabilized SOC. This proved robust for a large number of models and sites (Smith et al., 1997). For the good representation of decomposition patterns that they provide, while still being simple with only one decay parameter per pool, 1st order decomposition models became widely used. To this date, most models use 1st order decay for simulating SOC and soil nitrogen passing through a series of increasingly stabilized pools, losing a portion of SOC to the atmosphere at each transition. The amount of pools varies between models, but all of the models consist of at least one fresh plant material pool and at least one stabilized SOC pool (Campbell and Paustian, 2015). Most models additionally consider the role of microbes, having at least one microbial biomass pool or active carbon pool, as intermediate between plant material and SOC, thus directly simulating the involvement of microbes in the formation of SOC. It is due to this similarity in models that the improvement of important processes in one model, for example, the temperature function, can be translated relatively easily into similar models (Figure 1 - 1).

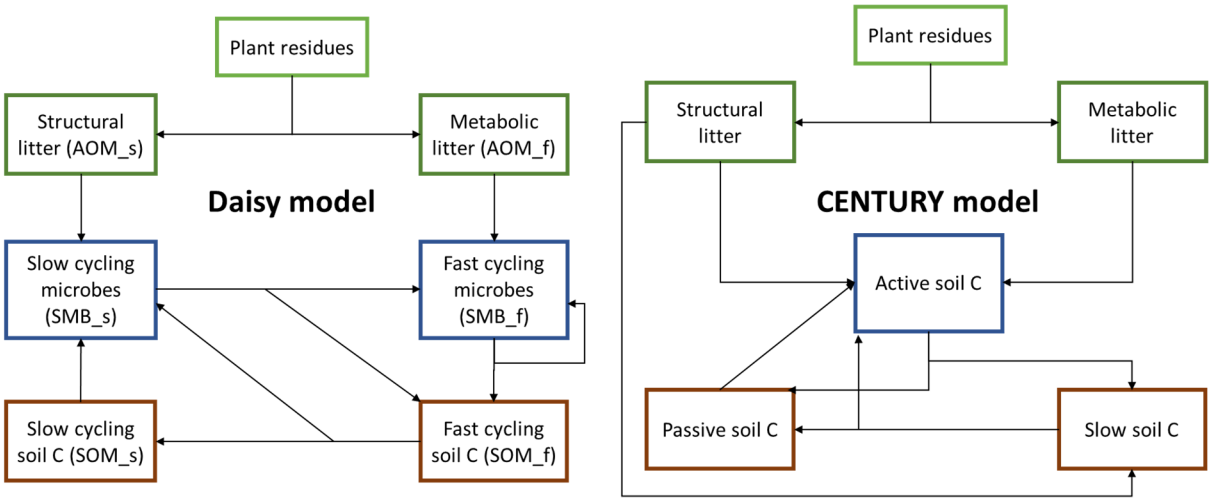

Figure 1 - 1 Comparison of the Daisy to the CENTURY model structure. Both have a similar representation of fast- and slow-cycling soil C, which are called slow and passive soil carbon in CENTURY. Thus, improved simulations of individual processes, such as the temperature response could be translated from one structure to the other.

To account for heterogeneity of SOC in the soil, most models divide stabilized SOC into at least two pools. There were two main approaches when dividing SOC into those different pools, either dividing SOC into a centennially stable fraction (which is not mineralized in simulations) and a fast decomposing fraction (RothC type models) or into fast- and slow-cycling SOC fractions, with a part of the fast cycling SOC being humified (transferred into the slow-cycling pool) while being decomposed (CENTURY type models). While both model approaches were robust and could be adjusted to a large range of sites, the different pool structures of commonly used models, such as CENTURY (Parton et al., 1987), RothC (Coleman and Jenkinson, 1996) and Daisy (Hansen et al., 1993), are usually not linked to measurable SOC fractions. Therefore, they have no direct relation to soil properties (Segoli et al., 2013). Because of this, the division of SOC between the pools had to be made either by expert guesses, inverse modeling (RothC) or standard equations (Daisy). For many regional to global ecosystem models, the multi pool SOC models represent the SOC mineralization coupled to the nitrogen mineralization and thus also directly influence crop simulations. For example Daisy is part of the MONICA (Nendel et al., 2011) and Expert-N (Klein et al., 2017) model ecosystem, which are both used for regional simulations of entire landscapes. Thus, especially for regional initialization, strong assumptions need to be made that are based on insufficient data. This poses an equifinality problem for calibration, as turnover rates and pool division are almost perfectly correlated (Bruun and Jensen, 2002). Depending on the pool sizes and structure, resulting turnover times between models will be vastly different. With calibration, the different model structures can reproduce field manipulation experiments with similar quality (Smith et al., 1997). However, the differences, resulting from model structure and equifinality lead to very different predictions for driving variables perturbation, and hence, to increased uncertainty in

extrapolations (Sierra et al., 2015a). This could be one of the main reasons for strongly diverging model results of different global carbon models under climate change (Todd-Brown et al., 2018).

Models that have more than one pool for a property that has only one measurable estimate are overparameterized from a statistical point of view, meaning that the data are insufficient to estimate all parameters. Most SOC models with several pools have exactly this main weakness. The missing link of different SOC pools to measurable fractions produces most uncertainty, if different reactions by the different SOC fractions are expected to environmental perturbations (e.g, a carbon complexity dependent difference in the reaction to temperature increase or moisture alteration). If SOC pools are not clearly defined, it cannot be established whether they actually react differently to perturbations. Thus, pools in SOC models need to be linked to measurable fractions of SOC or proxies for SOC fractions. Therefore, this was one of the main goals of this thesis. In the next subchapter, different potential proxies for SOC pools in models will be discussed, and the choice of DRIFTS a proxy will be elaborated.

1.3 Model proxies for SOC complexity related to stabilization mechanisms

The use of proxies in SOC models is very common, for example through the clay functions that alter SOC decomposition as a linear function of clay content. As a result, clay content is one of the main mediators of simulated SOC retention (Stella et al., 2019), demonstrating the potential of well-chosen proxies. Proxies have been linked to SOC stocks at global scales (Bailey et al., 2018) and are intimately connected to the soil forming factors proposed by Jenny (1941). However, proxies to divide SOC into the pools of different complexity are still lacking for most of the current SOC models. First attempts could correlate measured soil fractions to modeled pools with some initial success (e.g., Zimmermann et al., 2007), but did not establish a pool definition from clearly defined fractions. Also the newer proxies for pool allocation, such as the Rock-Eval pyrolysis-combustion method (Cécillon et al., 2018), are so far only correlative. Hence, more efforts need to directly link SOC model pools to measured SOC fractions (Segoli et al., 2013) or proxies for such fractions. This either calls for development of new models that simulate measurable fractions or adapting current models by linking their pools to measurable proxies of SOC complexity. The latter has the advantage, that there is a lot of expertise with the current models which are already widely used and implemented into global ecosystem modeling concepts. Hence, new proxies could easily be applied to many existing model frameworks and future studies.

It is clear, that any attempt to separate the continuous complex nature of SOC into defined pools will be an approximation at best. For example, even with separation by size and density fractionation, which should intuitively yield very clearly defined fractions, the results varied considerably between laboratories (Poeplau et al., 2013). Therefore, a conceptional fit of SOC fractions or proxies for pools

to established theories about the stabilization of SOC in the soil is required. If SOC pools through a model proxy are clearly defined and have uniquely different turnover, it could also be tested if unique responses to environmental factors (e.g., temperature or moisture) exist for each pool (i.e., complexity dependent temperature sensitivity).

The different mechanisms of SOC stabilization in soils can be roughly divided into three different concepts: 1) the concept of stability due to intrinsic chemical properties of SOC or plant material, 2) the concept of chemical protection of SOC through sorption to fine particles of silt and clay size, and 3) the concept of physical stabilization of SOC within and through the formation of soil aggregates of different sizes and hierarchy. In all three concepts, the SOC stabilization is linked to microbial decomposition of SOC, i.e., the unattractiveness or inaccessibility of SOC for microbes is the stabilizing mechanism.

The first of these concepts is probably the oldest and is linked strongly with the initial idea that SOC consists mainly of humins, fulvic and humic acids (Morrill et al., 1982), large molecular compounds that can be extracted from soils by different organic acids. These were thought to be the stable compounds of SOC and due to their high content of aromatics, it was concluded that they consist to a large extent of stable, mostly undecomposed plant residues (mostly lignin). However, recent evidence suggests that these extracted humic substances are not representative of the total carbon complexity profile within SOC (Amelung et al., 2018, pp. 157), and some evidence suggests that SOC consist mostly of much lower molecular size (Schmidt et al., 2011). New concepts assigned most stabilized SOC to microbial origin (Cotrufo et al., 2013), regardless of whether the sources were complex aromatic carbon or glucose (Kallenbach et al., 2016). Nevertheless, there is evidence from DRIFTS spectroscopy that more complex SOC structures, such as aromatic and carboxylic SOC constituents, are more persistent in soils than less complex SOC, for example aliphatic constituents (Demyan et al., 2012; Kunlanit et al., 2014). Hence, there are still indications of a relationship between SOC complexity and recalcitrance. This might be due to preferential use of more energy rich (e.g., aliphatic) SOC by soil microorganisms instead of the intrinsic recalcitrance of higher complexity SOC (Barré et al., 2016), but this is not entirely clear yet.

The second concept suggests chemical sorption of SOC to particles of silt and clay size to be one of the most important factors of SOC stabilization, limiting access of microbes to SOC via spatial separation (Sokol et al., 2019). This is generally due to the large surface area that these particle sizes provide. Larger surface area promotes more possibilities for sorption of SOC to the soil particles, which stabilizes SOC (Wiesmeier et al., 2019). This was already demonstrated by the concept of SOC saturation based on silt and clay content (Hassink, 1997) and is still used in recent models (e.g., Campbell et al., 2016). The mineral associated SOC is considered the most slowly cycling part of SOC

(Sokol et al., 2019) and often the largest portion of SOC in agricultural fields. It is also recognized and implemented as a proxy in many models, where it slows down the turnover of stabilized SOC.

The third concept explains the stabilization of SOC by physical protection within soil aggregates, mostly microaggregates, which are formed as a byproduct of microbial activity by providing gluing substances (Totsche et al., 2017). This aggregate-protected SOC is seen as the most vulnerable part of SOC, easily lost due to changes in land use and management practices (Six and Paustian, 2014). Aggregate-protected SOC could therefore correspond to SOC of intermediate turnover, because it seems to be easily released upon aggregate destruction (Puttaso et al., 2013). This is also acknowledged in more recent SOC models, such as the millennial model (Abramoff et al., 2018), which has both a mineral associated SOC pool of slow turnover and an aggregate stabilized SOC pool of intermediate turnover.

These three concepts are not excluding each other. It is very likely that all three are involved in the stability of SOC and they are all related. For example, it has been shown that even silt associated organic matter is aggregated (Schweizer et al., 2019) or that spectral ratio of aliphatic to aromatic-carboxyl SOC correlates well with the ratio of heavy to light fraction associated SOC (Demyan et al., 2012). This suggests that the relative importance of those individual concept depends mainly on the spatial and temporal scale in focus. From a modeling perspective, it is important that different pools are related to the concepts of stabilization. They should not only be uniquely measurable, but also provide insights into utility and importance of the theoretical concept. Furthermore, the different SOC fractions of the pools must have clearly different turnover in the soil. Lastly, the measurement of proxies must be repeatable and ideally be stable over a longer time period, as the change of SOC requires decades to centuries of manipulation experiments. Additionally, low derivation cost would be beneficial for large-scale applications.

There are a range of different techniques to classify SOC, which relate to the different stabilization mechanisms. Size and density separations of water stable aggregates, for example, try to separate SOC into aggregated SOC on the one hand and silt and clay mineral associated SOC on the other hand (e.g. Poeplau et al., 2013; Puttaso et al., 2013; Zimmermann et al., 2007). However, the hierarchical theory of aggregate formation suggests that it is difficult to separate SOC stabilization mechanisms, because macroaggregates contain microaggregates (Six and Paustian, 2014) and both contain silt and clay within the aggregates. Other techniques such as the use of traceable isotopes, often ^{14}C, can be used to classify SOC by age. Those are often used in combination with inverse modelling to derive ages of different SOC pools ranging from simple one SOC pool (Ahrens et al., 2014) to multi-pool models (Metzler et al., 2020). Hence, the isotope approaches are often combined with approaches such as size density separation or gas evolution from combustion at different temperatures. Furthermore, there are approaches that focus on SOC chemistry, such as nuclear magnetic resonance spectroscopy (Kiem

et al., 2000) or mid-infrared spectroscopy. These approaches point towards SOC stability due to intrinsic chemical properties and there is evidence that SOC constituents of higher complexity, such as aromatics, are preferentially preserved due to lower energy content (Barré et al., 2016). However there is also evidence that SOC chemistry correlates to the distribution of SOC in size density fractionation (Demyan et al., 2012). This could be due to depolymerized lignin molecules from plants directly attaching to minerals (Huang et al., 2019). Thus, while the understanding of the link between SOC chemistry and stability is enriched by newly proposed mechanisms of microbial processing and direct sorption, SOC chemistry seems still a highly informative proxy for SOC stability. Within the methods that classify SOC chemistry, one promising proxy is the use of infrared spectra as an SOC complexity proxy. The spectra contain information on the presence of different carbon bonds. Michel and Ludwig (2010) demonstrated that this information can be used for SOC pool allocation by predicting RothC model pools by near-infrared spectroscopy. With standardized equipment, DRIFTS should also be more reproducible than methods requiring manual labor, for example, size density fractionation. The use of DRIFTS spectra has shown special potential to represent carbon fractions of different complexity because different identified functional groups of carbon showed clearly different turnover times (Demyan et al., 2012). Therefore, the test of DRIFTS for pool partitioning was conducted within this thesis. The underlying principles will be further elaborated in the following chapter.

1.3.1 The use and limitations of DRIFTS as a proxy for complexity

Infrared spectroscopy, which measures absorbance of light at distinct wavenumbers (the inverse of the wavelength) gives information on the chemical bonds present in a sample. Hence, it is mainly related to the concept of intrinsic recalcitrance of SOC. Though the common sample preparation through milling destroys physical protection prior to measurement, the correlative nature of infrared absorption bands of different complexity to size density fractionation (Demyan et al., 2012; Sohi et al., 2001) shows the link to the other two concepts. However, the processes behind this link are incompletely understood and thus use of infrared spectra alone could be partly misleading if other measures of SOC stabilization are not considered at all. The main advantages of infrared spectroscopy are the cost efficiency, ease of preparation and the resulting potential for large scale application. Additionally, the SOC chemistry is likely less prone to change than soil aggregate distribution when storing soil samples for the long timespans to study changes in SOC quality and quantity. Infrared spectroscopy has been used for many years in the attempt to study SOC, with earliest applications analyzing the spectra gained from extracted humic substances (Stevenson, 1994). As it became more evident that those are only a small portion of SOC, the analysis of spectra from bulk soil and soil fractions (often mixed with potassium bromide) came into focus. Early studies already suggested that SOC stability could be inferred from spectral information, for example that stabilized SOC had a stronger absorption in the spectral regions linked to aromatic carbon (e.g., Sohi et al., 2001). The

aliphatic and aromatic-carboxyl absorption bands were the most clearly visible indicators of different SOC complexity (Ellerbrock and Gerke, 2004). More recently, faster and slower changes of the aliphatic and aromatic-carboxyl absorption bands, respectively, as a result of different amounts of carbon input, were demonstrated (Demyan et al., 2012). A lower thermal stability of aliphatic compared to aromatic-carboxyl compounds further proved their different recalcitrance (Demyan et al., 2013). Within this study aliphatic and aromatic-carboxyl absorption bands were selected as proxies for SOC of fast and slow turnover, respectively, due to their visibility, clear assignment and different turnover times. The choice of DRIFTS within this study was due to better representations of the SOC in the sample (Ma et al., 2019), as compared to attenuated total reflectance spectroscopy with a stronger signal from the mineral matrix and higher precision for inorganic compounds (Beasley et al., 2014). The main challenge of DRIFTS for the interpretation of SOC complexity was that apart from the organic absorption bands of interest, the spectra also contain inorganic absorption bands, for example from water (OH bonds) or minerals, which overlap with SOC absorption bands (Nguyen et al., 1991). Especially the absorption by OH is problematic and can even lead to negative areas of absorption bands for low SOC contents. The resulting interference is the major obstacle, when interpreting DRIFTS spectra across soils (Demyan et al., 2012) and thus it should be minimal for pool partition. Thus, an improvement of the DRIFTS measurement protocol to reduce OH interference was needed to best represent the proportions of different SOC constituents. This was the first study of this thesis. In the next step, the suitability of DRIFTS for SOC pool partitioning was tested. It was hypothesized that due to their different turnover times and chemical complexity, the aliphatic and aromatic-carboxyl absorption bands would be suitable proxies for fast- and slow-cycling SOC pools in SOC models.

1.4 Temperature sensitivity related to SOC complexity

The response of SOC stocks to global warming will largely depend on the response of their mineralization to temperature increase. As a result, estimating the effect of future climate scenarios on SOC stock development requires a good representation of the temperature effect on mineralization in SOC models. This so-called temperature sensitivity is often expressed as the Q_{10} value, the factor by which mineralization increases (i.e. is multiplied by) at a +10°C temperature increase. The Q_{10} value is usually positive and assumed to be between 1.0 and 3.0, which means that, with all other factors being constant, an increase of mineralization with temperature is expected in all but the most special cases. Through the close link of SOM to soil nitrogen, this could lead to a higher nitrogen supply in the short term, while reducing the stocks of mineralizable nitrogen in the long term (Nendel et al., 2019). Furthermore, the activation energy theory (Bosatta and Ågren, 1999) postulates that there is an inverse relationship between temperature sensitivity and carbon complexity. This is a direct result of the use of the Arrhenius equation, where higher activation energy is directly linked to higher temperature sensitivities (Sierra, 2012). This means that SOC model pools representing different

carbon complexities should be different in terms of Q_{10} values. However, most common SOC models apply the same temperature function and Q_{10} value for all pools. This is usually either an exponential function or derivative of an exponential function (Tuomi et al., 2008). While this approach captures the general effect of temperature on mineralization, it does not take the effects of carbon complexity and different stabilization mechanisms into account. This may be one of the main reasons for the high uncertainty of SOC models at global scales (Tang and Riley, 2015). For example, even when this single Q_{10} value was allowed to vary, the 95% confidence intervals for Q_{10} were between 1.6 and 2.7, which translated into global SOC stock changes until 2100 of between – 304 and + 114 Pg carbon under the RCP 8.5 scenario (Todd-Brown et al., 2018), meaning it could not be established whether this extreme scenario would lead to carbon loss or gain.

In addition to the activation energy theory, there is a lot of experimental evidence that Q_{10} values should be dissimilar for different carbon complexities. This applies for Q_{10} values of different soil enzymes (e.g., Ali et al., 2015), seasonally varying Q_{10} values of soil respiration (Demyan et al., 2016) or different inferred Q_{10} values for different model pools (Hararuk et al., 2017). It is unclear though, which of the possible Q_{10} values should be assigned to different complexities of soil carbon. The basic assumption of the Arrhenius equation, which is derived from theoretical chemistry (Tang et al., 2019), could be invalid in soils. The activation energy might not be the main limiting factor of mineralization in soils, where processes are highly interactive and complex: For example, living microorganisms alter activation energies by extracellular enzymes, substrate availability can be limited by factors such as aggregation, that are not linked to activation energy, and the denaturation of different enzymes could lead to reduced mineralization at higher temperatures. Thus, it is not yet clear whether it is valid for SOC to infer Q_{10} values based on carbon complexity alone, since the results of several studies opposed to the activation energy theory. For example, Gromova et al. (2020) found a much higher Q_{10} value of soil with glucose addition (~2.6) compared to soil basal respiration (~2); or Nottingham et al. (2016) found higher Q_{10} values for glucosidase (~1.6) than for phenoloxidase (~1.4).

As a consequence, there is a need to investigate pool specific Q_{10} values. Due to the conflicts of experimental evidence with the activation energy theory, the approach should not rely on theoretical assumptions, but instead could be directly developed within established models using temperature gradients. Two approaches seem promising to determine pool specific Q_{10} values. One option would be to statistically infer pool specific Q_{10} values from measured data. A second option would be to identify measurable proxies for different Q_{10} values of different carbon pools.

The first approach faces the challenge of Q_{10} values being a multiplicator of mineralization. Multiplicative structures are prone to equifinality problems (Bagnara et al., 2018), and turnover is itself strongly correlated with pool allocation (Bruun and Jensen, 2002). Therefore, a clear definition of SOC

model pools is a prerequisite for inferring or testing different Q_{10} values for different pools. Hence, the search for SOC complexity proxies and for pool specific temperature functions in modeling are synergetic. If pool definition is clear and experiments cover the temperature range of interest, it should be possible to infer Q_{10} values based on defined carbon complexity and temperature gradients. This would represent a direct test of the activation energy theory for natural soil systems, using the current generation of models. The inverse modeling technique furthermore needs to be able to establish whether different pools' Q_{10} values are significantly different, because any fitting routine will lead to different values for different pools. Probabilistic methods are therefore needed.

The second option are measurable proxies for pool specific Q_{10} values. Firstly, such a proxy would have to be linked to the temperature sensitivity of carbon mineralization and secondly distinguish different carbon qualities. Because of the importance of extracellular enzymes in SOC mineralization, measured enzyme activities and their Q_{10} values are a candidate for such a proxy. Enzyme activity Q_{10} is clearly linked to mineralization Q_{10} (Ali et al., 2015) and the measurement by substrate addition is simple. Further, the use of enzyme Q_{10} values as proxies has a mechanistic reason: extracellular enzymes play a central role in SOC mineralization. They are excreted by microbes with the central purpose of carbon or nitrogen acquisition (Sinsabaugh, 2010), where they regulate the breakdown of large SOC and plant macromolecules to smaller soluble molecules, which can then be assimilated by microbes (Sinsabaugh et al., 2008). The enzymatic reaction is therefore considered to be the rate-limiting step in the decomposition of SOC and plant material (Sinsabaugh and Follstad Shah, 2012). Different measured extracellular enzymes such as glucosidases, cellobiohydrolases, xylanases, phosphatases and phenoloxidases (Sinsabaugh et al., 2008) tackle carbon of different complexities, thus they should be a proxy for the respective targeted substrate. Under the assumption that the enzymatic reaction is the rate-limiting step of the mineralization, the Q_{10} values of enzyme activities could be used as Q_{10} values of different pools. Thus, the use of enzyme Q_{10} values also requires a measurable pool definition linked to the carbon sources that the different enzymes tackle. By testing for potential improvements in model performance, one could indirectly test the utility of enzyme Q_{10} values as pool specific Q_{10} values. This could add to inference by inverse modeling of Q_{10} values using measured data and ideally lead to similar conclusions as inferred pool specific model Q_{10} values. The approach of statistical inference would require probabilistic model optimization. The following chapter will explicate the background behind statistical interference for SOC models and introduce the method of Bayesian calibration which was used in this study.

1.5 Using Bayesian calibration to account for model uncertainty and the link to new model proxies

Soils are probably the most complex biomaterial on earth (Young, 2004). Therefore, SOC models are always a simplification of highly complex real-world processes, thus leading to uncertainty. While the common statistical models in all schools of science treat their parameters and output as probabilistic, this has not been commonly done in SOC process models. However, if the level of confidence in model outputs or a statistical testing of hypotheses, such as whether different Q_{10} values are justified for different pools, should be conducted within SOC models, there is a need for probabilistic approaches that account for uncertainty. Apart from the uncertainty due to the simplification of such a complex system, the model uncertainty originates mainly from soil heterogeneity and more model pools than measured fractions. Earlier approaches attempted to display uncertainty by an analysis of simulation and measurement misfit (Smith et al., 1997). However, this only derives a site-specific value and does not allow to propagate uncertainty to other simulations.

In contrast, probabilistic modeling approaches, such as Bayesian calibration, treat the model parameters, data and outputs as probability distributions instead of single values, while the models can still be deterministic in structure. They can therefore account for the uncertainty of the model parameters and the model output (Clifford et al., 2014), which would allow to propagate model errors from one site to another. They express the level of confidence in the model parameters (Van Oijen et al., 2005) and compare different model formulations by their likelihood (van Oijen et al., 2011). The downside of Bayesian calibration is high computational cost, because it requires thousands to millions of model runs. However, classical statistical approaches, which have exactly one analytical solution and are computationally cheap, fail for most SOC models. As most SOC models are noninvertible due to their internal carbon recycling structure (Todd-Brown et al., 2018) they are not mathematically solvable with least-square methods. Instead, solutions are obtained by methods of random sampling from the multidimensional space of possible parameters, using data to estimate the likelihood of each sample from the parameter space (Marcel van Oijen, 2008). The equivalence of Bayesian calibration measures of parameter uncertainty with linear statistical models has been shown for simple problems (Lu et al., 2012), but Bayesian calibration can also handle nonlinear problems. It is superior to gradient search algorithms, which tend to get trapped in local optima (Xu et al., 2018). This seems not to be the case for Bayesian calibration, even for complex synthetic examples (Lu et al., 2014). Hence, it should be ideal for hypothesis testing within the established SOC models of high nonlinearity. Through its capability to display uncertainty, Bayesian calibration is useful for model calibration and hypothesis testing as was the goal of this thesis. It can be applied to the two main questions of this thesis, firstly

assessing whether using DRIFTS as SOC complexity proxy is a meaningful improvement for an SOC model and secondly whether pool specific Q_{10} values are likely given the data.

The Bayesian calibration technique was originally developed by Metropolis et al. (1953) to find solutions to a chemical entropy problem that was not analytically solvable and was refined to classical Markov chain Monte Carlo by Hastings (1970). Bayesian calibration techniques are relatively straightforward and use available data, including information on data uncertainty, to derive model parameters and model output probability distributions. In Bayesian terms this is called to sample from the posterior distribution of model parameters, given the model and the data: $p(\vartheta|M,D)$, ϑ standing for the parameters, *M* for the model and *D* for the data. The algorithm performs a random walk in the parameter distribution space and uses the measured data weighted by its variance and the model output to evaluate the likelihood. This is done in a Markov Chain, where the likelihood of each simulation is evaluated against the prior simulation. Increased likelihoods are always accepted. Decreased likelihoods are accepted with a probability that depends on the quotient of the new likelihood, divided by the likelihood of the prior simulation, which is called the Metropolis ratio (Marcel van Oijen, 2008). The sample is accepted if this quotient is greater than a randomly drawn number between 1 and 0 (Vrugt, 2016). Modern Bayesian calibration techniques still use the Metropolis ratio, which makes it possible to sample from the posterior distribution. Primary changes to the original algorithm are methods for generating new proposals and for diagnosing the convergence of the algorithm, for example by running multiple Markov chains in parallel (Gelman and Rubin, 1992). The DREAM algorithm, which was used in this study, is one of the most advanced Bayesian calibration schemes, because it provides multiple Markov chains to ensure convergence of the Bayesian calibration and uses information gained from the different chains to fine tune the proposal distribution to not be trapped in local minima (Vrugt, 2016). Therefore, Bayesian calibration offers a better performance for global optimization of nonlinear problems, such as SOC models, compared to gradient search algorithms, such as Gauss-Newton optimizers, which tend to get trapped in local minima (Pullen and Morris, 2014; Xu et al., 2018). After convergence, Bayesian credibility intervals and posterior distributions can be directly taken from the distribution of accepted parameters.

In a Bayesian calibration, good proxies reduce the uncertainty of model parameters and outputs with clearly identifiable parameters (Sierra et al., 2015a). Thus, the utility of proxies could be inferred from the reduction of model uncertainty. An example of this was shown by Ahrens et al. (2014). In their publication, the use of a ^{14}C signal of carbon pools could reduce the uncertainty of their mineralization speed. Other examples of successful use of Bayesian calibration are the SOC pool partitioning for CENTURY (Yeluripati et al., 2009) or for a two pool RothC type model with one persistent pool (Cécillon et al., 2018). However, such a pool partitioning by Bayesian calibration can only be used under the assumption that either turnover is known, or that one of the two SOC pools is not subject to

decomposition, constraints that were considered too drastic within this study. Other examples of Bayesian calibration include assessing the light use efficiency of forest models (Bagnara et al., 2018) or inferring pools specific Q_{10} values for a forest model (Hararuk et al., 2017). More complex approaches, such as Bayesian model evidence, can also compare different model concepts of increasing complexity and estimate which model is most likely, given the available data (Menichetti et al., 2016). Those include considerations of model parsimony (Sierra et al., 2015a) posing the questions whether there is enough data to justify the use of complex models that are usually used for SOC modeling. However, this was beyond the scope of this study, which was limited to Bayesian calibration of SOC parameters.

The direct applicability to improve models, led to the choice of the Bayesian calibration technique within this study for hypothesis testing. Thus, it was used to evaluate the utility of DRIFTS for pool partitioning and to test the activation energy theory. Both of these were done within the framework of the Daisy SOC model. The Daisy model is a typical SOC model, which has two pools for each of the fractions, plant litter, microbes and stabilized SOC (Figure 1 - 1). It was hypothesized that application of probabilistic Bayesian calibration would lead to insights into the link between SOC complexity and turnover and the utility of pool specific Q_{10} values as informed by measured data. This should present an improvement of current generation SOC models with regards to making model pools measurable and to have explicitly different temperature functions for different SOC and litter pools.

1.6 Objectives and Hypotheses

The overall objective of this thesis was to contribute to overcoming some of the main challenges that the current generation of SOC models face when simulating future climate perturbations: The lack of clear SOC pool definitions, of pool specific Q_{10} values and of displaying model parameter confidence. A main topic was therefore the development of the DRIFTS stability index (DSI), which is the ratio of aliphatic to aromatic-carboxylate absorption band areas of DRIFTS spectra, as a proxy for SOC complexity. The goal was implementation of the DSI as a proxy for SOC complexity into the SOC model Daisy and thereafter inferring different pool specific Q_{10} values based on temperature gradient experiments as well as testing enzyme Q_{10} values as proxy for pool specific Q_{10}. This was done in a probabilistic way, to quantify the uncertainty of the Daisy SOC model parameters and to conduct hypothesis testing within the model.

The specific goals were addressed in three research papers, which built on each other, with the topics of:

1) Improving the measurement protocol of the DSI for model initialization
2) Implementing the DSI into the Daisy SOC model by Bayesian calibration
3) Deriving pool specific Q_{10} values by Bayesian calibration and testing enzyme Q_{10} values as proxies for pool specific Q_{10} values based on the DSI

The hypotheses were that i) the interference of residual sample moisture content in the DRIFTS spectra needs to be reduced through higher drying temperature for deriving a suitable proxy for SOC pool initialization; ii) the resulting improved DSI contains the necessary information about fast- and slow-cycling SOC pools, and implementing the DSI for SOC pool initialization reduces model error compared to assuming steady state; and iii) through its' measurable definition of the Daisy SOC pools, the DSI reduces parameter uncertainty in Bayesian calibration. Furthermore, it was hypothesized that iv) with the introduced pool definition, pool specific Q_{10} values can be inferred by Bayesian calibration, thus providing a test of the activation energy theory. A final hypothesis was that v) measured enzyme Q_{10} values (of glucosidase, xylanase, and phenoloxidase) are proxies for the pool specific Q_{10} values, thus, they improve model performance and have the same trend as Bayesian calibration inferred Q_{10} values.

1.7 Outline of this thesis

Three research papers are presented in this thesis. The aim of the first paper was to optimize the use of the diffuse reflectance Fourier transform mid-infrared spectroscopy stability index (DSI) as proxy of SOC complexity by testing the pretreatment effect of drying temperature (chapter 2). The derived DSI was then introduced into the SOC model Daisy to derive and test a partitioning of SOC into pools of different complexity in a probabilistic way, by using Bayesian calibration (chapter 3). Based on this partitioning, two ways of testing hypothesis about SOC complexity dependent Q_{10} values were followed in the last research paper: statistical inference of Q_{10} values by Bayesian calibration and linking measured enzyme Q_{10} values to model pools. Thus, the activation energy theory was tested based on the prior established pool definition (chapter 4). Finally, the implications of pool partitioning, Q_{10} allocation and dealing with model and data uncertainty, including the broader literature, are discussed and an outlook is given (chapter 4).

Figure 1 - 2 Locations of the origin of the soil samples used within this thesis. Coordinates may be found in Table S2 - 1.

A number of datasets were combined to develop this thesis. The modeling exercises of chapter 3 and chapter 4 made use of samples and datasets from the long-term bare fallow experiments in Ultuna, Sweden and Bad Lauchstädt, Germany. Furthermore, use was made of medium-term bare fallow and vegetation experiments from the Kraichgau and Swabian Jura regions in Southwest Germany and laboratory incubation of soil and plant samples conducted at different temperatures (Figure 1 - 2). To improve the measurement protocol of DRIFTS, a more global approach was used including tropical soils from the SURUMER project in China (Laub et al., 2018).

1.8 References general introduction

Abramoff, R., Xu, X., Hartman, M., O'Brien, S., Feng, W., Davidson, E., Finzi, A., Moorhead, D., Schimel, J., Torn, M. and Mayes, M. A.: The Millennial model: in search of measurable pools and transformations for modeling soil carbon in the new century, Biogeochemistry, 137(1–2), 51–71, doi:10.1007/s10533-017-0409-7, 2018.

Ahrens, B., Reichstein, M., Borken, W., Muhr, J., Trumbore, S. E. and Wutzler, T.: Bayesian calibration of a soil organic carbon model using Δ14C measurements of soil organic carbon and heterotrophic respiration as joint constraints, Biogeosciences, 11(8), 2147–2168, doi:10.5194/bg-11-2147-2014, 2014.

Ali, R. S., Ingwersen, J., Demyan, M. S., Funkuin, Y. N., Wizemann, H.-D., Kandeler, E. and Poll, C.: Modelling in situ activities of enzymes as a tool to explain seasonal variation of soil respiration from agro-ecosystems, Soil Biol. Biochem., 81, 291–303, doi:10.1016/j.soilbio.2014.12.001, 2015.

Amelung, W., Blume, H.-P., Fleige, H., Horn, R., Kandeler, E., Kögel-Knabner, I., Kretzschmar, R., Stahr, K. and Wilke, B.-M.: Scheffer/Schachtschabel Lehrbuch der Bodenkunde, Springer Berlin Heidelberg, Berlin, Heidelberg., 2018.

Bagnara, M., Van Oijen, M., Cameron, D., Gianelle, D., Magnani, F. and Sottocornola, M.: Bayesian calibration of simple forest models with multiplicative mathematical structure: A case study with two Light Use Efficiency models in an alpine forest, Ecol. Modell., 371(April 2017), 90–100, doi:10.1016/j.ecolmodel.2018.01.014, 2018.

Bailey, V. L., Bond-Lamberty, B., DeAngelis, K., Grandy, A. S., Hawkes, C. V., Heckman, K., Lajtha, K., Phillips, R. P., Sulman, B. N., Todd-Brown, K. E. O. and Wallenstein, M. D.: Soil carbon cycling proxies: Understanding their critical role in predicting climate change feedbacks, Glob. Chang. Biol., 24(3), 895–905, doi:10.1111/gcb.13926, 2018.

Barré, P., Plante, A. F., Cécillon, L., Lutfalla, S., Baudin, F., Bernard, S., Christensen, B. T., Eglin, T., Fernandez, J. M., Houot, S., Kätterer, T., Le Guillou, C., Macdonald, A., van Oort, F. and Chenu, C.: The energetic and chemical signatures of persistent soil organic matter, Biogeochemistry, 130(1–2), 1–12, doi:10.1007/s10533-016-0246-0, 2016.

Beasley, M. M., Bartelink, E. J., Taylor, L. and Miller, R. M.: Comparison of transmission FTIR, ATR, and DRIFT spectra: implications for assessment of bone bioapatite diagenesis, J. Archaeol. Sci., 46(1), 16–22, doi:10.1016/j.jas.2014.03.008, 2014.

Bosatta, E. and Ågren, G. I.: Soil organic matter quality interpreted thermodynamically, Soil Biol. Biochem., 31(13), 1889–1891, doi:10.1016/S0038-0717(99)00105-4, 1999.

Bruun, S. and Jensen, L. S.: Initialisation of the soil organic matter pools of the Daisy model, Ecol. Modell., 153(3), 291–295, doi:10.17665/1676-4285.20155108, 2002.

Campbell, E. E., Parton, W. J., Soong, J. L., Paustian, K., Hobbs, N. T. and Cotrufo, M. F.: Using litter chemistry controls on microbial processes to partition litter carbon fluxes with the Litter Decomposition and Leaching (LIDEL) model, Soil Biol. Biochem., 100, 160–174, doi:10.1016/j.soilbio.2016.06.007, 2016.

Campbell, E. E. E. and Paustian, K.: Current developments in soil organic matter modeling and the expansion of model applications: a review, Environ. Res. Lett., 10(12), 123004, doi:10.1088/1748-9326/10/12/123004, 2015.

Cécillon, L., Baudin, F., Chenu, C., Houot, S., Jolivet, R., Kätterer, T., Lutfalla, S., Macdonald, A., van Oort, F., Plante, A. F., Savignac, F., Soucémarianadin, L. N. and Barré, P.: A model based on Rock-Eval

thermal analysis to quantify the size of the centennially persistent organic carbon pool in temperate soils, Biogeosciences, 15(9), 2835–2849, doi:10.5194/bg-15-2835-2018, 2018.

Clifford, D., Pagendam, D., Baldock, J., Cressie, N., Farquharson, R., Farrell, M., Macdonald, L. and Murray, L.: Rethinking soil carbon modelling: a stochastic approach to quantify uncertainties, Environmetrics, 25(4), 265–278, doi:10.1002/env.2271, 2014.

Coleman, K. and Jenkinson, D. S.: RothC-26.3 - A Model for the turnover of carbon in soil, in Evaluation of Soil Organic Matter Models, pp. 237–246, Springer Berlin Heidelberg, Berlin, Heidelberg., 1996.

Cotrufo, M. F., Wallenstein, M. D., Boot, C. M., Denef, K. and Paul, E.: The Microbial Efficiency-Matrix Stabilization (MEMS) framework integrates plant litter decomposition with soil organic matter stabilization: do labile plant inputs form stable soil organic matter?, Glob. Chang. Biol., 19(4), 988–995, doi:10.1111/gcb.12113, 2013.

Demyan, M. S., Rasche, F., Schulz, E., Breulmann, M., Müller, T. and Cadisch, G.: Use of specific peaks obtained by diffuse reflectance Fourier transform mid-infrared spectroscopy to study the composition of organic matter in a Haplic Chernozem, Eur. J. Soil Sci., 63(2), 189–199, doi:10.1111/j.1365-2389.2011.01420.x, 2012.

Demyan, M. S., Rasche, F., Schütt, M., Smirnova, N., Schulz, E. and Cadisch, G.: Combining a coupled FTIR-EGA system and in situ DRIFTS for studying soil organic matter in arable soils, Biogeosciences, 10(5), 2897–2913, doi:10.5194/bg-10-2897-2013, 2013.

Demyan, M. S., Ingwersen, J., Funkuin, Y. N., Ali, R. S., Mirzaeitalarposhti, R., Rasche, F., Poll, C., Müller, T., Streck, T., Kandeler, E. and Cadisch, G.: Partitioning of ecosystem respiration in winter wheat and silage maize—modeling seasonal temperature effects, Agric. Ecosyst. Environ., 224, 131–144, doi:10.1016/j.agee.2016.03.039, 2016.

Ellerbrock, R. H. and Gerke, H. H.: Characterizing organic matter of soil aggregate coatings and biopores by Fourier transform infrared spectroscopy, Eur. J. Soil Sci., 55(2), 219–228, doi:10.1046/j.1365-2389.2004.00593.x, 2004.

Frey, S. D., Lee, J., Melillo, J. M. and Six, J.: The temperature response of soil microbial efficiency and its feedback to climate, Nat. Clim. Chang., 3(4), 395–398, doi:10.1038/nclimate1796, 2013.

Gelman, A. and Rubin, D. B.: Inference from Iterative Simulation Using Multiple Sequences, Stat. Sci., 7(4), 457–472, doi:10.1214/ss/1177011136, 1992.

Gromova, M. S., Matvienko, A. I., Makarov, M. I., Cheng, C. and Menyailo, O. V: Temperature Sensitivity (Q 10) of Soil Basal Respiration as a Function of Available Carbon Substrate , Temperature , and Moisture, Eurasian Soil Sci., 53(January), 376–381, doi:10.1134/S1064229320020052, 2020.

Hansen, S., Jensen, L. S., Nielsen, N. E. and Svendsen, H.: The Soil Plant System Model Daisy - Basic Principles and Modelling Approach, Copenhagen: The Royal Veterinary and Agricultural University., 1993.

Hararuk, O., Shaw, C. and Kurz, W. A.: Constraining the organic matter decay parameters in the CBM-CFS3 using Canadian National Forest Inventory data and a Bayesian inversion technique, Ecol. Modell., 364, 1–12, doi:10.1016/j.ecolmodel.2017.09.008, 2017.

Hassink, J.: The capacity of soils to preserve organic C and N by their association with clay and silt particles, Plant Soil, 191(1), 77–87, doi:10.1023/A:1004213929699, 1997.

Huang, W., Hammel, K. E., Hao, J., Thompson, A., Timokhin, V. I. and Hall, S. J.: Enrichment of lignin-derived carbon in mineral-associated soil organic matter, Environ. Sci. Technol., 53(13), 7522–7531, doi:10.1021/acs.est.9b01834, 2019.

Jenny, H.: Factors of Soil Formation, Soil Sci., 52(5), 415, doi:10.1097/00010694-194111000-00009, 1941.

Kallenbach, C. M., Frey, S. D. and Grandy, A. S.: Direct evidence for microbial-derived soil organic matter formation and its ecophysiological controls, Nat. Commun., 7, 1–10, doi:10.1038/ncomms13630, 2016.

Kiem, R., Knicker, H., Körschens, M. and Kögel-Knabner, I.: Refractory organic carbon in C-depleted arable soils, as studied by 13C NMR spectroscopy and carbohydrate analysis, Org. Geochem., 31(7–8), 655–668, doi:10.1016/S0146-6380(00)00047-4, 2000.

Klein, C., Biernath, C., Heinlein, F., Thieme, C., Gilgen, A. K., Zeeman, M. and Priesack, E.: Vegetation Growth Models Improve Surface Layer Flux Simulations of a Temperate Grassland, Vadose Zo. J., 16(13), 1–19, doi:10.2136/vzj2017.03.0052, 2017.

Kunlanit, B., Vityakon, P., Puttaso, A., Cadisch, G. and Rasche, F.: Mechanisms controlling soil organic carbon composition pertaining to microbial decomposition of biochemically contrasting organic residues: Evidence from midDRIFTS peak area analysis, Soil Biol. Biochem., 76, 100–108, doi:10.1016/j.soilbio.2014.05.006, 2014.

Lal, R.: Soil carbon sequestration to mitigate climate change, Geoderma, 123(1–2), 1–22, doi:10.1016/j.geoderma.2004.01.032, 2004.

Laub, M., Blagodatsky, S., Lang, R., Yang, X. and Cadisch, G.: A mixed model for landscape soil organic carbon prediction across continuous profile depth in the mountainous subtropics, Geoderma, 330(November 2018), 177–192, doi:10.1016/j.geoderma.2018.05.020, 2018.

Lu, D., Ye, M. and Hill, M. C.: Analysis of regression confidence intervals and Bayesian credible intervals for uncertainty quantification, Water Resour. Res., 48(9), 1–20, doi:10.1029/2011WR011289, 2012.

Lu, D., Ye, M., Hill, M. C., Poeter, E. P. and Curtis, G. P.: A computer program for uncertainty analysis integrating regression and Bayesian methods, Environ. Model. Softw., 60(October), 45–56, doi:10.1016/j.envsoft.2014.06.002, 2014.

Ma, F., Du, C. W., Zhou, J. M. and Shen, Y. Z.: Investigation of soil properties using different techniques of mid-infrared spectroscopy, Eur. J. Soil Sci., 70(1), 96–106, doi:10.1111/ejss.12741, 2019.

Marcel van Oijen: Bayesian Calibration (BC) and Bayesian Model Comparison (BMC) of process-based models: Theory, implementation and guidelines, Edinburgh, United Kingdom. [online] Available from: http://nora.nerc.ac.uk/id/eprint/6087/1/BC&BMC_Guidance_2008-12-18_Final.pdf (Accessed 8 May 2020), 2008.

Menichetti, L., Kätterer, T. and Leifeld, J.: Parametrization consequences of constraining soil organic matter models by total carbon and radiocarbon using long-term field data, Biogeosciences, 13(10), 3003–3019, doi:10.5194/bg-13-3003-2016, 2016.

Metropolis, N., Rosenbluth, A. W., Rosenbluth, M. N., Teller, A. H. and Teller, E.: Equation of State Calculations by Fast Computing Machines, J. Chem. Phys., 21(6), 1087–1092, doi:10.1063/1.1699114, 1953.

Metzler, H., Zhu, Q., Riley, W., Hoyt, A., Müller, M. and Sierra, C. A.: Mathematical Reconstruction of Land Carbon Models From Their Numerical Output: Computing Soil Radiocarbon From C Dynamics, J. Adv. Model. Earth Syst., 12(1), doi:10.1029/2019MS001776, 2020.

Michel, K. and Ludwig, B.: Prediction of model pools for a long-term experiment using near-infrared spectroscopy, J. Plant Nutr. Soil Sci., 173(1), 55–60, doi:10.1002/jpln.200800181, 2010.

Minasny, B., Malone, B. P., McBratney, A. B., Angers, D. A., Arrouays, D., Chambers, A., Chaplot, V., Chen, Z.-S., Cheng, K., Das, B. S., Field, D. J., Gimona, A., Hedley, C. B., Hong, S. Y., Mandal, B., Marchant,

B. P., Martin, M., McConkey, B. G., Mulder, V. L., O'Rourke, S., Richer-de-Forges, A. C., Odeh, I., Padarian, J., Paustian, K., Pan, G., Poggio, L., Savin, I., Stolbovoy, V., Stockmann, U., Sulaeman, Y., Tsui, C.-C., Vågen, T.-G., van Wesemael, B. and Winowiecki, L.: Soil carbon 4 per mille, Geoderma, 292, 59–86, doi:10.1016/j.geoderma.2017.01.002, 2017.

Morrill, L. G., Mahilum, B. C., Mohiuddin, S. H. and others: Organic compounds in soils: sorption, degradation and persistence., Ann Arbor Science Publishers, Inc., Michigan, USA., 1982.

Nelson, D. W. and Sommers, L. E.: Total carbon, organic carbon, and organic matter, Soil Science Society of America, American Society of Agronomy., 1996.

Nendel, C., Berg, M., Kersebaum, K. C., Mirschel, W., Specka, X., Wegehenkel, M., Wenkel, K. O. and Wieland, R.: The MONICA model: Testing predictability for crop growth, soil moisture and nitrogen dynamics, Ecol. Modell., 222(9), 1614–1625, doi:10.1016/j.ecolmodel.2011.02.018, 2011.

Nendel, C., Kersebaum, K. C., Mirschel, W. and Wenkel, K. O.: Testing farm management options as climate change adaptation strategies using the MONICA model, Eur. J. Agron., 52, 47–56, doi:10.1016/j.eja.2012.09.005, 2014.

Nendel, C., Melzer, D. and Thorburn, P. J.: The nitrogen nutrition potential of arable soils, Sci. Rep., 9(1), 5851, doi:10.1038/s41598-019-42274-y, 2019.

Nguyen, T., Janik, L. and Raupach, M.: Diffuse reflectance infrared fourier transform (DRIFT) spectroscopy in soil studies, Soil Res., 29(1), 49–67, doi:10.1071/SR9910049, 1991.

Nottingham, A. T., Turner, B. L., Whitaker, J., Ostle, N., Bardgett, R. D., McNamara, N. P., Salinas, N. and Meir, P.: Temperature sensitivity of soil enzymes along an elevation gradient in the Peruvian Andes, Biogeochemistry, 127(2–3), 217–230, doi:10.1007/s10533-015-0176-2, 2016.

van Oijen, M., Cameron, D. R., Butterbach-Bahl, K., Farahbakhshazad, N., Jansson, P.-E., Kiese, R., Rahn, K.-H., Werner, C. and Yeluripati, J. B.: A Bayesian framework for model calibration, comparison and analysis: Application to four models for the biogeochemistry of a Norway spruce forest, Agric. For. Meteorol., 151(12), 1609–1621, doi:10.1016/j.agrformet.2011.06.017, 2011.

Van Oijen, M., Rougier, J. and Smith, R.: Bayesian calibration of process-based forest models: bridging the gap between models and data, Tree Physiol., 25(7), 915–927, doi:10.1093/treephys/25.7.915, 2005.

Parton, W. J., Schimel, D. S., Cole, C. V. and Ojima, D. S.: Analysis of Factors Controlling Soil Organic Matter Levels in Great Plains Grasslands1, Soil Sci. Soc. Am. J., 51(5), 1173, doi:10.2136/sssaj1987.03615995005100050015x, 1987.

Poeplau, C., Don, A., Dondini, M., Leifeld, J., Nemo, R., Schumacher, J., Senapati, N. and Wiesmeier, M.: Reproducibility of a soil organic carbon fractionation method to derive RothC carbon pools, Eur. J. Soil Sci., 64(6), 735–746, doi:10.1111/ejss.12088, 2013.

Pullen, N. and Morris, R. J.: Bayesian Model Comparison and Parameter Inference in Systems Biology Using Nested Sampling, edited by S. Rogers, PLoS One, 9(2), e88419, doi:10.1371/journal.pone.0088419, 2014.

Puttaso, A., Vityakon, P., Rasche, F., Saenjan, P., Treloges, V. and Cadisch, G.: Does Organic Residue Quality Influence Carbon Retention in a Tropical Sandy Soil?, Soil Sci. Soc. Am. J., 77(3), 1001, doi:10.2136/sssaj2012.0209, 2013.

Schmidt, M. W. I., Torn, M. S., Abiven, S., Dittmar, T., Guggenberger, G., Janssens, I. A., Kleber, M., Kögel-Knabner, I., Lehmann, J., Manning, D. A. C., Nannipieri, P., Rasse, D. P., Weiner, S. and Trumbore, S. E.: Persistence of soil organic matter as an ecosystem property, Nature, 478(7367), 49–56, doi:10.1038/nature10386, 2011.

Schweizer, S. A., Bucka, F. B., Graf-Rosenfellner, M. and Kögel-Knabner, I.: Soil microaggregate size composition and organic matter distribution as affected by clay content, Geoderma, 355(March), 113901, doi:10.1016/j.geoderma.2019.113901, 2019.

Segoli, M., De Gryze, S., Dou, F., Lee, J., Post, W. M., Denef, K. and Six, J.: AggModel: A soil organic matter model with measurable pools for use in incubation studies, Ecol. Modell., 263, 1–9, doi:10.1016/j.ecolmodel.2013.04.010, 2013.

Sierra, C. A.: Temperature sensitivity of organic matter decomposition in the Arrhenius equation: some theoretical considerations, Biogeochemistry, 108(1–3), 1–15, doi:10.1007/s10533-011-9596-9, 2012.

Sierra, C. A., Malghani, S. and Müller, M.: Model structure and parameter identification of soil organic matter models, Soil Biol. Biochem., 90, 197–203, doi:10.1016/j.soilbio.2015.08.012, 2015a.

Sierra, C. A., Trumbore, S. E., Davidson, E. A., Vicca, S. and Janssens, I.: Sensitivity of decomposition rates of soil organic matter with respect to simultaneous changes in temperature and moisture, J. Adv. Model. Earth Syst., 7(1), 335–356, doi:10.1002/2014MS000358, 2015b.

Sinsabaugh, R. L.: Phenol oxidase, peroxidase and organic matter dynamics of soil, Soil Biol. Biochem., 42(3), 391–404, doi:10.1016/j.soilbio.2009.10.014, 2010.

Sinsabaugh, R. L. and Follstad Shah, J. J.: Ecoenzymatic Stoichiometry and Ecological Theory, Annu. Rev. Ecol. Evol. Syst., 43(1), 313–343, doi:10.1146/annurev-ecolsys-071112-124414, 2012.

Sinsabaugh, R. L., Lauber, C. L., Weintraub, M. N., Ahmed, B., Allison, S. D., Crenshaw, C., Contosta, A. R., Cusack, D., Frey, S., Gallo, M. E., Gartner, T. B., Hobbie, S. E., Holland, K., Keeler, B. L., Powers, J. S., Stursova, M., Takacs-Vesbach, C., Waldrop, M. P., Wallenstein, M. D., Zak, D. R. and Zeglin, L. H.: Stoichiometry of soil enzyme activity at global scale, Ecol. Lett., 11(11), 1252–1264, doi:10.1111/j.1461-0248.2008.01245.x, 2008.

Six, J. and Paustian, K.: Aggregate-associated soil organic matter as an ecosystem property and a measurement tool, Soil Biol. Biochem., 68, A4–A9, doi:10.1016/j.soilbio.2013.06.014, 2014.

Smith, P., Smith, J. U., Powlson, D. S., McGill, W. B., Arah, J. R. M., Chertov, O. G., Coleman, K., Franko, U., Frolking, S., Jenkinson, D. S., Jensen, L. S., Kelly, R. H., Klein-Gunnewiek, H., Komarov, A. S., Li, C., Molina, J. A. E., Mueller, T., Parton, W. J., Thornley, J. H. M. and Whitmore, A. P.: A comparison of the performance of nine soil organic matter models using datasets from seven long-term experiments, Geoderma, 81(1–2), 153–225, doi:10.1016/S0016-7061(97)00087-6, 1997.

Sohi, S. P., Mahieu, N., Arah, J. R. M., Powlson, D. S., Madari, B. and Gaunt, J. L.: A Procedure for Isolating Soil Organic Matter Fractions Suitable for Modeling, Soil Sci. Soc. Am. J., 65(4), 1121, doi:10.2136/sssaj2001.6541121x, 2001.

Sokol, N. W., Sanderman, J. and Bradford, M. A.: Pathways of mineral-associated soil organic matter formation: Integrating the role of plant carbon source, chemistry, and point of entry, Glob. Chang. Biol., 25(1), 12–24, doi:10.1111/gcb.14482, 2019.

Spaccini, R., Piccolo, A., Haberhauer, G., Stemmer, M. and Gerzabek, M. .: Decomposition of maize straw in three European soils as revealed by DRIFT spectra of soil particle fractions, Geoderma, 99(3–4), 245–260, doi:10.1016/S0016-7061(00)00073-2, 2001.

Specka, X., Nendel, C., Hagemann, U., Pohl, M., Hoffmann, M., Barkusky, D., Augustin, J., Sommer, M. and van Oost, K.: Reproducing CO2 exchange rates of a crop rotation at contrasting terrain positions using two different modelling approaches, Soil Tillage Res., 156, 219–229, doi:10.1016/j.still.2015.05.007, 2016.

Stella, T., Mouratiadou, I., Gaiser, T., Berg-Mohnicke, M., Wallor, E., Ewert, F. and Nendel, C.: Estimating the contribution of crop residues to soil organic carbon conservation, Environ. Res. Lett., 14(9), 094008, doi:10.1088/1748-9326/ab395c, 2019.

Stevenson, F. J.: Humus chemistry: genesis, composition, reactions, John Wiley & Sons, New York., 1994.

Tang, J. and Riley, W. J.: Weaker soil carbon–climate feedbacks resulting from microbial and abiotic interactions, Nat. Clim. Chang., 5(1), 56–60, doi:10.1038/nclimate2438, 2015.

Tang, J., Bradford, M. A., Carey, J., Crowther, T. W., Machmuller, M. B., Mohan, J. E. and Todd-Brown, K.: Temperature sensitivity of soil carbon, in Ecosystem Consequences of Soil Warming, pp. 175–208, Elsevier., 2019.

Todd-Brown, K., Zheng, B. and Crowther, T. W.: Field-warmed soil carbon changes imply high 21st-century modeling uncertainty, Biogeosciences, 15(12), 3659–3671, doi:10.5194/bg-15-3659-2018, 2018.

Totsche, K. U., Amelung, W., Gerzabek, M. H., Guggenberger, G., Klumpp, E., Knief, C., Lehndorff, E., Mikutta, R., Peth, S., Prechtel, A., Ray, N. and Kögel-Knabner, I.: Microaggregates in soils, J. Plant Nutr. Soil Sci., 1–33, doi:10.1002/jpln.201600451, 2017.

Tuomi, M., Vanhala, P., Karhu, K., Fritze, H. and Liski, J.: Heterotrophic soil respiration—Comparison of different models describing its temperature dependence, Ecol. Modell., 211, 182–190, doi:10.1016/j.ecolmodel.2007.09.003, 2008.

Van Veen, J. A., Ladd, J. N. and Frissel, M. J.: Modelling C and N turnover through the microbial biomass in soil, Plant Soil, 76(1–3), 257–274, doi:10.1007/BF02205585, 1984.

Vrugt, J. A.: Markov chain Monte Carlo simulation using the DREAM software package: Theory, concepts, and MATLAB implementation, Environ. Model. Softw., 75, 273–316, doi:10.1016/j.envsoft.2015.08.013, 2016.

Wiesmeier, M., Urbanski, L., Hobley, E., Lang, B., von Lützow, M., Marin-Spiotta, E., van Wesemael, B., Rabot, E., Ließ, M., Garcia-Franco, N., Wollschläger, U., Vogel, H.-J. and Kögel-Knabner, I.: Soil organic carbon storage as a key function of soils - A review of drivers and indicators at various scales, Geoderma, 333(November 2017), 149–162, doi:10.1016/j.geoderma.2018.07.026, 2019.

Xu, H., Zhang, T., Luo, Y., Huang, X. and Xue, W.: Parameter calibration in global soil carbon models using surrogate-based optimization, Geosci. Model Dev., 11(7), 3027–3044, doi:10.5194/gmd-11-3027-2018, 2018.

Yeluripati, J. B., van Oijen, M., Wattenbach, M., Neftel, A., Ammann, A., Parton, W. J. and Smith, P.: Bayesian calibration as a tool for initialising the carbon pools of dynamic soil models, Soil Biol. Biochem., 41(12), 2579–2583, doi:10.1016/j.soilbio.2009.08.021, 2009.

Young, I. M.: Interactions and Self-Organization in the Soil-Microbe Complex, Science (80-.)., 304(5677), 1634–1637, doi:10.1126/science.1097394, 2004.

Zimmermann, M., Leifeld, J., Schmidt, M. W. I., Smith, P. and Fuhrer, J.: Measured soil organic matter fractions can be related to pools in the RothC model, Eur. J. Soil Sci., 58(3), 658–667, doi:10.1111/j.1365-2389.2006.00855.x, 2007.

2 Soil sample drying temperature affects specific organic mid-DRIFTS peaks and quality indices*

Moritz Laub[1], Sergey Blagodatsky[1], Yvonne Funkuin Nkwain[1], Georg Cadisch[1]

[1]Institute for Agronomy in the Tropics and Subtropics (Hans-Ruthenberg-Institute), University of Hohenheim, 70593 Stuttgart, Germany

*This chapter has been reprinted from Laub, M., Blagodatsky, S., Nkwain, Y. F. and Cadisch, G.: Soil sample drying temperature affects specific organic mid-DRIFTS peaks and quality indices, *Geoderma*, **355**, 113897, doi:10.1016/j.geoderma.2019.113897, 2019. The original short communication is available at: https://www.sciencedirect.com/science/article/abs/pii/S0016706119313874?via%3Dihub

2.1 Abstract

Peak area (PA) integration of diffuse reflectance mid infrared Fourier transform spectroscopy (DRIFTS) spectra is useful to study soil organic matter (SOM) quality and as a potential modelling proxy. Residual water of soil samples after drying affects DRIFTS spectra, mainly in the region > 2500 cm^{-1}. Therefore, SOM quality related PA at different wavenumbers should be influenced to varying degrees. We studied how absolute, normalized and relative PA related to SOM functional groups (at 2930, 1620, 1530 and 1159 cm^{-1}), as well as their ratios were influenced by oven drying of soil samples at increasing temperatures (from 32° C to 105° C). All organic and even mineral associated PA significantly increased with drying temperature. The PA of aliphatic C-H stretching (2930 cm^{-1}), located on the shoulder of the broad O-H stretching PA, was influenced most strongly. Our results indicate that using 105° C as drying temperature and storing samples in a desiccator is the best way to minimize water interference. These findings apply to relative PA and ratios of organic compounds, while no effect of drying temperatures on PA correlations to C or N were found.

2.2 Short communication article

Ratios of peak areas (PA) from diffuse reflectance mid infrared Fourier transform spectroscopy (DRIFTS), which is typically used for soil properties prediction like soil texture, C and N content, inform about soil organic matter (SOM) quality (Demyan et al., 2012). One example is the ratio of PA 2930 cm^{-1} (C-H stretching, hypothesized proxy for labile SOM) to 1620 cm^{-1} (aromatic C=C and/or COO^- stretching, hypothesized proxy of recalcitrant SOM), as measure of SOM hydrophobicity (Ellerbrock and Gerke, 2004) or SOM stability (Demyan et al., 2012; Margenot et al., 2015). The SOM related peaks of bulk soil DRIFTS spectra have interference by minerals and water, for example the 2930 cm^{-1} PA is superimposed on the broad O-H peak (Demyan et al., 2012). Since regions of DRIFTS spectra > 2500 cm^{-1} are most strongly influenced by O-H bonds, it is likely that residual water and hence drying temperature has an unwanted impact. Nevertheless, no consensus on optimal drying temperature exists: different authors applied a wide range of drying temperatures from 32°C (Demyan et al., 2012), 65°C (Matamala et al., 2017), up to 105°C (Parolo et al., 2017). To our knowledge, the influence on PA has not been comprehensively studied, so this was our studies objective. We hypothesized, that intensities of organic matter functional peaks with O-H interference are more affected by drying temperatures than others, and that an optimal drying temperature exist where the effect of temperatures on PA and their ratios plateaus.

To test our hypothesis, we inspected four SOM quality related DRIFTS PA after increasing drying temperatures. We used 21 archive soil samples, representing a broad range of soil types, textures and SOM contents from topsoil and subsoil. They originated from long-term experiments in Bad Lauchstädt in Germany, the Frame Experiment at Ultuna, Sweden, field sites of University of Hohenheim and the

SURUMER project in subtropical China (Table S2 - 1). These ball-milled, air dried soil samples had been stored since collection. Prior DRIFTS measurements they were dried at increasing temperatures, i.e. 32°C, 55°C, 65°C, 75°C, 85°C, 95°C and 105°C for 24 h. After each 24 h drying, samples were cooled in a desiccator. Four sub-samples of each soil were then measured in an HTS-XT microplate extension, mounted to a Tensor-27 spectrometer (Bruker Optik GmbH, Ettlingen, Germany) with the settings proposed by Demyan (2012), but using gold instead of KBr as background. Due to limited amounts, the same samples were used for all temperatures (only with increasing temperature), as a previous test indicated no difference to using new sample material each time. After baseline correction and vector normalization of spectra, four PA of interest related to SOM functional groups at 2930 cm^{-1} (mainly C-H, limits 3010-2800 cm^{-1}), 1620 cm^{-1} (mainly aromatic C=C/COO^-, 1660-1580 cm^{-1}), 1530 cm^{-1} (mainly aromatic C=C, 1546-1520 cm^{-1}) and 1159 cm^{-1} (mainly C-O, 1170-1148 cm^{-1}) were extracted as the integral on top of a local baseline constructed between the intersect of the spectra and a vertical line at the integration limits (Demyan et al., 2012) as shown in Figure 2 - 1 b. Other potential assignments are in Table S2 -2. The average PA of four sub-samples were taken for further calculations. All PA, including inorganic peaks increased with drying temperatures. Therefore, PA of interest were normalized by dividing them by the 1880 cm^{-1} quartz/silicates PA (1925cm^{-1} - 1835 cm^{-1}) (Parolo et al., 2017), designated hereafter with subscript ($_n$). Finally, relative ($_r$) PA (each peak divided by the sum of all four PA (Demyan et al., 2012)) were computed. A mixed model (***lmer*** of ***lme4*** package in R Software 3.4.3) was used to test for significant drying temperature effects on PA, ratios of aliphatic to aromatic PA and the integrated full spectra (4000 – 400 cm^{-1}). A random slope and intercept of the "drying temperature" effect was allowed for each sample, to account for autocorrelation of data due to repeated measurements. Least square means of the temperature effect and PA were calculated with the ***emmeans*** R package. Additionally, Pearson's correlations of PA at different drying temperatures and organic C and N were computed.

The broad O-H peak centered at 3400 cm^{-1} significantly decreased with increasing drying temperature (~2% reduction from 32° C to 105° C, Figure S2 - 1), while the absorbance of the entire DRIFTS spectra increased (Figure 2 - 1 and S2 - 1). All PA (including inorganic vibrational peaks) increased significantly with increased drying temperatures. Samples with low organic C content (< 0.8%) with initially small to negative 2930 cm^{-1} PA at 32° C (Figure 2 - 1 a, c) were increasingly visible at higher drying temperatures. The normalized PA $_n$2930 cm^{-1} and $_n$1530 cm^{-1} increased significantly with drying temperature, while $_n$1159 cm^{-1} decreased (all $p < 0.0001$) but $_n$1620 cm^{-1} had no trend (Figure 2 - 2). Also relative PA were significantly affected by drying temperature with the $_r$2930 cm^{-1} increasing, while all others decreased. An effect also existed for both ratios of peaks (2930 cm^{-1}/1620 cm^{-1} and 2930 cm^{-1}/1530 cm^{-1}), all strongly and significantly increasing with higher temperatures (Figure 2 - 2).

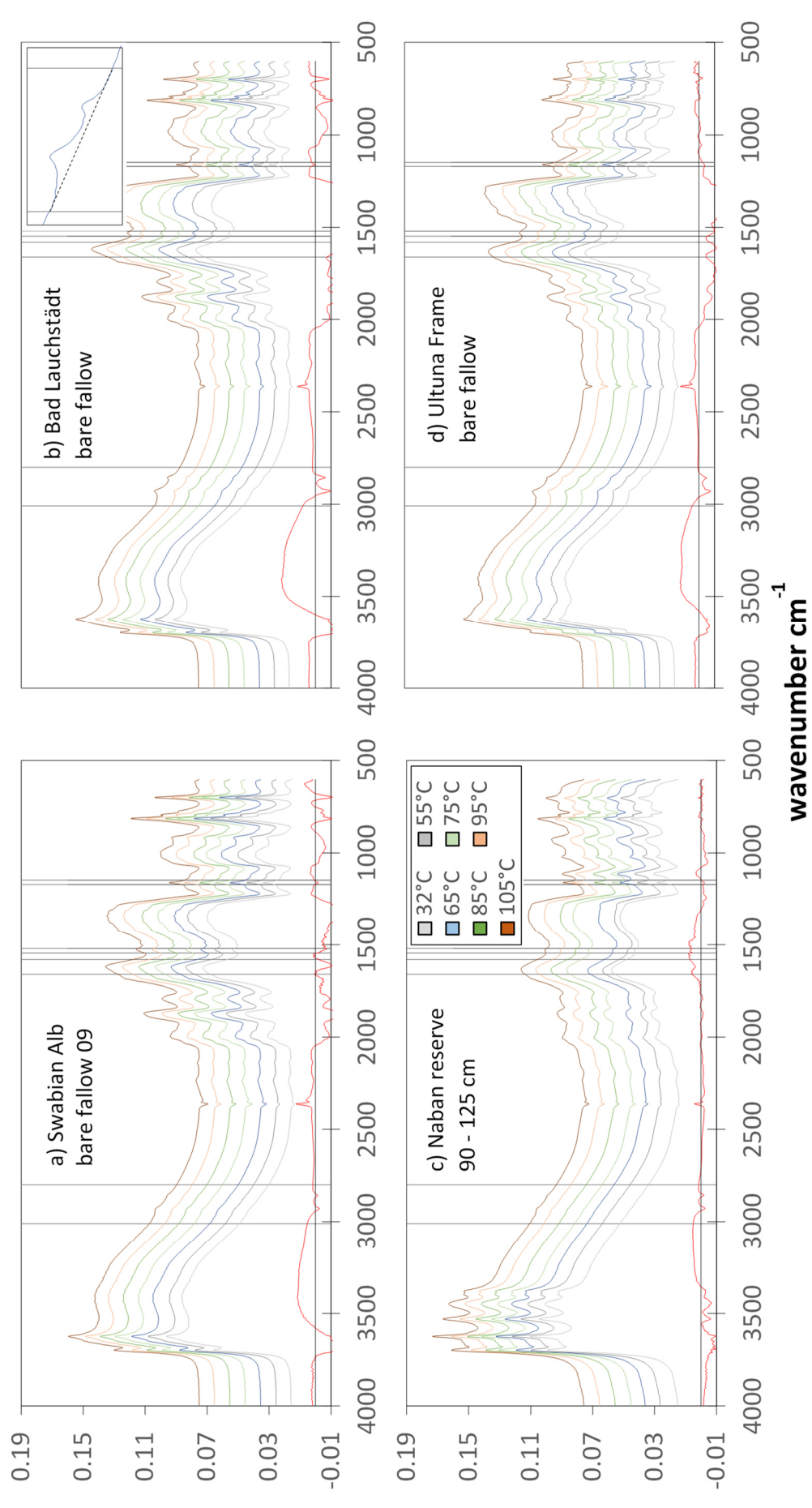

Figure 2 - 1 Baseline corrected example DRIFTS Spectra of four different bulk soils (**Table S2 - 1**) dried at different temperatures. The red line indicates the difference of the 32°C – 105°C absorbance (3X scaled for better illustration). The integration limits of the four peak areas of interest are shown by vertical lines. An example of an integrated 2930 cm^{-1} peak area is given in b) top right. For integration, a local baseline is drawn between the intersects of the vertical lines at the integration limits (3010 and 2800 cm^{-1}) with the spectra, which is the lower boundary of the integral. More details on the integration can be found in (Demyan et al., 2012).

Strong correlations of all PA with C or N content existed, but were not influenced by drying temperatures (Table S2 - 3). The correlations of $_n$2930 cm^{-1} and $_n$1530 cm^{-1} with C and N were stronger than for the original PA at 2930 cm^{-1} and 1530 cm^{-1}, while normalizing changed correlations of $_n$1620 cm^{-1} and $_n$1159 cm^{-1} from significant and negative to nonsignificant and positive.

While all peak areas and the absorbance of the total spectra increased with drying temperature, the visibility of the 2930 cm^{-1} PA increased the most. This phenomenon lead to a strong positive effect of drying temperature on the PA ratios of aliphatic to aromatic SOM functional groups. For example, the means of the 2930 cm^{-1}/1620 cm^{-1} ratio between 32°C and 105°C changed from 0.2 to 0.6 and the 2930 cm^{-1}/1530 cm^{-1} ratio means from 2 to 4. In fact, it seems as if the broad O-H can strongly over shade the 2930 cm^{-1} PA at low drying temperatures (Figure 2 - 1), which is reduced with drying. This challenge with a small 2930 cm^{-1} PA might also be the reason why several authors (Demyan et al., 2012; Margenot and Hodson, 2016) used rank correlations instead of Pearson correlations to relate relative PA/ratios to SOM fractions.

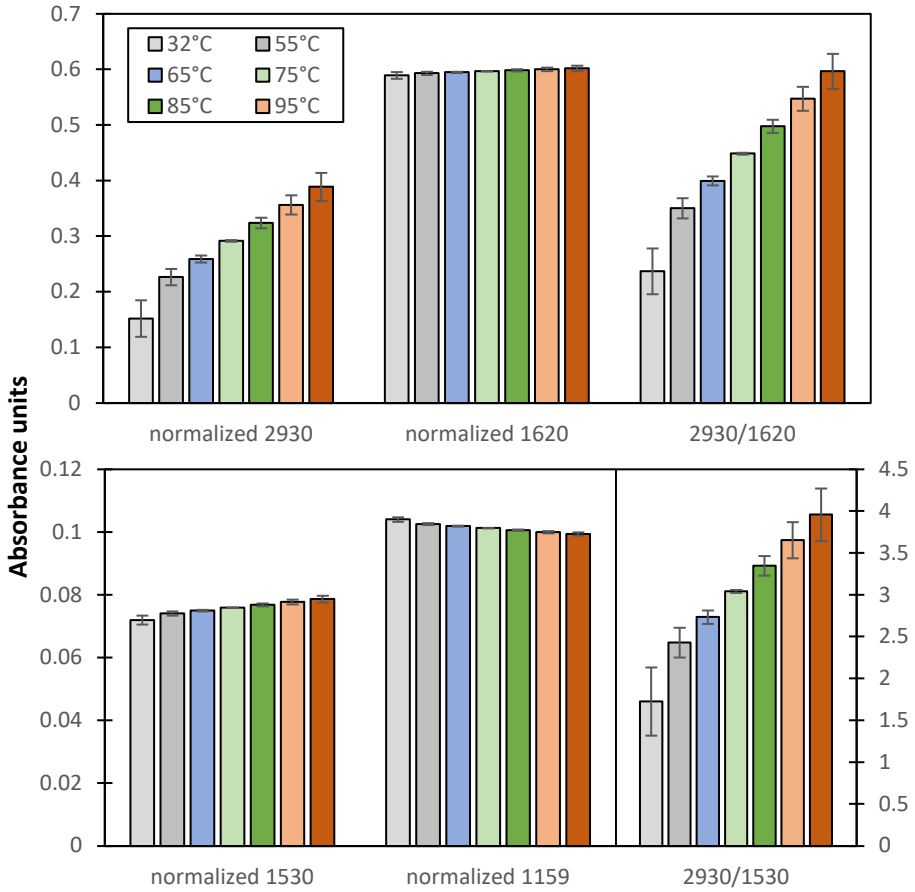

Figure 2 - 2 Least square means estimations for quartz/silicates normalized peak areas of interest and two stability indices ratios across all samples. Significant differences between all temperatures existed for all peaks and ratios (excluding the 1620 cm^{-1} peak). Error bars indicate 95% confidence intervals of the drying temperature effect.

Several research groups have directly interpreted 2930 cm^{-1}/1620 cm^{-1} ratios as a measure of hydrophobicity, applying different drying temperatures (Bernier et al., 2013 at 105°C ; Nadav et al.,

2013 at 65° C; Parolo et al., 2017 at 105°C) but the results of this study suggest, that temperature should be standardized. At first, it looks like our results for DRIFTS spectroscopy contradict the results of Duboc et al., (2016), who found no significant effect of drying temperature for ATR spectroscopy. However, they assumed that samples equilibrated moisture with ambient air as they did not store samples in a desiccator. In fact, our samples also regained ambient air water outside the desiccator, which also spectra showed within just a few hours. Combining the two studies results suggest that 1) organic matter functional groups are not changed by temperatures up to 105° C, so 2) the change in DRIFTS spectra relates to loss of the residual water, which over shaded peaks in the broad O-H region, and which the soil can regain from ambient air.

Contrary to the initial hypothesis, no plateau of PA was detected in this study. As temperatures above 105° C might start altering SOM, and it is standard for measuring water content, higher temperatures likely have a negligible effect on water evaporation compared to possible SOM alterations. To make future studies comparable, we therefore suggest using 105° C as standard drying temperature for DRIFTS ratios or relative PA and to keep samples in desiccators.

As correlations were not affected by drying temperatures, the water was mainly interfering with relative PA and ratios, especially for samples with small SOM contents (very small or negative 2930 cm^{-1} peaks compared to baseline). Comparison across different temperatures might still be possible, using the regression slopes between temperature and PA (Table S2 - 4) gained from the mixed model, for example:

$$2930\ cm^{-1}/1620\ cm^{-1} = 0.07888 + 0.00492\ T\ (\text{in}\ ^\circ C) \qquad (2\text{-}1)$$

It would be interesting to see, whether the regressions are universally applicable, as we used a range of soil samples from around the world. We would advise further test for different soils (e.g. with high sand contents) and different DRIFTS equipment. We invite others to share their datasets, if they measured the same samples at different drying temperatures.

While the PA approach is promising to study SOM quality, this study showed that the drying temperature considerably affects relative PA and ratios, but not correlations. The ratios could then give valuable information on SOM quality for large scale datasets or for SOM modelling.

2.3 Acknowledgement

We thank Thomas Kätterer, Swedish University of Agricultural Sciences and Elke Schulz, Helmholtz Centre for Environmental Research, for the samples from Ultuna and Bad Lauchstädt. The first author was funded by the German Research Foundation (DFG) project FOR1695 “Agricultural Landscapes under Global Climate Change – Processes and Feedbacks on a Regional Scale” within subproject P3 (CA 598/6-1).

2.4 References

Bernier, M.-H., Levy, G. J., Fine, P. and Borisover, M.: Organic matter composition in soils irrigated with treated wastewater: FT-IR spectroscopic analysis of bulk soil samples, Geoderma, 209–210, 233–240, doi:10.1016/j.geoderma.2013.06.017, 2013.

Coates, J.: Interpretation of Infrared Spectra, A Practical Approach, in Encyclopedia of Analytical Chemistry, pp. 10815–10837, John Wiley & Sons, Ltd, Chichester, UK., 2006.

Demyan, M. S., Rasche, F., Schulz, E., Breulmann, M., Müller, T. and Cadisch, G.: Use of specific peaks obtained by diffuse reflectance Fourier transform mid-infrared spectroscopy to study the composition of organic matter in a Haplic Chernozem, Eur. J. Soil Sci., 63(2), 189–199, doi:10.1111/j.1365-2389.2011.01420.x, 2012.

Duboc, O., Tintner, J., Zehetner, F. and Smidt, E.: Does sample drying temperature affect the molecular characteristics of organic matter in soil and litter? A statistical proof using ATR infrared spectra, Vib. Spectrosc., 85, 215–221, doi:10.1016/j.vibspec.2016.05.002, 2016.

Ellerbrock, R. H. and Gerke, H. H.: Characterizing organic matter of soil aggregate coatings and biopores by Fourier transform infrared spectroscopy, Eur. J. Soil Sci., 55(2), 219–228, doi:10.1046/j.1365-2389.2004.00593.x, 2004.

Margenot, A. J. and Hodson, A. K.: Relationships between labile soil organic matter and nematode communities in a California oak woodland, Nematology, 18(10), 1231–1245, doi:10.1163/15685411-00003027, 2016.

Margenot, A. J., Calderón, F. J., Bowles, T. M., Parikh, S. J. and Jackson, L. E.: Soil Organic Matter Functional Group Composition in Relation to Organic Carbon, Nitrogen, and Phosphorus Fractions in Organically Managed Tomato Fields, Soil Sci. Soc. Am. J., 79(3), 772–782, doi:10.2136/sssaj2015.02.0070, 2015.

Matamala, R., Calderón, F. J., Jastrow, J. D., Fan, Z., Hofmann, S. M., Michaelson, G. J., Mishra, U. and Ping, C.-L.: Influence of site and soil properties on the DRIFT spectra of northern cold-region soils, Geoderma, 305(December 2016), 80–91, doi:10.1016/j.geoderma.2017.05.014, 2017.

Nadav, I., Tarchitzky, J. and Chen, Y.: Induction of soil water repellency following irrigation with treated wastewater: Effects of irrigation water quality and soil texture, Irrig. Sci., 31(3), 385–394, doi:10.1007/s00271-011-0316-y, 2013.

Parolo, M. E., Savini, M. C. and Loewy, R. M.: Characterization of soil organic matter by FT-IR spectroscopy and its relationship with chlorpyrifos sorption, J. Environ. Manage., 196, 316–322, doi:10.1016/j.jenvman.2017.03.018, 2017.

Socrates, G.: Infrared and Raman characteristic group frequencies: tables and charts, John Wiley & Sons., 2004.

Stevenson, F. J.: Humus chemistry: genesis, composition, reactions, John Wiley & Sons, New York., 1994.

3 DRIFTS band areas as measured pool size proxy to reduce parameter uncertainty in soil organic matter models*

Moritz Laub[1], Michael Scott Demyan[2], Yvonne Funkuin Nkwain[1], Sergey Blagodatsky[1,3], Thomas Kätterer[4], Hans-Peter Piepho[5], Georg Cadisch [1]

[1] Institute of Agricultural Sciences in the Tropics (Hans-Ruthenberg-Institute), University of Hohenheim, Garbenstrasse 13, 70599 Stuttgart, Germany

[2] School of Environment and Natural Resources, The Ohio State University, Columbus, 2021 Coffey Rd., OH, USA, 43210

[3] Institute of Physicochemical and Biological Problems in Soil Science, Russian Academy of Sciences, 142290 Pushchino, Russia

[4] Department of Ecology, Swedish University of Agricultural Sciences, Ulls Väg 16, Uppsala, Sweden

[5] Biostatistics Unit, Institute of Crop Science, University of Hohenheim, Fruwirthstr. 23, 70599 Stuttgart, Germany

*This chapter has been reprinted from Laub, M., Demyan, M. S., Nkwain, Y. F., Blagodatsky, S., Kätterer, T., Piepho, H. and Cadisch, G.: DRIFTS band areas as measured pool size proxy to reduce parameter uncertainty in soil organic matter models, *Biogeosciences*, **17(6)**, 1393–1413, doi:10.5194/bg-17-1393-2020, 2020, under the Creative Commons Attribution 4.0 License. The original article is available at: https://www.biogeosciences.net/17/1393/2020/

3.1 Abstract

Soil organic matter (SOM) turnover models predict changes in SOM due to management and environmental factors. Their initialization remains challenging as partitioning of SOM into different hypothetical pools is intrinsically linked to model assumptions. Diffuse reflectance mid-infrared Fourier transform spectroscopy (DRIFTS) provides information on SOM quality and could yield a measurable pool-partitioning proxy for SOM. This study tested DRIFTS-derived SOM pool partitioning using the Daisy model. The DRIFTS stability index (DSI) of bulk soil samples was defined as the ratio of the area below the aliphatic absorption band (2930 cm^{-1}) to the area below the aromatic-carboxylate absorption band (1620 cm^{-1}). For pool partitioning, the DSI (2930 cm^{-1} / 1620 cm^{-1}) was set equal to the ratio of fast-cycling / slow-cycling SOM. Performance was tested by simulating long-term bare fallow plots from the Bad Lauchstädt extreme farmyard manure experiment in Germany (Chernozem, 25 years), the Ultuna continuous soil organic matter field experiment in Sweden (Cambisol, 50 years) and 7 year duration bare fallow plots from the Kraichgau and Swabian Jura regions in Southwest Germany (Luvisols). All experiments were at sites that were agricultural fields for centuries before fallow establishment, so classical theory would suggest that a steady-state can be assumed for initializing SOM pools. Hence, steady state and DSI initializations were compared, using two published parameter sets, that differed in turnover rates and humification efficiency. Initialization using the DSI significantly reduced Daisy model error for total soil organic carbon and microbial carbon in cases where assuming a steady state had poor model performance. This was irrespective of the parameter set, but faster turnover performed better for all sites except for Bad Lauchstädt. These results suggest that soils, although under long-term agricultural use, were not necessarily at a steady state. In a next step, Bayesian-calibration-inferred best-fitting turnover rates for Daisy using the DSI were evaluated for each individual site or for all sites combined. Two approaches significantly reduced parameter uncertainty and equifinality in Bayesian calibrations: (1) adding physicochemical meaning with the DSI (for humification efficiency and slow SOM turnover) and (2) combining all sites (for all parameters). Individual-site-derived turnover rates were strongly site specific. The Bayesian calibration combining all sites suggested a potential for rapid SOM loss with 95% credibility intervals for the slow SOM pools' half-life being 278 to 1095 years (highest probability density at 426 years). The credibility intervals of this study were consistent with several recently published Bayesian calibrations of similar two-pool SOM models, i.e., with turnover rates being faster than earlier model calibrations suggested: hence they likely underestimated potential SOM losses.

3.2 Introduction

Process-based models of plant-soil ecosystems are used from plot to global scales as tools of research and to support policy decisions (Campbell and Paustian, 2015). In soil organic matter (SOM) models,

SOM is traditionally divided into several pools, representing fast- and slow-cycling or even inert SOM (Hansen et al., 1993; Parton et al., 1993). However, these theoretical SOM pools cannot easily be linked to measurable fractions. As a workaround, common methods of SOM pool initialization require that one assumes SOM at a steady state or includes a model spin-up run, attempting to simulate SOM dynamics according to history and carbon inputs for the decades to several millennia prior to the period of actual interest (e.g., O'Leary et al., 2016). Theoretically if SOM pools are at a steady state and turnover times of SOM pools are known, models could be initialized, i.e., pool sizes calculated, either by simple equations (e.g., for Daisy, Bruun and Jensen, 2002) or by inverse modeling (for RothC, Coleman and Jenkinson, 1996). In most cases, data are insufficient to guarantee that the assumptions of a SOM steady state or long-term land use history and inputs are correct, given the lack of data on residue and manure input and weather variability on the required long-term timescales (> 200 years to millennia). Furthermore, exact turnover times of different SOM pools are unknown, which makes the results of inverse modeling and steady-state initializations a direct result of model assumptions (Bruun and Jensen, 2002). Hence, it is critical to find measurable proxies, such as soil size density fractionation or infrared spectra (Sohi et al., 2001), that can provide information on the quality of SOM and help to disconnect the intrinsic link between turnover times and SOM pool division for SOM pool initialization.

As was shown by Zimmermann et al. (2007), and recently confirmed by Herbst et al. (2018), a link exists between soil fractions obtained by size and density fractionation and fast- and slow-cycling SOM pools. However, Poeplau et al. (2013) showed that the same fractionation protocol led to considerably different results in six different laboratories which regularly applied the technique (coefficient of variation from 14 to 138%). The resulting differences in the model initializations for simulated SOM loss after 40 years of fallow, led to differences in SOM losses that were to up to 30% of initial SOM. Hence there is a need for a reproducible proxy for SOM pool initialization to reduce the high uncertainty in SOM models. We hypothesized that such a proxy could be obtained from inexpensive, high-throughput diffuse reflectance mid-infrared Fourier transform spectroscopy (DRIFTS).

As a novel approach, this study uses information gained from DRIFTS spectra to partition measured SOM into pools of different complexity. DRIFTS can provide information on SOM quality but also on texture and even mineralogy (Nocita et al., 2015; Tinti et al., 2015). The absorbance of mid-infrared light by molecular bonds in the soil sample vibrating at the same frequency produces typical absorption bands at distinct wavelengths (Stevenson, 1994). The area below absorption bands (in short, band area), can be linked to different molecular bonds of carbohydrates, amides, silicates and others. Two important absorption bands that provide information on SOM quality are the aliphatic carbon band (2930 cm^{-1}; limits, 3010-2800 cm^{-1}) and the aromatic-carboxylate band (1620 cm^{-1}; limits, 1660-1580 cm^{-1}; Giacometti et al., 2013; Margenot et al., 2015; Pengerud et al., 2013). While both

bands are subject to interference (2930 cm^{-1} mainly from water and 1620 cm^{-1} mainly from minerals; Nguyen et al., 1991), it should be possible to limit the interference using subregions of the absorption bands with carefully selected integration limits. Indeed, Demyan et al. (2012) found aliphatic carbon to be enriched under long-term farmyard manure application and depleted in mineral fertilizer or control treatments and showed that the ratio of the 1620 cm^{-1} to 2930 cm^{-1} band area had a significant positive correlation with the ratio of stable to labile SOM obtained by size and density fractionation. It was further corroborated that the band areas they used, which mainly selected the top subregion of the absorption bands, are strongly reduced or lost during combustion (Demyan et al., 2013). Hence, we hypothesized that the ratio of areas below aliphatic to aromatic-carboxylate carbon absorption bands can be used as proxy for the ratio of fast- to slow-cycling SOM for pool initialization, thus providing a major improvement over assuming steady-state SOM. The ratio of areas below absorbance bands of aliphatic to aromatic-carboxylate carbon will be referred to as the DRIFTS stability index (DSI) hereafter. Testing, improvement and proper use of the DSI were the central topics of this study. Recent findings have highlighted that the residual water content in bulk soil samples after drying at different temperatures affects the DSI considerably. Water absorbance affects significant parts of the mid-infrared spectra and particularly influences the 2930 and 1620 cm^{-1} band areas (Laub et al., 2019). For this reason, we also tested how the drying temperature prior to DRIFTS measurements affects the use of the DSI proxy, using 32, 65 and 105°C as pretreatment temperatures.

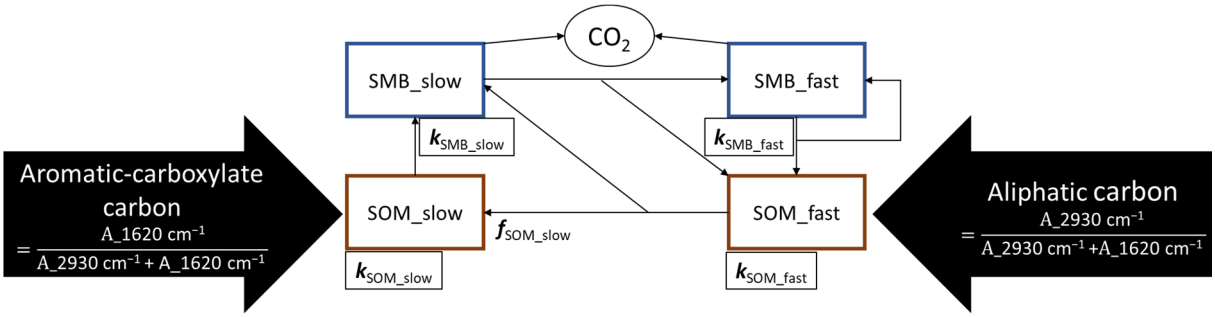

Figure 3 - 1 Original structure of the internal cycling of SOM in the Daisy model, as it was used in this study. A_2930 cm^{-1} and A_1620 cm^{-1} refer to the areas below the DRIFTS absorption bands at 2930 cm^{-1} and 1620 cm^{-1} (Equation 3-3), k_{SOM} and k_{SMB} (fast and slow) are turnover rates of the fast and slow SOM and SMB pools, respectively, and f_{SOM_slow} is the humification efficiency. All model parameters can be found in Table 3 - 2.

To test our hypotheses about DSI performance, we used the Daisy SOM model (Hansen et al., 2012). Daisy is a commonly used SOM model (Campbell and Paustian, 2015) with a typical multipool structure, which includes two soil microbial biomass (SMB) pools as well as two pools for stabilized SOM (fast and slow cycling). With first-order turnover kinetics and a humification efficiency parameter (Figure 3 - 1), the Daisy structure is similar to other widely used SOM models such as CENTURY (Parton et al., 1993) or ICBM (Andrén and Kätterer, 1997). Model SOM pool initialization using the DSI was compared to initialization via a steady-state assumption with different published turnover rates. For this comparison bare fallow experiments from a range of different sites and over timescales of 1 to 5

decades were included. Bare fallow experiments were used to avoid the added complexity caused by the conversion of different plant compounds into SOM of varying stabilities during decomposition.

As SOM pool sizes and turnover rates are closely linked, it could also be necessary to recalibrate Daisy parameters for the use of the DSI. Therefore, a Bayesian calibration of turnover rates was used to adjust Daisy turnover rates to the pool division and time dynamics of the measured DSI throughout the fallow period. Thus, the Daisy parameterization was evaluated with respect to equifinality and uncertainty as well as to dependence on model structure. The final hypothesis was that, through a Bayesian calibration using the DSI, Daisy pools will correspond to measured, i.e., physiochemically meaningful fractions, thus reducing uncertainty. The posterior credibility intervals and optima of turnover rates should correspond to the results of other Bayesian calibrations carried out for similarly structured two-pool models. If such relations could be confirmed, this would point towards fundamental insights about the intrinsic SOM turnover in temperate agroecosystems.

3.3 Material and methods

3.3.1 Study sites and data used for modeling

Datasets originating from bare fallow treatments of four different sites with different experimental durations and measurement frequencies were used in this study. Topsoil (0-20 cm) samples were received from the long-term experiments of (a) the Ultuna continuous soil organic matter field experiment (established in 1956, with additional samples from 1979, 1995 and 2005 taken in autumn (Kätterer et al., 2011), four replicates) and (b) the Bad Lauchstädt extreme farmyard manure experiment (established in 1983, with additional samples from 2001, 2004 and 2008 taken in autumn (Blair et al., 2006), two replicates; https://www.ufz.de/index.php?de=37008, date accessed 10.01.2019). Additional data from two medium-term bare fallow experiments (established in autumn 2009 with data until 2016) from Southwest German regions were included. In these experiments three fields in the region of (c) the Kraichgau and three fields in the region of (d) the Swabian Jura, representing different climatic and geological conditions, were intensely monitored. The bare fallow plots (5 m × 5 m size) in these experiments were established within agricultural fields with three replicates per field (Ali et al., 2015). Up to four topsoil samples (0-30 cm) were taken throughout the year. Further details on all the sites can be found in Table 3 - 1. All sites had been under cultivation for at least several hundred years prior to establishing the bare fallow plots, which would suggest that a steady state could be assumed.

All available bulk soil samples of Ultuna and Bad Lauchstädt were analyzed for total organic carbon and DRIFTS spectra. For the Kraichgau and Swabian Jura sites, total organic carbon and DRIFTS spectra were measured about once every 2 years, while soil microbial biomass carbon (SMB-C) was measured

up to four times per year. All bulk soil samples (except for SMB-C) were passed through a 2 mm sieve, then air-dried, ball-milled (for 2 min) to powder and stored until further analysis was carried out. Soil organic carbon (SOC) content was analyzed with a vario MAX CNS (Elementar Analysensysteme GmbH, Hanau, Germany). Soil samples for DRIFTS analysis were obtained after 24 h of drying at 32, 65 and 105°C. The dried samples were kept in a desiccator until measurement. DRIFTS spectra of bulk soil samples (with four subsamples per sample) were obtained using an HTS-XT microplate extension, mounted to a TENSOR 27 spectrometer using the processing software OPUS 7.5 (Bruker Optik GmbH, Ettlingen, Germany). A potassium bromide (KBr) beam splitter with a nitrogen-cooled HTS-XT reflection detector was used to record spectra in the mid-infrared range (4000 – 400 cm^{-1}). Each spectrum was a combination of 16 coadded scans with a 4 cm^{-1} resolution. Spectra were recorded and then converted to absorbance units (AU); the acquisition mode *double-sided, forward-backward* and the apodization function Blackman-Harris 3 were used. After baseline correction and vector normalization of the spectra, areas below absorptions bands of interest were obtained by integration using a local baseline with the integration limits of Demyan et al. (2012). Integrated band areas of the four subsamples were then averaged. The local baselines were drawn between the intersection of the spectra and a vertical line at the integration limits (3010 – 2800 cm^{-1} for the aliphatic carbon band, 1660 – 1580 cm^{-1} for the aromatic-carboxylate carbon band). Example spectra and integrated band areas are displayed in Figure S 3 - 1. The integration limits were selected with the goal of reducing signal interference from water and minerals, using spectra of pure substances, clay minerals and DRIFTS spectra gained during heating samples up to 700°C (Demyan et al., 2013). Particularly, the mineral interference close to the 1620 cm^{-1} band makes accurate selection of integration limits necessary so that only its top part (assumed to consist mostly of aromatic-carboxylate carbon) is selected. In the case of our samples, the selected specific band area of the 1620 cm^{-1} band accounted for approximately 10 to 30% of the band area of the larger surrounding band (Figure S 3 - 1, ca. 1755-1555 cm^{-1}). Integration limits were chosen so that the band area best corresponds to the portion that is lost with combustion or chemical oxidation (Demyan et al., 2013; Yeasmin et al., 2017). A strong correlation between the DSI and the percentage of centennially persistent SOC ($r = 0.84$) from the combined long-term experiments used in this study (using values of centennially persistent SOC from Cécillon et al., 2018; and Franko and Merbach, 2017) showed that the DSI selected in this manner did in fact explain a large portion of the SOC quality change across sites (Figure S 3 - 2).

Table 3 - 1 Locations, soil type according to IUSS Working Group WRB - 2007, initial soil organic carbon (SOC) stocks and other properties of the simulated bare fallow study sites

Study Site	UTM Degrees Latitude	UTM Degrees Longitude	Soil type	Depth of sampling (cm)	Rep.	Clay (%)	Silt (%)	Initial SOC (%)	Bulk density (Mg m^{-3})	Initial SOC stocks in the sampled depth at fallow start (Mg ha^{-1})	Year of experiment and bare fallow establishment	Bulk soil samples available from years	Types of available measurements
Ultuna[a]	59.821879	17.656348	Eutric Cambisol	0 - 20	4	37	41	1.50	1.44	43.22	1956	1956, 79, 95, 2005	SOC, DRIFTS
Bad Lauchstädt[b]	51.391605	11.877028	Haplic Chernozem	0 - 20	2	21	68	1.82	1.24	45.08	1985	1985, 2001, 04, 08	SOC, DRIFTS
Kraichgau 1	48.928517	8.702794	Stagnic Luvisol	0 - 30	3	18	97	0.90	1.37	37.10	2009	2009 - 16	SOC, DRIFTS, SMB-C
Kraichgau 2	48.927748	8.708884	Stagnic Luvisol	0 - 30	3	18	80	1.04	1.33	41.61	2009	2009 - 16	SOC, DRIFTS, SMB-C
Kraichgau 3	48.927197	8.715891	Stagnic Luvisol	0 - 30	3	17	81	0.89	1.44	38.50	2009	2009 - 16	SOC, DRIFTS, SMB-C
Swabian Jura 1	48.527510	9.769429	Calcic Luvisol	0 - 30	3	38	56	1.78	1.32	70.33	2009	2009 - 16	SOC, DRIFTS, SMB-C
Swabian Jura 2	48.529857	9.773253	Anthrosol	0 - 30	3	29	68	1.95	1.38	80.85	2009	2009 - 13	SOC, DRIFTS, SMB-C
Swabian Jura 3	48.547035	9.773176	Rendzic Leptosol	0 - 30	3	45	51	1.91	1.07	61.27	2009	2009 - 13	SOC, DRIFTS, SMB-C

UTM, Universal Transverse Mercator reference system; SOC, soil organic carbon; Rep, replicates; SOC, soil organic carbon; DRIFTS, Diffuse reflectance mid-infrared Fourier transform spectroscopy; SMB-C, soil microbial biomass carbon; [a] Ultuna continuous soil organic matter field experiment (Kätterer et al., 2011), [b] Bad Lauchstädt extreme farmyard manure experiment (Blair et al., 2006).

Additionally, soils from the experiments in Kraichgau and Swabian Jura were analyzed for SMB-C using the chloroform fumigation extraction method (Joergensen and Mueller, 1996). Briefly, field-moist samples were transported to the lab in a cooler, with extractions beginning within 24 h of field sampling and the final SMB-C values corrected to an oven-dried (105° C) basis. The SMB-C was measured two to four times throughout the whole year. Stocks of SOC and SMB-C for 0-30 cm were calculated by multiplying the percentage of SOC and SMB-C with the bulk density and sampled layer thickness (Table 3 - 1), respectively. Bulk density was assumed constant for Bad Lauchstädt, Kraichgau and Swabian Jura, while for Ultuna the initial 1.44 Mg m^{-3} (Kirchmann et al., 2004) in the beginning was used for all but the last measurement, where 1.43 Mg m^{-3} (Kätterer et al., 2011) was used. Due to low coarse-fragment contents (< 5% for Swabian Jura 3, < 2% for Swabian Jura 1 and < 1% for the other six sites), and because changes in stone content throughout the simulation periods are unlikely, no correction for coarse-fragment content was done.

3.3.2 Description of the simulation model: Daisy Expert-N 5.0

All simulations were conducted using the Daisy SOM model (Hansen et al., 2012) integrated into the Expert-N 5.0 modeling framework. Expert-N 5.0 allows for a wide range of soil, plant and water models to be combined and interchanged (Heinlein et al., 2017; Klein et al., 2017; Klein, 2018). Expert-N can be compiled for both Windows and Linux systems. The Daisy model consists of two pools (fast and slow cycling) for each of the measurable fractions of 1) litter, 2) SMB and 3) stabilized SOM (Figure 3 - 1). Due to bare fallow, litter pools were disregarded in this study, and the focus was on initializing the two SOM pools. A detailed description of the Daisy SOM submodule as it was implemented into the Expert-N 5.0 framework can be found in Mueller et al. (1997). The additional modules available for selection in the Expert-N 5.0 framework consist of a selection of established models for all simulated processes in the soil-plant continuum. The evaporation, ground heat, net radiation and emissivity were simulated according to the Penman-Monteith equation (Monteith, 1976). Water flow through the soil profile was simulated by the HYDRUS flow module (van Genuchten, 1982) with the hydraulic functions according to Mualem (1976). Heat transfer through the soil profile was simulated with the Daisy heat module (Hansen et al., 1993). In the first step of the DSI evaluation, simulations were conducted with two established parameter sets for Daisy SOM. The first set was from Mueller et al. (1997) and was a modification of the original parameter set of turnover rates reported by Jensen et al. (1997). The second set was established after calibrations made by Bruun et al. (2003) using the Askov long-term experiments, in which they introduced considerable changes to the turnover rates of the slow SOM pool and the humification efficiency. An equation developed by Bruun and Jensen (2002) was used to compute the proportions of the slow- and fast-cycling SOM pools for both parameter sets at a steady state (see next section). Parameters of both sets are given in Table 3 - 2.

Table 3 - 2 Values of the two Daisy parameter sets used in this study. The parameters consist of turnover rates (k), maintenance respiration (only for SMB, added to the turnover rate), carbon use efficiency (CUE -which divides between carbon assimilated by SMB and lost as CO_2), the humification efficiency (f_{SOM_slow}) and microbial recycling (part of SMB going directly back to SMB fast at turnover of either SMB pool). A graphical display of the model structure and pools considered within this study is found in Figure 3 - 1.

Parameter	Mueller et al. (1997)	Bruun et al. (2003)	Unit
k_{SOM_slow}	2.70×10^{-6} [a]	4.30×10^{-5} [c]	d^{-1}
k_{SOM_fast}	1.40×10^{-4} [a]	1.40×10^{-4} [a]	d^{-1}
k_{SMB_slow}	1.85×10^{-4} [b]	1.85×10^{-4} [b]	d^{-1}
k_{SMB_fast}	1.00×10^{-2} [b]	1.00×10^{-2} [b]	d^{-1}
k_{AOM_slow}	1.20×10^{-2} [b]	1.20×10^{-2} [b]	d^{-1}
k_{AOM_fast}	5.00×10^{-2} [b]	5.00×10^{-2} [b]	d^{-1}
Maint_SMB_slow	1.80×10^{-3} [b]	1.80×10^{-3} [b]	d^{-1}
Maint_SMB_fast	1.00×10^{-2} [b]	1.00×10^{-2} [b]	d^{-1}
CUE_SMB	0.60 [a]	0.60 [a]	kg kg^{-1}
CUE_SOM_slow	0.40 [b]	0.40 [b]	kg kg^{-1}
CUE_SOM_fast	0.50 [b]	0.50 [b]	kg kg^{-1}
CUE_AOM_slow	0.13 [b]	0.13 [b]	kg kg^{-1}
CUE_AOM_fast	0.69 [b]	0.69 [b]	kg kg^{-1}
f_{SOM_slow} (humification efficiency)	0.10 [a]	0.30 [c]	kg kg^{-1}
Part. SMB > SOM_fast (microbial recycling)	0.40 [a]	0.40 [a]	kg kg^{-1}
Fraction of SOM_slow at steady-state Bruun (2002) equation	0.83	0.49	kg kg^{-1}

k, turnover rate (death rate for SMB); Maint, maintenance respiration (SMB only); CUE, carbon use efficiency; SOM, soil organic matter pools; SMB, soil microbial biomass pools; AOM, added organic matter pools (not considered in this study); Part., partitioning. [a] Original Jensen (1997), [b] Modified by Mueller et al. (1997), [c] Modified by Bruun et al. (2003).

For simulating soil temperature and moisture in Expert-N, daily averages of radiation, temperature, precipitation, relative humidity and wind speed are needed. For the long-term experiments they were extracted from the nearest weather station with complete data (Ultuna source specifications are as follows: Swedish Agricultural University; European Climate Assessment Station ID 5506; elevation 15 m; 59.8100° N, 17.6500° E. Bad Lauchstädt specifications are as follows: Deutsche Wetter Dienst Station 2932; elevation 131 m; 51.4348 N, 12.2396 E; locality name, Leipzig-Halle). For the fields of the Kraichgau and Swabian Jura, the driving variables were measured by weather stations installed next to eddy covariance stations located at the center of each field. Details on the measurements and instrumentation as well as the gap-filling methods of those eddy covariance weather stations are described in Wizemann et al. (2015).

3.3.3 SOM pool initializations with the DRIFTS stability index and at a steady state

Measured bulk soil SOC includes SMB-C; therefore the amount of SOC in the fast- and slow-cycling SOM pools combined consists of bulk soil SOC minus measured SMB-C. Partitioning of measured SMB-C into slow-cycling (90%) and fast-cycling (10%) microbial pools was carried out similarly to Mueller et al. (1998).

The remaining carbon (difference between bulk soil SOC and SMB-C) was divided between fast- and slow-cycling SOM pools either by the DRIFTS stability index (DSI) or according to the steady-state assumption. For steady-state division, the equation of Bruun and Jensen (2002) was used, which estimates the fraction of SOM in the slow pool from the model parameters under an assumed steady state:

$$\text{slow SOM fraction} = \frac{1}{1+\frac{k_{SOM\_slow}}{f_{SOM\_slow} * k_{SOM\_fast}}}, \quad (3\text{-}1)$$

with k_{SOM_slow} and k_{SOM_fast} representing the turnover (per day) of the slow and fast SOM pools, respectively, and f_{SOM_slow} representing the fraction of the fast SOM pool directed towards the slow SOM pool (humification efficiency). This resulted in 83% of SOM in the slow pool for the original Daisy turnover rates and 49% in the slow pool for the Bruun et al. (2003) turnover rates (Table 3 - 2). For the DSI initialization, the ratio of the area below the aliphatic absorption bands to the area below the aromatic-carboxylate absorption band was used as the ratio of SOM in the fast-cycling SOM pool to SOM in the slow-cycling SOM pool:

$$\frac{\text{fast SOM}}{\text{slow SOM}} = \frac{\text{A\_2930cm}^{-1}}{\text{A\_1620cm}^{-1}} = DSI, \quad (3\text{-}2)$$

Thus, analogous to Equation 3-1, the fraction of SOM in the slow pool was calculated with the formula

$$\text{slow SOM fraction} = \frac{\text{A\_1620cm}^{-1}}{\text{A\_1620cm}^{-1}+\text{A\_2930cm}^{-1}}, \quad (3\text{-}3)$$

With A_2930 cm^{-1} and A_1620 cm^{-1} being the specific area under the aliphatic and aromatic-carboxylate band, respectively (described in section 3.3.1). The remaining carbon was allocated to the fast SOM pool. As was mentioned before, three different data inputs for the DSI were used, obtained at drying temperatures of 32, 65 and 105°C, in order to test which drying temperature derived the best proxy for modeling. An example of the change in DRIFTS spectra occurring after several years of bare fallow can be found in Figure 3 - 2. All DSI model initializations were simulated with both published sets of model parameters. Steady-state initializations using Equation 3-1 were only simulated with the corresponding parameter set from which they were calculated.

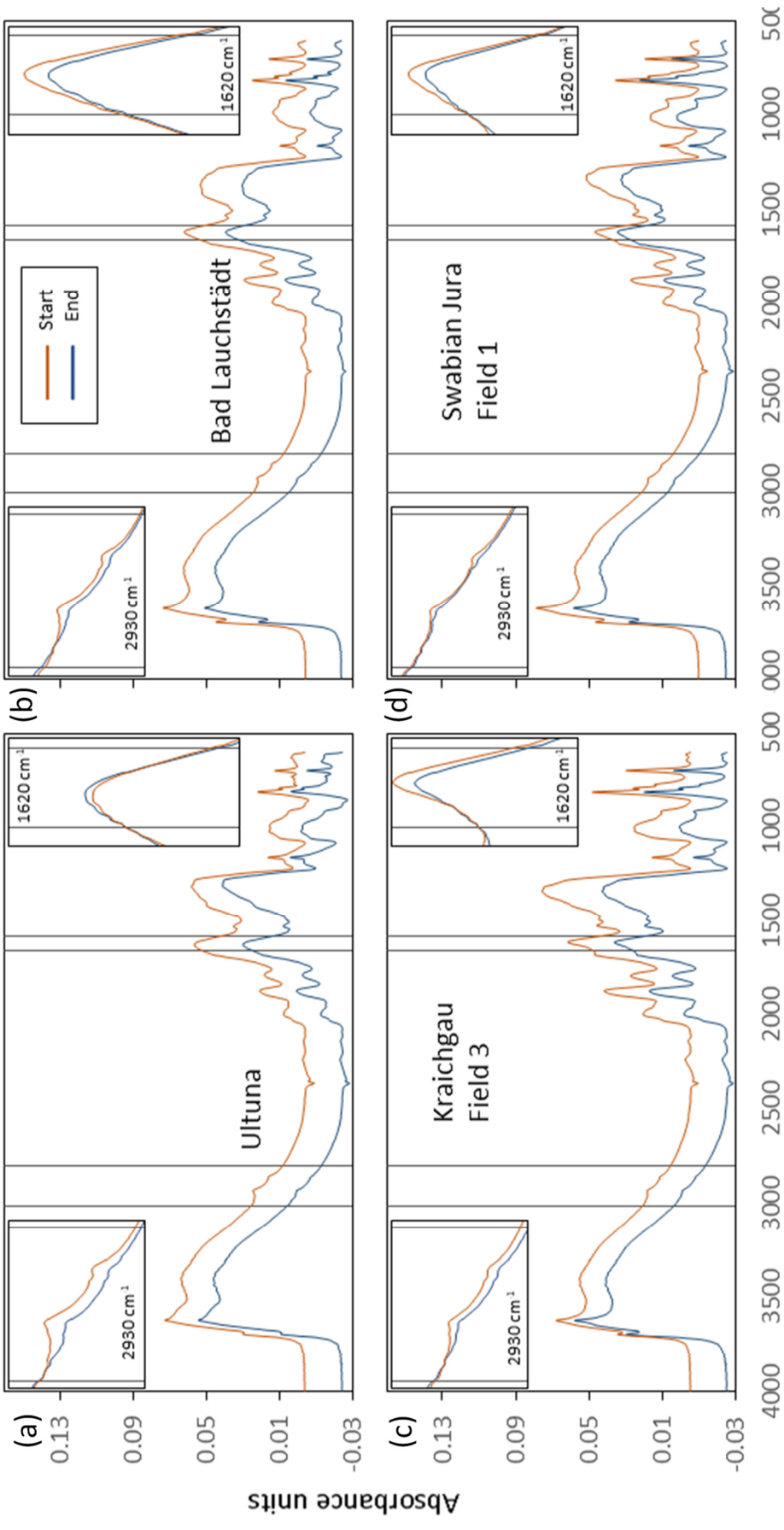

Figure 3 - 2 Examples of baseline-corrected and vector-normalized DRIFTS spectra of bulk soil samples (dried at 105°C) of the first and last year of the bare fallow plots at four sites. Fallow periods were 50 years (a, Ultuna), 24 years (b, Bad Lauchstädt) and 7 years (c, Kraichgau and d, Swabian Jura). Small pictures in (a) to (d) are zoomed-in versions of the 2930cm^{-1} band (left) and the 1620cm^{-1} band (right). For better visibility, the full spectra pictures have a y-axis offset (+0.02 for samples from the start), while zoomed-in versions share a common baseline. More details on the sites are in Table 3 - 3.

3.3.4 Statistical evaluation of model performance

Statistical analysis was performed with SAS version 9.4 (SAS Institute Inc., Cary, NC, USA). To compare different model initializations, a statistical analysis of squared model errors (SME) was conducted:

$$SME_x = (obs_x - pred_x)^2, \quad (3\text{-}4)$$

with obs_x being the observed value, $pred_x$ the predicted value and x the simulated variable of interest. A linear mixed model with SME as the response was then used to test for significant differences between initialization methods. This approach allowed for us to make use of the statistical power of the three Kraichgau and Swabian Jura fields to analyze which initialization was most accurate and to evaluate the trend of the model error with increasing simulation time. In some cases, SME were transformed to ensure a normal distribution of residuals (square root transformation for Ultuna SOC and Kraichgau and Swabian Jura SMB-C and fourth root for Kraichgau and Swabian Jura SOC), which was checked by a visual inspection of the normal Q-Q plots and histograms of residuals (Kozak and Piepho, 2018). Random effects were included to account for temporal autocorrelation of SME within (a) the same field and (b) the same simulation. The model reads as follows:

$$y_{ijkl} = \phi_0 + \alpha_{0i} + ß_{0j} + \gamma_{0ij} + \phi_1 t_k + \alpha_{1i} t_k + ß_{1j} t_k + \gamma_{1ij} t_k + u_{kl} + u_{ijkl}, \quad (3\text{-}5)$$

where y_{ijkl} are the SME_x of the simulation using the *i*th initialization with the *j*th parameter set, at the *k*th time in the *l*th field; ϕ_0 is an overall intercept; α_{0i} is the main effect of the *i*th initialization; $ß_{0j}$ is the main effect of the *j*th parameter set; γ_{0ij} is the *ij*th interaction effect of initialization × parameter set; $\phi_1$is the slope of the time variable t_k; $\alpha_{1i} t_k$ is the interaction of the *i*th initialization with time; $ß_{1j} t_k$ is the interaction of the *j*th parameter set with time; $\gamma_{1ij} t_k$ is the *ij*th interaction effect of initialization × parameter set × time; u_{kl} is the autocorrelated random deviation at the *k*th time in the *l*th field; and u_{ijkl} is the autocorrelated residual error term corresponding to y_{ijkl}. The detailed SAS code can be found in the supplementary material. For Ultuna and Bad Lauchstädt, the u_{kl} term was left out, as both trials only had one field. As the Kraichgau and Swabian Jura sites had the exact same experimental setup and duration, these sites were jointly analyzed in the statistical model, but due to completely different setups and durations, this was not possible for Bad Lauchstädt and Ultuna. The full models with all fixed effects were used to compare different correlation structures for the random effects including (i) temporal autocorrelation (exponential, spherical, Gaussian), (ii) compound symmetry, (iii) a simple random effect for each different field and simulation, and (iv) a random intercept and slope of the time variable (with allowed covariance between both) for each field and initialization method. A residual maximum-likelihood estimation of model parameters was used, and the best-fitting random-effect structure for this model was selected using the Akaike information criterion as specified by Piepho et al. (2004). Then a stepwise model reduction was conducted until only the significant effects ($p < 0.05$) remained in the final statistical model. Because a mixed model

was used, the Kenward-Roger method was applied for estimating the degrees of freedom (Piepho et al., 2004) and to compute post hoc Tukey-Kramer pairwise comparisons of means.

3.3.5 Model optimization and observation weighting for Bayesian calibration

Optimization of parameters k_{SOM_slow}, k_{SOM_fast} and the humification efficiency (f_{SOM_slow}) was performed using a Bayesian calibration approach. These parameters were chosen as only they have a considerable impact on the rate of native SOM loss (see further details in the supplementary chapter S 6.2.3). The Bayesian calibration method uses an iterative process to simulate what the distribution of parameters would be given the data and the model. It combines a random walk through the parameter space with a probabilistic approach on parameter selection.

The differential evolution adaptive metropolis algorithm (Vrugt, 2016) implemented in UCODE_2014 (Lu et al., 2014; Poeter et al., 2014) was used for the Bayesian calibration in this study. As no Bayesian calibration of Daisy SOM parameters has been done before, noninformative priors were used. The main drawback of noninformative priors is that they can have longer computing times, but as was shown by Lu et al. (2012), with sufficient data and simulation durations, the posterior distributions are very similar to using informed priors. Ranges were set far beyond published parameters with 1.4×10^{-2} to 1.4×10^{-6} d^{-1} for k_{SOM_fast} and 1.4×10^{-3} to 5×10^{-7} d^{-1} for k_{SOM_slow}. The parameter f_{SOM_slow} had to be more strongly constrained as without constraints it tended to run into unreasonable values of up to 99% humification. The limits were therefore set to 0.05 to 0.35, which are ± 5% of the two published parameter sets and represent the upper boundaries of other similar models (e.g., Ahrens et al., 2014). The default UCODE_2014 Gelman-Rubin criterion (Gelman and Rubin, 1992) value of 1.2 was chosen for the convergence criteria. A total of 15 chains were run in parallel with a time step of 0.09 d in Expert-N 5.0 (this was the largest time step and fastest computation where the simulation results of water flow, temperature and hence SOM pools were unaltered compared to smaller time steps). It was ensured that at least 300 runs per chain were carried out after the convergence criterion was satisfied.

In Bayesian calibration, a proper weighing of observations is needed in order to achieve a diagonal weight matrix of residuals (proportional to the inverse of the variance-covariance matrix) and to ensure that residuals are in the same units (Poeter et al., 2005, p18 ff). This included several steps. A differencing removed autocorrelation in the individual errors in each model run of the Bayesian calibration itself (the first measurement of each kind of data at each field was taken as raw data, for any repeated measurement the difference from this first measurement was taken instead of the raw data). Details on differencing are provided in chapter 3 of the UCODE_2005 manual (Poeter et al., 2005). To account for varying levels of heterogeneity of different fields in the weighting, a linear mixed model was used to separate the variance in observations from different fields originating from natural

field heterogeneity from the variance originating from measurement error. To do so, a linear mixed model with a random slope and intercept of the time effect for each experimental plot was fitted to the SOC, SMB-C and DSI data for each field individually:

$$y_{kl} = \phi_0 + \phi_1 t_k + u_l + u_k + u_{kl}, \quad (3\text{-}6)$$

where y_{kl} is the modeled variable at the *k*th time on the *l*th plot, ϕ_0 is the intercept, $\phi_1$is the slope of the time variable t_k, u_l is the random intercept, u_k is the autocorrelated random deviation of the slope and u_{kl} is the autocorrelated residual error term corresponding to y_{kl}.

The error variance in each type of measurement (DSI, SMC-C, SOC) at each field ${\sigma_{fM}}^2 = \sigma_{u_k}^2 + \sigma_{u_{kl}}^2$ was then used for weighting of observations, excluding the field variance $\sigma_{u_l}^2$ from the weighting scheme. This error variance was used in UCODE_2014 to compute weighted model residuals for each observation as follows:

$$w\_SME_x = \frac{(obs_x - pred_x)^2}{{\sigma^2}_{fM}}, \quad (3\text{-}7)$$

where w_SME_x is the weighted squared model residual, obs_x is the observed value, $pred_x$ is the predicted value and ${\sigma^2}_{fM}$ is the error variance in the *M*th type of measurement at each field. All w_SME_x values are summed up to the sum of squared weighted residuals, which is the objective function used in UCODE_2014 (Poeter et al., 2014). By this procedure, observations with higher measurement errors have a lower influence in the Bayesian calibration.

Since the medium-term experiments had a much higher measurement frequency, it was also tested whether giving each experiment the same weight would improve the results of the Bayesian calibration (equal weight calibration). In this case an additional group weighting term was introduced for groups of observations, representing different datasets at the different sites. This weighting term is internally multiplied with each w_SME_x value in UCODE_2014 and was calculated as

$$w\_G_x = \frac{1}{(n_{obs} * n_{par} * n_f)}, \quad (3\text{-}8)$$

where w_G_x is the weight multiplier for each observation, n_{obs} is the number of observations per parameter, n_{par} is the number of parameters per field, and n_f is the number of fields per site. This weighing assures that, with the exact same percentage of errors, each site would have the exact weight of 1.

The influence of several factors was assessed in this Bayesian calibration: the use of individual sites compared to combining sites, including an equal weight (EW, as described above) vs. original weight (OW) weighting only by error variance, and the effect of including or excluding the DSI (± DSI) in the Bayesian calibration. Therefore, seven Bayesian calibrations were conducted in total: (1-4) four for

each individual site with original weight and the DSI, i.e., Ultuna, Bad Lauchstädt, Kraichgau, and Swabian Jura; (5) equal weight calibration for all sites combined using the DSI; (6) original weight calibration for all sites combined without using the DSI in the Bayesian calibration (only for initial pool partitioning); and (7) original weight calibration for all sites combined using the DSI. The comparison of these seven Bayesian calibrations was designed to assess the effect of the site on the calibration, as well as the effect of the DSI and of user weighting decisions.

Table 3 - 3 Measured soil properties of the bare fallow experiments at each site corresponding to the start of the bare fallow experiment and the end of the simulated period. Measurements include SOC and SMB-C stocks in the modeled layer and the percentage of SOC that would be assigned to the slow pool according to the DRIFTS stability index (DSI) measured at 105°C.

Site	Start year of experiment	End year of simulation	Depth of modeled layer (cm)	Bulk density of modeled layer (Mg m^{-3})	SOC at start Mg ha^{-1} [a]	SOC at end Mg ha^{-1} [a]	SMB-C at start Mg ha^{-1} [a]	SMB-C at end Mg ha^{-1} [a]	% SOC in slow pool at start (DSI 105°C)	% SOC in slow pool at end (DSI 105°C)	% of initial SOC lost	Number of years	% of initial SOC lost per year
Ultuna	1956	2005	0 - 20	1.44	43.22	26.51	NA	NA	54	91	39%	50	0.8%
Bad Lauchstädt	1983	2008	0 - 20	1.24	45.08	41.91	NA	NA	70	80	7%	26	0.3%
Kraichgau 1	2009	2015	0 - 30	1.37	37.10	32.59	0.847	0.408	80	98	12%	7	1.7%
Kraichgau 2	2009	2015	0 - 30	1.33	41.61	38.66	0.853	0.314	73	93	7%	7	1.0%
Kraichgau 3	2009	2015	0 - 30	1.44	38.50	35.06	0.672	0.261	76	99	9%	7	1.3%
Swabian Jura 1	2009	2015	0 - 30	1.32	70.33	63.29	1.566	0.654	64	83	10%	7	1.4%
Swabian Jura 2	2009	2013	0 - 30	1.38	80.85	79.61	1.805	0.970	66	83	2%	5	0.3%
Swabian Jura 3	2009	2013	0 - 30	1.07	61.27	70.29	1.350	0.990	61	76	-15%	5	-2.9%

SOC, soil organic carbon; SMB-C, soil microbial biomass carbon; DSI, Diffuse reflectance mid-infrared Fourier transform spectroscopy stability index; NA, no data available for this site; [a]stocks in Mg ha^{-1} refer to stocks within the depth of the modelled layer.

3.4 Results

3.4.1 Dynamics of SOC, SMB-C and DRIFTS during bare fallow

All bare fallow plots lost SOC over time, with the severity of SOC loss varying between soils and climates at the different sites. The Bad Lauchstädt site experienced the slowest carbon loss (7% of initial SOC in 26 years), while SOC at Ultuna and Kraichgau was lost at much faster rates (Ultuna, 39% of initial SOC in 50 years; Kraichgau, on average 9% of initial SOC in 7 years; Table 3 - 3). In the Swabian Jura Field 1 the SOC loss was comparable to that of Kraichgau (about 10% of initial SOC in 7 years) but was much less in fields 2 and 3. Some miscommunication with the field owner's contractors led to unwanted manure addition and field ploughing in Swabian Jura fields 2 and 3 in 2013; hence results of these two fields after the incident in 2013 were excluded. The DRIFTS spectra revealed that the aliphatic carbon band area (2930 cm^{-1}) decreased rather fast after the establishment of bare fallow plots, while the aromatic-carboxylate band area (1620 cm^{-1}) showed only minor changes and no consistent trend (Figure 3 - 2). The assumed fraction of SOC in the slow SOM pool according to the DSI at 105°C changed from the initial range of 54 to 80% to the range of 76 to 99% at the end of the observational period (Table 3 - 3, Figure S 3 - 3). The SMB-C reacted even more rapidly to the establishment of fallow and halved on average for all fields within a 7 year duration (Table 3 - 3).

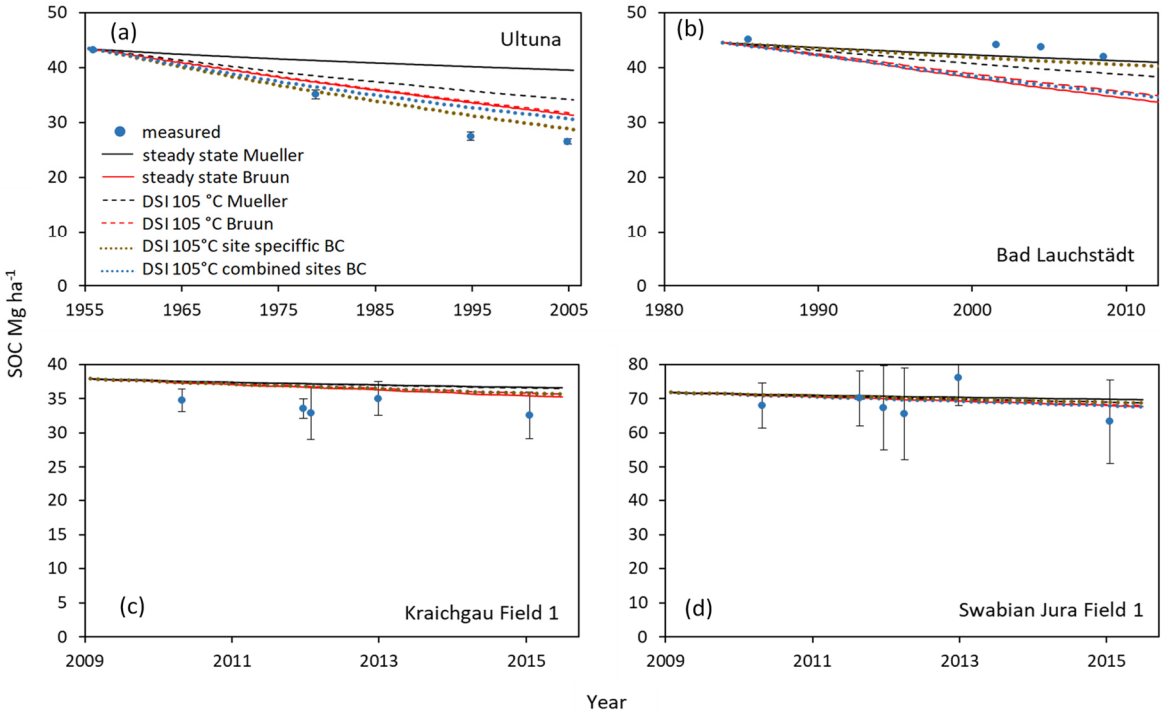

Figure 3 - 3 Example of SOC simulations from Ultuna (a), Bad Lauchstädt (b), Kraichgau Field 1 (c) and Swabian Jura Field 1 (d). Initializations were carried out (i) assuming a steady state using the formula of Bruun and Jensen (2002) (Equation 3-1) with turnover rates of both Mueller et al. (1997) and Bruun et al. (2003) and (ii) by the DRIFTS stability index (DSI) at a 105°C drying temperature using both turnover rates for simulations (simulations using the other drying temperatures for the DSI are in the supplementary material). The site-specific and the combined-sites Bayesian calibrations (BC) are also displayed. Bars indicate the standard deviation of measured values of all plots (n = 3) per field.

3.4.2 Comparison of the different model initializations

The observed trend of SOC loss with ongoing bare fallow duration was also found in all simulations (Figure 3 - 3 and Figure S 3 - 4). For Ultuna, simulated SOC loss in all cases underestimated measured loss, while for Bad Lauchstädt, simulated SOC losses consistently overestimated measured losses. At Kraichgau sites SOC loss was underestimated by the models, but with the Bruun et al. (2003) parameter set yielding simulated values closer to actual measurements. In the Swabian Jura, both parameter sets underestimated SOC loss. The decline of SMB-C in the Kraichgau and Swabian Jura (Figure 3 - 4) occurred more rapidly than that of SOC, though SMB-C had higher variability in measurements. The parameter sets with steady-state assumptions marked the upper and lower boundaries of the SMB-C simulations, but the DRIFTS stability index (DSI) initializations were closer to the measured values (with the exception of Swabian Jura Field 3). For brevity only simulations of Field 1 for Kraichgau and Swabian Jura are shown. Simulation results for fields 2 and 3 are found in the supplemental material (Figure S 3 - 5 for SOC simulations and Figure S 3 - 6 for SMB-C).

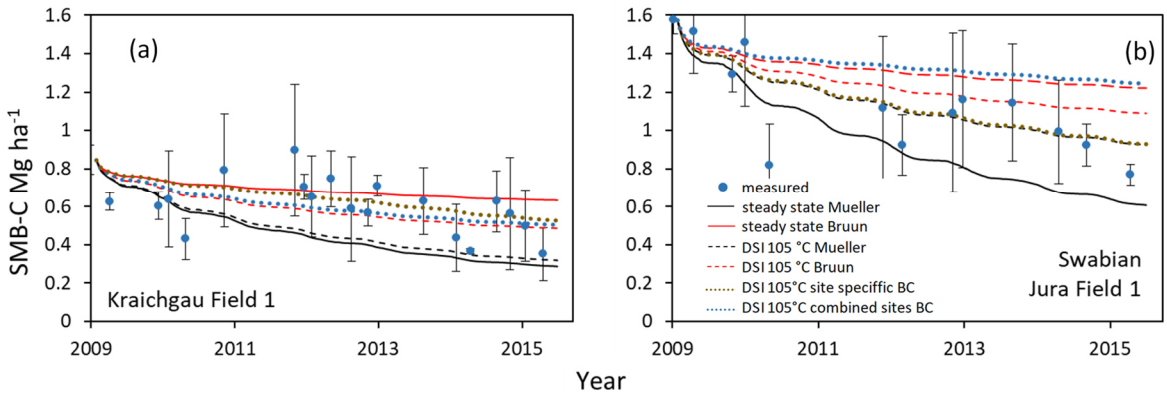

Figure 3 - 4 Example SMB-C simulations for Kraichgau Field 1 (a) and Swabian Jura Field 1 (b). Initializations were carried out (i) assuming a steady state using the formula of Bruun and Jensen (2002) with turnover rates of Mueller et al. (1997) and Bruun et al. (2003) and (ii) by the DRIFTS stability index (DSI) at a 105°C drying temperature using both turnover rates for simulations (simulations using the other drying temperatures for DRIFTS are in the supplementary material). The site-specific and the combined sites Bayesian calibrations (BC) are also displayed. Bars indicate the standard deviation of measured values of all plots (n =3) per field.

The statistical analysis of the model error revealed a site dependency of the effect of the parameter set. The three-way interaction of initialization, parameter set and time $\gamma_{1ij}t_k$ was significant for all but Bad Lauchstädt SOC, where only the parameter set had a significant effect. In the case of Bad Lauchstädt, the model error was significantly lower with the slower Mueller et al. (1997) SOM turnover parameter set, while for the rest of the tested cases, the faster Bruun et al. (2003) set performed significantly better (Table 3 - 4) . For Ultuna and Kraichgau and Swabian Jura SOC, the steady-state assumption with Mueller et al. (1997) parameters had the highest model error, while the steady state assumption with Bruun et al. (2003)parameters had the lowest model error of all simulations, being similar to DSI initializations at Kraichgau and Swabian Jura. However, there was a statistically significantly lower SOC model error with the DSI using the 105°C drying temperature than there was

using the lower drying temperatures for the Ultuna site. For SMB-C simulations at the Kraichgau and Swabian Jura sites, however, the errors were lowest for the DSI initialization using the 105° C drying temperature with Bruun et al. (2003) parameters and significantly lower than both steady-state initializations. Of the DSI initializations using different drying temperatures, the model error was always lowest when using the 105°C drying temperature initialization compared to 32°C and 65°C (significant for Ultuna, as well as for Kraichgau and Swabian Jura SMB-C using Mueller et al. (1997) parameters). As initializations with the DSI using the 105°C drying temperature consistently performed best of all three DSI initializations, only DSI spectra of soils dried at 105°C were used for the Bayesian calibration.

Table 3 - 4 Effect of the initialization method on simulation errors. Displayed are estimated least-square means of the absolute error of Daisy bare fallow simulations of SOC and SMB-C for the sites of Ultuna, Bad Lauchstädt, and Kraichgau and Swabian Jura combined. Means are the estimate for the end of the simulation period (number of years in brackets). Different capital letters indicate significant differences ($p < 0.05$) within columns (not tested between sites). For Bad Lauchstädt, the initialization effect was nonsignificant, so only the least-square means for the effect of the parameter set are displayed.

		Ultuna (50yr)	Bad Lauchstädt (23yr)	Kraichgau and Swabian Jura (7 yr)	Kraichgau and Swabian Jura (7 yr)
Parameter set	**Initialization method of SOM pools**	**Least-square means of errors (SOC Mg/ha)**	**Back transformed least-square means of errors (SOC Mg/ha)**	**Back transformed least-square means of errors (SOC Mg/ha)**	**Least-square means of errors (SMB-C Mg/ha)**
Mueller et al. (1997)	Ratio of steady-state assumption	13.91 A	2.22 A	4.50 A	0.354 A
	Band area ratio of DRIFTS at 32°C	10.86 B		4.50 A	0.317 AB
	Band area ratio of DRIFTS at 65°C	10.06 C		4.42 A	0.274 ABC
	Band area ratio of DRIFTS at 105°C	8.52 D		4.28 A	0.205 CD
Bruun et al. (2003)	Ratio of steady-state assumption	5.84 H	6.01 B	3.12 B	0.231 BCD
	Band area ratio of DRIFTS at 32°C	7.06 E		3.31 B	0.179 CDE
	Band area ratio of DRIFTS at 65°C	6.75 F		3.30 B	0.160 DE
	Band area ratio of DRIFTS at 105°C	6.15 G		3.25 B	0.131 E

SOM, soil organic matter pools; SOC, soil organic carbon; SMB-C, soil microbial biomass carbon; DRIFTS, Diffuse reflectance mid-infrared Fourier transform spectroscopy.

3.4.3 Informed turnover rates of the Bayesian calibration

The posterior distribution of parameters from the Bayesian calibration differed considerably between the different calibrations for individual sites, but there were also differences between different weighting schemes or when performing the Bayesian calibration without using the DSI (Figure 3 - 5). The highest probability turnover of the fast SOM pool (k_{SOM_fast}) was 1.5 and 3 times faster for Ultuna and Kraichgau, respectively, when compared to initial rates (1.4×10^{-4} d^{-1} for both parameters sets),

which fitted well for Bad Lauchstädt and Swabian Jura. For the slow SOM pools (k_{SOM_slow}), the Bad Lauchstädt, Kraichgau and Swabian Jura site calibrations were in between the two published parameter sets but tended towards the slower rates (2.7×10^{-6} d^{-1} by Mueller, 1997), while the optimum for Ultuna was exactly at the fast rates of Bruun et al. (2003; 4.3×10^{-5} d^{-1}). The humification efficiency (f_{SOM_slow}) was not strongly constrained in the Bayesian calibration, except for the Kraichgau site, where it ran into the upper boundary of 0.35. This trend towards higher humification also existed for the other sites, but to a lesser extent than for Kraichgau.

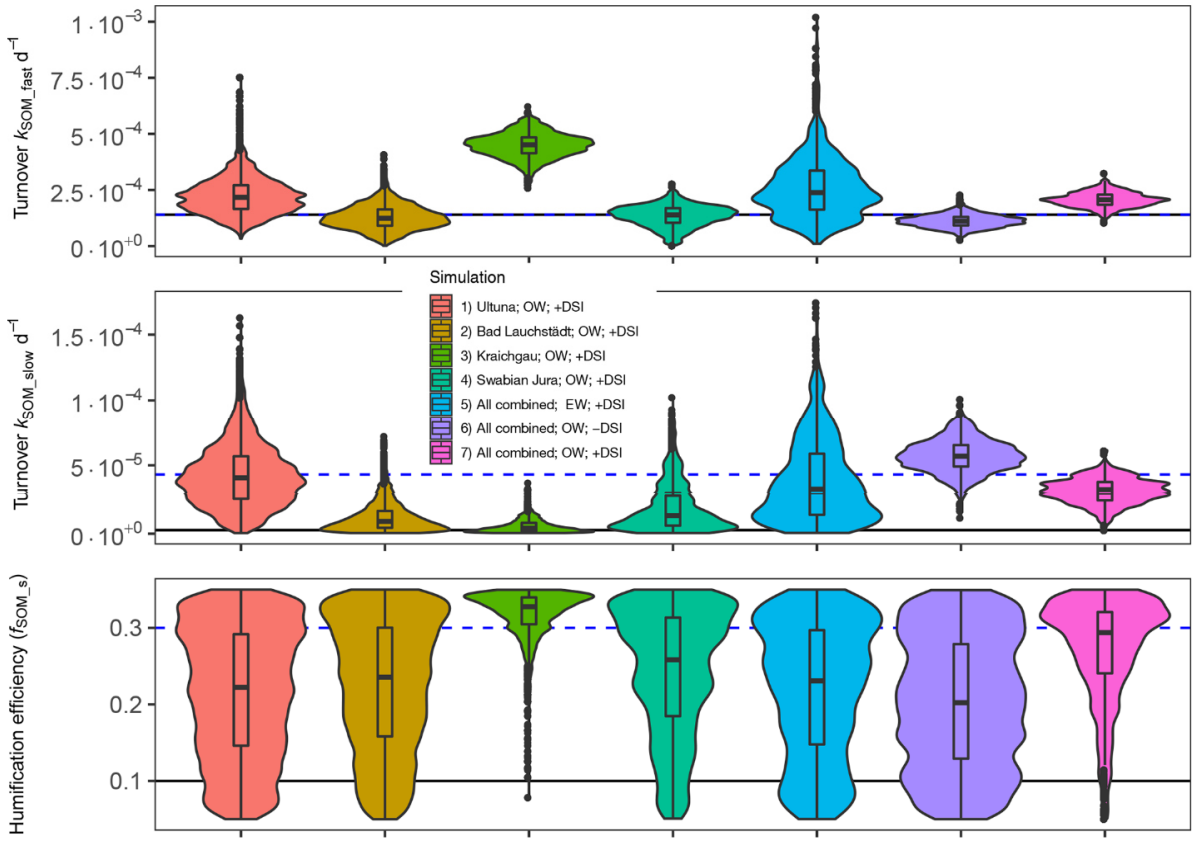

Figure 3 - 5 Violin plots of the parameter distributions, obtained by the Bayesian calibration using only the individual sites (1-4) and all sites combined (5-7) with different weighing schemes (OW, original weight; EW, equal weight calibration; ± DSI indicates whether the DSI data were used for calibration). The black line corresponds to the parameters of Mueller et al. (1997) and the dashed blue line to the parameters of Bruun et al. (2003). Note that the turnover k_{SOM_fast} parameter (top of the figure) is the same in both Mueller et al. (1997) and Bruun et al. (2003).

The different calibrations of the combination of all sites under different weightings and with or without the DSI led to considerable differences in the posteriors (Figure 3 - 5). When combining the sites with the artificial equal weighting, the posterior distribution of all three parameters was the widest, basically covering the range of all four site calibrations. With the original weighting scheme, only informed by the variance in the data, the posteriors were narrower for all parameters, with the optima of k_{SOM_fast} being slightly faster than the two (similar) published rates. The optima of k_{SOM_slow} were slightly slower than Bruun et al. (2003) but much faster than Mueller et al. (1997), and f_{SOM_slow} was even above the higher Bruun et al. (2003)value of 0.3. The use of the original weighting scheme without

the use of the DSI in the Bayesian calibration did not constrain the f_{SOM_slow} at all and had faster k_{SOM_slow} and slower k_{SOM_fast} than the one using the DSI. Both these Bayesian calibrations using the original weighting (with and without the DSI) showed a trend towards slightly faster turnover than suggested by Bruun et al. (2003).

There was a strong negative correlation between k_{SOM_fast} and k_{SOM_slow} parameters for all but the Bad Lauchstädt calibration (Figure S 3 - 7). When the DSI was not included in the Bayesian calibration, this negative correlation was stronger than when it was included (Figure 3 - 6). The parameters k_{SOM_fast} and f_{SOM_slow} were always positively correlated, most strongly for Kraichgau (0.49) and Swabian Jura (0.38), but only weakly for the long-term sites. The correlations between the parameters k_{SOM_slow} and f_{SOM_slow} were generally low and both positive and negative. The parameters with the highest probability density of the calibrations combining all sites for f_{SOM_slow} , k_{SOM_fast} and k_{SOM_slow} in that order were 0.34, 2.29×10^{-4} and 3.25×10^{-5} for the original weight calibration and 0.06, 9.58×10^{-5} and 5.54×10^{-5} for the calibration using original weights and no DSI. These results suggest that turnover rates of k_{SOM_slow} could be similar or faster than those of k_{SOM_fast} without the use of the DSI. About 10% of the simulations of the Bayesian calibration without the DSI even had a faster k_{SOM_slow} *than* k_{SOM_fast}.

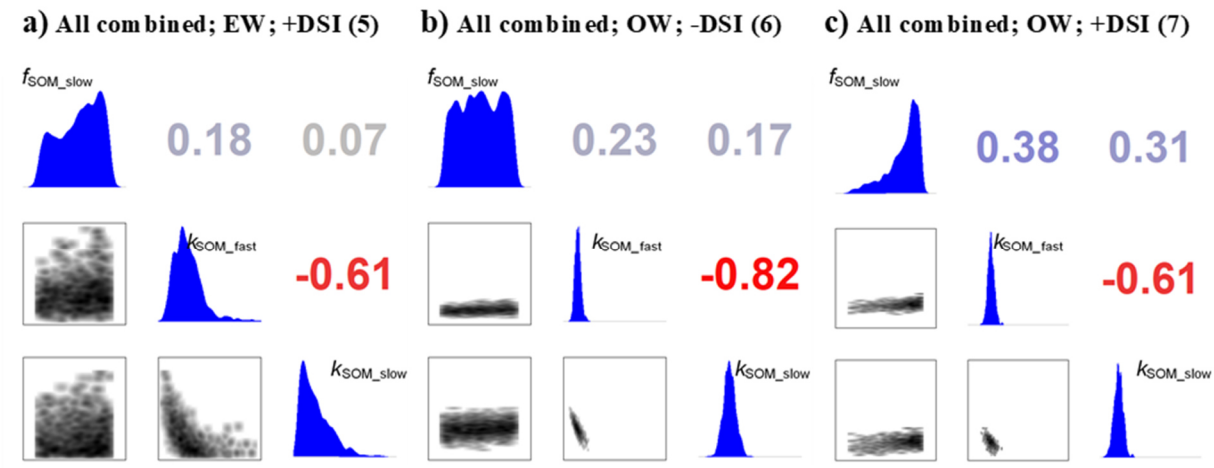

Figure 3 - 6 Correlation matrices of posterior distributions from the Bayesian calibrations of a) equal weight calibration for all sites combined using the DSI (calibration 5), b) original weight calibration for all sites combined without using the DSI (calibration 6), and c) original weight calibration for all sites combined using the DSI (calibration 7). The plots of individual site simulations (calibrations 1-4) can be found in the Supplement.

3.5 Discussion

3.5.1 How useful is the DRIFTS stability index?

A search for suitable proxies for SOM pool partitioning into SOM model pools that correspond to measurable and physicochemically meaningful quantities is of high interest (Abramoff et al., 2018; Bailey et al., 2018; Segoli et al., 2013). The results of this study confirm the hypothesized usefulness of the DSI proxy in assessing the current state of SOM for pool partitioning to model SOC for several soils

across Europe. This is particularly relevant given that changes in crop genotype and rotation and agricultural management and the rise of average temperatures in recent decades as well as land use changes, such as draining of soils or deforestation, in recent centuries have altered the quality and quantity of carbon inputs to soil. Consequently, the steady-state assumption for model initialization is not likely to be valid. Demyan et al. (2012) showed that, with a careful selection of integration limits for absorbance band areas, the DSI through identifying organic contributions in DRIFTS spectra is a sensitive indicator of SOM stability if mineralogy is similar (despite acknowledged mineral interference). Combined with a higher temperature (105°C) for soil drying prior to DRIFTS analysis, a strong correlation between the portion of centennially persistent SOC and the DSI (Figure S 3 - 2) was found in our study, which supports the hypothesis that the DSI might be of general applicability across sites. Results from modeling corroborated the usefulness of the DSI for SOM pool partitioning for soils of different properties across Europe. The statistical analysis of the model error for both SOC and SMB-C showed clearly that the DSI can improve poor model performance, especially when the slower turnover rates of Mueller et al. (1997) were used. When model performance is already satisfactory, the natural variability in the DSI can make model performance worse, as in the case of Ultuna SOC with Bruun et al. (2003) parameters, but this reduction was minor compared to the improvement the DSI had over steady-state assumptions at Ultuna with Mueller et al. (1997) rates. The better results for Ultuna with the Bruun et al. (2003) steady state might also just be an effect of turnover times still being too slow, and hence the more SOC in the fast pool, the faster turnover is in general and the lower the model error. This was also indicated by faster optima by the Bayesian calibration compared to both published turnover rates. In the case of the Chernozem of Bad Lauchstädt, only turnover rates had an influence on model performance and its SOC turnover was overestimated by both parameter sets (Figure 3 - 3). It was previously suggested that the high SOC storage capacity of this site is a result of cation-bridging due to a high content of adsorbed cations (Ellerbrock and Gerke, 2018). Additionally, there is evidence of black carbon at the site (e.g., the high thermal stability found by Demyan et al., 2013). Therefore, a possible reason for an overestimation of SOC turnover in Bad Lauchstädt might be that Daisy only considers clay content as a stabilizing mechanism. Nevertheless, the use of the DSI was also suitable for Bad Lauchstädt, as there was no significant difference in model performance compared to a steady state.

The range of different sites, soils and climatic conditions of Europe represented within this study suggests the robustness of the DSI as a proxy for SOM quality and SOM pool division for a large environmental gradient. Hence, it would be an improvement over assuming a steady state of SOM wherever there is a lack of detailed information on carbon inputs and climatic conditions. Considering the timescales at which SOM develops, this is almost anywhere, as detailed data are available at best for <200 years, which is not even one half-life of the slow SOM pool.

So far, studies that have assessed SOM quality and pool division proxies, using either the thermal stability of SOM (Cécillon et al., 2018) or size-density fractionation (Zimmermann et al., 2007), only indirectly related the proxies to inversely modeled SOM pool distributions, using machine learning and rank correlations. In contrast, our study showed that the DSI is a proxy which can be directly used for pool initialization. The DSI also makes sense from the perspective of energy content, as microorganisms can obtain more energy from the breakdown of aliphatic than aromatic-carboxylate carbon compounds (e.g., Good and Smith, 1969), and therefore aliphatic carbon is primarily targeted by microorganisms (hence has faster turnover), as previously shown for bare fallow (Barré et al., 2016).

The two distinct absorption bands for aliphatic and aromatic-carboxylate carbon bonds of the DSI fit well to the two SOM pool structures of Daisy and the simulation of carbon flow through the soil in Daisy is very similar to several established SOM models such as SoilN, ICBM and CENTURY. It is therefore likely that, with calibration, the DSI could be used as a general proxy for SOM models with two SOM pools and a humification efficiency (f_{SOM_slow} in Daisy). The parameter correlations between k_{SOM_slow}, k_{SOM_fast} and f_{SOM_slow} according to the Bayesian calibrations also suggest that without a pool-partitioning proxy, modifying any one parameter can lead to similar results in terms of SOC and SMB-C simulation. A clear distinction between fast and slow pools needs a pool-partitioning proxy, as can be seen by faster k_{SOM_slow} than k_{SOM_fast} for some of the simulations of the Bayesian calibration without using the DSI. Assigning the DSI to Daisy reduced parameter correlations and led to a clear distinction between fast and slow SOM pools.

The DRIFTS absorption band for aliphatic carbon is most resolved when applying a 105°C drying temperature to samples prior to analysis (Laub et al., 2019). The current study's modeling results corroborated the finding that the DSI should be obtained from measurements after drying at 105°C, with the performance of the DRIFTS initializations being always in the order 105°C > 65°C > 32°C drying temperature (differences being sometimes but not always significant).

Compared with the other proxies for SOM quality discussed above, the measurements by DRIFTS are inexpensive and relatively simple, and the equipment of the same manufacturer is standardized. This should also constrain variability between different laboratories and be attractive for large-scale applications with large sample numbers, for example to initialize simulations at the regional scale. However, for standardization of the DSI for model initialization, one needs to address how the type of spectrometer (e.g., detector type) influences the spectra, if water and mineral interferences (Nguyen et al., 1991) in the spectra can be further reduced, and if a mathematical standardization of the spectra and the DSI (across instruments and water contents) is possible. While a complete elimination of mineral interference is not possible, a careful selection of integration limits and the use of a local baseline minimize mineral interference of DRIFTS spectra from bulk soils. This mostly selects the top

part of the 1620 cm^{-1} band area, which corresponds to the part that is reduced or completely lost when SOC is destroyed (Demyan et al., 2013; Yeasmin et al., 2017). Other approaches such as spectral subtraction of ashed samples or HF destruction of minerals prior to DRIFTS analysis have been developed in the attempt to obtain spectra of pure SOC. All are rather labor intensive and still produce artifacts, as it is not possible to destroy only the minerals or only the SOC without altering the respective other fraction (Yeasmin et al., 2017). Hence, we think that the selected integration limits might represent at this point the most feasible option for obtaining a robust and cost-effective proxy of SOC quality for modeling. The strong correlation of the DSI and centennially persistent SOC as well as the model results of this study seem to corroborate this. The method of DSI estimation might be improved by a study of the best integration limits optimizing the fit of the DSI and centennially persistent SOC, which would require more bare fallow experiments than in this study. From a conceptual perspective the DSI probably relates mainly to chemical recalcitrance of SOM present in different SOM fractions. In that respect it is different from physical light and heavy fraction separation approaches as each of these fractions is very heterogeneous. For example, the light fraction has strong absorbance at both aliphatic and aromatic-carboxylate carbon bands (Calderón et al., 2011), so it could be that within each fraction, aliphatic carbon is preferentially consumed by microorganisms. Thus, the DSI reflects physicochemically stabilized SOC (mainly mineral association in the case of bare soils) as also suggested by the correlation of the ratio of 1620 cm^{-1}/2930 cm^{-1} absorption bands to the ratio of mineral-associated carbon/light fraction carbon (Demyan et al. 2012). The relationship to mineral association in many models is represented by a texture adjustment factor. On the other hand, the DSI does not directly relate to aggregated (i.e., occluded) SOM, and its applicability in models focusing on aggregation needs to be evaluated (i.e., by a separate spectral analysis of occluded and remaining fractions).

The recent coupling of pyrolysis with DRIFTS (Nkwain et al., 2018) might be a further analytical advancement of the DSI, as it overcomes mineral interferences in the spectra. However, this technique is more complex due to a larger number of visible organic absorption bands, including CO_2 that develops from the pyrolysis, which makes it not easily applicable to established two-pool models such as Daisy. In addition, a considerable portion (30 – 40%) of SOM is not pyrolyzed and therefore not recorded in the spectra. In summary, despite the acknowledged shortcomings, the DSI was useful to partition SOM between pools and will be even more so when the optimized parameters for the DSI are used for future applications. It seems more robust than steady-state or long-term spin-up runs which rely on strong assumptions. Further tests are needed before using the DSI for mineralogy that differs considerably from the soils of this study.

3.5.2 Parameter uncertainty as estimated with Bayesian calibration

According to our Bayesian calibrations, a wide range of parameter values are possible for Daisy going far beyond the initial published parameter sets. By combining various sites and including meaningful proxies, such as the DSI, the parameter uncertainty and equifinality could be reduced and the credibility intervals narrowed. The predictions of mechanistic models usually fail to account for the three main statistical uncertainties in (1) inputs, (2) scientific judgments resulting in different model setups and (3) driving data (Wattenbach et al., 2006). However, with a Bayesian calibration framework such as that implemented in UCODE 2014, almost any model can be made probabilistic, so uncertainties in parameters and outputs can be assessed, even for projections into the future (Clifford et al., 2014). As this study focused on Bayesian calibration and we used an established model, we mainly address parameter uncertainty, although input uncertainty was also included through the weighting process. We clearly demonstrated an effect of the individual site used for Bayesian calibration on the resulting model parameters and uncertainties. Similarly diverging site-specific turnover rates were also found by Ahrens et al. (2014) in a study of soil carbon in forests. Diverging results for different sites generally point towards a need for a better understanding of the modeled system and model improvements (Poeter et al., 2005), but this often requires a deeper understanding of the system and new measurements – hence it is not always feasible. A Bayesian calibration asks the following question: what would be the probability distribution of parameters, given that the measured data should be represented by the selected model? Hence, if only one site is used, it can only answer this question for that specific site. As this study showed, the parameter set could then be highly biased for other sites. For a more robust calibration, several sites should be combined to obtain posterior distributions of parameters for a gradient of sites, though this might reduce model performance for individual sites. The introduction of the equal weighting scheme, which gave similar weights to the different sites, highlights how much bias may be introduced by user decisions of artificial weighting: this Bayesian calibration parameter set had the highest uncertainties, and it appears as if the Ultuna site had by far the strongest influence. In contrast to that, the combination of all four sites with the original weights based on the error variances or measurements led to a very clear reduction in parameter uncertainty and the narrowest parameter credibility intervals (Figure 3 - 6 a compared to Figure 3 - 6 b and c).

The results of the statistical analysis of model errors (Table 3 - 4) suggest that the DSI is suitable for SOC model pool initialization. This was corroborated by the Bayesian calibration, as the inclusion of the DSI narrowed credibility intervals for the slow SOM pool turnover and humification efficiency and reduced the correlation between fast and slow SOM turnover compared to the simulation without the DSI as a constraint. Especially in the case of the clear differentiation between k_{SOM_slow} and k_{SOM_fast}, our results show the advantage of attaching a physiochemical meaning to the pools that was not provided

before. Other effective approaches, such as using time series of ^{14}C data, could be combined with the DSI for better results.

Of all three parameters, the humification efficiency (f_{SOM_slow}) was the only parameter that consistently ran into the upper boundaries, set to 35%. In fact, initial calibrations were carried out where f_{SOM_slow} was constrained to 95%; even then, it tended to run into that constraint (Figure S 3 - 8) and led to much faster turnover rates (k_{SOM_slow}) than were published before. These values of f_{SOM_slow} were much greater than the 10% for the Mueller et al. (1997) dataset, 30% for Bruun et al. (2003) and other published two-pool models. Therefore, we considered the cause of the poorly constrained f_{SOM_slow} parameter to be a model formulation problem, which did not depend on whether the DSI was included in the Bayesian calibration or not. Only when the humification efficiency was restricted in the Bayesian calibration did the turnover of fast and slow SOM align with the earlier published rates. If a parameter is problematic, such as f_{SOM_slow}, it could mean that there are a lack of data. However, if parameters are constrained but run into implausible values, it usually means that the model structure is suboptimal (Poeter et al., 2005) and should be altered.

3.5.3 Model structure determines SOM turnover times in two-pool models

The rate of SOM decomposition remains of major interest, especially with respect to the potential of SOM as a global carbon sink (Minasny et al., 2017). Some of the first conceptual approaches proposed SOM pools with residence times of 1000 years and longer (e.g., in CENTURY, Parton et al., 1987), but the SOM models were calibrated to fit data measured in long-term experiments that included vegetation. The pool structure of early SOM models such as Daisy and CENTURY were rather similar as were the turnover rates of SOM pools (see summary in Table 3 - 5). An improved understanding of the actual number of carbon inputs to the soil, which remains challenging to measure, led to faster turnover rates in more recent model versions (e.g., by Bruun et al., 2003). The reason is probably that inputs of carbon and nitrogen to the soil were initially underestimated as it is very difficult to measure root turnover and rhizosphere exudation inputs without expensive in situ ^{13}C or ^{14}C labeling. The underestimated inputs were then likely counterbalanced in the model calibration by slower turnover rates resulting in acceptable model outputs (SOM dynamics and CO_2 emissions) for the time being. However, as our summary of more recent studies underlines (Table 3 - 5), the earlier published turnover rates seem to be subject to a systematic underestimation. As the comparison of our Bayesian calibration to other recent Bayesian calibration studies suggests, the relatively fast turnover rates of this study are in alignment with other recent findings (Table 3 - 5), as all five examples have published turnover rates for the slow SOM pool, which are at least 1 order of magnitude faster than early assumptions from the 1980s and 90s.

Table 3 - 5 Optimized turnover rates and humification efficiency of this study (using the combined site analysis with original weighting and the DSI) compared to other Bayesian calibrations and standard values of commonly used models. Turnover rates of other models were normalized to the Daisy standard of 10°C using an exponential equation (an exception was Clifford et al. (2014), where no temperature was given).

Model	Daisy	ICBM	CBM-CFS3	APSIM	Own creation*	CENTURY	Daisy	Daisy
Reference	This study	Ahrens	Hararuk	Luo	Clifford	Parton	Mueller	Bruun
Year	2019	2014	2017	2016	2014	1993	1997	2003
Turnover rates of the fast pool at 10°C (d^{-1})								
minimum	1.07×10^{-4}	4.57×10^{-4}	6.30×10^{-4}					
optimum	2.29×10^{-4}	4.57×10^{-3}	1.97×10^{-4}			9.32×10^{-5}	1.40×10^{-4}	1.40×10^{-4}
maximum	3.27×10^{-4}	2.28×10^{-2}	1.05×10^{-3}					
Turnover rates of the slow pool at 10°C (d^{-1})								
minimum	2.99×10^{-6}	4.57×10^{-7}	9.86×10^{-6}	1.00×10^{-4}	1.10×10^{-4}			
optimum	3.25×10^{-5}	2.28×10^{-5}	1.10×10^{-5}	3.00×10^{-4}	1.67×10^{-4}	2.10×10^{-6}	2.70×10^{-6}	4.30×10^{-5}
maximum	6.14×10^{-5}	4.57×10^{-5}	1.32×10^{-5}	6.00×10^{-4}	2.19×10^{-4}			
Portion of fast to slow pool = humification efficiency (dimensionless)								
minimum	0.05	0.05						
optimum	0.34	0.2				0.3	0.1	0.3
maximum	0.35	0.35						

References: Ahrens et al. (2014), Bruun et al. (2003), Clifford et al. (2014), Hararuk et al. (2017), Luo et al. (2016), Mueller et al. (1997), Parton et al. (1993). * Clifford et al. (2014) did not specify a base temperature for their model.

It is critical to understand model uncertainties and to test fundamental assumptions of how SOM is transferred between the pools (Sulman et al., 2018). The comparison between constrained and unconstrained humification efficiency in the Bayesian calibrations suggests that the sequential flow of carbon through the system might be assuming a condensation of stabile carbon that does not actually explain the vast majority of more stable SOM formation. From a theoretical perspective, one may wonder how large amounts of less complex SOM should become complex SOM without any involvement of living soil organisms. The way that the formation of complex carbon is represented in Daisy is probably a remainder of earlier humification theories from the 1990s that mostly ignored microbe involvement, while most of the recent studies suggest that the vast majority of SOM is of microbial origin (Cotrufo et al., 2013). A simple adaption for two-pool SOM models such as Daisy that include SMB pools could acknowledge this paradigm shift: the partitioning between slow- and fast-turnover SOM could be at the death of the microbial biomass (Figure 3 - 7) without any transfer of SOM from fast to slow pools (a brief test of this new structure is provided in Figure S 3 - 10). This would also be in alignment with the DSI concept, as aliphatic carbon should not spontaneously transform to aromatic-carboxylate carbon on its own. Then Daisy would fit better to the DSI and other proxies linking measurable fractions to SOM pools (the same is true for CENTURY and other models, which apply the same humification principle). The way that pools are linked in the current model configuration, is such that the actual turnover time of recalcitrant SOM consists of the turnover of the fast and slow SOM pools combined as it moves through these pools sequentially (Figure 3 - 1).

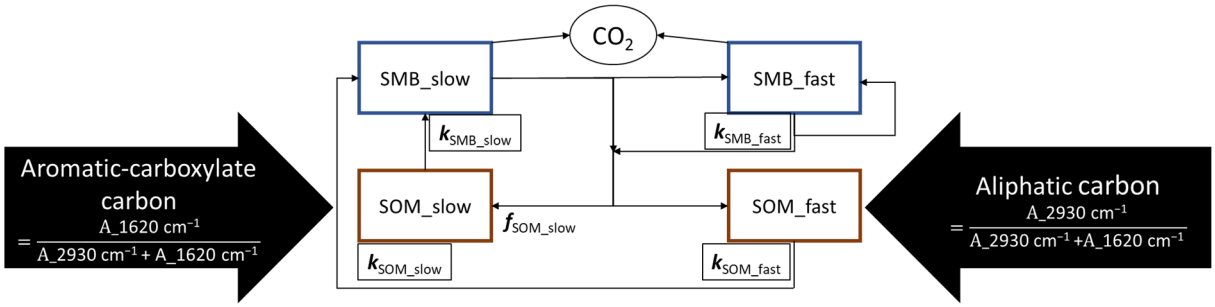

Figure 3 - 7 Suggested improvements to the internal cycling structure of SOM in the Daisy model. The division into fast- and slow-cycling SOM, corresponding to aliphatic and aromatic-carboxylate carbon follows the turnover or death of either SMB pool. Aliphatic carbon no longer becomes aromatic-carboxylate carbon without the involvement of microbes.

How strongly the basic model assumptions influence SOM simulations is also reflected when differences between one- and two-pool SOM models are compared. The turnover rates of the one-pool models are in between those of slow and fast SOM pools. However, our comparison shows that models with similar structure come to similar conclusions for SOM turnover. For example, the one-pool model in Clifford et al. (2014) was quite similar in turnover rates to that in Luo et al. (2016) but does not match well with two-pool models. Then again, the rates for the two-pool models of this study, and the studies by Ahrens et al. (2014) and Hararuk et al. (2017), were very similar in their minima and maxima, for both the slow and fast SOM pools, which shows that only models with a similar number of pools and transformations could be compared.

The 95% credibility intervals of half-lives in Daisy were in the range from 278 to 1095 years for the slow SOM pool and from 47 to 90 years for the fast SOM pool for the combination of sites presented in this study. If these values were reasonable – and as the three recently published Bayesian calibrations including this study are quite close in turnover rates (Table 3 - 5), this seems to be the case - SOM could be lost at much faster rates under mismanagement and global warming than earlier modeling results suggest. The rates may also be biased towards an underestimation of turnover, as even with intense efforts it is next to impossible to keep bare fallow plots completely free of vegetation (weeds) and roots from neighboring plots. Recent studies are in alignment with the possibility of relatively fast SOC loss across various scales from field scale (Poyda et al., 2019) to country scale. For example in Germany, agricultural soils are much more often a carbon source than a sink (Jacobs et al., 2018). This highlights the importance of adequate SOM management and a deeper understanding of the processes at different scales. Especially in the context of understanding the response of SOM to climate change, it is not enough if the SOM balance is simulated appropriately, but fluxes within the plant-soil system also need to be quantified. The reason is that under a warmer climate and changing soil moisture levels, the plant-derived carbon inputs will change. Furthermore, soil enzymatic analysis at regional and field levels (Ali et al., 2015, 2018) suggest that pools of different complexity have different temperature sensitivities (Lefèvre et al., 2014), which is also realized in new models (Hararuk et al.,

2017). If different pools have different responses to temperature, the formula by Bruun and Jensen (2002) for SOM pool distribution could not be used anymore, as it implicitly assumes a similar temperature sensitivity for all pools. In light of this, new proxies such as the DSI, soil fractionation or ^{14}C use (Menichetti et al., 2016), which could also be combined, are crucial for making SOM pools chemically or physically meaningful and for reducing model uncertainty and equifinality. As the DSI also had a good correlation with structurally protected SOM (Demyan et al., 2012), it could also fit very well to models that directly simulate the protection of SOM as a function of microbial activity (Sulman et al., 2014). A better understanding and the use of meaningful proxies such as DRIFTS, pyrolysis with DRIFTS (Nkwain et al., 2018) or thermal deconvolution (Cécillon et al., 2018; Demyan et al., 2013) in combination with Bayesian calibration and a wide range of long-term experiments are needed. The discrepancy between simulating SOM of tropical and temperate soils, which points towards a lack of understanding of fundamental differences in processes at work on the global scale would be the best test for future proxies and SOM models, which should be facilitated by freely available datasets for model testing and calibration.

3.6 Conclusion

We tested the use of the DRIFTS stability index as a proxy for initializing the two SOM pools in the Daisy model and used a Bayesian calibration to implement this proxy. A statistical analysis of model errors suggested that the use of the DRIFTS stability index to initialize the fast and slow SOM pools significantly reduced model errors in most cases, especially those with initially poor performance. The DSI therefore seems to be a robust proxy for distinguishing between fast- and slow-cycling SOM in order to initialize two-pool models and adds physicochemical meaning to the pools. As other studies have also shown, statistically sound approaches such as Bayesian calibration are needed to grasp the high uncertainty in SOM turnover, which is often neglected in modeling exercises. The results of the Bayesian optimization procedure further suggest that model performance could be improved by adjusting model parameters (turnover rates, humification efficiency) in the DSI initialization approach. Meaningful proxies such as DRIFTS, physical and chemical fractionation, or ^{14}C age assessments are likely to be the most robust way to initialize SOM pools, but their measurement method needs to be optimized to overcome known constraints, such as water and mineral interference in the case of the DSI. The results of this study suggest that the turnover of SOM could be much faster than assumed by commonly used SOM models. For example, the Daisy slow SOM pool half-life estimated in our study ranged from 278 to 1095 years (95% credibility intervals). The variability in parameters highlights the importance of including meaningful proxies in SOM models and conducting research on a larger gradient of soils with bare fallow and planted sites and over longer time frames.

3.7 Acknowledgements

This research was supported by the German Research Foundation (DFG) under the projects PAK 346 and the following research unit, FOR1695 Agricultural Landscapes under Global Climate Change – Processes and Feedbacks on a Regional Scale, within subproject P3 (CA 598/6-1 and CA 598/6-2). We would like to thank Elke Schulz from the Department of Soil Ecology, Helmholtz Centre for Environmental Research in Halle (Saale), for the provision of samples from Bad Lauchstädt. We would also like to thank Steffen Mehl, from the UCODE development team, for his help with the weighing of observations and the troubleshooting during the setup of UCODE_2014 on the bwUniCluster. Finally, we thank the editor and all the reviewers, especially Lauric Cécillon for the fruitful discussions during the review process. The authors acknowledge support by the state of Baden-Württemberg through the bwHPC project.

3.8 Data availability

Data of SOC from Ultuna and Bad Lauchstädt have already been published in the last decades and are cited in the text. The data of Kraichgau and Swabian Jura has not been published yet, but is provided in the graphs. The raw data which was used in this study is available in the supplement of this article.

3.9 References

Abramoff, R., Xu, X., Hartman, M., O'Brien, S., Feng, W., Davidson, E., Finzi, A., Moorhead, D., Schimel, J., Torn, M. and Mayes, M. A.: The Millennial model: in search of measurable pools and transformations for modeling soil carbon in the new century, Biogeochemistry, 137(1–2), 51–71, doi:10.1007/s10533-017-0409-7, 2018.

Ahrens, B., Reichstein, M., Borken, W., Muhr, J., Trumbore, S. E. and Wutzler, T.: Bayesian calibration of a soil organic carbon model using Δ14C measurements of soil organic carbon and heterotrophic respiration as joint constraints, Biogeosciences, 11(8), 2147–2168, doi:10.5194/bg-11-2147-2014, 2014.

Ali, R. S., Ingwersen, J., Demyan, M. S., Funkuin, Y. N., Wizemann, H.-D., Kandeler, E. and Poll, C.: Modelling in situ activities of enzymes as a tool to explain seasonal variation of soil respiration from agro-ecosystems, Soil Biol. Biochem., 81, 291–303, doi:10.1016/j.soilbio.2014.12.001, 2015.

Ali, R. S., Kandeler, E., Marhan, S., Demyan, M. S., Ingwersen, J., Mirzaeitalarposhti, R., Rasche, F., Cadisch, G. and Poll, C.: Controls on microbially regulated soil organic carbon decomposition at the regional scale, Soil Biol. Biochem., 118(December 2017), 59–68, doi:10.1016/j.soilbio.2017.12.007, 2018.

Andrén, O. and Kätterer, T.: ICBM: The introductory carbon balance model for exploration of soil carbon balances, Ecol. Appl., 7(4), 1226–1236, doi:10.1890/1051-0761(1997)007[1226:ITICBM]2.0.CO;2, 1997.

Bailey, V. L., Bond-Lamberty, B., DeAngelis, K., Grandy, A. S., Hawkes, C. V., Heckman, K., Lajtha, K., Phillips, R. P., Sulman, B. N., Todd-Brown, K. E. O. and Wallenstein, M. D.: Soil carbon cycling proxies: Understanding their critical role in predicting climate change feedbacks, Glob. Chang. Biol., 24(3), 895–905, doi:10.1111/gcb.13926, 2018.

Barré, P., Plante, A. F., Cécillon, L., Lutfalla, S., Baudin, F., Bernard, S., Christensen, B. T., Eglin, T., Fernandez, J. M., Houot, S., Kätterer, T., Le Guillou, C., Macdonald, A., van Oort, F. and Chenu, C.: The energetic and chemical signatures of persistent soil organic matter, Biogeochemistry, 130(1–2), 1–12, doi:10.1007/s10533-016-0246-0, 2016.

Blair, N., Faulkner, R. D., Till, A. R., Korschens, M. and Schulz, E.: Long-term management impacts on soil C, N and physical fertility. Part II: Bad Lauchstadt static and extreme FYM experiments, Soil Tillage Res., 91(1–2), 39–47, doi:10.1016/j.still.2005.11.001, 2006.

Bruun, S. and Jensen, L. S.: Initialisation of the soil organic matter pools of the Daisy model, Ecol. Modell., 153(3), 291–295, doi:10.17665/1676-4285.20155108, 2002.

Bruun, S., Christensen, B. T., Hansen, E. M., Magid, J. and Jensen, L. S.: Calibration and validation of the soil organic matter dynamics of the Daisy model with data from the Askov long-term experiments, Soil Biol. Biochem., 35(1), 67–76, doi:10.1016/S0038-0717(02)00237-7, 2003.

Calderón, F. J., Reeves, J. B., Collins, H. P. and Paul, E. A.: Chemical Differences in Soil Organic Matter Fractions Determined by Diffuse-Reflectance Mid-Infrared Spectroscopy, Soil Sci. Soc. Am. J., 75(2), 568–579, doi:10.2136/sssaj2009.0375, 2011.

Campbell, E. E. E. and Paustian, K.: Current developments in soil organic matter modeling and the expansion of model applications: a review, Environ. Res. Lett., 10(12), 123004, doi:10.1088/1748-9326/10/12/123004, 2015.

Cécillon, L., Baudin, F., Chenu, C., Houot, S., Jolivet, R., Kätterer, T., Lutfalla, S., Macdonald, A., van Oort, F., Plante, A. F., Savignac, F., Soucémarianadin, L. N. and Barré, P.: A model based on Rock-Eval thermal analysis to quantify the size of the centennially persistent organic carbon pool in temperate soils, Biogeosciences, 15(9), 2835–2849, doi:10.5194/bg-15-2835-2018, 2018.

Clifford, D., Pagendam, D., Baldock, J., Cressie, N., Farquharson, R., Farrell, M., Macdonald, L. and Murray, L.: Rethinking soil carbon modelling: a stochastic approach to quantify uncertainties, Environmetrics, 25(4), 265–278, doi:10.1002/env.2271, 2014.

Coleman, K. and Jenkinson, D. S.: RothC-26.3 - A Model for the turnover of carbon in soil, in Evaluation of Soil Organic Matter Models, pp. 237–246, Springer Berlin Heidelberg, Berlin, Heidelberg., 1996.

Cotrufo, M. F., Wallenstein, M. D., Boot, C. M., Denef, K. and Paul, E.: The Microbial Efficiency-Matrix Stabilization (MEMS) framework integrates plant litter decomposition with soil organic matter stabilization: do labile plant inputs form stable soil organic matter?, Glob. Chang. Biol., 19(4), 988–995, doi:10.1111/gcb.12113, 2013.

Demyan, M. S., Rasche, F., Schulz, E., Breulmann, M., Müller, T. and Cadisch, G.: Use of specific peaks obtained by diffuse reflectance Fourier transform mid-infrared spectroscopy to study the composition of organic matter in a Haplic Chernozem, Eur. J. Soil Sci., 63(2), 189–199, doi:10.1111/j.1365-2389.2011.01420.x, 2012.

Demyan, M. S., Rasche, F., Schütt, M., Smirnova, N., Schulz, E. and Cadisch, G.: Combining a coupled FTIR-EGA system and in situ DRIFTS for studying soil organic matter in arable soils, Biogeosciences, 10(5), 2897–2913, doi:10.5194/bg-10-2897-2013, 2013.

Ellerbrock, R. H. and Gerke, H. H.: Explaining soil organic matter composition based on associations between OM and polyvalent cations, J. Plant Nutr. Soil Sci., 181(5), 721–736, doi:10.1002/jpln.201800093, 2018.

Franko, U. and Merbach, I.: Modelling soil organic matter dynamics on a bare fallow Chernozem soil in Central Germany, Geoderma, 303(May), 93–98, doi:10.1016/j.geoderma.2017.05.013, 2017.

Gelman, A. and Rubin, D. B.: Inference from Iterative Simulation Using Multiple Sequences, Stat. Sci., 7(4), 457–472, doi:10.1214/ss/1177011136, 1992.

van Genuchten, M. T.: A comparison of numerical solutions of the one-dimensional unsaturated—saturated flow and mass transport equations, Adv. Water Resour., 5(1), 47–55, doi:10.1016/0309-1708(82)90028-8, 1982.

Giacometti, C., Demyan, M. S., Cavani, L., Marzadori, C., Ciavatta, C. and Kandeler, E.: Chemical and microbiological soil quality indicators and their potential to differentiate fertilization regimes in temperate agroecosystems, Appl. Soil Ecol., 64, 32–48, doi:10.1016/j.apsoil.2012.10.002, 2013.

Good, W. D. and Smith, N. K.: Enthalpies of combustion of toluene, benzene, cyclohexane, cyclohexene, methylcyclopentane, 1-methylcyclopentene, and n-hexane, J. Chem. Eng. Data, 14(1), 102–106, doi:10.1021/je60040a036, 1969.

Hansen, S., Jensen, L. S., Nielsen, N. E. and Svendsen, H.: The Soil Plant System Model Daisy - Basic Principles and Modelling Approach, Copenhagen: The Royal Veterinary and Agricultural University., 1993.

Hansen, S., Abrahamsen, P., Petersen, C. T. and Styczen, M.: Daisy: Model Use, Calibration, and Validation, Trans. ASABE, 55(4), 1317–1335, doi:10.13031/2013.42244, 2012.

Hararuk, O., Shaw, C. and Kurz, W. A.: Constraining the organic matter decay parameters in the CBM-CFS3 using Canadian National Forest Inventory data and a Bayesian inversion technique, Ecol. Modell., 364, 1–12, doi:10.1016/j.ecolmodel.2017.09.008, 2017.

Heinlein, F., Biernath, C., Klein, C., Thieme, C. and Priesack, E.: Evaluation of Simulated Transpiration from Maize Plants on Lysimeters, Vadose Zo. J., 16(1), 1–16, doi:10.2136/vzj2016.05.0042, 2017.

Herbst, M., Welp, G., Macdonald, A., Jate, M., Hädicke, A., Scherer, H., Gaiser, T., Herrmann, F., Amelung, W. and Vanderborght, J.: Correspondence of measured soil carbon fractions and RothC pools for equilibrium and non-equilibrium states, Geoderma, 314(November 2017), 37–46, doi:10.1016/j.geoderma.2017.10.047, 2018.

Jacobs, A., Flessa, H., Don, A., Heidkamp, A., Prietz, R., Dechow, R., Gensior, A., Poeplau, C., Riggers, C., Schneider, F., Tiemeyer, B., Vos, C., Wittnebel, M., Müller, T., Säurich, A., Fahrion-Nitschke, A., Gebbert, S., Hopfstock, R., Jaconi, A., Kolata, H., Lorbeer, M., Schröder, J., Laggner, A., Weiser, C. and Freibauer, A.: Landwirtschaftlich genutzte Böden in Deutschland – Ergebnisse der Bodenzustandserhebung - Thünen Report 64, Johann Heinrich von Thünen-Institut, Bundesallee 50, 38116 Braunschweig, Germany., 2018.

Jensen, L. S., Mueller, T., Nielsen, N. E., Hansen, S., Crocker, G. J., Grace, P. R., Klír, J., Körschens, M. and Poulton, P. R.: Simulating trends in soil organic carbon in long-term experiments using the soil-plant-atmosphere model DAISY, Geoderma, 81(1), 5–28, doi:http://dx.doi.org/10.1016/S0016-7061(97)88181-5, 1997.

Joergensen, R. G. and Mueller, T.: The fumigation-extraction method to estimate soil microbial biomass: Calibration of the kEC value, Soil Biol. Biochem., 28(1), 25–31, doi:10.1016/0038-0717(95)00102-6, 1996.

Kätterer, T., Bolinder, M. A., Andrén, O., Kirchmann, H. and Menichetti, L.: Roots contribute more to refractory soil organic matter than above-ground crop residues, as revealed by a long-term field experiment, Agric. Ecosyst. Environ., 141(1–2), 184–192, doi:10.1016/j.agee.2011.02.029, 2011.

Kirchmann, H., Haberhauer, G., Kandeler, E., Sessitsch, A. and Gerzabek, M. H.: Effects of level and quality of organic matter input on carbon storage and biological activity in soil: Synthesis of a long-term experiment, Global Biogeochem. Cycles, 18(4), 1–9, doi:10.1029/2003GB002204, 2004.

Klein, C., Biernath, C., Heinlein, F., Thieme, C., Gilgen, A. K., Zeeman, M. and Priesack, E.: Vegetation Growth Models Improve Surface Layer Flux Simulations of a Temperate Grassland, Vadose Zo. J., 16(13), 1–19, doi:10.2136/vzj2017.03.0052, 2017.

Klein, C. G.: Modeling fluxes of energy and water between land surface and atmosphere for grass- and cropland system, Fakultät Wissenschaftszentrum Weihenstephan., 2018.

Kozak, M. and Piepho, H. P.: What's normal anyway? Residual plots are more telling than significance tests when checking ANOVA assumptions, J. Agron. Crop Sci., 204(1), 86–98, doi:10.1111/jac.12220, 2018.

Laub, M., Blagodatsky, S., Nkwain, Y. F. and Cadisch, G.: Soil sample drying temperature affects specific organic mid-DRIFTS peaks and quality indices, Geoderma, 355, 113897, doi:10.1016/j.geoderma.2019.113897, 2019.

Lefèvre, R., Barré, P., Moyano, F. E., Christensen, B. T., Bardoux, G., Eglin, T., Girardin, C., Houot, S., Kätterer, T., van Oort, F. and Chenu, C.: Higher temperature sensitivity for stable than for labile soil organic carbon - Evidence from incubations of long-term bare fallow soils, Glob. Chang. Biol., 20(2), 633–640, doi:10.1111/gcb.12402, 2014.

Lu, D., Ye, M. and Hill, M. C.: Analysis of regression confidence intervals and Bayesian credible intervals for uncertainty quantification, Water Resour. Res., 48(9), 1–20, doi:10.1029/2011WR011289, 2012.

Lu, D., Ye, M., Hill, M. C., Poeter, E. P. and Curtis, G. P.: A computer program for uncertainty analysis integrating regression and Bayesian methods, Environ. Model. Softw., 60(October), 45–56, doi:10.1016/j.envsoft.2014.06.002, 2014.

Luo, Z., Wang, E., Shao, Q., Conyers, M. K. and Liu, D. L.: Confidence in soil carbon predictions undermined by the uncertainties in observations and model parameterisation, Environ. Model. Softw., 80, 26–32, doi:10.1016/j.envsoft.2016.02.013, 2016.

Margenot, A. J., Calderón, F. J., Bowles, T. M., Parikh, S. J. and Jackson, L. E.: Soil Organic Matter Functional Group Composition in Relation to Organic Carbon, Nitrogen, and Phosphorus Fractions in Organically Managed Tomato Fields, Soil Sci. Soc. Am. J., 79(3), 772–782, doi:10.2136/sssaj2015.02.0070, 2015.

Menichetti, L., Kätterer, T. and Leifeld, J.: Parametrization consequences of constraining soil organic matter models by total carbon and radiocarbon using long-term field data, Biogeosciences, 13(10), 3003–3019, doi:10.5194/bg-13-3003-2016, 2016.

Minasny, B., Malone, B. P., McBratney, A. B., Angers, D. A., Arrouays, D., Chambers, A., Chaplot, V., Chen, Z.-S., Cheng, K., Das, B. S., Field, D. J., Gimona, A., Hedley, C. B., Hong, S. Y., Mandal, B., Marchant, B. P., Martin, M., McConkey, B. G., Mulder, V. L., O'Rourke, S., Richer-de-Forges, A. C., Odeh, I., Padarian, J., Paustian, K., Pan, G., Poggio, L., Savin, I., Stolbovoy, V., Stockmann, U., Sulaeman, Y., Tsui, C.-C., Vågen, T.-G., van Wesemael, B. and Winowiecki, L.: Soil carbon 4 per mille, Geoderma, 292, 59–86, doi:10.1016/j.geoderma.2017.01.002, 2017.

Monteith, J. L.: Evaporation and surface temperature, Q. J. R. Meteorol. Soc., 12, 513–522, doi:10.1002/qj.49710745102, 1976.

Mualem, Y.: A new model for predicting the hydraulic conductivity of unsaturated porous media, Water Resour. Res., 12(3), 513–522, doi:10.1029/WR012i003p00513, 1976.

Mueller, T., Jensen, L. S. S., Magid, J. and Nielsen, N. E. E.: Temporal variation of C and N turnover in soil after oilseed rape straw incorporation in the field: simulations with the soil-plant-atmosphere model DAISY, Ecol. Modell., 99(2), 247–262, doi:http://dx.doi.org/10.1016/S0304-3800(97)01959-5, 1997.

Mueller, T., Magid, J., Jensen, L. S., Svendsen, H. and Nielsen, N. E.: Soil C and N turnover after incorporation of chopped maize, barley straw and blue grass in the field: Evaluation of the DAISY soil–organic-matter submodel, Ecol. Modell., 111(1), 1–15, doi:10.1016/S0304-3800(98)00094-5, 1998.

Nguyen, T., Janik, L. and Raupach, M.: Diffuse reflectance infrared fourier transform (DRIFT) spectroscopy in soil studies, Soil Res., 29(1), 49–67, doi:10.1071/SR9910049, 1991.

Nkwain, F. N., Demyan, M. S., Rasche, F., Dignac, M.-F., Schulz, E., Kätterer, T., Müller, T. and Cadisch, G.: Coupling pyrolysis with mid-infrared spectroscopy (Py-MIRS) to fingerprint soil organic matter bulk chemistry, J. Anal. Appl. Pyrolysis, 133(April 2017), 176–184, doi:10.1016/j.jaap.2018.04.004, 2018.

Nocita, M., Stevens, A., van Wesemael, B., Aitkenhead, M., Bachmann, M., Barthès, B., Ben Dor, E., Brown, D. J., Clairotte, M., Csorba, A., Dardenne, P., Demattê, J. A. M., Genot, V., Guerrero, C., Knadel, M., Montanarella, L., Noon, C., Ramirez-Lopez, L., Robertson, J., Sakai, H., Soriano-Disla, J. M., Shepherd, K. D., Stenberg, B., Towett, E. K., Vargas, R. and Wetterlind, J.: Soil Spectroscopy: An Alternative to Wet Chemistry for Soil Monitoring, in Advances in Agronomy, vol. 132, pp. 139–159., 2015.

O'Leary, G. J., Liu, D. L., Ma, Y., Li, F. Y., McCaskill, M., Conyers, M., Dalal, R., Reeves, S., Page, K., Dang, Y. P. and Robertson, F.: Modelling soil organic carbon 1. Performance of APSIM crop and pasture modules against long-term experimental data, Geoderma, 264(November 2015), 227–237, doi:10.1016/j.geoderma.2015.11.004, 2016.

Parton, W. J., Schimel, D. S., Cole, C. V. and Ojima, D. S.: Analysis of Factors Controlling Soil Organic Matter Levels in Great Plains Grasslands1, Soil Sci. Soc. Am. J., 51(5), 1173, doi:10.2136/sssaj1987.03615995005100050015x, 1987.

Parton, W. J., Scurlock, J. M. O., Ojima, D. S., Gilmanov, T. G., Scholes, R. J., Schimel, D. S., Kirchner, T., Menaut, J.-C., Seastedt, T., Garcia Moya, E., Kamnalrut, A. and Kinyamario, J. I.: Observations and modeling of biomass and soil organic matter dynamics for the grassland biome worldwide, Global Biogeochem. Cycles, 7(4), 785–809, doi:10.1029/93GB02042, 1993.

Pengerud, A., Cécillon, L., Johnsen, L. K., Rasse, D. P. and Strand, L. T.: Permafrost Distribution Drives Soil Organic Matter Stability in a Subarctic Palsa Peatland, Ecosystems, 16(6), 934–947, doi:10.1007/s10021-013-9652-5, 2013.

Piepho, H. P., Büchse, A. and Richter, C.: A Mixed Modelling Approach for Randomized Experiments with Repeated Measures, J. Agron. Crop Sci., 190(4), 230–247, doi:10.1111/j.1439-037X.2004.00097.x, 2004.

Poeplau, C., Don, A., Dondini, M., Leifeld, J., Nemo, R., Schumacher, J., Senapati, N. and Wiesmeier, M.: Reproducibility of a soil organic carbon fractionation method to derive RothC carbon pools, Eur. J. Soil Sci., 64(6), 735–746, doi:10.1111/ejss.12088, 2013.

Poeter, E. P., Hill, M. C., Banta, E. R., Mehl, S. and Christensen, S.: UCODE_2005 and six other computer codes for universal sensitivity analysis, inverse modeling, and uncertainty evaluation, U.S. Geological Survey Techniques and Methods 6-A11, 283p. (As updated in Feb 2008)., 2005.

Poeter, E. P., Hill, M. C., Lu, D., Tiedeman, C. R. and Mehl, S.: UCODE_2014, with New Capabilities to Define Parameters Unique to Predictions, Calculate Weights using Simulated Values, Estimate Parameters with SVD, Evaluate Uncertainty with MCMC, and More, Integrated Groundwater Modeling Center Report Number: GWMI 2014-02., 2014.

Poyda, A., Wizemann, H.-D., Ingwersen, J., Eshonkulov, R., Högy, P., Demyan, M. S., Kremer, P., Wulfmeyer, V. and Streck, T.: Carbon fluxes and budgets of intensive crop rotations in two regional climates of southwest Germany, Agric. Ecosyst. Environ., 276, 31–46, doi:10.1016/j.agee.2019.02.011, 2019.

Segoli, M., De Gryze, S., Dou, F., Lee, J., Post, W. M., Denef, K. and Six, J.: AggModel: A soil organic matter model with measurable pools for use in incubation studies, Ecol. Modell., 263, 1–9, doi:10.1016/j.ecolmodel.2013.04.010, 2013.

Sohi, S. P., Mahieu, N., Arah, J. R. M., Powlson, D. S., Madari, B. and Gaunt, J. L.: A Procedure for Isolating Soil Organic Matter Fractions Suitable for Modeling, Soil Sci. Soc. Am. J., 65(4), 1121, doi:10.2136/sssaj2001.6541121x, 2001.

Stevenson, F. J.: Humus chemistry: genesis, composition, reactions, John Wiley & Sons, New York., 1994.

Sulman, B. N., Phillips, R. P., Oishi, A. C., Shevliakova, E. and Pacala, S. W.: Microbe-driven turnover offsets mineral-mediated storage of soil carbon under elevated CO2, Nat. Clim. Chang., 4(12), 1099–1102, doi:10.1038/nclimate2436, 2014.

Sulman, B. N., Moore, J. A. M., Abramoff, R., Averill, C., Kivlin, S., Georgiou, K., Sridhar, B., Hartman, M. D., Wang, G., Wieder, W. R., Bradford, M. A., Luo, Y., Mayes, M. A., Morrison, E., Riley, W. J., Salazar, A., Schimel, J. P., Tang, J. and Classen, A. T.: Multiple models and experiments underscore large uncertainty in soil carbon dynamics, Biogeochemistry, 141(2), 109–123, doi:10.1007/s10533-018-0509-z, 2018.

Tinti, A., Tugnoli, V., Bonora, S. and Francioso, O.: Recent applications of vibrational mid-infrared (IR) spectroscopy for studying soil components: A review, J. Cent. Eur. Agric., 16(1), 1–22, doi:10.5513/JCEA01/16.1.1535, 2015.

Vrugt, J. A.: Markov chain Monte Carlo simulation using the DREAM software package: Theory, concepts, and MATLAB implementation, Environ. Model. Softw., 75, 273–316, doi:10.1016/j.envsoft.2015.08.013, 2016.

Wattenbach, M., Gottschalk, P., Hatterman, C., Rachimow, C., Flechsig, M. and Smith, P.: A framework for assessing uncertainty in ecosystem models, in Proceedings of the iEMSs Third Biennial Meeting, p. Paper 373, International Environmental Modeling and Software Society. [online] Available from: https://abdn.pure.elsevier.com/en/publications/a-framework-for-assessing-uncertainty-in-ecosystem-models, 2006.

Wizemann, H.-D., Ingwersen, J., Högy, P., Warrach-Sagi, K., Streck, T. and Wulfmeyer, V.: Three year observations of water vapor and energy fluxes over agricultural crops in two regional climates of Southwest Germany, Meteorol. Zeitschrift, 24(1), 39–59, doi:10.1127/metz/2014/0618, 2015.

Yeasmin, S., Singh, B., Johnston, C. T. and Sparks, D. L.: Evaluation of pre-treatment procedures for improved interpretation of mid infrared spectra of soil organic matter, Geoderma, 304, 83–92, doi:10.1016/j.geoderma.2016.04.008, 2017.

Zimmermann, M., Leifeld, J., Schmidt, M. W. I., Smith, P. and Fuhrer, J.: Measured soil organic matter fractions can be related to pools in the RothC model, Eur. J. Soil Sci., 58(3), 658–667, doi:10.1111/j.1365-2389.2006.00855.x, 2007.

4 Modeling temperature sensitivity of soil organic matter decomposition: splitting the pools*

Moritz Laub[1], Rana Shahbaz Ali[2], Michael Scott Demyan[3], Yvonne Funkuin Nkwain[1], Christian Poll[2], Petra Högy[4], Arne Poyda[5], Joachim Ingwersen[6], Sergey Blagodatsky[1], Ellen Kandeler[2], Georg Cadisch[1]

[1]Institute of Agricultural Sciences in the Tropics (Hans-Ruthenberg-Institute), University of Hohenheim, 70599 Stuttgart, Germany

[2]Institute of Soil Science and Land Evaluation, Soil Biology Department, University of Hohenheim, 70599 Stuttgart, Germany

[3]School of Environment and Natural Resources, The Ohio State University, Columbus, OH, USA, 43210

[4]Institute of Landscape and Plant Ecology-Plant, Plant Ecology Section, University of Hohenheim, 70599 Stuttgart, Germany

[5]Institute of Crop Science and Plant Breeding, Grass and Forage Science/ Organic Agriculture, Kiel University, 24118 Kiel, Germany

[6]Institute of Soil Science and Land Evaluation-Biogeophysics Section, University of Hohenheim, 70599 Stuttgart, Germany

*This chapter has been reprinted from Laub, M., Ali, R.S., Demyan, M.S., Nkwain, Y.F., Poll, C., Högy, P., Poyda, A., Ingwersen, J., Blagodatsky, S., Kandeler, E., Cadisch, G., 2021. Modeling temperature sensitivity of soil organic matter decomposition: Splitting the pools. *Soil Biol. Biochem.* 153, 108108. The original article is available at:

https://www.sciencedirect.com/science/article/abs/pii/S0038071720304041?via%3Dihub

4.1 Abstract

The direction and magnitude of change of soil organic carbon (SOC) stocks due to global warming depend strongly on the temperature sensitivity (e.g., Q_{10}) of carbon mineralization. To date, most multi-pool SOC models assume a general Q_{10} of 2 despite experimental evidence suggesting different Q_{10} for different carbon fractions. The aim of this study was to test if the use of experimentally derived pool specific Q_{10} values improves the performance of SOC models. Five contrasting data sets from three field experiments and two laboratory incubations were used to study the link between carbon pool recalcitrance and Q_{10} using two different approaches: a) Bayesian calibration of the Daisy SOC model parameters to infer Q_{10} of SOC and crop-litter pools, and b) using measured Q_{10} values of carbon degrading enzymes as proxies for Q_{10} of different Daisy pools. Namely β-glucosidase (median Q_{10} of 1.82) was assigned to metabolic litter and phenol/peroxidase (1.35) to structural litter and both SOC pools. To partition litter-carbon and SOC into model pools, the lignin-to-nitrogen ratio and the ratio of aliphatic/aromatic-carboxylate carbon were used, respectively. Measurements included soil microbial biomass, soil carbon dioxide (CO_2) evolution and remaining carbon in soils and crop-litter. In the Bayesian calibration, strong differences in inferred Q_{10} values of the same pools between experiments suggested that intrinsic substrate recalcitrance was not the main driver of temperature sensitivity. For field experiment simulations, both the Q_{10} values derived by Bayesian calibration and measured enzyme Q_{10} were centered around values below 2, contrasting with high Q_{10} values for mineralization under laboratory incubations (close to 3). Furthermore, assigning measured phenol/peroxidase Q_{10} values to the slow crop-litter as well as both SOC pools and ß-glucosidase to the fast crop-litter pool (approach b), could significantly improve model performance compared to using the default Q_{10} value of 2 for all pools. Root-mean-squared-deviation reductions were between 3-10% for field experiments, with no change in the laboratory experiments. Thus, site specific Q_{10} values of soil enzymes show potential as proxies for pool specific Q_{10}. We present a new conceptual framework to explain the observed differences in temperature sensitivities between experiments as a result of two fundamental driving factors classified in a) state variables, that fluctuate in time, and b) soil properties, that are constant over decades. Measured enzyme Q_{10} values were interpreted as a proxy incorporating both factors. More than intrinsic substrate recalcitrance, the state variables such as physical protection, substrate abundance and unfavorable conditions for microorganisms control temperature sensitivity of mineralization. To reduce the uncertainty in global SOC simulations under a changing climate, their relative contributions should be disentangled and then implemented into SOC models.

4.2 Introduction

The increase in global temperature will most likely enhance the activity of soil organic carbon (SOC) degrading microorganisms, possibly increasing losses of global soil carbon stocks (Davidson and Janssens, 2006). The extent of such losses will largely depend on the temperature sensitivity (TS) of SOC mineralization. Chemical substrate recalcitrance (Bosatta and Ågren, 1999) and physical protection of substrate (Benbi et al., 2014) were suggested to control the apparent TS (Davidson and Janssens, 2006) observed in the field by either determining the required energy for decomposition and thus the attractiveness for microbes (recalcitrance), or by limiting the access of microbes to substrate (protection). In the long run, the interplay of both determines the microbial community (Alster et al., 2016b, 2016a) as another potential influencer on TS (Robertson et al., 2019; Wieder et al., 2018). The debate whether substrate properties or protection mechanisms are more important for the apparent TS has been ongoing for decades (e.g. Ågren and Wetterstedt, 2007; Conant et al., 2011; Sierra et al., 2015b) and is yet to be resolved (Moinet et al., 2020).

The TS in soil organic matter (SOM) process models is often expressed in the form of a Q_{10} value, the multiplicator of decomposition activity with 10 °C temperature increase (e.g. a Q_{10} of 2 means a doubling of reaction rate with +10 °C ; see equation S4 - 1 and S4 - 2). Due to difficulties in defining recalcitrance and a lack of consensus, a Q_{10} value of 2 is assumed in most models for all carbon complexities (Sierra et al., 2015b). However, experimentally evaluated Q_{10} values vary largely at regional scales depending on soil types. The measured ranges can be as high as 1.2 to 2.8 (Meyer et al., 2018), which would translate to a range of 10 to 70% faster mineralization, with an exemplary warming of 5 C. Thus, the simplified constancy of Q_{10} presents one of the largest uncertainties in global carbon models (Tang and Riley, 2015). Therefore, a better understanding of what ultimately determines TS of SOC mineralization and how to implement varying TS into models is needed for modeling the potential impact of global climate change on SOC stocks.

The well-established carbon–quality–temperature (CQT) theory suggests that TS of SOC is an intrinsic property of each carbon compound (Bosatta and Ågren, 1999; Sierra, 2012), increasing with carbon recalcitrance - a direct result of the number of enzymatic steps and activation energy needed for decomposition. The term recalcitrance is often not clearly defined, so to be able to measure recalcitrance, within this study we defined recalcitrance as having a higher aromaticity of carbon compounds (Kiem et al., 2000; Wagai et al., 2013; Wang et al., 2019). In SOC models with discrete pools, the CQT theory would mean pool specific TS for each pool. Different TS of different SOC constituents could explain why a single temperature function for all constituents becomes increasingly uncertain at higher temperatures (Lloyd and Taylor, 1994). However, the connection between recalcitrance and temperature sensitivity has been cast into doubt by molecular analysis of SOC and

it's age (Kleber et al., 2011). Thus, pool specific TS need to be based on measurements instead of theoretical assumptions.

The activity of soil enzymes and their TS are closely linked to soil organic carbon degradation (Ali et al., 2015; Sinsabaugh and Follstad Shah, 2012). Measured TS of different soil enzyme activities could thus be a potential proxy for mineralization TS of different pools. Differences in TS between enzyme activities of β-glucosidase, xylanase and phenol/peroxidase (Nottingham et al., 2016) could then represent TS differences between different carbon compounds or different carbon pools in models. Testing this link is particularly interesting, because phenol/peroxidase in comparative studies was the enzyme with lowest TS (Ali et al., 2015; Nottingham et al., 2016), thus contradicting the CQT theory. As enzymes are rate limiting (Sinsabaugh et al., 2008), their TS could be representative of apparent TS for SOC decomposition. Another option to gain insights into the relation between recalcitrance and apparent TS could come from inverse modelling (e.g., Hararuk et al., 2017). Bayesian calibration, which provides probabilistic information on process variables, given a model and measured data, is a useful tool to infer variables, which are not directly measurable in the field. The combination of several field sites in Bayesian calibration can reduce parameter uncertainty (Laub et al., 2020), and so pool specific TS could be inferred as a general pool property in case TS reflects an intrinsic pool property like recalcitrance.

The aim of this study was to clarify whether the measured enzymes' TS can help in modeling the overall TS of SOM mineralization. Furthermore, we tested if the CQT theory could be confirmed trough Bayesian calibration using the established SOC multi-pool model Daisy (Hansen et al., 2012).

The following hypotheses were tested:

1) Bayesian calibration can infer different TS of different organic carbon pools from measured experimental data, if pools are clearly defined, and
2) these inferred TS are a consistent property of each pool.
3) Measured enzyme activity TS's represent suitable proxies for these different carbon pools' TS, thus
4) Bayesian calibration derived TS and measured enzyme activity TS show similar patterns for similar pool definitions.

This study relied on measurable pool definitions to distinguish carbon pools of different recalcitrance and activation energies. For SOC pools, the recently developed pool partitioning method by mid-infrared spectroscopy was used, which classifies SOC into aliphatic carbon in the fast pool and aromatic-carboxylate carbon in the slow pool. This pool partitioning was superior to using the default Daisy assumption that SOC is at steady state (Laub et al., 2020). For litter inputs the long-established

lignin-to-nitrogen ratio (Parton et al., 1987) was used for pool partitioning. Due to the aim to derive TS as a general pool property, five different datasets were combined for this study, including fallow and cropped soils in laboratory and field experiments, covering the time span of weeks to several decades.

4.3 Material and methods

4.3.1 Overview of the five experiments and their datasets

To infer and test pool specific TS for SOC models under a range of different conditions and draw general conclusions, five different experiments were combined, including new and already published data. These were bare fallow plots (Exp. 1) and cropped plots (Exp. 2) of an agricultural field of medium duration; a crop-litter decomposition study using litterbags in fields (Exp. 3); as well as laboratory incubations of crop-litter in soil at two different temperatures (Exp. 4); and of soils from long-term bare fallow plots at four different temperatures (Exp. 5). Several variables were measured in the different experiments including soil microbial biomass (SMB), SOC and CO_2 evolution.

4.3.1.1 Experiments 1 and 2: Bare fallow and cropped plots within agricultural fields

The seven-year monitoring experiments 1 and 2 consisted of bare fallow (Exp. 1; soil data from Laub et al., 2020) and cropped (Exp. 2) plots in six agricultural fields in two different regions (Kraichgau and Swabian Jura) in Southwest Germany with measurements carried out in three replicated plots per field, placed at representative locations at the edge of eddy covariance station footprints (Demyan et al., 2016). Mean annual temperatures (Table 4 - 1) of the Kraichgau region (9.4 °C;) are warmer, while mean annual precipitation (890 mm) is lower than in the Swabian Jura region (7.5 °C; 1040 mm; measured in 1981-2010; Eshonkulov et al., 2019). The bare fallow plots (5 x 5 m) were established in spring 2009 and maintained by manual weeding and spot application of glyphosate. The adjacent cropped plots of the same size (Ali et al., 2015) were subject to normal management and crop rotations including winter wheat, silage maize, winter rapeseed, winter barley, spring barley and cover crops (specific rotation details in Poyda et al., 2019; Table 2). Soils of both treatments were sampled to 30 cm depth at the start of experiments and then up to four times per year to measure soil microbial biomass (SMB) by the chloroform fumigation extraction method (Joergensen, 1996). This was done from 2009 to 2016 for fallow plots (~20 serial measurements per plot in total) and 2012 to 2016 in cropped plots (~10 serial measurements in total). Additionally, soil surface CO_2 efflux was measured several times throughout the growing period of different years (2009, 5x; 2010, 15x; 2014, 3x; 2015, 7x) and an intensive campaign in 2012-13 (May 2012 – June 2013, 40x), where measurements were conducted weekly to biweekly. Portable infrared gas analyzers (EGM-2 and EGM-4, PP Systems Amesbury, Massachusetts, USA) were used for soil surface CO_2 efflux measurements (further details in Demyan et al., 2016, who used the data until 2012). Enzyme activities were measured in monthly intervals from

April 2012 to April 2013 (dates in Table S4 - 4). Furthermore, plant development was intensely monitored in Exp. 2, including development stage, and measurements of biomass carbon and nitrogen at shoot development, full flouring and maturity (supplement section S4), and used for calibrating the crop-growth model.

Table 4 - 1 Soil characteristics of the manipulation experiments used in this study; soil types classified according to IUSS Working Group WRB 2007. Experiment 3 was conducted in the same region as experiment 1 and 2, but as it had 13 sites, the detailed information was moved to Table S4 - 3.

Study Site or origin of soil/ Experiment no.	UTM Degrees Latitude	UTM Degrees Longitude	Mean annual temperature (°C)/ precipitation (mm)	Study type	Soil type	Clay (%)	Silt (%)	Initial SOC (%)	Bulk density (Mg/m^3)	Initial SOC stocks 0-30 cm (Mg/ha)	Years used in this study	Replicates per trial (n)
Kraichgau 1 **/1+2**	48.928517	8.702794		Field manipulation (fallow/ vegetated)	Stagnic Luvisol	18	77	0.90	1.37	37.10	2009 - 16	3
Kraichgau 2 **/1+2**	48.927748	8.708884	9.4/890[A]	Field manipulation (fallow/ vegetated)	Stagnic Luvisol	18	80	1.04	1.33	41.61	2009 - 16	3
Kraichgau 3 **/1+2**	48.927197	8.715891		Field manipulation (fallow/ vegetated)	Stagnic Luvisol	17	81	0.89	1.44	38.50	2009 - 16	3
Swabian Jura 4 **/1+2**	48.527510	9.769429		Field manipulation (fallow/ vegetated)	Calcic Luvisol	38	56	1.78	1.32	70.33	2009 - 16	3
Swabian Jura 5 **/1+2**	48.529857	9.773253	7.5/1040[A]	Field manipulation (fallow/ vegetated)	Anthrosol	29	68	1.95	1.38	80.85	2009 - 16	3
Swabian Jura 6 **/1+2**	48.547035	9.773176		Field manipulation (fallow/ vegetated)	Rendzic Leptosol	45	51	1.91	1.07	61.27	2009 - 16	3
Kraichgau and Swabian Jura **/3**	For data on the 13 sites of experiment 3 please refer to Table S 4 - 1										2015 - 16	3
Crop-litter laboratory incubation **/4**	48.739626	8.931971	NA	Incubation of crop residues in bulk soil	Haplic Luvisol	23	75	2.25	1.21		2018	3
Ultuna **/5**	59.821879	17.656348	5.4/570[B]	Incubation of bulk soil	Eutric Cambisol	37	41	1.50	1.44		1956, 2009	4

UTM = Universal Transverse Mercator reference system; [A] (Eshonkulov et al., 2019); [B] (Menichetti et al., 2013)

4.3.1.2 Experiment 3: Regional litterbag decomposition study

The litterbag decomposition study was conducted in the adjacent areas of Exp. 1 and 2. At 10 sites per region (Table S4 - 3), three crop-litter types (wheat, maize and rapeseed straw; Table 4 - 2) were buried at 10 cm depth on October 24, 2015 in Kraichgau and October 29, 2015 in Swabian Jura, using three replicates for each crop-litter type at each recovery date. They were buried in litterbags (50 µm mesh,

7 x 7 cm bag size), each containing 4 g of dry matter-based air-dried litter, cut to 2 cm size. Three replicate litterbags of each litter type were retrieved at each sampling date, i.e. one, six and nine months after burial (Table 4 - 2). The remaining litter inside each litterbag (10 sites x 2 regions x 3 litter types x 3 times x 3 replicates = 540 litterbags) was dried, weighed and analyzed for carbon and nitrogen content using an elemental analyzer. Measurements were corrected to ash free dry matter content. Soil moisture and temperature at 15 cm depth were continuously monitored since 2009 at these sites (details including instrumentation in Poltoradnev et al., 2015). Due to sensor breakdown, only 13 out of the 20 sites could be simulated in the end.

Table 4 - 2 Characteristics the crop-litters that were used in the litter incubation experiments in the laboratory as well as in the regional litterbag incubations.

Experiment No/type	Crop residue	Carbon content (%DM)	Nitrogen content (%DM)	Lignin content (%DM)	Carbon/ Nitrogen ratio	Lignin/ Nitrogen ratio	Dates of litterbag retrieval (after 1,6 and 10 months)	
							Kraichgau	Swabian Jura
3/ Regional litterbag incubation	Rapeseed	37.3	0.7	8.3	55.7	12.4	23.11.15; 23.04.16; 01.07.16	25.11.15; 25.04.16; 08.07.16
	Wheat	41.8	0.48	6.4	86.6	13.3		
	Maize	43.1	0.61	5.8	70.1	9.4		
							Amount applied g g^{-1} soil *100 (DM)	
4/ Crop-litter laboratory incubation	Maize	43.3	0.83	4.8	52.1	5.8	1.83	
	Wheat	42.9	1.06	7.1	40.5	6.7	1.85	
	Barley	43.1	0.57	7.0	76.1	12.4	1.84	
	Soybean	43.1	0.88	14.1	48.9	16.0	1.84	
	Sunflower	41.4	0.36	12.1	115.6	33.7	1.92	

DM = dry matter;

4.3.1.3 Experiment 4: Laboratory crop-litter incubations at different temperatures

For the laboratory crop-litter incubation, air dried litter of different quality was used, harvested in 2016 from fields of Exp. 2. Litter (8.58 µg C g^{-1} soil) of maize, wheat, barley, soybean and sunflower (Table 4 - 2), cut to 1 cm size, was incubated in soil within airtight glass jars (750 ml) in climate chambers at 15 °C or 25 °C. The experiment was a randomized complete block design with three replications per treatment including a soil only control at each temperature. Samples for CO_2 and SMB-C measurements were incubated in different jars. The CO_2 jars contained 50 g of soil, while SMB-C jars contained initially 150 g of soil, from which a subsample was taken at each measurement. The soil originated from 0-10 cm topsoil of a *Miscanthus giganteus* (C4) experiment (Gauder et al., 2016), located 25 km Southwest of Kraichgau fields with similar soil texture. Soil was sieved (< 2 mm) to remove roots and rhizomes and then submerged in water and agitated to remove floating fine roots, dried at 40 °C and preincubated at 70% water holding capacity and 25 °C for two weeks. Evolution of CO_2 was measured by passive trapping in 1 M NaOH at day 1, 3, 6, 10, 15, 23, 31, 38, 50, 63 and 80, precipitation of carbonates with 1M $BaCl_2$ (Poll et al., 2008), and titration with 0.1 M HCl. For the SMB

measurements, by the chloroform fumigation extraction method (Joergensen, 1996), 20 g of sample were removed from the 150 g soil jars at days 0, 7, 15, 41 and 78. Experiment 4 resulted in 396 CO_2 (6 treatments x 3 replicates x 2 temperatures x 11 times) and 144 microbial biomass samples (6 treatments x 3 replicates x 2 temperatures x 4 times).

4.3.1.4 Experiment 5: Laboratory incubation of fallow soils of different age at different temperatures

The data from Lefèvre et al. (2014) from a laboratory incubation experiment of soils from a long-term bare fallow experiment, established in 1956 in Ultuna, Sweden (Kätterer et al., 2011) was used to study the TS of soils of the same texture and mineral composition but with different contents of recalcitrant carbon. Lefèvre et al. (2014) conducted the incubations of this soil without any residue addition from the beginning of the experiment in 1956 and after long-term bare fallow in 2009. The experiment was conducted in sealed flasks using 5 g of air-dried sieved soil (< 2 mm) under optimal moisture (pF = 2.5), with incubation temperatures of 4, 12, 20, and 35 °C and 4 replicates. They calculated remaining SOC from CO_2 evolution at day 14, 28, 42, 70, 105, 182, 310 and 427 (leading to 2 treatments x 4 replicates x 4 temperatures x 8 times in Exp. 5). The CO_2 in the flask headspace was measured with a Micro-GC (Agilent 3000A and Agilent 490, Santa Clara, CA, USA). The two data series we used had an initial C content of 1.53% for 1956 samples and 1.06% for 2009 samples. The Daisy model simulates C in kg ha^{-1}, so simulations were conducted with an assumed soil mass of 10^6 kg ha^{-1} and all data converted to kg C ha^{-1}.

4.4 Laboratory analyses as basis for pool partitioning and Q_{10} values

Analysis of crop-litter quality and SOC recalcitrance was done to partition carbon between Daisy model pools (Figure 4 - 1). Crop-litter quality was analyzed by acid detergent lignin (Van Soest and Wine, 1968). Total carbon and nitrogen contents of all crop-litter and soil samples were measured in a Vario Max CNS (Elementar Analysensysteme GmbH, Hanau, Germany). Information on SOC recalcitrance was gained from diffuse reflectance mid-infrared Fourier transform spectroscopy (DRIFTS) of bulk soil samples. The specific areas below absorption bands at 2930 cm^{-1} and 1620 cm^{-1} are related to aliphatic and aromatic-carboxylate carbon, respectively, and were used to partition SOC between pools (section 4.4.1.2). The spectra of ball milled bulk soil samples (dried for 24 h at 105 °C and stored in a desiccator) were recorded with an HTS-XT microplate extension, mounted to a Tensor-27 spectrometer using the processing software OPUS 7.5 (all from Bruker Optik GmbH, Ettlingen, Germany). The rationale and details of this approach are discussed in Laub et al. (2020). For Exp. 5, samples from 1956 and 2005

were available, but not from 2009. Therefore, DRIFTS spectra from 2005 were used for initializing the SOC pools of 2009 samples.

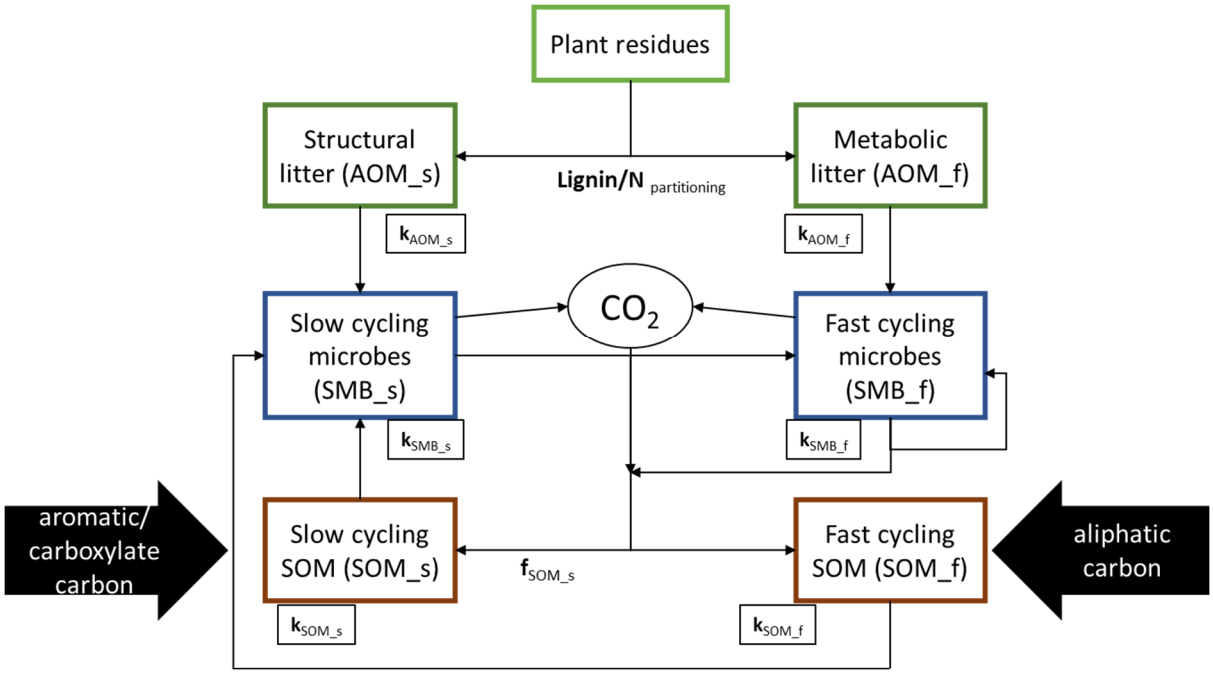

Figure 4 - 1 Structure of the adapted Daisy soil organic matter model, as used in this study. The partitioning of litter into structural and metabolic is controlled by the lignin to nitrogen (L/N) ratio, kSOM, kSMB and kAOM are turnover rates of the pools and fSOM_slow is the amount of recalcitrant materials from SMB. Other parameters are found in Table S4 - 5.

The Q_{10} values of β-glucosidase and xylanase data were taken directly from the supplement of Ali et al. (2015), while phenol/peroxidase measurements were redone using an optimized method with substantially improved results. All details on the derivation of Q_{10} values are displayed in the supplement section 6.3.1, summary histograms of all enzymes Q_{10} are presented in Figure 4 - 2.

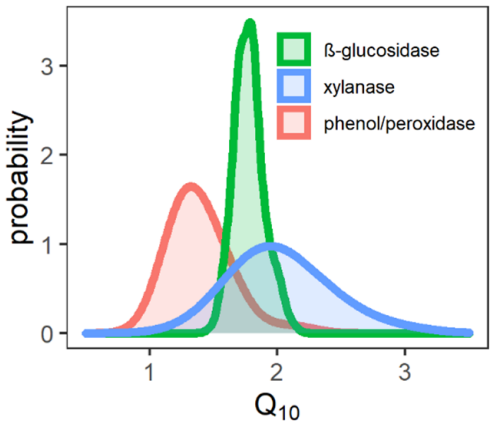

Figure 4 - 2 Probability densities of measured ß-glucosidase, xylanase and phenol/peroxidase Q_{10}, from experiment 1 and 2, that matched the quality criteria (modelling efficiency >0.65) and were used in this study.

4.4.1 Model setup

For modeling of carbon and nitrogen dynamics, the agroecosystem modelling framework Expert-N 5.0 (Heinlein et al., 2017; Klein et al., 2017) was used, which allows the user to select different modules for simulating different processes (organic matter decomposition, crop growth, etc.). The selected soil carbon and nitrogen model was Daisy (Hansen et al., 2012). Daisy considers three fractions of carbon in soil through which carbon moves sequentially: crop-litter (added organic matter - AOM), soil microbial biomass (SMB) and soil organic matter (SOM) each divided into a fast (_f) and a slow (_s) pool (Figure 4 - 1). Thus, Daisy has six pools, which contain both carbon and nitrogen, with nitrogen coupled to carbon by fixed carbon/nitrogen (C/N) ratios, which determine nitrogen mineralization. Further details on the sub-models used for the simulation of Daisy driving factors are in the supplement 6.3.2Simulated laboratory incubations (Exp. 4 and Exp. 5) used fixed temperature and moisture. Experiments 1 and 2 used weather data of the stations within each field (Laub et al., 2020; Wizemann et al., 2015). For Exp. 3, measured temperature and moisture were used instead of simulating both. Therefore, crop-litter decomposition of Exp. 3 was thus simulated with code written in R (R version 3.4.3; R Core Team, 2017) instead of Expert-N 5.0. This code was translated from Expert-N 5.0 code, which simulates soil moisture and temperature based on climatic variables and can therefore not use measured inputs. The R code used the exact same HYDRUS routine to compute matric potential from measured volumetric water content and Daisy code to compute litter decomposition on a daily timestep as implemented in Expert-N 5.0. Some missing data of soil moisture had to be gap filled (Site S26, November 2015; S27, a 6-day and a 3-day interval in March 2016). Gap filling was done by a linear interpolation between soil moisture of the last measurement before and the first measurement after the gap. This simple method was amongst the most effective methods for soil moisture data gap filling up to 50 days, with similar accuracy than artificial neural networks (Kornelsen and Coulibaly, 2014). Several sites had gaps of more than 50 days and as a result, only 12 (5 from Kraichgau) out of 20 sites of Exp. 3 were simulated.

4.4.1.1 Modifications of the Daisy model

The Daisy model (Figure 4 - 1, parameters in Table S4 - 5) was subject to two modifications compared to the original structure (Mueller et al., 1997). First, the flow of carbon and nitrogen from SMB to SOM pools was changed: instead of sequentially moving from SMB through SOM_f into SOM_s, SMB was divided immediately into SOM_s and SOM_f at SMB turnover/death, and the flow of SOM_f into SOM_s eliminated. This was suggested by Laub et al. (2020) as fast cycling carbon should not become slow cycling carbon without involvement of SMB (Cotrufo et al., 2013). Secondly, because the lignin-to-nitrogen is to date considered one of the best proxies for litter pool partitioning (Zhang et al., 2018), we replaced the default empirical Daisy partitioning. Thus, partitioning of crop-litter by the lignin-to-nitrogen ratio as in the CENTURY model (Parton et al., 1987) was introduced, as it is a direct

measurement of our definition of recalcitrance, and able to handle the different litter types and lignin contents of the several experiments (e.g. Exp. 3 and 4).

The equation used to partition litter was:

$$F_m = M_0 - S_{L/N} * L/N \quad (4 - 1)$$

F_m is the fraction of AOM_f, *L/N* stands for the lignin-to-nitrogen ratio, M_0 is the intercept (0.85 per default) and $S_{L/N}$ denotes the slope of reduction with *L/N* (default 0.018; Parton et al., 1987). For the two litter incubation experiments (Exp. 3 and 4), lignin and nitrogen contents were measured (Van Soest and Wine, 1968). For simulated crop-litter (Exp. 2), measurements of the lignin-to-nitrogen ratio were not available throughout the full simulation period. Therefore, the lignin-to-nitrogen was calculated using the simulated plant nitrogen content from GECROS and crop specifically fixed lignin contents, which differed between the root, leaves and stem and were estimated by literature values (Table S4 - 6). In the absence of measured values, this was seen the best available option, but could ultimately make the results of Exp. 2 less robust than of Exp. 3 and 4. For initialization of Exp. 1 and 2, measured residue amounts from the season 2009 were applied at simulation start (August 2009) using estimated lignin contents (4, 7 and 11% for maize, wheat and rapeseed; Table S4 - 6).

4.4.1.2 Initialization of the Daisy soil pools and parameters used for Daisy

The Daisy model parameters under which the measured enzyme activity as TS proxy (Table S4 - 5) were tested, were a combination of standard Daisy parameters with turnover rates and carbon use efficiencies of litter from Parton et al. (1987), and a recent Bayesian calibration for SOM pools (Laub et al., 2020). The amount of litter in AOM pools at the start of experiments was based on the measured amount of crop residues. AOM_s nitrogen was added based on carbon content (assigned fixed C/N ratio of 150), the remaining nitrogen was partitioned to the AOM_f pool. The SMB pools of Daisy were initialized using measured SMB assuming 93% being in the slow pool (SMB_s) and 7% in the fast pool (SMB_f) according to Mueller et al. (1997). The C/N ratio of SMB measured at start, was applied to both SMB pools. The amount of SOC and nitrogen minus SMB-C and SMB-N was assigned to SOM pools. It was distributed between fast and slow cycling soil organic matter pools (SOM_f, SOM_s) by the band area approach using infrared DRIFTS spectra as detailed above (4.4.1.2). This approach classifies the aliphatic proportion as fast cycling SOC, while aromatic-carboxylate proportion is slow cycling SOC. The advantages of the approach are distinct chemical recalcitrance of the pools, reproducibility and cost-efficiency, while mineral interference in the spectra poses a potential shortcoming (Laub et al., 2020). Using several medium- to long-term fallow experiments across Europe, the authors could show that, even with mineral artifacts in the spectra, this partition of pools outperformed the initial Daisy partitioning that assumes that SOC is at steady state. The ratio of the two SOC pools is estimated by

their absorption bands in DRIFTS spectra. A local baseline between integration limits delineated the lower boundary of absorption band areas. The ratio of areas below absorption bands at 2930 cm^{-1} (integration limits 3010–2800 cm^{-1}; assumed to be labile aliphatic carbon) and 1620 cm^{-1} (integration limits 1660–1580 cm^{-1}; assumed to be recalcitrant aromatic-carboxylate carbon) was set equal to the ratio of the fast to slow cycling carbon. The SOM_s pool were given a C/N ratio of 11, while the rest of nitrogen was distributed to SOM_f (Jensen et al., 1997). Measured soil mineral nitrogen (NH_4^+ and NO_3^-) was initialized from field measured samples for Exp. 1 and 2. For Exp. 4, only mineral nitrogen content was available and initialized as NO_3^-, which is usually the majority of mineral N in these soils.

4.4.2 Inferring Q_{10} and other parameters by Bayesian calibration

The Bayesian calibration approach obtains probability distributions of parameters that are conditional on the model and the available measured data. Its application for plant-soil models has been well described by Ahrens et al. (2014) and Van Oijen et al. (2005). Bayesian calibrations were done with UCODE_2014 Software (Lu et al., 2014; Poeter et al., 2014), which uses the Differential Evolution Adaptive Metropolis algorithm (Vrugt, 2016). To enable combining different experiments and types of measurements, it is necessary to apply a weighting scheme which brings different types of measurements to the same scale and reflects the relative accuracy of measurements (Poeter et al., 2005). Then, different experiments can be combined in one Bayesian calibration, given that the model is suitable for all of them. The weight of each measurement is usually the inverse of the variance. In this study, mixed linear models of SAS version 9.4 (SAS Institute Inc., Cary, NC, USA) were used to derive weights which account for different experimental designs of the different experiments. By doing so, it was possible to separate systematic parts of the variance (e.g. due to block effects) from the residual error term, which was used for the weighting. The procedure for weight derivation is explained in detail in the supplement (section 6.3.4).

The Q_{10} value priors were uniform, so that they would be only informed by the data, but their limits were 1 and 3. For the turnover rates of SOM_f and SOM_s, priors were taken from the results of a recent Bayesian calibration of Daisy SOM pools (Laub et al., 2020). For all other turnover rates, the carbon use efficiency, and the SOM partitioning coefficient (fSOM_s), priors were centered around the standard parameter set (Table S4 - 5). For those parameters, the selected standard deviations of the priors were chosen based on the level of certainty about them. For carbon use efficiency the standard deviation was 0.15, which approximately represented the spread observed in meta-analyses (e.g. Manzoni et al., 2012; Sinsabaugh et al., 2016). The exception, with 0.07, was the carbon use efficiency of AOM_s, which deliberately limited to values below 0.45, in order to be clearly distinguishable from AOM_f. For the rest of turnover rates and fSOM_s, broad priors were chosen, to reflect the level of

certainty about them. These priors even contained the 0 within two standard deviations (which was technically prevented by setting limits close to 0).

The default UCODE_2014 convergence criterion was used, a Gelman-Rubin value of 1.2, which is considered an indicator of approximate convergence (Brooks and Gelman, 1998; Gelman and Rubin, 1992). It was computed from 15 parallel chains. All samples after convergence were taken as the posterior distributions. The number of available samples differed between different Bayesian calibrations, but no sample was smaller than 1000 simulations (equivalent to 15,000 samples). Though more samples would be preferable, the sample generation was limited by computation times of up to two weeks of the available super computer clusters. To draw a general conclusion about Q_{10} all experiments were combined into one Bayesian calibration. Due to contrasting conditions of the experiments also a separate analysis was conducted resulting in four different setups (number of posterior samples in parentheses) :

1) Combining all experiments (combined_BC; 1800 x 15 samples)
2) Combining field Exp. 1, 2 and 3 (field_BC; 1200 x 15 samples)
3) Crop-litter incubation Exp. 4 alone (litter_inc_BC; 6000 x 15 samples)
4) Laboratory bare soil incubation Exp. 5 alone (bare_soil_inc_BC; 2700 x 15 samples)

Experiment 1 to 3 were always combined because of their similar setup (same sites, all were field experiments and same litter), whereas Exp. 4 and 5 differed in soil and methodology and thus were analyzed individually.

4.4.3 Allocating measured enzyme TS to different Daisy pools

Testing different allocations of enzyme TS to different Daisy pools was performed independently from the Bayesian calibration. The rationale behind this was that certain enzymes are considered the rate limiting step of the depolymerization of carbon in the soil (Sinsabaugh et al., 2008). Thus, the TS of enzyme activities could be a strong predictor of TS of carbon mineralization, which Ali et al. (2015) could show for soil surface CO_2 evolution which they predicted by the measured TS of β-glucosidase. It is known that β-glucosidase depolymerizes cellulose (Jeng et al., 2011). Within the Daisy model, as used in this study, this would be best represented by metabolic litter (AOM_f). In contrast, phenol/peroxidase depolymerizes phenolic molecules, for example lignin (Sinsabaugh, 2010), thus it should be related to structural litter, as determined by the lignin-to-nitrogen ratio, and potentially also to aromatic-carboxylate carbon in the slow SOC pool (SOM_s). Due to this conceptual overlap, using measured enzyme TS as pool TS should improve model simulations compared to using the same default TS (Q_{10} = 2) for each pool. To test this, the evaluation of model performance applying different enzyme TS was done, using the fixed standard model parameters (Table S4 - 5). According to Shapiro-Wilk test, the distribution of measured enzyme Q_{10} values, determined in Exp. 1 and 2, diverged from

normality (Table S4 - 5), even after Q_{10} values with only satisfactory modelling efficiencies and below (< 0.65; Moriasi et al., 2007) were excluded. Thus, the median Q_{10} value of each enzyme was considered a more robust estimate than the mean. This was a Q_{10} of 1.35 for phenol/peroxidase and 1.82 for β-glucosidase (xylanase, with 1.98, was too similar to 2 and thus not used). Different hypotheses, linking enzymes TS with SOM pools, were tested, based on the recalcitrance of carbon pools. The Q_{10} of β-glucosidase was assigned to the AOM_f pool and three possible assignments for phenol/peroxidase, were tested, including AOM_s, SOM_s, SOM_f and combinations of these. As a result, nine possible assignment combinations of β-glucosidase (Gl) and phenol/peroxidase (Po) were formulated, which were all compared to the default (D) Q_{10} assignment of 2 for all pools: either only the Q_{10} of β-glucosidase was assigned to AOM_f, or only the Q_{10} of phenol/peroxidase was assigned to AOM_s, or both options were combined (hypotheses D_Gl, Po_D and Po_Gl, respectively, corresponding to AOMs_AOMf). These three possibilities were combined with either standard temperature sensitivity (Q_{10} = 2) for SOM_s and SOM_f, phenol/peroxidase Q_{10} only for SOM_s or phenol/peroxidase Q_{10} for SOM_s and SOM_f (hypotheses /D_D, /Po_D and /Po_Po, respectively, corresponding to /SOMs_SOMf; Table 4 - 3). Model statistics of the combined nine alternative hypotheses were then compared to the default (Q_{10} = 2) by common evaluation criteria, described in detail in the supplement section 6.3.5.

Table 4 - 3 Hypotheses that were formulated to test the link between the Q_{10} values of model pools and measured soil enzyme activity Q_{10} values. They were evaluated by assessing changes in the model performance (Table 4 - 5). The different hypotheses represent possible combinations of enzyme Q_{10} assignments to pools, which were compared to the standard Q_{10} value of 2 (D). The AOM pools represent crop-litter, SMB the microbial biomass and SOM the stabilized soil organic matter pools of Daisy, which each having a fast (_f) and a slow pool (_s). Measured median Q_{10} values of ß-glucosidase (Gl, 1.82) and phenol/peroxidase (Po, 1.35) were used.

Hypothesis	NO	AOM_s	AOM_f	SMB	SOM_s	SOM_f
D_D/D_D(0)	1	default	default	default	default	default
D_Gl/D_D	2	default	*ß-glucosidase*	default	default	default
D_Gl/Po_D	3	default	*ß-glucosidase*	default	*phenol/peroxidase*	default
D_Gl/Po_Po	4	default	*ß-glucosidase*	default	*phenol/peroxidase*	*phenol/peroxidase*
Po_D/D_D	5	*phenol/peroxidase*	default	default	default	default
Po_D/Po_D	6	*phenol/peroxidase*	default	default	*phenol/peroxidase*	default
Po_D/Po_Po	7	*phenol/peroxidase*	default	default	*phenol/peroxidase*	*phenol/peroxidase*
Po_Gl/D_D	8	*phenol/peroxidase*	*ß-glucosidase*	default	default	default
Po_Gl/Po_D	9	*phenol/peroxidase*	*ß-glucosidase*	default	*phenol/peroxidase*	default
Po_Gl/Po_Po	10	*phenol/peroxidase*	*ß-glucosidase*	default	*phenol/peroxidase*	*phenol/peroxidase*

4.4.3.1 The Daisy temperature function

The temperature function of Daisy is a multiplication factor for turnover rates. The multiplier has a linear interpolation from 0 to 1 between 0 and 10 °C, with 10 °C as reference temperature for all turnover in Daisy. An exponential increase follows above 10 °C with a standard Q_{10} of 2. In alignment

with this temperature function and because enzyme Q_{10} were only measured > 5 °C, Q_{10} values of measured enzyme were assigned only to the exponential part above 10 °C , replacing the standard Q_{10} of 2 (Figure 4 - 3 a). A second reason for keeping the linear function < 10 °C was that the standard turnover rate in Daisy is given for 10 °C, which, when using standard parameters, would lead to an overestimation of turnover < 10 °C with an exponential function. Examples of Exp. 1 in 2009 show that the relationship between soil temperature and CO2 release is roughly exponential (Figure 4 - 3 b).

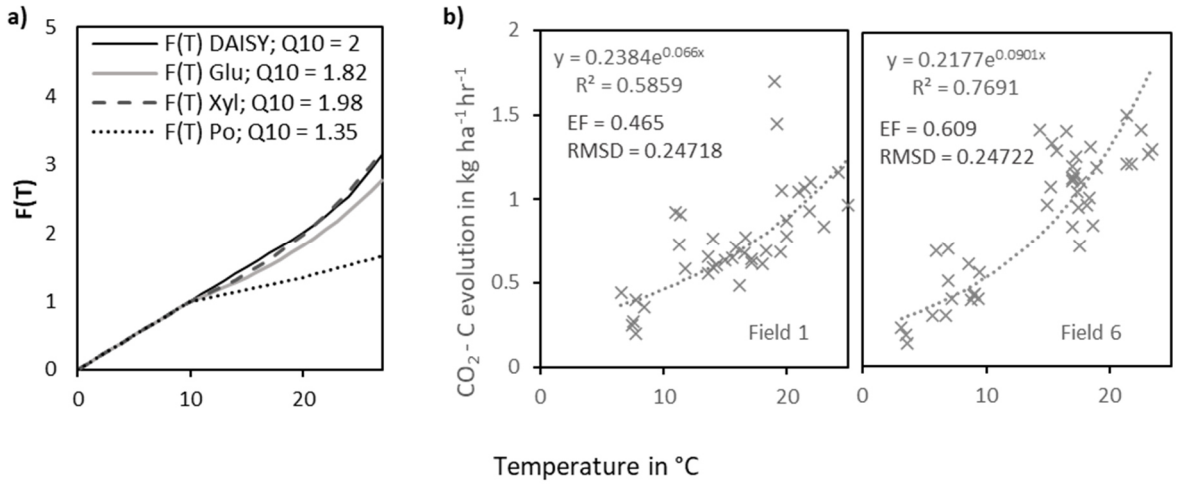

Figure 4 - 3 The temperature function of Daisy as modified in this study is represented by the multiplication factor F(T) with turnover (a). Examples of measured soil respiration from experiment 1 in 2009 plotted against temperature indicate deviations from a single exponential function (b). The Daisy functions have a linear increase from 0 to 1 between 0 and 10 °C, then exponential increase based on measured enzyme Q_{10}. Abbreviations: Glu, ß-glucosidase; Xyl, xylanase; Po, phenol/peroxidase

4.5 Results

4.5.1 Model fit using the default parameter set and Q_{10}

With the initial set of parameters, the different experiments were simulated with both positive and negative modelling efficiencies. Simulations of measured SMB-C of experiment 1 and 2 (Figure 4 - 4 a) had low modeling efficiency (EF; -0.63/-0.64), but the high lack of correlation (LC; 67/74%) suggested that deviations were mostly random (Table 4 - 4). Simulations of soil CO_2 efflux within Exp. 1 and 2 systematically underestimated measured values (Figure 4 - 4 b), as indicated by a squared bias (SB) greater than 70% and the negative model EF (Exp. 1 -38; Exp. 2 -399). The simulated crop-litter carbon decomposition of Exp. 3 (Figure 4 - 5 a) had a high model EF of 0.66 while the 90% LC indicated little systematic bias. The change of CO_2 evolution rate of Exp. 4 was generally captured (EF = 0.38), but the initial flush of CO_2 evolution was underestimated, resulting in overestimations towards the end of the experiment. Therefore, cumulative CO_2 evolution (Figure 4 - 5 b) of Exp. 4 was better captured than daily CO_2 evolution (Table 4 - 4, Figure S4 - 3). The development of SMB following residue addition of Exp. 4 was poorly captured by all simulations. While SMB-N simulations could roughly follow the

measured trend (Figure 4 - 5 c), SMB-C was systematically overestimated by the model (SB of 54.5%,Table 4 - 4) for all except for the control treatments. Simulations of Exp. 5 with an R^2 of 0.99 showed a strong correlation between simulated and observed SOC, but a low EF (-0.48) and a high SB suggested systematic underestimation of mineralization (Figure 4 - 5 d). Due to the large amount of simulated experiments and sites, only a sub-selection of graphs is presented in the paper, but graphs of all simulations are in the supplement (Figure S4 - 1 to Figure S4 - 4) as is a detailed discussion on the model goodness-of-fit (section 6.3.6) and about the Daisy temperature function (section 6.3.7).

Table 4 - 4 Performance statistics of the hypothesis 0 model, using a standard Q_{10} (=2) for all pools. The performance of simulated compared to measured values within the different experiments were assessed. Used were measurements of soil microbial biomass (SMB) C and N, CO_2 evolution from the soil remaining C in litterbags and remaining C of incubated soil Squared bias (SB), nonunity slope (NU) and lack of correlation (LC) are displayed as their percentage of the mean squared deviation. The properties of each experiment are explained in detail in Table 4 - 1.

Experiment	Property	Unit	EF	RMSD	R^2	MSD	SB (%)	NU (%)	LC (%)
1	SMB-C	kg C ha^{-1}	-0.64	282.9	0.67	80052	22.6	10.5	67.0
1	CO_2 evolution	kg CO_2-C ha^{-1} hr^{-1}	-38.92	2.5	0.10	6.14	70.4	27.3	2.3
2	SMB-C	kg C ha^{-1}	-0.63	380.2	0.44	144565	1.1	24.8	74.0
2	CO_2 evolution	kg CO_2-C ha^{-1} hr^{-1}	-399.00	17.5	0.06	305	72.8	27.0	0.2
3	C in litterbag	g C per bag	0.66	0.2	0.75	0.03	3.2	6.5	90.3
4	CO_2 evolution	kg CO_2-C ha^{-1} hr^{-1}	0.38	39.9	0.61	1592	6.8	3.6	89.6
4	SMB-C	kg C ha^{-1}	-38.23	415.1	0.21	172276	54.5	38.2	7.3
4	SMB-N	kg N ha^{-1}	-4.78	27.7	0.21	768	1.8	44.5	53.7
5	C remaining	kg C ha^{-1}	-0.48	213.9	0.99	45766	51.0	16.8	32.1

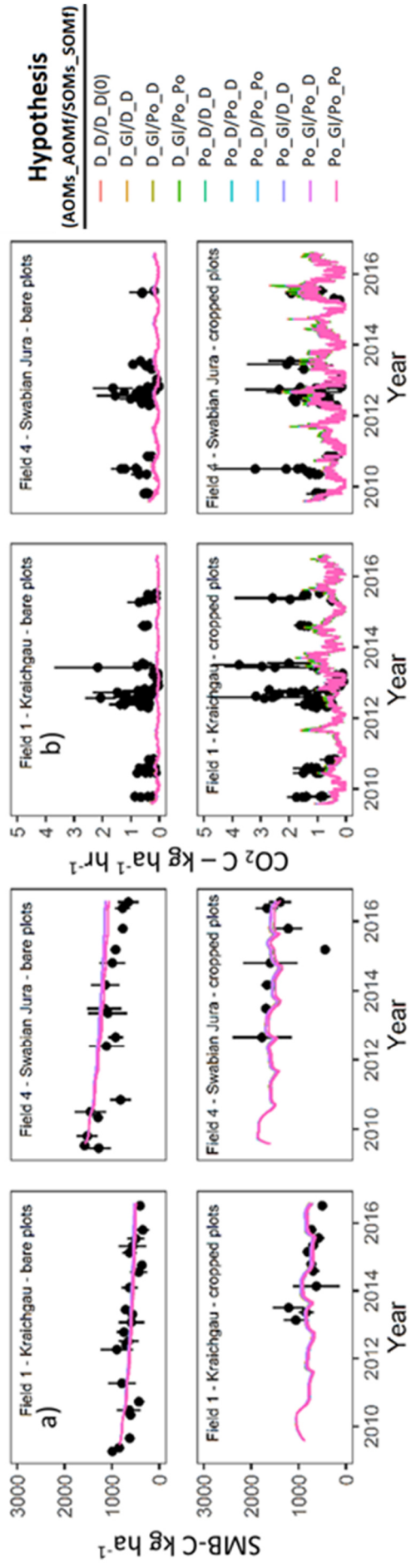

Figure 4 - 4 Example simulations of all hypotheses assigning enzyme TS as TS of different pools (assignments of hypotheses in Table 4 - 3). Displayed are experiment 1 (bare plots - top) and 2 (cropped plots - bottom), for soil microbial biomass - SMB-C (a) and CO_2 evolution (b). Dots represent the average and error bars the standard deviation of the three replicates per field. For SMB, there were 20 (fallow) and 10 (cropped plots) measurements throughout the simulation period, for CO_2 there were 70 measurements for both. Graphs of all simulations can be found in Figure S4 - 1, Figure S4 - 2, Figure S4 - 3, Figure S4 - 4.

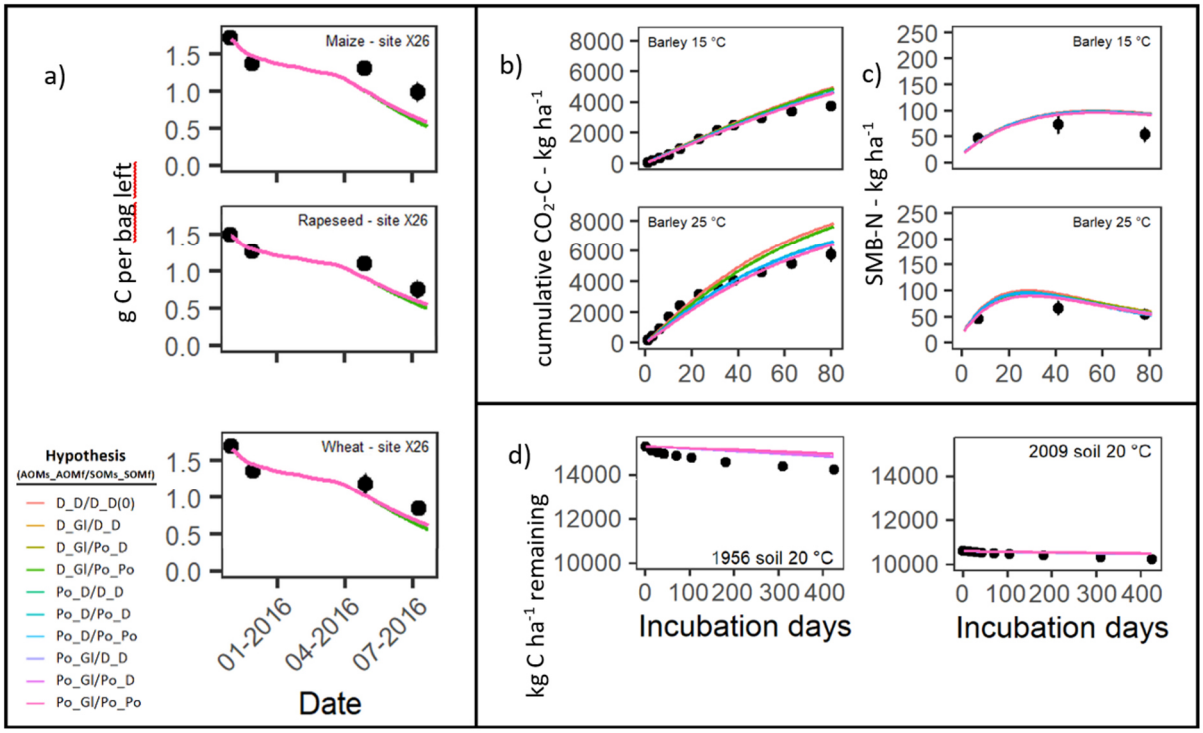

Figure 4 - 5 Example simulations of all hypotheses assigning enzyme TS as TS of different pools (assignments of hypotheses in Table 4 - 3). Displayed are experiment 3 remaining litter carbon (a); experiment 4 cumulative CO_2 evolution (b) and SMB-N (c); and experiment 5 remaining carbon at 20 °C (d). Dots represent the average and error bars the standard deviation of the three replicates Simulations of all hypotheses are displayed but often overlap. Graphs of all simulations can be found in Figure S4 - 1, Figure S4 - 1, Figure S4 - 2, Figure S4 - 3, Figure S4 - 4.

4.5.2 Q_{10} assigned by Bayesian calibration

In the combined_BC, Q_{10} values close to 3 for SMB, AOM_s and SOM_f were assigned and a Q_{10} around 2.4 for AOM_f (Figure 4 - 6 a) while SOM_s covered the full range from 1 to 3. Many model parameters differed strongly from initial assignments such as a carbon use efficiency of 20% for AOM_f, 90% for dead SMB consumed by SMB_f, and with 10% for SOM_f much lower than the 50% for SOM_s (Figure S4 - 5). Furthermore, strong negative correlations between turnover rates and Q_{10} of the same pools existed in combined_BC (Figure S4 - 7) for AOM_f (-0.81) and SOM_f (-0.6). These strong correlations between turnover and Q_{10} were also present for AOM_f (-0.71) and AOM_s (-0.88) in Exp. 4 individually (litter_inc_BC, Figure S4 - 6). The litter_inc_BC clearly constrained the Q_{10} values, with 95% credibility intervals being 2.76 to 3.00 for AOM_f, 1.59 to 2.74 for AOM_s and 2.87 to 3.00 for SMB (Figure 4 - 6 c). This experiment was mostly driven by litter decomposition and suggested low optima of Q_{10} values for both SOM pools close to 1 but credibility intervals covered the full range from 1 to 3.

Experiment 5 (bare_soil_inc_BC), which included no AOM, clearly constrained the Q_{10} values of both SOM pools (Figure 4 - 6 d) to 95% credibility intervals being 2.37 to 2.99 for SOM_s and 2.83 to 3.00 for SOM_f. This suggested a drastic increase of mineralization up to the maximum temperature of 35 °C of this experiment.

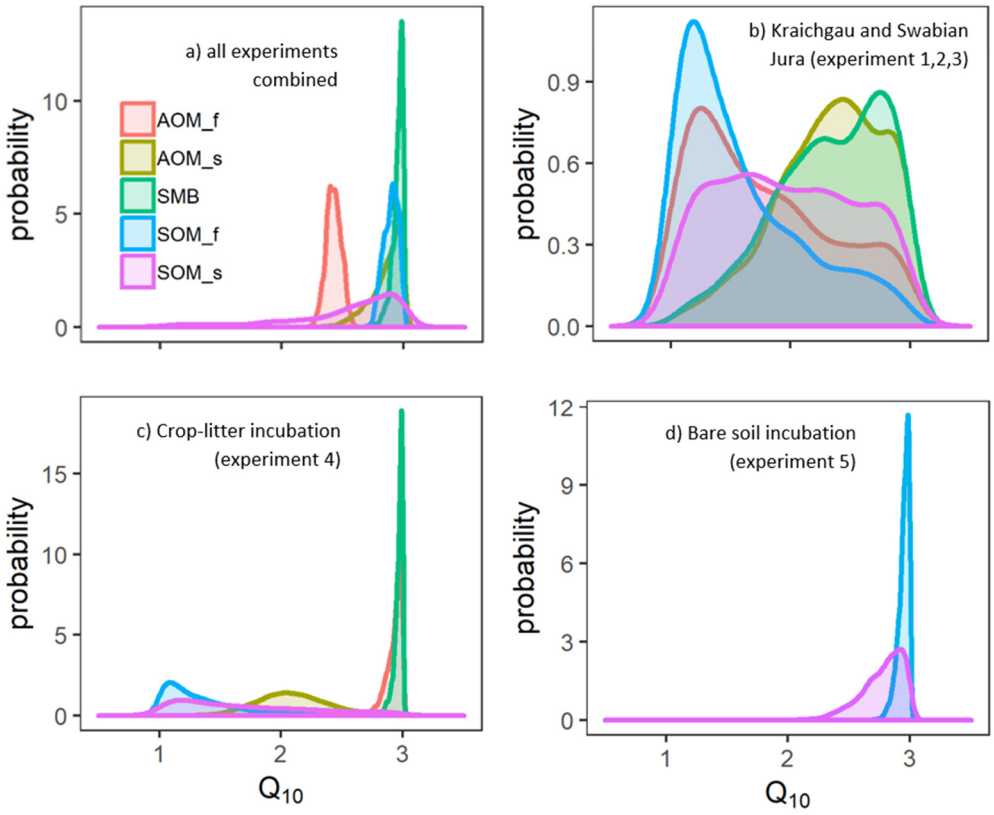

Figure 4 - 6 The Q_{10} values of different SOM pools which were assigned by the combined and the three individual Bayesian calibrations when all other Daisy parameters were allowed to vary at the same time (a = combined_BC, combining all experiments; b = field_BC, combining agricultural bare fallow plots, cropped plots and a litterbag experiment , all in the field, Exp. 1,2 and 3; c = litter_inc_BC, incubating crop-litter at different temperatures in the laboratory, Exp. 4; d = bare_soil_inc_BC, incubation of long term fallow soil from Ultuna using soil of year 0 and 54, Exp. 5).

While both laboratory temperature manipulation experiments simultaneously could constrain Q_{10} values and other parameters, the Bayesian calibration of field Exp. 1, 2 and 3 combined (field_BC) covered the full range of allowed Q_{10} values (1 to 3) for all pools (Figure 4 - 6 b), only showing tendencies. These were a Q_{10} value above 2 for SMB and AOM_s as well as below 2 for SOM_f and AOM_f with no tendency for SOM_s. The inability to constrain Q_{10} values to values beyond the initial limits, was despite field_BC having the highest number of measurements (Figure S4 - 1 and Figure S4 - 2) and temperatures above 10 °C, where differences in Q_{10} become effective, being present between June and October.

4.5.3 Model performance of using enzyme Q_{10} with default parameters

Using enzyme measured Q_{10} values obtained from samples of Exp. 1 and 2 as corresponding model pool Q_{10}, reduced simulation errors of all field experiments (1, 2 and 3), but not for the incubation experiments. The difference between the simulations using the different hypotheses (Table 4 - 3) for Exp. 1, 2 and 3 was most visible in summer months and for CO_2 evolution from the cropped plots (Figure 4 - 4 b). The overall lowest error and AIC for simulated CO_2, SMB-C and remaining litter carbon of Exp. 1, 2 and 3 was obtained with hypothesis Po_D/Po_Po (for pools AOMs_AOMf/SOMs_SOMf;

Table 4 - 5), where phenol/peroxidase Q_{10} was assigned to AOM_s, SOM_f and SOM_s. Assigning only β-glucosidase to AOM_f (D_Gl/D_D) reduced RMSD by 0.1% which according to AIC was not significant. The AIC suggested best performance of applying phenol/peroxidase Q_{10} to AOM_s and both SOM pools (Po_D/Po_Po), while further adding β-glucosidase Q_{10} to AOM_f (Po_Gl/Po_Po) would only improve CO_2 simulation of Exp. 2 and the initially overestimated SMB-C of Exp. 4. The main reduction of RMSD for Exp. 1 CO_2 as well as Exp. 1 and 2 SMB-C was achieved by assigning phenol/peroxidase to both SOM pools (Po_D/Po_Po), whereas assignment of phenol/peroxidase to the AOM_s pool only (Po_D/D_D) reduced errors only for Exp. 2 CO_2 and Exp. 3 litterbag C.

For Exp. 5, where the standard Q_{10} (=2) already underestimated SOC loss, field measured enzyme Q_{10} assignments, having all Q_{10} values below 2, further reduced model performance. Hence, while assignment of field obtained phenol/peroxidase Q_{10} improved field and litterbag simulations (Exp. 1-3), assigning enzyme Q_{10} to laboratory incubation experiments mostly reduced model performance, even for Exp. 4, which had a soil that was similar to Kraichgau soils and used plant residues harvested in Exp. 2.

Table 4 - 5 Result of the modelling of different temperature sensitivity hypotheses (Table 4 - 3). Displayed are the root mean squared deviations (RMSD) as percentage of the RMSD of the 0 hypotheses (D_D/D_D; all Q_{10} being the default of 2) for measurements of soil microbial biomass (SMB) C and N, CO_2 evolution from the soil, remaining C in litterbags and remaining C of incubated fallow soil. Additionally, the numbers in parentheses represent the Akaike information criterion (AIC). Hypotheses were named in the pool order AOMs_AOMf/SOMs_SOMf, with: D, default; Gl, β-glucosidase, Po, phenol/peroxidase.

RMSD of alternative hypotheses as % of the default (Q_{10} =2) values (AIC in brackes)

Expe-riment	Hypothesis / Property	D_D/D_D(0)	D_Gl/D_D	D_Gl/Po_D	D_Gl/Po_Po	Po_D/D_D	Po_D/Po_D	Po_D/Po_Po	Po_Gl/D_D	Po_Gl/Po_D	Po_Gl/Po_Po
1	SMB-C	100 (1485)	100 (1487)	98 (1485)	90 (1466)	100 (1487)	98 (1483)	90 (1464)	100 (1489)	98 (1485)	90 (1466)
1	CO_2 evolution	100 (1784)	100 (1785)	98 (1772)	91 (1719)	100 (1782)	98 (1766)	91 (1714)	99 (1784)	98 (1768)	91 (1715)
2	SMB-C	100 (915)	100 (916)	99 (918)	96 (914)	100 (916)	99 (916)	96 (912)	100 (918)	99 (917)	96 (914)
2	CO_2 evolution	100 (3145)	100 (3147)	99 (3145)	98 (3132)	96 (3110)	95 (3107)	94 (3091)	95 (3108)	95 (3104)	93 (3090)
3	C in litterbag	100 (-67)	100 (-65)	100 (-63)	100 (-63)	98 (-71)	98 (-71)	98 (-71)	98 (-69)	98 (-69)	98 (-69)
4	CO_2 evolution	100 (1329)	103 (1340)	103 (1342)	103 (1342)	104 (1340)	104 (1340)	104 (1341)	109 (1356)	109 (1357)	109 (1357)
4	SMB-C	100 (419)	96 (419)	95 (420)	94 (419)	95 (418)	95 (418)	94 (417)	91 (418)	90 (417)	89 (417)
4	SMB-N	100 (267)	98 (268)	98 (270)	97 (270)	98 (268)	98 (268)	98 (268)	96 (269)	96 (269)	96 (269)
5	C remaining	100 (518)	100 (520)	102 (523)	111 (530)	100 (520)	102 (521)	111 (528)	100 (522)	102 (523)	111 (530)

4.6 Discussion

4.6.1 Is there a need for pool specific Q_{10}'s?

The results of the Bayesian calibrations and enzyme Q_{10} based SOC modelling suggested that temperature sensitivity is pool specific but also varying across experiments for each pool. Hence, observed deviations from an exponential trend between soils heterotrophic respiration and temperature (Figure 4 - 3 b) could be due to differences in recalcitrance of SOC, meaning that there are several temperature functions simultaneously at play. For example, Bayesian calibration assigned significantly different Q_{10} values to different pools of litter in incubation Exp. 4, with credibility intervals of AOM_s and AOM_f not overlapping. While Bayesian calibration of field simulations could not further constrain Q_{10} (credibility intervals covered the full initial limits from 1 to 3), using pool specific Q_{10} values derived from measured enzyme activities improved the field simulations. This corroborated a connection between measured TS of potential enzyme activity and TS of carbon mineralization in the field (Ali et al., 2015). By using the phenol/peroxidase Q_{10} as a proxy of Q_{10} for AOM_s and both SOM pools, reductions in RMSD of up to 10% for Exp. 1 or 4-7% for Exp. 2 and 3 could be achieved. This is considerable, given common variability of field data and uncertainties from other parts of the model, e.g., the moisture function or root inputs. However, the improvement of model predictions by applying pool specific enzyme Q_{10} could also be interpreted as a mere indicator that Q_{10} of field Exp. 1 to 3 was lower than 2 in general.

Based on the observed fundamental differences in TS between laboratory and field experiments, pool specific Q_{10} values as fixed intrinsic pool property across a range of experiments appear unlikely, even with measurable pool definitions. It has been postulated that intrinsic TS of substrates becomes obsolete, once one moves away from the classical model of humification towards evidence based models that include sorption and aggregation processes (Lehmann and Kleber, 2015). *In situ* enzyme TS could thus be a better predictor of mineralization TS than recalcitrance. For example, phenol/peroxidase Q_{10} as proxy for more recalcitrant substrate was the lowest of all enzymes, which contradicts the CQT theory, but also the Bayesian calibrations suggested that Q_{10} of AOM_f was significantly higher than of AOM_s in Exp. 4.

The present results suggest that Q_{10} are experiment and quality specific, but recalcitrance was subordinate to experimental conditions. Enzyme derived Q_{10} values were reasonable proxies for pool specific Q_{10} in Exp. 1 to 3 but are expensive to measure. Furthermore, measurements of locally differing enzyme activities are not possible with purely data driven modeling exercises frequently used for global SOC studies. Thus, the environmental factors that cause the variation in TS need a closer attention. It has been long proposed that the drivers of apparent TS are much more complex than recalcitrance alone (Schmidt et al., 2011), and some systematical examinations exist. An explorative

study at a regional scale, showed that texture and the abundance of aliphatic carbon were significant explanatory covariates for the Q_{10} of respiration and enzymes (Ali et al., 2018). From such regional assessments, it can be seen that the spatial variability of TS can be of the same magnitudes as the variability of TS between laboratory and field. Thus, future research should focus on the environmental factors influencing TS apart from substrate recalcitrance. In modeling, parsimony could make it necessary to drop either spatial variability or the difference between pools, so, it would be practical to know which is more important.

4.6.2 Microorganisms' main source of carbon had high TS regardless of recalcitrance

Our results indicate that TS was mainly controlled by experimental conditions and not by intrinsic chemical properties of SOM and litter (i.e., recalcitrance of carbon compounds). The high Q_{10} values close to 3 corresponded to the main carbon source for microorganisms in both incubation experiments (litter in Exp. 4 and SOM in Exp. 5; Figure 4 - 6) despite the hypothesized difference of carbon compounds in AOM_f and SOM. High Q_{10} values obtained in incubation experiments for contrasting carbon sources could instead point to opportunistic microbial behavior regardless of carbon complexity. If microbes increase enzyme excretion and activity rapidly under optimal conditions, these conditions might increase TS. Such opportunistic behavior was recently reported by Blagodatskaya et al. (2016) and by Gromova et al. (2020) who found Q_{10} for glucose addition close to 3 compared to 2 for the control without any addition. The bare_soil_inc_BC results suggest that this is also possible for carbon of higher recalcitrance.

The clearly constrained Q_{10} values of the two incubation experiments with Bayesian calibration highlight the relevance of measurable SOC pools for models simulating climate change. However, caution is needed with multiplicative parameters such as Q_{10}, which are prone to equifinality problems (Bagnara et al., 2018). For example, the very low parameter values of combined_BC, i.e., 20% carbon use efficiencies for AOM_f and much lower efficiencies of SOM_f than SOM_s, as well as high correlations between turnover and Q_{10} for several pools, (Figure S4 - 7), suggested the rejection of the initial hypothesis that intrinsic Q_{10} values exist for specific carbon pools. Thus, interpreting the results of the combined_BC as TS dependent on carbon quality, would lead to incorrect conclusions, because factors such as physical protection would be ignored. The insufficient consideration of those factors could be the reason for high uncertainty of TS in climate models. Due to the observed autocorrelations, there is a danger that Q_{10} serves as an additional degree of freedom for the turnover rates. For example, for the litter_inc_BC, both litter pools Q_{10} were correlated to the turnover of the same pool, probably because only two incubation temperatures existed.

With the highest number of measurements, the inability of field_BC to effectively constrain Q_{10} beyond preset limits could seem surprising, but the reason could be the higher uncertainty of field

measurements where temperature and moisture changes occur continuously. The field moisture was at optimal conditions according to the Daisy moisture function 75% of time (Figure S4 - 8), so the main difference between field and laboratory was that there is fluctuation of moisture conditions and temperature in the field. The fluctuation of moisture rather than the moisture content itself could lead to unfavorable conditions for microorganisms. Higher Q_{10} values in incubation compared to field experiments thus suggested higher TS under optimal laboratory conditions regardless of recalcitrance and reduced TS under suboptimal field conditions. In the light of the high uncertainty regarding the Q_{10} under field conditions, a better understanding of processes affecting carbon turnover and their temperature sensitivity under field conditions is needed. Especially their relative relevance is important to decide what processes to include in future models and what to ignore for parsimony.

4.6.3 What drives TS of respiration and measured enzyme activities?

While a consistent difference between enzymes' TS across studies, such as lower phenol/peroxidase than β-glucosidase derived Q_{10} values (e.g., Nottingham et al., 2016; Pope et al., 2020), points towards an effect of intrinsic carbon recalcitrance on TS, the fundamental differences in TS between field and laboratory experiments suggest greater importance of external controlling factors. We present a conceptual model (Figure 4 - 7) that tries to explain the difference between TS derived from laboratory incubation experiments and field data. We hypothesize that a dynamic soil enzyme pool mediates the TS of carbon mineralization. Measured potential enzyme activities and Q_{10} are then proxies for the current state of this soil enzyme pool and mineralization TS (Ali et al., 2015). For example, the averages of measured enzyme and Bayesian calibration Q_{10} for the field were in a similar range: field_BC had an overall mean Q_{10} of 1.99, while the field measured enzyme Q_{10} overall mean was 1.79. The release of enzymes by microorganisms can change the TS of mineralization and is increased under optimal conditions, while reduced under unfavorable conditions. This could explain why within our study, the calibrated Q_{10} values of the laboratory incubations under optimal conditions were much higher than for the field. Thus, apparent TS would be a function of intrinsic substrate TS and environmental controlling factors, with measured enzyme TS being a proxy for apparent TS. While no measurements of enzyme TS existed from the laboratory incubation experiments in this study, others reported higher enzyme activities' TS for laboratory incubations than we measured in the field. Examples are a β-glucosidase Q_{10} of 2.7 by Min et al. (2019) and $Q_{10} > 2$ for several enzymes and temperatures up to 25 °C (Razavi et al., 2017).

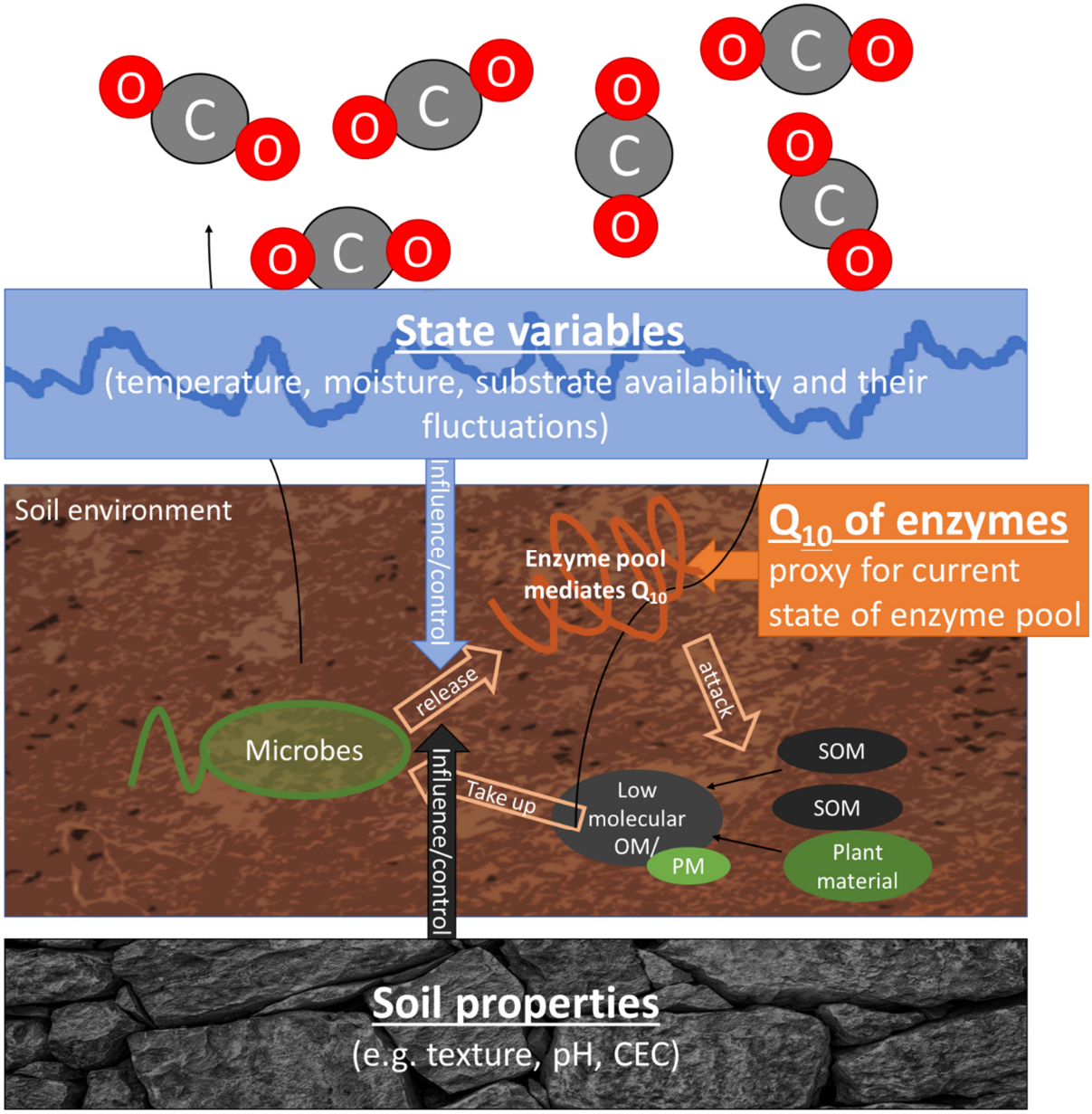

Figure 4 - 7 Conceptual model of the environmental controlling factors influencing soil microorganisms' enzyme production and release. This influences the measured TS of enzyme activity and soil respiration. The factors can be classified into the fluctuating state variables and the mostly constant soil properties. Both influence the lifecycle and activity of microorganisms. For state variables, unfavorable conditions could be due to fluctuations rather than the state per se.

Within our conceptual model, environmental controlling factors are divided into soil properties and state variables. Soil properties, such as texture, climate or pH in natural ecosystem, which can be linked to Q_{10} variability at large scales (Zheng et al., 2009), are constant for decadal timespans and longer. In contrast, state variables such as temperature, moisture (Ding et al., 2016), physical protection by aggregates (Benbi et al., 2014) and substrate availability (Gromova et al., 2020) are more dynamic. The fluctuations of state variables could alter TS mainly by inducing unfavorable conditions (e.g. by frequent drought) for microorganisms. Changes in state variables could thus explain, why there is temporal variability of soil respiration Q_{10} (Demyan et al., 2016) and enzyme Q_{10} (Ali et al., 2015). High Q_{10} under laboratory incubations could then be due to state variables, such as moisture, being at the

optima for microorganisms. Another example would be partly disrupted soil structure and SOC protection in most incubation studies in alignment with findings that SOC physical protection lowers TS (Benbi et al., 2014). However, the soil properties can still explain up to 40% of the variation in soil respiration Q_{10} (Ali et al., 2018). It seems that measured Q_{10} of enzymes is a proxy for the current TS of the soil enzyme pool, effectively incorporating soil properties and state variables. This view is also supported by the findings of Diáková et al. (2016), who found a strong positive correlation ($R^2 = 0.64$) between Q_{10} of enzymes and mineralization Q_{10}. Intriguingly, most studies found lower enzyme Q_{10} than mineralization Q_{10}, which could mean that despite the strong correlation between both (Ali et al., 2018; Blagodatskaya et al., 2016; Diáková et al., 2016), enzymatic reaction speed cannot be considered as the only bottleneck for mineralization. The strong effect of physical protection could mean that substrate availability is another important limiting factor (Benbi and Khosa, 2014; Karhu et al., 2019). Another explanation could be a reduced carbon use efficiency at higher temperatures (Frey et al., 2013), leading to a change in the ratio between SOC mineralization and CO_2 evolution. Thus, the effects of soil properties and state variables on TS need to be disentangled for reasonable long-term predictions in climate change simulations. For short-term simulations, using regionally differing measured Q_{10} of different enzymes as proxies for regionally varying Q_{10} of soil pools seems better than using a single Q_{10} at all sites. They reflect at least the spatial variability of soil properties and a snapshot of the state variables. It would then be important to know at which timescales field TS change when state variables experience a permanent shift, because the high Q_{10}'s derived from laboratory incubations indicate that state variables could have a stronger effect on TS than soil properties. As state variables are altered by climate change, a mechanistic understanding is indispensable – increased heat and drought stress for microorganisms could partly counteract temperature changes.

As Abramoff et al. (2019) pointed out, spatial gradients at the regional level are insufficient to derive optimal temperature response functions, so manipulation experiments are needed to better understand the effect of time variable factors on TS. Thus, future laboratory work should focus on how enzyme Q_{10} along with mineralization Q_{10} is altered through changes in moisture, temperature, or substrate availability of differing recalcitrance. Also, the effects of physical stabilization mechanisms need to be examined in detail, for example comparing TS of intact soil cores with homogenized soil. Determining which state variables connected to Q_{10} are under human control may also help in improved agricultural management for carbon sequestration.

4.7 Conclusion

To understand the potential effects of climate change on global SOC stocks, it is crucial to understand what drives the apparent temperature sensitivity of SOC mineralization. The Bayesian calibrations of Q_{10} values within this study suggested that intrinsic substrate recalcitrance was not the main or sole

driver of apparent temperature sensitivity of SOC mineralization. Instead, the apparent temperature sensitivity seems to be a function of both substrate recalcitrance and environmental controlling factors. These controlling factors were divided into relatively constant soil properties and state variables which can change rapidly (e.g. substrate availability or conditions inducing unfavorable conditions for microbial persistence). High temperature sensitivities under optimal conditions of laboratory soil incubations suggested that the state variables could be more relevant for apparent temperature sensitivities than soil properties or substrate recalcitrance. With an improved model performance, our results provide first evidence that temperature sensitivities of measured activities of different enzymes are valuable proxies for apparent temperature sensitivities of different SOC and litter fractions. They could thus be a proxy for pool specific Q_{10} in SOC models, effectively incorporating state variables and soil properties. To be able to simulate SOC dynamics under a changing climate it is crucial to disentangle the effects of substrate recalcitrance, soil properties and state variables on mineralization temperature sensitivities and explicitly model them. Understanding the state variables is probably of highest importance because they change the most rapid with climate change.

4.8 Acknowledgements

We thank Ladan Maghsoodiganjeh for carrying out the major portion of Exp. 4 and Martin Gauder for access to the soil for Exp. 4. Furthermore, we thank Pierre Barré and Claire Chenu for their kindness in providing the data of Exp. 5. This research was supported by the German Research Foundation (DFG) under the project FOR1695 “Agricultural Landscapes under Global Climate Change – Processes and Feedbacks on a Regional Scale” within subproject P3 (CA 598/6-1 and 6-2). The authors acknowledge support by the state of Baden-Württemberg through bwHPC.

4.9 References

Abramoff, R.Z., Torn, M.S., Georgiou, K., Tang, J., Riley, W.J., 2019. Soil Organic Matter Temperature Sensitivity Cannot be Directly Inferred From Spatial Gradients. Global Biogeochemical Cycles 33, 761–776. doi:10.1029/2018GB006001

Ågren, G.I., Wetterstedt, J.Å.M., 2007. What determines the temperature response of soil organic matter decomposition? Soil Biology & Biochemistry 39, 1794–1798. doi:10.1016/j.soilbio.2007.02.007

Ahrens, B., Reichstein, M., Borken, W., Muhr, J., Trumbore, S.E., Wutzler, T., 2014. Bayesian calibration of a soil organic carbon model using Δ14C measurements of soil organic carbon and heterotrophic respiration as joint constraints. Biogeosciences 11, 2147–2168. doi:10.5194/bg-11-2147-2014

Ali, R.S., Ingwersen, J., Demyan, M.S., Funkuin, Y.N., Wizemann, H.-D., Kandeler, E., Poll, C., 2015. Modelling in situ activities of enzymes as a tool to explain seasonal variation of soil respiration from agro-ecosystems. Soil Biology & Biochemistry 81, 291–303. doi:10.1016/j.soilbio.2014.12.001

Ali, R.S., Kandeler, E., Marhan, S., Demyan, M.S., Ingwersen, J., Mirzaeitalarposhti, R., Rasche, F., Cadisch, G., Poll, C., 2018. Controls on microbially regulated soil organic carbon decomposition at the regional scale. Soil Biology & Biochemistry 118, 59–68. doi:10.1016/j.soilbio.2017.12.007

Alster, C.J., Baas, P., Wallenstein, M.D., Johnson, N.G., von Fischer, J.C., 2016a. Temperature Sensitivity as a Microbial Trait Using Parameters from Macromolecular Rate Theory. Frontiers in Microbiology 7, 1–10. doi:10.3389/fmicb.2016.01821

Alster, C.J., Koyama, A., Johnson, N.G., Wallenstein, M.D., von Fischer, J.C., 2016b. Temperature sensitivity of soil microbial communities: An application of macromolecular rate theory to microbial respiration. Journal of Geophysical Research: Biogeosciences 121, 1420–1433. doi:10.1002/2016JG003343

Bagnara, M., Van Oijen, M., Cameron, D., Gianelle, D., Magnani, F., Sottocornola, M., 2018. Bayesian calibration of simple forest models with multiplicative mathematical structure: A case study with two Light Use Efficiency models in an alpine forest. Ecological Modelling 371, 90–100. doi:10.1016/j.ecolmodel.2018.01.014

Benbi, D.K., Boparai, A.K., Brar, K., 2014. Decomposition of particulate organic matter is more sensitive to temperature than the mineral associated organic matter. Soil Biology & Biochemistry 70, 183–192. doi:10.1016/j.soilbio.2013.12.032

Benbi, D.K., Khosa, M.K., 2014. Effects of Temperature, Moisture, and Chemical Composition of Organic Substrates on C Mineralization in Soils. Communications in Soil Science and Plant Analysis 45, 2734–2753. doi:10.1080/00103624.2014.950423

Blagodatskaya, E., Blagodatsky, S., Khomyakov, N., Myachina, O., Kuzyakov, Y., 2016. Temperature sensitivity and enzymatic mechanisms of soil organic matter decomposition along an altitudinal gradient on Mount Kilimanjaro. Scientific Reports 6, 1–11. doi:10.1038/srep22240

Bosatta, E., Ågren, G.I., 1999. Soil organic matter quality interpreted thermodynamically. Soil Biology & Biochemistry 31, 1889–1891. doi:10.1016/S0038-0717(99)00105-4

Brooks, S.P., Gelman, A., 1998. General Methods for Monitoring Convergence of Iterative Simulations. Journal of Computational and Graphical Statistics 7, 434–455. doi:10.1080/10618600.1998.10474787

Conant, R.T., Ryan, M.G., Ågren, G.I., Birge, H.E., Davidson, E.A., Eliasson, P.E., Evans, S.E., Frey, S.D., Giardina, C.P., Hopkins, F.M., Hyvönen, R., Kirschbaum, M.U.F., Lavallee, J.M., Leifeld, J., Parton, W.J., Megan Steinweg, J., Wallenstein, M.D., Martin Wetterstedt, J.Å., Bradford, M.A., 2011. Temperature and soil organic matter decomposition rates - synthesis of current knowledge and a way forward. Global Change Biology 17, 3392–3404. doi:10.1111/j.1365-2486.2011.02496.x

Cotrufo, M.F., Wallenstein, M.D., Boot, C.M., Denef, K., Paul, E., 2013. The Microbial Efficiency-Matrix Stabilization (MEMS) framework integrates plant litter decomposition with soil organic matter

stabilization: do labile plant inputs form stable soil organic matter? Global Change Biology 19, 988–995. doi:10.1111/gcb.12113

Davidson, E.A., Janssens, I.A., 2006. Temperature sensitivity of soil carbon decomposition and feedbacks to climate change. Nature 440, 165–173. doi:10.1038/nature04514

Demyan, M.S., Ingwersen, J., Funkuin, Y.N., Ali, R.S., Mirzaeitalarposhti, R., Rasche, F., Poll, C., Müller, T., Streck, T., Kandeler, E., Cadisch, G., 2016. Partitioning of ecosystem respiration in winter wheat and silage maize—modeling seasonal temperature effects. Agriculture, Ecosystems & Environment 224, 131–144. doi:10.1016/j.agee.2016.03.039

Diáková, K., Čapek, P., Kohoutová, I., Mpamah, P.A., Bárta, J., Biasi, C., Martikainen, P.J., Šantrůčková, H., 2016. Heterogeneity of carbon loss and its temperature sensitivity in East-European subarctic tundra soils. FEMS Microbiology Ecology 92, fiw140. doi:10.1093/femsec/fiw140

Ding, J., Chen, L., Zhang, B., Liu, L., Yang, G., Fang, K., Chen, Y., Li, F., Kou, D., Ji, C., Luo, Y., Yang, Y., 2016. Linking temperature sensitivity of soil CO2 release to substrate, environmental, and microbial properties across alpine ecosystems. Global Biogeochemical Cycles 30, 1310–1323. doi:10.1002/2015GB005333

Eshonkulov, R., Poyda, A., Ingwersen, J., Wizemann, H.-D., Weber, T.K.D., Kremer, P., Högy, P., Pulatov, A., Streck, T., 2019. Evaluating multi-year, multi-site data on the energy balance closure of eddy-covariance flux measurements at cropland sites in southwestern Germany. Biogeosciences 16, 521–540. doi:10.5194/bg-16-521-2019

Frey, S.D., Lee, J., Melillo, J.M., Six, J., 2013. The temperature response of soil microbial efficiency and its feedback to climate. Nature Climate Change 3, 395–398. doi:10.1038/nclimate1796

Gauder, M., Billen, N., Zikeli, S., Laub, M., Graeff-Hönninger, S., Claupein, W., 2016. Soil carbon stocks in different bioenergy cropping systems including subsoil. Soil and Tillage Research 155, 308–317. doi:10.1016/j.still.2015.09.005

Gelman, A., Rubin, D.B., 1992. Inference from Iterative Simulation Using Multiple Sequences. Statistical Science 7, 457–472. doi:10.1214/ss/1177011136

Gromova, M.S., Matvienko, A.I., Makarov, M.I., Cheng, C., Menyailo, O. V, 2020. Temperature Sensitivity (Q10) of Soil Basal Respiration as a Function of Available Carbon Substrate , Temperature , and Moisture. Eurasian Soil Science 53, 376–381. doi:10.1134/S1064229320020052

Hansen, S., Abrahamsen, P., Petersen, C. T. and Styczen, M.: Daisy: Model Use, Calibration, and Validation, Trans. ASABE, 55(4), 1317–1335, doi:10.13031/2013.42244, 2012.

Hararuk, O., Shaw, C., Kurz, W.A., 2017. Constraining the organic matter decay parameters in the CBM-CFS3 using Canadian National Forest Inventory data and a Bayesian inversion technique. Ecological Modelling 364, 1–12. doi:10.1016/j.ecolmodel.2017.09.008

Heinlein, F., Biernath, C., Klein, C., Thieme, C., Priesack, E., 2017. Evaluation of Simulated Transpiration from Maize Plants on Lysimeters. Vadose Zone Journal 16, 1–16. doi:10.2136/vzj2016.05.0042

Jeng, W.-Y., Wang, N.-C., Lin, M.-H., Lin, C.-T., Liaw, Y.-C., Chang, W.-J., Liu, C.-I., Liang, P.-H., Wang, A.H.J., 2011. Structural and functional analysis of three β-glucosidases from bacterium Clostridium cellulovorans, fungus Trichoderma reesei and termite Neotermes koshunensis. Journal of Structural Biology 173, 46–56. doi:10.1016/j.jsb.2010.07.008

Jensen, L.S., Mueller, T., Nielsen, N.E., Hansen, S., Crocker, G.J., Grace, P.R., Klír, J., Körschens, M., Poulton, P.R., 1997. Simulating trends in soil organic carbon in long-term experiments using the soil-plant-atmosphere model DAISY. Geoderma 81, 5–28. doi:http://dx.doi.org/10.1016/S0016-7061(97)88181-5

Joergensen, R.G., 1996. The fumigation-extraction method to estimate soil microbial biomass: Calibration of the kEC value. Soil Biology & Biochemistry 28, 25–31. doi:10.1016/0038-0717(95)00102-6

Karhu, K., Hilasvuori, E., Järvenpää, M., Arppe, L., Christensen, B.T., Fritze, H., Kulmala, L., Oinonen, M., Pitkänen, J.-M., Vanhala, P., Heinonsalo, J., Liski, J., 2019. Similar temperature sensitivity of soil mineral-associated organic carbon regardless of age. Soil Biology & Biochemistry 136, 107527. doi:10.1016/j.soilbio.2019.107527

Kätterer, T., Bolinder, M.A., Andrén, O., Kirchmann, H., Menichetti, L., 2011. Roots contribute more to refractory soil organic matter than above-ground crop residues, as revealed by a long-term field experiment. Agriculture, Ecosystems & Environment 141, 184–192. doi:10.1016/j.agee.2011.02.029

Kiem, R., Knicker, H., Körschens, M., Kögel-Knabner, I., 2000. Refractory organic carbon in C-depleted arable soils, as studied by 13C NMR spectroscopy and carbohydrate analysis. Organic Geochemistry 31, 655–668. doi:10.1016/S0146-6380(00)00047-4

Kleber, M., Nice, P.S., Plante, A., Filley, T., Kramer, M., Swanston, C., Sollins, P., 2011. Old and stable soil organic matter is not necessarily chemically recalcitrant: implications for modeling concepts and temperature sensitivity. Global Change Biology 17, 1097–1107. doi:10.1111/j.1365-2486.2010.02278.x

Klein, C., Biernath, C., Heinlein, F., Thieme, C., Gilgen, A.K., Zeeman, M., Priesack, E., 2017. Vegetation Growth Models Improve Surface Layer Flux Simulations of a Temperate Grassland. Vadose Zone Journal 16, 1–19. doi:10.2136/vzj2017.03.0052

Kornelsen, K., Coulibaly, P., 2014. Comparison of Interpolation, Statistical, and Data-Driven Methods for Imputation of Missing Values in a Distributed Soil Moisture Dataset. Journal of Hydrologic Engineering 19, 26–43. doi:10.1061/(ASCE)HE.1943-5584.0000767

Laub, M., Demyan, M.S., Nkwain, Y.F., Blagodatsky, S., Kätterer, T., Piepho, H., Cadisch, G., 2020. DRIFTS band areas as measured pool size proxy to reduce parameter uncertainty in soil organic matter models. Biogeosciences 17, 1393–1413. doi:10.5194/bg-17-1393-2020

Lefèvre, R., Barré, P., Moyano, F.E., Christensen, B.T., Bardoux, G., Eglin, T., Girardin, C., Houot, S., Kätterer, T., van Oort, F., Chenu, C., 2014. Higher temperature sensitivity for stable than for labile soil organic carbon - Evidence from incubations of long-term bare fallow soils. Global Change Biology 20, 633–640. doi:10.1111/gcb.12402

Lehmann, J., Kleber, M., 2015. The contentious nature of soil organic matter. Nature 528, 60–68. doi:10.1038/nature16069

Lloyd, J., Taylor, J.A., 1994. On the Temperature Dependence of Soil Respiration. Functional Ecology 8, 315. doi:10.2307/2389824

Lu, D., Ye, M., Hill, M.C., Poeter, E.P., Curtis, G.P., 2014. A computer program for uncertainty analysis integrating regression and Bayesian methods. Environmental Modelling & Software 60, 45–56. doi:10.1016/j.envsoft.2014.06.002

Manzoni, S., Taylor, P., Richter, A., Porporato, A., Ågren, G.I., 2012. Environmental and stoichiometric controls on microbial carbon-use efficiency in soils. New Phytologist 196, 79–91. doi:10.1111/j.1469-8137.2012.04225.x

Menichetti, L., Ekblad, A., Kätterer, T., 2013. Organic amendments affect δ13C signature of soil respiration and soil organic C accumulation in a long-term field experiment in Sweden. European Journal of Soil Science 64, 621–628. doi:10.1111/ejss.12077

Meyer, N., Welp, G., Amelung, W., 2018. The Temperature Sensitivity (Q10) of Soil Respiration: Controlling Factors and Spatial Prediction at Regional Scale Based on Environmental Soil Classes. Global Biogeochemical Cycles 32, 306–323. doi:10.1002/2017GB005644

Min, K., Buckeridge, K., Ziegler, S.E., Edwards, K.A., Bagchi, S., Billings, S.A., 2019. Temperature sensitivity of biomass-specific microbial exo-enzyme activities and CO2 efflux is resistant to change across short- and long-term timescales. Global Change Biology 25, 1793–1807. doi:10.1111/gcb.14605

Moinet, G.Y.K., Moinet, M., Hunt, J.E., Rumpel, C., Chabbi, A., Millard, P., 2020. Temperature sensitivity of decomposition decreases with increasing soil organic matter stability. Science of The Total Environment 704, 135460. doi:10.1016/j.scitotenv.2019.135460

Moriasi, D.N., Arnold, J.G., Van Liew, M.W., Bingner, R.L., Harmel, R.D., Veith, T.L., 2007. Model Evaluation Guidelines for Systematic Quantification of Accuracy in Watershed Simulations. Transactions of the ASABE 50, 885–900. doi:10.13031/2013.23153

Mueller, T., Jensen, L.S.S., Magid, J., Nielsen, N.E.E., 1997. Temporal variation of C and N turnover in soil after oilseed rape straw incorporation in the field: simulations with the soil-plant-atmosphere model DAISY. Ecological Modelling 99, 247–262. doi:http://dx.doi.org/10.1016/S0304-3800(97)01959-5

Nottingham, A.T., Turner, B.L., Whitaker, J., Ostle, N., Bardgett, R.D., McNamara, N.P., Salinas, N., Meir, P., 2016. Temperature sensitivity of soil enzymes along an elevation gradient in the Peruvian Andes. Biogeochemistry 127, 217–230. doi:10.1007/s10533-015-0176-2

Parton, W.J., Schimel, D.S., Cole, C. V., Ojima, D.S., 1987. Analysis of Factors Controlling Soil Organic Matter Levels in Great Plains Grasslands. Soil Science Society of America Journal 51, 1173–1179. doi:10.2136/sssaj1987.03615995005100050015x

Poeter, E.P., Hill, M.C., Banta, E.R., Mehl, S., Christensen, S., 2005. UCODE_2005 and six other computer codes for universal sensitivity analysis, inverse modeling, and uncertainty evaluation. U.S. Geological Survey Techniques and Methods 6-A11, 283p. (As updated in Feb 2008). doi:10.3133/TM6A11

Poeter, E.P., Hill, M.C., Lu, D., Tiedeman, C.R., Mehl, S., 2014. UCODE_2014, with New Capabilities to Define Parameters Unique to Predictions, Calculate Weights using Simulated Values, Estimate Parameters with SVD, Evaluate Uncertainty with MCMC, and More. Integrated Groundwater Modeling Center Report Number: GWMI 2014-02.

Poll, C., Marhan, S., Ingwersen, J., Kandeler, E., 2008. Dynamics of litter carbon turnover and microbial abundance in a rye detritusphere. Soil Biology & Biochemistry 40, 1306–1321. doi:10.1016/j.soilbio.2007.04.002

Poltoradnev, M., Ingwersen, J., Streck, T., 2015. Calibration and Application of Aquaflex TDT Soil Water Probes to Measure the Soil Water Dynamics of Agricultural Topsoil in Southwest Germany. Journal of Irrigation and Drainage Engineering 141, 04014072. doi:10.1061/(ASCE)IR.1943-4774.0000838

Pope, C.A., Halvorson, H.M., Findlay, R.H., Francoeur, S.N., Kuehn, K.A., 2020. Light and temperature mediate algal stimulation of heterotrophic activity on decomposing leaf litter. Freshwater Biology 65, 1210–1222. doi:10.1111/fwb.13465

Poyda, A., Wizemann, H.-D., Ingwersen, J., Eshonkulov, R., Högy, P., Demyan, M.S., Kremer, P., Wulfmeyer, V., Streck, T., 2019. Carbon fluxes and budgets of intensive crop rotations in two regional climates of southwest Germany. Agriculture, Ecosystems & Environment 276, 31–46. doi:10.1016/j.agee.2019.02.011

R Core Team, 2017. R: A Language and Environment for Statistical Computing.

Razavi, B.S., Liu, S., Kuzyakov, Y., 2017. Hot experience for cold-adapted microorganisms: Temperature sensitivity of soil enzymes. Soil Biology & Biochemistry 105, 236–243. doi:10.1016/j.soilbio.2016.11.026

Robertson, A.D., Paustian, K., Ogle, S., Wallenstein, M.D., Lugato, E., Cotrufo, M.F., 2019. Unifying soil organic matter formation and persistence frameworks: the MEMS model. Biogeosciences 16, 1225–1248. doi:10.5194/bg-16-1225-2019

Schmidt, M.W.I., Torn, M.S., Abiven, S., Dittmar, T., Guggenberger, G., Janssens, I.A., Kleber, M., Kögel-Knabner, I., Lehmann, J., Manning, D.A.C., Nannipieri, P., Rasse, D.P., Weiner, S., Trumbore, S.E., 2011. Persistence of soil organic matter as an ecosystem property. Nature 478, 49–56. doi:10.1038/nature10386

Sierra, C.A., 2012. Temperature sensitivity of organic matter decomposition in the Arrhenius equation: some theoretical considerations. Biogeochemistry 108, 1–15. doi:10.1007/s10533-011-9596-9

Sierra, C.A., Trumbore, S.E., Davidson, E.A., Vicca, S., Janssens, I., 2015. Sensitivity of decomposition rates of soil organic matter with respect to simultaneous changes in temperature and moisture. Journal of Advances in Modeling Earth Systems 7, 335–356. doi:10.1002/2014MS000358

Sinsabaugh, R.L., 2010. Phenol oxidase, peroxidase and organic matter dynamics of soil. Soil Biology & Biochemistry 42, 391–404. doi:10.1016/j.soilbio.2009.10.014

Sinsabaugh, R.L., Follstad Shah, J.J., 2012. Ecoenzymatic Stoichiometry and Ecological Theory. Annual Review of Ecology, Evolution, and Systematics 43, 313–343. doi:10.1146/annurev-ecolsys-071112-124414

Sinsabaugh, R.L., Lauber, C.L., Weintraub, M.N., Ahmed, B., Allison, S.D., Crenshaw, C., Contosta, A.R., Cusack, D., Frey, S., Gallo, M.E., Gartner, T.B., Hobbie, S.E., Holland, K., Keeler, B.L., Powers, J.S., Stursova, M., Takacs-Vesbach, C., Waldrop, M.P., Wallenstein, M.D., Zak, D.R., Zeglin, L.H., 2008. Stoichiometry of soil enzyme activity at global scale. Ecology Letters 11, 1252–1264. doi:10.1111/j.1461-0248.2008.01245.x

Sinsabaugh, R.L., Turner, B.L., Talbot, J.M., Waring, B.G., Powers, J.S., Kuske, C.R., Moorhead, D.L., Follstad Shah, J.J., 2016. Stoichiometry of microbial carbon use efficiency in soils. Ecological Monographs 86, 172–189. doi:10.1890/15-2110.1

Tang, J., Riley, W.J., 2015. Weaker soil carbon–climate feedbacks resulting from microbial and abiotic interactions. Nature Climate Change 5, 56–60. doi:10.1038/nclimate2438

Van Oijen, M., Rougier, J., Smith, R., 2005. Bayesian calibration of process-based forest models: bridging the gap between models and data. Tree Physiology 25, 915–927. doi:10.1093/treephys/25.7.915

Van Soest, P.J., Wine, R.H., 1968. Determination of Lignin and Cellulose in Acid-Detergent Fiber with Permanganate. Journal of AOAC INTERNATIONAL 51, 780–785. doi:10.1093/jaoac/51.4.780

Vrugt, J.A., 2016. Markov chain Monte Carlo simulation using the DREAM software package: Theory, concepts, and MATLAB implementation. Environmental Modelling & Software 75, 273–316. doi:10.1016/j.envsoft.2015.08.013

Wagai, R., Kishimoto-Mo, A.W., Yonemura, S., Shirato, Y., Hiradate, S., Yagasaki, Y., 2013. Linking temperature sensitivity of soil organic matter decomposition to its molecular structure, accessibility, and microbial physiology. Global Change Biology 19, 1114–1125. doi:10.1111/gcb.12112

Wang, X., Chen, G., Wang, S., Zhang, L., Zhang, R., 2019. Temperature sensitivity of different soil carbon pools under biochar addition. Environmental Science and Pollution Research 26, 4130–4140. doi:10.1007/s11356-018-3822-0

Wieder, W.R., Hartman, M.D., Sulman, B.N., Wang, Y.-P., Koven, C.D., Bonan, G.B., 2018. Carbon cycle confidence and uncertainty: Exploring variation among soil biogeochemical models. Global Change Biology 24, 1563–1579. doi:10.1111/gcb.13979

Wizemann, H.-D., Ingwersen, J., Högy, P., Warrach-Sagi, K., Streck, T., Wulfmeyer, V., 2015. Three year observations of water vapor and energy fluxes over agricultural crops in two regional climates of Southwest Germany. Meteorologische Zeitschrift 24, 39–59. doi:10.1127/metz/2014/0618

Zhang, H., Goll, D.S., Manzoni, S., Ciais, P., Guenet, B., Huang, Y., 2018. Modeling the effects of litter stoichiometry and soil mineral N availability on soil organic matter formation using CENTURY-CUE (v1.0). Geoscientific Model Development 11, 4779–4796. doi:10.5194/gmd-11-4779-2018

Zheng, Z., Yu, G., Fu, Y., Wang, Y.-S.Y., Sun, X., Wang, Y.-S.Y., 2009. Temperature sensitivity of soil respiration is affected by prevailing climatic conditions and soil organic carbon content: A trans-China based case study. Soil Biology & Biochemistry 41, 1531–1540. doi:10.1016/j.soilbio.2009.04.01

5 General Discussion

The present thesis aimed to link conceptional carbon pools of soil organic carbon (SOC) models to measurable proxies of SOC quality and to derive pool specific temperature functions. This was conducted in a probabilistic way, acknowledging the uncertainty in the models and measurements. Bayesian calibration was used to test and implement the two promising proxies, the DRIFTS stability index (DSI) and measured Q_{10} values of soil enzymes. Hereby two key model structures that control the mineralization of soil were linked: The division of soil organic matter into discrete pools with fast and slow turnover and pool specific Q_{10} values. Improved understanding of both is important for better assessing the potential impact of a changing climate on carbon stocks of agricultural soils.

The following section will discuss and relate the three presented studies and put them in the broader context of recent literature. The improved DSI implemented into the Daisy model (chapter 3 and chapter 4) will be discussed and compared to other available proxies. Then the temperature sensitivity (chapter 4) and its interlinkage to pool definition and will be addressed, followed by an assessment of the role or Bayesian probabilistic approaches in connecting models to proxies and addressing uncertainties. The chapter will be closed by recommendations for the focus of future studies and elaborate the most promising concepts to advance models of the agricultural plant-soil system and soil organic carbon models.

5.1 The DRIFTS stability index compared to other proxies for SOC quality in modeling

The study of SOC constituents by infrared spectroscopy has been around since decades, using different absorption bands to study SOC quality (Stevenson, 1994). Early approaches were marked by the attempt to classify extractants of SOC from bulk soil, such as humic acids, but with time the use of spectra of bulk soil became the most popular. Michel and Ludwig (2010) first predicted inversely modeled RothC model pools by near-infrared spectroscopy using partial least-square regression. This made it evident that the information about the quality of SOC in the spectra of bulk soils can be linked to model pools. The successful use of DRIFTS aliphatic and aromatic-carboxyl absorption bands as proxies for fast- and slow-cycling SOC for the tested soils (chapter 3) thus presents the first practical realization of this concept for a range of common soils of temperate regions in Europe. The value of the DSI for modeling lies in the cost-effective representation of SOC quality linked to different turnover times. By using spectral information from long-term bare-fallow experiments, the aliphatic and aromatic-carboxyl absorption bands were successfully linked to SOC of rapid and slow loss, respectively. This corroborated earlier hypotheses about their different turnover (Demyan et al., 2012)

and increased the range of soils where the approach is valid (Ultuna, Sweden and Southwest Germany - chapter 3). The lower turnover of aromatic-carboxyl absorption bands is also corroborated by higher thermal stability (Demyan et al., 2013), which is directly linked to higher biogeochemical stability and persistence in ecosystems (Cécillon et al., 2018).

The direct use of DRIFTS band areas to infer SOC quality is a promising possibility as soil infrared spectroscopy is a rapidly evolving field. New handheld spectrometers will advance this development as they already achieve the same performance as bench-top instruments, when used under controlled laboratory conditions (Hutengs et al., 2018). A high cover of spatially explicit DRIFTS spectra could therefore soon become reality, generating an abundance of data to further improve the DSI.

The unwanted interference in spectra thus presents a major obstacle to universal applicability of SOC quality assessment by DRIFTS spectra and the DSI. Particularly the interference from water, is the major challenge for the application of handheld spectrometers under field conditions. The strong effect of water on the aliphatic absorption band at 2930 cm^{-1} and the whole spectra points towards increased complexity when interpreting spectra from field conditions, where soil moisture is inconsistent. Hence, an increased understanding of the effect of water on spectra gained from this study will benefit further research. For DRIFTS spectra of this study, the drying at 105°C was necessary to best resolve the 2930 cm^{-1} absorption band, especially for samples with low SOC content. It was thus needed to best resolve the aliphatic absorption band as a SOC quality indicator. The drying at 105°C and storing in a desiccator was also found the best representation for model initialization (chapter 2). Obviously, drying samples at high temperatures comes with trade-offs. First, the high temperatures carry the potential risk to alter SOC. Additionally the drying at high temperatures and storing samples in a desiccator increases the efforts and cost of DRIFTS measurements significantly and is impossible under field conditions. The risk to alter SOC seems limited up to 105°C for two reasons: The visibility of aliphatic absorption band, which is considered the least stable SOC, only increased with drying temperatures up to 105°C. Also, the changes in absorption and CO_2 evolution during heating by Demyan et al. (2013) were only observed above 200°C, and Duboc et al. (2016) found no lasting spectra alteration for ATR spectra for samples stored outside the desiccator. For large scale applications, however, better solutions than high drying temperatures need to be found to reduce water interference. The highly significant increase and strong correlation of absorption band area with drying temperature across a global collection of soils, shows that there could be the possibility to correct mathematically for the effect of water on absorption bands of interest. Such an approach was demonstrated by Mirzaeitalarposhti et al. (2016) for the interference by carbonate and could be similarly possible for other interferences. It is likely that 105°C drying temperatures were necessary to remove intralayer water from clay minerals, as this water is most persistent, and the effect of drying temperature was absent for tropical sandy soils (personal communication with Benjapon Kunlanit,

unpublished data). Since DRIFTS spectra contain information on the clay content correction factors could be possible with large enough datasets. However it could be difficult to derive correction factors, since not only the clay content, but also the clay type determine water holding capacity of a soil and there could be many interactions between clay type and carbon, which are difficult to describe mathematically.

The mineral interference for the absorption bands at 1620 cm^{-1} and 1530 cm^{-1} is more difficult to eliminate or reduce compared to the water interference. In contrast to the 2930 cm^{-1}, the limits of integration cannot easily be identified by visual inspection as they directly overlap with mineral absorption bands in the same region. However, there does not yet seem to be a simple solution to this problem. Efforts to obtain spectra of only SOC, e.g. by spectral subtraction of the mineral background, represented by ashed samples (Yang, 2014), or pretreatment with hydrofluoric acid to remove soil minerals and silicates (Yeasmin et al., 2017) showed only limited success. Both treatments have high risk of alterations of the remaining SOC or mineral fraction. For example, high temperatures likely alter clay minerals, producing unwanted noise in the spectra whereas mineral artifacts in the silicate region around 1880 cm^{-1} (e.g., spectra of Yeasmin et al., 2017) indicate that silicates cannot be completely dissolved. Since the unwanted changes of SOC cannot be quantified by neither technique, they do not lead to spectra only representing SOC. The increase of the absorption bands at 1620 cm^{-1} and 1530 cm^{-1} with higher drying temperatures in our studies must be a secondary consequence as there is no absorbance of OH in those regions. This demonstrates the complex interactions of absorption bands within spectra. Hence, absorbance in one spectral region seems to affect other regions. This could be related to a change in relative masses of water and soil, or to interactions between the diffuse light and the soil sample, as light could interact several times with the soil before reaching the sensor.

Given the mineral interference cannot be eliminated to this point the integration limits for the absorption bands at 1620 cm^{-1} and 1530 cm^{-1} should be selected with special care. Different integration limits between studies using these absorption bands (e.g., Kunlanit et al., 2014; Parolo et al., 2017; Yeasmin et al., 2017) show a lack of consensus, but with a spectrometer resolution of 4 cm^{-1} it could also be a result of resolution differences. Pure substrates of carbon were used to define limits, but the effect of possible interactions of minerals and SOC in could not be estimated. Therefore, it is likely that the different mineral background from different soils add noise specific to each soil type (Demyan et al., 2012). This means that although the DSI approach proved to be very useful for the soils tested, it is likely that it will have to be adapted to soils of different mineralogy in order to infer SOC quality and pool initialization, and that integration limits could be refined through in depth research. Especially for applications outside the temperate region soils, further testing in a similar way than conducted in this study should be done prior DSI application. For the sites under study, the noise from different mineralogies was less important than the information gained about SOC quality from the

spectra. This was highlighted by the fact that the DSI had a higher correlation with the percentage of centennially persistent carbon compared to SOC when the Ultuna and Bad Lauchstädt sites were combined into one dataset (Figure S 3 - 2). The test is relevant because SOC content alone is already an indicator of SOC stability. This is based on the saturation concept (e.g., Hassink et al., 1997) which assume that each part of newly added SOC to a soil is less recalcitrant than the prior. This principle also reflects in the 1st order decay of SOC models where the total decay per unit of time is a function of SOC content. The higher correlation of the DSI with centennially persistent carbon compared to SOC alone shows that the DSI contains additional site-specific information about SOC stability. Combined with a better performance of models initialized with the DSI compared to steady state initialization in most cases lends strong support to the advantage of the DSI for initializing models compared to inverse modeling approaches using assumptions about site history or turnover times of pools. The results generalize and add to prior existing studies, relating DRIFTS information to SOC quality, specifying an improved method for deriving the DSI. At this time, the DSI is therefore operational for similar soils in temperate zones in Europe, both for inferring the SOC quality and for model initialization.

A conceptionally open question with regard to the DSI is how exactly it relates to the stabilization processes for SOC. Experimentally, the faster turnover times of aliphatic compared to aromatic-carboxyl carbon were clearly proven, i.e., with reduced carbon inputs, the aliphatic absorption band was subject to much faster change than the aromatic-carboxyl absorption band. The understanding of the corresponding mechanism is, however, less clear. Observations of changes in the DSI under fallow seem mostly in line with the theory that recalcitrance of SOC is due to chemical structure, i.e., the degree of unsaturated carbon bonds. This concept was linked to early theories according to which most of SOC represents mostly un-decomposable part of plant litter, especially “recalcitrant” lignin structures. This view has been cast into doubt and most of SOC is now attributed to form from microbial residues which are often physically protected by the soil matrix (Cotrufo et al., 2013). However, the DSI only indicates the presence of different carbon bonds that are related to quality of SOC molecules but does not contain information about their origin. Against the background that microbial residues naturally contain a significant amount of aromatic compounds (Kallenbach et al., 2016), the DSI does not contradict the new understanding. Preferential preservation of aromatic-carboxylate structures could thus be due to their low attractiveness for microbes (Barré et al., 2016) resulting from their low carbon use efficiency (Frey et al., 2013) rather than the intrinsic recalcitrance of lignin constituents of the plant material.

Obviously, DRIFTS is only one of several techniques to study SOC quality. Several other proxies are promising and show potential to represent different SOC pools. The coupling of flash pyrolysis with mid infrared spectroscopy, for example, removes mineral interference from the spectra itself, while still yielding aliphatic and aromatic absorption bands (Nkwain et al., 2018). The results of this technique

could provide similar analysis of SOC chemistry as nuclear magnetic resonance spectroscopy but at a lower cost. However, this technique produces a large CO_2 absorption band, which indicates that SOC is altered by the pyrolysis. Furthermore, a part of SOC remains in the sample after pyrolysis, so that not the entire SOC profile is characterized. The thermal stability theory would suggest that this part corresponds to the most stable SOC. Both points mentioned could further depend on the soil type. The Rock-Eval analysis overcomes this partly, by combining pyrolysis with combustion thereafter (Cécillon et al., 2018) but the resulting multidimensional data are more complex to interpret. The presence of CO and CO_2 under pyrolysis also indicates alterations of SOC. Therefore, the connection between SOC pools and Rock-Eval spectra has to date only been made by random-forest machine learning and it remains to be solved how the data could be directly linked to the two SOC pools most models use to date. Other approaches such as the use of ^{14}C as a tracing element do not yield a proxy for SOC distribution but can be used to estimate ages of either bulk soil SOC (Ahrens et al., 2014) or of several SOC pools of different turnover (Metzler et al., 2020). Thus, they are especially useful for inverse modeling approaches using longer time series and in combination with other techniques such as thermal gas analysis or physical fractionation procedures. New imaging techniques such as nanoscale secondary ion mass spectrometry (NanoSIMS) can also help to study the mechanisms of SOC stabilization mainly on particles of silt and clay size. For example, they provide evidence of the importance of mineral associated organic matter for SOC stabilization forming rapidly at initial soil formation (Schweizer et al., 2018). Combined with isotopic labeling by ^{13}C and ^{15}N, NanoSIMS images showed, that dissolved organic carbon attaches primarily to already present patches of carbon (Kopittke et al., 2020) while microbially derived carbon can directly attach to the uncoated surface of clay (Kopittke et al., 2018). While not yielding direct modeling proxies, yet, these approaches help to refine the understanding about the relative importance of different SOC forming mechanisms, which can then be implemented into SOC models. For example, Huang et al. (2019) found evidence that lignin derived aromatic carbon can directly sorb to iron oxides where it is stabilized. This suggests that not all SOC is metabolized by microorganisms and could also explain, why heavy mineral fractions were enriched in aromatic carbon (Demyan et al., 2012). Thus, simulating spatial arrangement, microbial processing but also extracellular enzymes and sorption show the potential to improve SOC models in the future by a better representation of important processes.

For classical SOC models, that do not consider spatial arrangement, the physical soil fractionation to derive SOC pools, which was the first attempt to measure model pools (Zimmermann et al., 2007), is still a promising option. However, with the diversity of protocols, for example different densities of the sodium polytungstate solution used (between 1.4 and 2.0 g cm^{-3}), a clear standard is lacking. Even with a clear standard, it is prone to differences between conductors (Poeplau et al., 2013). Also, physical fractionation has the disadvantage that for the long timescales needed to examine changes in SOC

(e.g., 50 years and longer) the fractions are more prone to change than proxies based on chemistry. A clear advantage of physical soil fractionation compared to other techniques is that nitrogen for each fraction, and hence, each pool, can be directly measured and would not have to be estimated by a fix carbon to nitrogen ratio for each pool, as is the case for the other techniques which focus on carbon. An interesting intermediate between the DSI approach was proposed by Baldock et al. (2013), who separated soil by size fractionation and then determined aromatic carbon by ^{13}C NMR within the coarse and fine fraction which they called resistant SOC. It was shown that such fractions could be used to initialize the RothC model and can be derived from environmental covariates of proximal sensing techniques (Lee and Viscarra Rossel, 2020).

Given the shortcomings of each technique alone, comparative studies of the different SOC quality proxies would be of added value. Assessing where different proxies match in terms of SOC quality and turnover, and investigating their major differences, could improve them simultaneously. If better proxies for pool initialization than the DSI could be found, or the mineral interference be overcome, DRIFTS could still prove useful. Even though DRIFTS spectra are measured on ball milled samples, there are indications that the SOC complexity represented in the spectra is correlated to SOC in different soil density fractions (Demyan et al., 2012) and thus liked to physicochemical stabilization. For example, its chemometric prediction capacities, such as partial lest square regression, can be used to predict other proxies for large regions at low cost demonstrated by the success for other quality indices including enzyme activity (Rasche et al., 2013).

In summary, the performance improvements from using the DSI, corroborated by statistical tests (chapter 3) and the Bayesian calibration, suggest that directly applying the DSI for model initialization represents a step forward in the attempt to model the measurable. The DSI is, to the knowledge of the author, the first operational proxy to directly partition SOC into different quality pools which was tested against measured long-term data. This presents an advancement over the indirect link between proxies and pools by machine learning or partial least square regressions. Future studies should focus on resolving the shortcomings of the DSI approach which are mineral and water interference. It would be desirable to test several proxies in parallel, following their development over time and calibrating models to them. As was shown in chapter 3, long term datasets with repeated measurements of controlled field experiments including bare fallow are needed for this evaluation and calibration. Combining several datasets of similar studies would be a good way forward.

5.2 The complexity of pool specific Q_{10} values, their link to pool definition and the potential of enzyme Q_{10} values as proxy

As was mentioned before, the lack of knowledge about pool specific temperature sensitivity and Q_{10} values is one of the biggest uncertainties in global carbon models (Tang and Riley, 2015; Todd-Brown et al., 2014) and a better understanding of Q_{10} values is crucial. It was shown that statistical inference using a combination of several experiments can provide deeper insights into the nature of Q_{10} values than single experiments (e.g., Carey et al., 2016). Thus, it should also be feasible to derive pool specific Q_{10} values for process models by combining experiments. Within this study, the assumption was that the carbon complexity of a pool would be the main determining factor of pool specific Q_{10} values (Bosatta and Ågren, 1999; Wetterstedt and Ågren, 2011). The strong parameter correlations between the turnover of the pools with their Q_{10} values (chapter 4) showed why a clear definition of pools was needed: Without clear pool definition, a shift in pool allocation or Q_{10} values could lead to the same results in model calibration.

With the DRIFTS and lignin-to-nitrogen pool division, the derived Q_{10} values for the defined pools of individual laboratory incubations (Figure 4 - 6 c and d) showed the utility of Bayesian calibration to derive model parameters that cannot directly be measured. In the case of this study, this were the Q_{10} values. This general utility of Bayesian calibration to derive Q_{10} values was also shown by a few other studies (Hararuk et al., 2014, 2017; Hararuk and Luo, 2014). However, the diverging results of the different individual Bayesian calibrations Q_{10} values (chapter 4) and the strong parameter correlations show that derived Q_{10} values have to be interpreted with caution. In fact, the impossibility of deriving unique Q_{10} values as a function of clearly defined pools by carbon quality contradicts the initial hypothesis that intrinsic substrate temperature sensitivity is the main driver of mineralization Q_{10} values: Inferred Q_{10} values of the same pool, varied strongly between different experimental conditions (e.g., close to either 1 or 3 for fast cycling SOC; chapter 4), which should not be the case if quality were the main determinant of Q_{10} values. Quality might be the main determinant of Q_{10} values in cultures of pure substrate and microbes where soil aggregation and stress are absent, but this seems not to be the case for soils. Therefore, other processes need to be considered and modeled. The conceptual model we developed combined insights from the experiment and the literature. It summarizes which other factors exert the major control on the soil carbon mineralization Q_{10} values, which are so far poorly represented in SOC models. Identified were the gain and loss of physical protection, substrate availability and absence or presence of microbial stress.

The increase of Q_{10} values by loss of physical protection is in alignment with several studies comparing Q_{10} values of protected and unprotected carbon (Benbi et al., 2014; Karhu et al., 2019). It is further supported by incubated intact soil cores, having only a Q_{10} value of 2 (Vaughn and Torn, 2019). Also

Todd-Brown et al. (2018) summarized that lower field estimated Q_{10} values than laboratory incubation Q_{10} values were reported in the literature. Loss of physical protection could also be the explanation, why the Q_{10} values of the Ultuna incubation experiment were so high (~3; Figure 4 - 6 c). Given the evidence for high Q_{10} values of unprotected carbon, it is somewhat concerning that Poeplau et al. (2017) reported physically protected SOC is lost fastest under extreme warming, though the study considered high temperature increases up to +40°C. This highlights the effect of aggregation on mineralization Q_{10} values and vice versa need to be better understood. Given the importance of physical protection for Q_{10} values, soil fractionation methods as pool division proxy (Poeplau et al., 2013) might be better for inferring Q_{10} values compared to the DSI, which is only indirectly linked to physical protection (Demyan et al., 2012).

A second factor is the increase of Q_{10} values with higher substrate availability (Blagodatskaya et al., 2016; Gromova et al., 2020). This was supported within this study by much higher inferred Q_{10} values for the fast cycling crop-litter pool (added organic matter; AOM) of the incubation experiment around 3 compared to values around 2 for the field experiments (Figure 4 - 6 a). There is a clear link to physical protection as the loss of protection makes substrate available for microbes. Hence, substrate availability might be the actual driver behind the effect of physical protection on mineralization Q_{10} values. However, processes of gain and loss of physical protection are probably the main controls on substrate availability in natural soils: Any unprotected carbon source in the soil is usually consumed within a few months and converted to a form of microbial residue (Cotrufo et al., 2013) which are aggregated between soil particles. Another part of the plant material is occluded in aggregates and therefore partly protected from decomposition. This occluded particulate organic matter in the aggregates forms as a byproduct of fungal and microbial activity (Totsche et al., 2017), so also its availability also depends on aggregate disruption.

The third potential factor is environmental stress for microbes, which inhibits their strong opportunistic increase in activity observed under optimal conditions. Rather than their state per se, the fluctuations of temperature and moisture in the field could be the stressing factor which shift microbial community (Liu et al., 2019). Evans and Wallenstein (2012) showed that microbial reactions to moisture change was influenced by frequent moisture stress before the experiment. If microbial stress can affect the reaction to changes in moisture, it should also influence the reaction to temperature changes. Heat stress for microbes, for example, can lead to increased maintenance respiration and less growth (Li et al., 2020) which could be suppressing microbial biomass and hence, reduce microbial activity and Q_{10} values. An extreme example for this effect is the study of Chang et al. (2012), who even reported some Q_{10} values for microbial respiration <1 for alpine soils, as a result of induced heat stress at up to 30°C for a soil with mean annual temperature close to 0°C . The effect

of microbial stress on Q_{10} values is the least researched of the three mechanisms. This would initially require manipulation experiments under controlled conditions.

Another effect of potentially high relevance under climate change, which could not be studied here, is the reduction of carbon use efficiency at higher temperatures (Frey et al., 2013). A trend for lower efficiencies with higher temperatures can also be found at global level (Qiao et al., 2019). For the input of new carbon into soils, this is probably the most relevant factor, as reduced carbon use efficiency due to higher temperatures would dramatically reduce carbon inputs.

The challenge of common SOC models is that the three discussed controlling factors of Q_{10} values are implemented in very simple ways and do not influence Q_{10} values. Physical protection, for example, is usually a function of clay content only: In Daisy there is a linear decline of SOM turnover from 100 to 60% between 0 and 25% clay (Mueller et al., 1997), staying at 60% for clay contents >25%. In CENTURY it is a linear decrease of turnover with silt and clay content for the active SOC pool and the fraction lost to respiration (Parton et al., 1987). These functions have not been altered in the last three decades, even though they were rough estimations, based on laboratory incubation data (Parton et al., 1987) – which, as discussed earlier, destroy physical protection. The inability to simulate loss of protection represents a limitation for the simulation of incubation experiments, ploughing or freeze-thaw cycles. In the light of the oversimplified representation compared to the importance of physical protection, it becomes clear that it is difficult to infer pools specific Q_{10} values as a function of SOC quality, which is subordinate to protection. Thus, the conceptual model presented in chapter 4 is in alignment with Sulman et al. (2018), who postulated the hypothesis that the Q_{10} values of formation and destruction of physical protection is one of the key uncertainties in SOC models. Physical protection should be a research priority and recent model developments attempt to implement it (e.g., Milennial model, Abramoff et al., 2018). The results of this study suggest that not only the simulation of physical protection but also the effect of physical protection on Q_{10} values and the Q_{10} values of destruction of physical protection need to be included for simulations of climate change.

All discussed factors, formation of physical protection, substrate availability, stress, and stress related carbon use efficiency reduction (Frey et al., 2013; Gromova et al., 2020; Li et al., 2020; Totsche et al., 2017) are linked to the microbial lifecycle . Hence, the microbial biomass should be at the core of new SOC cycling models (Woolf and Lehmann, 2019). With their lifecycle so closely linked to many soil processes, it is clear, that models originating mostly from non-living systems and chemical reactions, such as 1st order kinetics or intrinsic temperature sensitivity fall short of matching observations from experiments. Their static approach misses the dynamic adaptions of living organisms. This does not mean that the carbon quality effect on Q_{10} values is not measurable under controlled conditions where other factors remain constant. However, experimental evidence indicates that in soils the theoretical

intrinsic substrate Q_{10} values is subordinate to the discussed other factors (Leifeld and von Lützow, 2014; Poeplau et al., 2017). This was also found in this study.

While the many involved processes make it difficult to theoretically derive pool specific Q_{10} values, the Q_{10} values of soil enzymes showed potential as a proxy for mineralization Q_{10} values. Because they are considered to be a rate-limiting factor, they represent a direct connection to the microbial mineralization processes happening in the soil (Sinsabaugh et al., 2008). Ali et al. (2015) showed that this connection exists in situ and a correlation between enzyme Q_{10} values and mineralization Q_{10} values of different sites was also found by Diáková et al. (2016). The results of the application of enzyme Q_{10} values to the model pools (chapter 4) provided further evidence that the enzyme Q_{10} values contain important information about mineralization Q_{10} values of different carbon complexities: Applying measured Q_{10} values reduced model errors. Specifically, applying the Q_{10} value of phenoloxidase to SOM pools and the slow AOM pool and the Q_{10} value of β-glucosidase to fast AOM pool, yielded significantly lower model errors. Additionally, the enzyme Q_{10} values and Bayesian calibration inferred Q_{10} values for the same field experiments were in similar ranges.

However, several questions remain unanswered regarding how the enzyme Q_{10} values exactly link to mineralization Q_{10} values. For example, a tendency for measured enzymes Q_{10} values being lower than measured mineralization Q_{10} values exists across studies (e.g., Ali et al., 2015, 2018; Blagodatskaya et al., 2016; Diáková et al., 2016, this studies infered Q_{10} values vs. enzyme Q_{10} values). The direct application of enzyme Q_{10} values might thus underestimate the actual mineralization Q_{10} values of all pools combined. However, the difference could also be an effect of methodological differences. Studies were usually measuring mineralization Q_{10} values at optimal moisture conditions with disturbed soils (mixed and sieved) and after pre-incubation, whereas potential enzyme activities measured the enzyme Q_{10} values as it was at time of sampling. While this thesis provides first evidence for the utility of enzyme Q_{10} values as model proxy, the question of how to best introduce the connection between enzyme and mineralization Q_{10} values into models is still open. Also, it is not finally clarified which measured enzymes fit best to which predefined SOC pools or if completely new models are better when using enzyme Q_{10} values. For example, applying phenoloxidase to the fast SOC pool in this study was done for the lack of a better option. The enzymes β-glucosidase and xylanase which depolymerize cellulose (Jeng et al., 2011) and hemicellulose (Beg et al., 2001) of plant litter, respectively, were considered unsuitable for the fast SOC pool. Also phenoloxidase, which depolymerizes phenolic molecules such as lignin (Sinsabaugh, 2010) has only a conceptual fit to the slow SOC pool defined as aromatic-carboxylate carbon. It was considered the most feasible of all enzymes for fast SOC because the lack of a better enzyme. Hence, the fact that this application further reduced model error could be due to the general tendency towards a lower Q_{10} value of the field experiment rather than a conceptual fit. However, even the Q_{10} values of the same enzyme varies

between microbial communities (Alster et al., 2016) and hence, enzyme Q_{10} values are always a proxy and will never have a perfect conceptional fit. Nevertheless, the link of pools to enzymes could be conceptionally improved. For example, for AOM pools, with appointing only lignin to the slow AOM pool and all the rest into the AOM fast pool. Then phenoloxidase Q_{10} values would fit better to the slow AOM pool. The use of the correlated lignin-to-nitrogen ratio was used due to its well-established utility to date (Parton et al., 1987; Zhang et al., 2018) and availability of calibrated parameters. Another option would be dividing the non-lignin plant components into a medium turnover AOM pool representing cell wall structures and a very fast AOM pool representing water soluble cell content. If the pools would represent such clearly defined measurable fractions, it would be less ambiguous which enzymes belongs to which pool. However, it could also be, that treating different AOM compartments as isolated fractions would be misleading due to interactions between the compartments, for example lignin structures protecting cellulose or slow pools requiring energy from faster pools for decomposition. Finally, with regards to the importance of physical protection of SOC on Q_{10} values, there is the option than enzyme Q_{10} values only reflect the Q_{10} values of unprotected carbon. This is because enzymes are only rate-limiting when carbon is accessible (Schimel and Schaeffer, 2012). As the Q_{10} values of potential enzyme activity is measured by substrate addition (Ali et al., 2018) it neglects the Q_{10} values of physical protection by definition, which again points to the importance of understanding the effect of physical protection on Q_{10} values.

New model concepts, simulating microbial and physical processes (Abramoff et al., 2018; Robertson et al., 2019; Woolf and Lehmann, 2019), question the model pools that have no measurable counterpart, thus new models could design pools with an exact fit to enzymes. As the discussion showed, there remain a lot of open questions about which processes influence Q_{10} values the most. However, they are all connected to the microbial life cycle, which in classical SOC models using 1st order kinetics (e.g., Daisy and CENUTRY) has no feedback to carbon decomposition. Thus, many models try to include microbial processes into global carbon models (Wang et al., 2017; Wieder et al., 2018) and would benefit from enhanced understanding of clearly observable trends of Q_{10} values on the global scale (Chen et al., 2020).

Summarizing, there are many processes at play that influence Q_{10} values: physical protection, substrate availability, soil moisture, prior conditions, microbial stress and carbon complexity, which are possibly all interlinked. As the number of relevant factors shows, this leads to a mathematically highly dimensional problem in modeling. This means that prioritizing of the most relevant processes affecting Q_{10} values is necessary to improve the simulation of the effects of climate change. Those seem to be Q_{10} values of physical protection for the loss SOC, and Q_{10} values of carbon use efficiencies and stress for the microbial lifecycle on the input of new carbon to SOC. A better understanding on their connection to measurable enzyme Q_{10} values is also needed. The prioritization means that some

processes will be neglected as a trade-off for implementing others. The choice of model structure then determines inferred Q_{10} values (Hararuk and Luo, 2014). This subjective choice and the equifinality of parameters lead to uncertainties of the model and its future predictions (Sierra et al., 2015a). Those uncertainties need to be accounted for. Therefore, model frameworks such as Bayesian calibration are needed because they can account for uncertainty in the models in a probabilistic way.

5.3 The utility of Bayesian calibration in displaying uncertainty, model testing and model development

Understanding the uncertainty of SOC models is important for predictive applications, especially if models are a basis for policy decisions (Campbell and Paustian, 2015), but also to direct further research and model development. While model performance statistics such as the root mean square error of simulations against observed data (e.g., chapter 4) can provide a measure of simulation success if data is available, they cannot display the uncertainty of model predictions into the future. Due to the complex nonlinear nature of SOC models, even established statistical approaches fail at this. Bayesian calibration can be applied to nonlinear models for analyzing and propagating error (Benke et al., 2018; Lu et al., 2012) and offers a way forward.

Classical measures of model performance, such as modeling efficiencies, often are overly optimistic due to prior calibration. Bayesian calibration credibility intervals in contrast are usually wider and show that the uncertainties are larger than other measures would suggest. However, their validity is shown by comparative studies, for example the similar parameter uncertainties of this and several other studies applying Bayesian calibration to SOC models (Table 3 - 5). The here identified 95% credibility intervals for the half-life of the slow SOC pool, with 278 to 1095 years, show a large uncertainty in model parameters. It is therefore essential to acknowledge this uncertainty, especially in predictive studies. Apart from the similarity of credibility intervals across studies, there are other indications that the large credibility intervals are a realistic representation of the actual uncertainty. For example, different SOC models on a global scale simulated a change of global SOC stocks between -30 and +25 Pg carbon in the last century (Wieder et al., 2018), roughly ±1% of total stocks. Even the global SOC stock simulations of Todd-Brown et al. (2018) under the extreme RCP 8.5 climate change scenario could not establish whether SOC would be lost or gained until 2100.

Although the depiction of uncertainty is important for a realistic representation of the actual knowledge about a process, this is only the first step. The real utility of Bayesian calibration is not only the depiction of parameter uncertainty but lies in the interpretation and reduction of uncertainty about important processes, for example by applying new proxies. New proxies or model structures can be directly assessed by the reduction of uncertainty they provide, which leads to a better

understanding of the processes and measures the relevance of different sub-processes. For example, Ahrens et al. (2014) showed that the addition of ^{14}C data could reduce the width of credibility intervals of humification efficiency and of slow SOC turnover between 60 and 90%. Better model structures also reduce uncertainty as was shown by the introduction of priming into the CENTURY based SOC model ORCHIDEE (Guenet et al., 2016), which shows how improved system understanding can lead to better models. Also within this thesis (chapter 3), the addition of the DSI as physicochemical meaningful proxy for pool partitioning reduced uncertainty of SOC pools turnover and furthermore showed that humification should be replaced by a separation between fast- and slow cycling SOC at microbial death (Figure 3 - 7).

This shows that Bayesian calibration does not eliminate the need for qualitative considerations of plausibility, for example of the unrealistic high humification efficiencies >90%, by using the original DAISY structure without constraints, could be eliminated by a new structure (Figure S 3 - 10). Another example were the Q_{10} values of several pools which could be constrained for individual experiments (chapter 4), but were only interpreted as a local property of each experiment. Bayesian calibration provides the parameters given the data and the model. Hence, if the model is weak or the data represents a very special case, the results will be suboptimal for other sites or experiments, which shows in high parameter uncertainty or unrealistic parameter combinations (Poeter et al., 2014). That model parameters are highly dependent on the setting is a typical modelling problem that also shows in crop models, for example in different parameter sensitivity scores which strongly depend on the simulated crop (Specka et al., 2015). Thus, additional qualitative user considerations are important in the interpretation of model results. In this study, the interpretation of unrealistic parameters was that the original Daisy structure was suboptimal for the application of the DSI because it would represent a change in SOC chemistry without microbial involvement (chapter 3). Also, intrinsic Q_{10} values as a function of SOC and litter quality was considered unlikely as main determinant of whole soil mineralization Q_{10} values because of diverging parameter optima (chapter 4). The Q_{10} values were identified as a multiplicative structure, which are particularly susceptible to equifinality (Bagnara et al., 2018) and thus unrealistic values. The qualitative analysis of Bayesian calibration outputs provides in depth insight into models but is to some extent subjective. However, even the choice of model is a subjective decision for one model against another, so a more neutral approach would be to compare different plausible model formulations with respect to available data. In this regard, Bayesian calibration is limited, because it takes the model as given (Van Oijen et al., 2005). A logical step forward is then to use Bayesian model evidence, which provides a basis for model comparisons computing integrated likelihoods across the whole parameter space and compare likelihoods of different models given the data (Schöniger et al., 2014). Possible model structure comparisons arising from the results of this thesis would be to compare the use of one Q_{10} value for all pools vs. different pool specific Q_{10}

values, testing new model structures, such as simulation of physical protection compared to traditional SOC models, or different temperature functions of higher complexity compared to the exponential functions (Tuomi et al., 2008).

A novelty of the Bayesian calibrations of this study was a statistical accounting for autocorrelation structures in the data by using error variance terms estimated by linear mixed models. This helped addressing the challenge of autocorrelation within data, which is one of the main drivers of uncertainty in Bayesian calibration (Elshall et al., 2019). It enabled the combination of different experiments and data types into one single Bayesian calibration, thus providing the basis for robust parameter estimations that were superior to site dependent calibrations (Figure 3 - 5). This is important, because as was seen at the example of very different Q_{10} values of the same pools between experiments (chapter 4), individual calibrations could be strongly misleading. Therefore, a combination for sites is preferable. As the sums of squares objective function at the center of the Bayesian calibration approach strongly depends on the measurement variance (as discussed in chapter 3), it is important to account for the data structure. From this follows, that the choice of variance for weighting has a major influence on parameter posterior distributions, when different sites are combined. This was shown for example by higher uncertainties of the Bayesian calibration using the artificial equal weighting (Figure 3 - 5). An unbiased weighting scheme is therefore important if different experiments and types of data, including state variables and matter flows, are to be combined, since different field experiments naturally differ in their heterogeneity due to soil site characteristics and/or different size of experimental fields. There could also be temporally autocorrelated measurements errors due to instrument or human error (Piepho et al., 2004), all which are usually ignored in Bayesian inference approaches. It is not clear how this autocorrelations could be directly represented in a Bayesian calibration algorithm but through the use of the statistical linear mixed effects model, modeling the temporal autocorrelation of repeated measurements (Piepho et al., 2004) and separating the natural heterogeneity of a field from the measurement error was possible. This natural heterogeneity would correspond to a block effect in design experiments, and it is preferable to remove its variance component for the estimation of error variance by adding this effect. Thus, the presented approach allows to mostly eliminate the unwanted autocorrelated error in residuals in the Bayesian calibration, weighing only by the random and residual error variance. This should prove superior when different experiments are combined. It is not common in Bayesian inference approaches and most approaches do not combine different sites in their calibrations (e.g., Ahrens et al., 2014; Yeluripati et al., 2009), but as was shown in chapter 4, it is preferable for parameter robustness. For regional to global scale simulations and climate perturbations, robust parameter credibility intervals are needed to serve as priors for the SOC part of climate models (e.g., Arisido et al., 2017). For nonlinear SOC models, those

can only be inferred by Bayesian calibrations combining a larger number of sites and measurements, for which the mixed approach presented here, is well suited.

While Bayesian calibration proves of high value for model calibration, several limitations of models still hold. For extrapolation of model results, high caution is needed, and it must be assured that the system behavior follows the applied equations beyond the calibration range. For climate change scenarios, this especially concerns the temperature function. The exponential temperature function of Daisy, for example, fits reasonably well up to 30°C (Carey et al., 2016), but for cases >30°C a gaussian function is superior (Tuomi et al., 2008). Would the Daisy temperature function be extrapolated to simulate turnover under temperatures of 40°C or higher, it would be wrong. However, with the Bayesian calibration using only temperatures below 30°C, this would not be represented in credibility intervals. Hence, one needs to be extremely cautious when extrapolating and make sure that the assumptions hold, for example, by tests with manipulation experiments. If the experiments are too specific or important processes are missing in the models, the parameters cannot be used for other sites or conditions. This is illustrated for the inferred Q_{10} values from the Ultuna incubation for example, which would not fit at all to the laboratory incubation of residues. As simulations of temperature increase under future climates are most likely extrapolations beyond temperatures present today, such an extrapolation needs experimental evidence. The climate we could have in Europe in the future could already be present somewhere else on the globe or in special conditions, such as low elevations, and the principle of uniformity could be applied in modeling, given that soils behave similar. This might be difficult because older soils are usually found at warmer climates and some special sites with similar conditions could prove important. However, the space-for-time approach is often insufficient to constrain temperature responses (Abramoff et al., 2019), which shows that it is crucial that all important mechanisms are explicitly understood and implemented. Given that higher temperature incubation experiments in the laboratory were unsuitable to infer Q_{10} values for field experiments, the combination of heating experiments around the globe would be most preferable (e.g., Carey et al., 2016).

As shown, the Bayesian calibration framework is very useful for thorough evaluation and improvement of nonlinear SOC models. With a qualitative assessment of parameter plausibility and correlations, the combination of several sites, or potentially even global datasets provides robust estimates for regional and global modeling approaches. This presents the next logical step in combining SOC modeling and system understanding. Bayesian calibration can help to improve models, show uncertainty and therefore can direct future studies and can be used to do hypothesis testing with established SOC models. A next step would be to compare different model formulations that require Bayesian model evidence techniques.

5.4 How model structures could be improved the Bayesian way

As outlined in the previous chapters, deriving better SOC and agricultural system models using Bayesian techniques will require rapid iterations of testing with combined data and solid model selection schemes. As shortcomings in the current SOC models became evident in the Bayesian calibration results, Bayesian model evidence schemes (Pullen and Morris, 2014; Schöniger et al., 2014) would be the next logical step. Bayesian model evidence has been used for plant models (Wöhling et al., 2015), but according to literature research has to this point not been used for SOC model selection (Scopus search: TITLE-ABS-KEY (soil AND carbon AND model AND Bayesian AND model AND (selection OR evidence); date accessed: 18.05.20).

As became evident, it is not the models themselves that are per se suboptimal. Rather some individual structures, such as the flow of carbon between pools or temperature moisture functions, need to be optimized. Contrary to earlier model comparison approaches where each model needs to be calibrated before (e.g., Smith et al., 1997), we suggest an approach that aims at developing a deeper common understanding: Instead of comparing completely different SOC models or even agricultural models, important sub-functions, such as the temperature or moisture function of different models (e.g., of Daisy vs CENTURY), should be compared by their potential to represent field data. Ideally the models would have a hierarchical modular structure, meaning they would have a common agreed basic structure (e.g., the same standard temperature which parameters are calibrated for – which is 10°C of Daisy and 30°C for Century). This would benefit the entire modeling community, as sub-functions could easily be exchanged. In doing so, it would be advisable to have a common framework for models and model testing, such as cascade vs. feedback models (Todd-Brown et al., 2018). A commonly agreed upon structure and joint datasets would be good, on which tests of new structures and sub-functions could be based, with the goal of importing newly developed features if they prove important. An example of such a broader conceptual model approach is the Millennial model structure, aiming at simulating SOC storage through soil aggregates (Abramoff et al., 2018). Within the here presented thesis, the two important questions of temperature sensitivity and of measurable SOC pool division were addressed. Further arising questions of high priority were identified by the model shortcomings of Daisy, where literature pointed towards important missing processes: The stabilization mechanisms which are linked to the soil microbial lifecycle and influence temperature sensitivity and the simulation of microbial stress. The living conditions of the soil microbiome and its limitations are highly relevant for a better understanding of the SOC mineralization process. Hence, future experiments and next generation models should focus on improving the simulation of the most relevant controls for the microbial lifecycle, how they are affected by climate change and to develop models in parallel experiments to test new concepts in an integrated fashion.

5.5 References general discussion

Abramoff, R., Xu, X., Hartman, M., O'Brien, S., Feng, W., Davidson, E., Finzi, A., Moorhead, D., Schimel, J., Torn, M. and Mayes, M. A.: The Millennial model: in search of measurable pools and transformations for modeling soil carbon in the new century, Biogeochemistry, 137(1–2), 51–71, doi:10.1007/s10533-017-0409-7, 2018.

Abramoff, R. Z., Torn, M. S., Georgiou, K., Tang, J. and Riley, W. J.: Soil Organic Matter Temperature Sensitivity Cannot be Directly Inferred From Spatial Gradients, Global Biogeochem. Cycles, 33(6), 761–776, doi:10.1029/2018GB006001, 2019.

Ahrens, B., Reichstein, M., Borken, W., Muhr, J., Trumbore, S. E. and Wutzler, T.: Bayesian calibration of a soil organic carbon model using Δ14C measurements of soil organic carbon and heterotrophic respiration as joint constraints, Biogeosciences, 11(8), 2147–2168, doi:10.5194/bg-11-2147-2014, 2014.

Ali, R. S., Ingwersen, J., Demyan, M. S., Funkuin, Y. N., Wizemann, H.-D., Kandeler, E. and Poll, C.: Modelling in situ activities of enzymes as a tool to explain seasonal variation of soil respiration from agro-ecosystems, Soil Biol. Biochem., 81, 291–303, doi:10.1016/j.soilbio.2014.12.001, 2015.

Ali, R. S., Kandeler, E., Marhan, S., Demyan, M. S., Ingwersen, J., Mirzaeitalarposhti, R., Rasche, F., Cadisch, G. and Poll, C.: Controls on microbially regulated soil organic carbon decomposition at the regional scale, Soil Biol. Biochem., 118(December 2017), 59–68, doi:10.1016/j.soilbio.2017.12.007, 2018.

Alster, C. J., Baas, P., Wallenstein, M. D., Johnson, N. G. and von Fischer, J. C.: Temperature Sensitivity as a Microbial Trait Using Parameters from Macromolecular Rate Theory, Front. Microbiol., 7(NOV), 1–10, doi:10.3389/fmicb.2016.01821, 2016.

Arisido, M. W., Gaetan, C., Zanchettin, D. and Rubino, A.: A Bayesian hierarchical approach for spatial analysis of climate model bias in multi-model ensembles, Stoch. Environ. Res. Risk Assess., 31(10), 2645–2657, doi:10.1007/s00477-017-1383-2, 2017.

Bagnara, M., Van Oijen, M., Cameron, D., Gianelle, D., Magnani, F. and Sottocornola, M.: Bayesian calibration of simple forest models with multiplicative mathematical structure: A case study with two Light Use Efficiency models in an alpine forest, Ecol. Modell., 371(April 2017), 90–100, doi:10.1016/j.ecolmodel.2018.01.014, 2018.

Baldock, J. A., Sanderman, J., Macdonald, L. M., Puccini, A., Hawke, B., Szarvas, S. and McGowan, J.: Quantifying the allocation of soil organic carbon to biologically significant fractions, Soil Res., 51(8), 561, doi:10.1071/SR12374, 2013.

Barré, P., Plante, A. F., Cécillon, L., Lutfalla, S., Baudin, F., Bernard, S., Christensen, B. T., Eglin, T., Fernandez, J. M., Houot, S., Kätterer, T., Le Guillou, C., Macdonald, A., van Oort, F. and Chenu, C.: The energetic and chemical signatures of persistent soil organic matter, Biogeochemistry, 130(1–2), 1–12, doi:10.1007/s10533-016-0246-0, 2016.

Beg, Q. K., Kapoor, M., Mahajan, L. and Hoondal, G. S.: Microbial xylanases and their industrial applications: a review, Appl. Microbiol. Biotechnol., 56(3–4), 326–338, doi:10.1007/s002530100704, 2001.

Benbi, D. K., Boparai, A. K. and Brar, K.: Decomposition of particulate organic matter is more sensitive to temperature than the mineral associated organic matter, Soil Biol. Biochem., 70, 183–192, doi:10.1016/j.soilbio.2013.12.032, 2014.

Benke, K. K., Norng, S., Robinson, N. J., Benke, L. R. and Peterson, T. J.: Error propagation in computer models: analytic approaches, advantages, disadvantages and constraints, Stoch. Environ. Res. Risk Assess., 32(10), 2971–2985, doi:10.1007/s00477-018-1555-8, 2018.

Blagodatskaya, E., Blagodatsky, S., Khomyakov, N., Myachina, O. and Kuzyakov, Y.: Temperature sensitivity and enzymatic mechanisms of soil organic matter decomposition along an altitudinal gradient on Mount Kilimanjaro, Sci. Rep., 6(February), 1–11, doi:10.1038/srep22240, 2016.

Bosatta, E. and Ågren, G. I.: Soil organic matter quality interpreted thermodynamically, Soil Biol. Biochem., 31(13), 1889–1891, doi:10.1016/S0038-0717(99)00105-4, 1999.

Campbell, E. E. E. and Paustian, K.: Current developments in soil organic matter modeling and the expansion of model applications: a review, Environ. Res. Lett., 10(12), 123004, doi:10.1088/1748-9326/10/12/123004, 2015.

Carey, J. C., Tang, J., Templer, P. H., Kroeger, K. D., Crowther, T. W., Burton, A. J., Dukes, J. S., Emmett, B., Frey, S. D., Heskel, M. A., Jiang, L., Machmuller, M. B., Mohan, J., Panetta, A. M., Reich, P. B., Reinsch, S., Wang, X., Allison, S. D., Bamminger, C., Bridgham, S., Collins, S. L., de Dato, G., Eddy, W. C., Enquist, B. J., Estiarte, M., Harte, J., Henderson, A., Johnson, B. R., Larsen, K. S., Luo, Y., Marhan, S., Melillo, J. M., Peñuelas, J., Pfeifer-Meister, L., Poll, C., Rastetter, E., Reinmann, A. B., Reynolds, L. L., Schmidt, I. K., Shaver, G. R., Strong, A. L., Suseela, V. and Tietema, A.: Temperature response of soil respiration largely unaltered with experimental warming, Proc. Natl. Acad. Sci., 113(48), 13797–13802, doi:10.1073/pnas.1605365113, 2016.

Cécillon, L., Baudin, F., Chenu, C., Houot, S., Jolivet, R., Kätterer, T., Lutfalla, S., Macdonald, A., van Oort, F., Plante, A. F., Savignac, F., Soucémarianadin, L. N. and Barré, P.: A model based on Rock-Eval thermal analysis to quantify the size of the centennially persistent organic carbon pool in temperate soils, Biogeosciences, 15(9), 2835–2849, doi:10.5194/bg-15-2835-2018, 2018.

Chang, X., Wang, S., Luo, C., Zhang, Z., Duan, J., Zhu, X., Lin, Q. and Xu, B.: Responses of soil microbial respiration to thermal stress in alpine steppe on the Tibetan plateau, Eur. J. Soil Sci., 63(3), 325–331, doi:10.1111/j.1365-2389.2012.01441.x, 2012.

Chen, S., Wang, J., Zhang, T. and Hu, Z.: Climatic, soil, and vegetation controls of the temperature sensitivity (Q10) of soil respiration across terrestrial biomes, Glob. Ecol. Conserv., 22, e00955, doi:10.1016/j.gecco.2020.e00955, 2020.

Cotrufo, M. F., Wallenstein, M. D., Boot, C. M., Denef, K. and Paul, E.: The Microbial Efficiency-Matrix Stabilization (MEMS) framework integrates plant litter decomposition with soil organic matter stabilization: do labile plant inputs form stable soil organic matter?, Glob. Chang. Biol., 19(4), 988–995, doi:10.1111/gcb.12113, 2013.

Demyan, M. S., Rasche, F., Schulz, E., Breulmann, M., Müller, T. and Cadisch, G.: Use of specific peaks obtained by diffuse reflectance Fourier transform mid-infrared spectroscopy to study the composition of organic matter in a Haplic Chernozem, Eur. J. Soil Sci., 63(2), 189–199, doi:10.1111/j.1365-2389.2011.01420.x, 2012.

Demyan, M. S., Rasche, F., Schütt, M., Smirnova, N., Schulz, E. and Cadisch, G.: Combining a coupled FTIR-EGA system and in situ DRIFTS for studying soil organic matter in arable soils, Biogeosciences, 10(5), 2897–2913, doi:10.5194/bg-10-2897-2013, 2013.

Diáková, K., Čapek, P., Kohoutová, I., Mpamah, P. A., Bárta, J., Biasi, C., Martikainen, P. J. and Šantrůčková, H.: Heterogeneity of carbon loss and its temperature sensitivity in East-European subarctic tundra soils, edited by D. Wagner, FEMS Microbiol. Ecol., 92(9), fiw140, doi:10.1093/femsec/fiw140, 2016.

Duboc, O., Tintner, J., Zehetner, F. and Smidt, E.: Does sample drying temperature affect the molecular characteristics of organic matter in soil and litter? A statistical proof using ATR infrared spectra, Vib. Spectrosc., 85, 215–221, doi:10.1016/j.vibspec.2016.05.002, 2016.

Elshall, A. S., Ye, M., Niu, G.-Y. and Barron-Gafford, G. A.: Bayesian inference and predictive performance of soil respiration models in the presence of model discrepancy, Geosci. Model Dev., 12(5), 2009–2032, doi:10.5194/gmd-12-2009-2019, 2019.

Evans, S. E. and Wallenstein, M. D.: Soil microbial community response to drying and rewetting stress: does historical precipitation regime matter?, Biogeochemistry, 109(1–3), 101–116, doi:10.1007/s10533-011-9638-3, 2012.

Frey, S. D., Lee, J., Melillo, J. M. and Six, J.: The temperature response of soil microbial efficiency and its feedback to climate, Nat. Clim. Chang., 3(4), 395–398, doi:10.1038/nclimate1796, 2013.

Gromova, M. S., Matvienko, A. I., Makarov, M. I., Cheng, C. and Menyailo, O. V: Temperature Sensitivity (Q 10) of Soil Basal Respiration as a Function of Available Carbon Substrate , Temperature , and Moisture, Eurasian Soil Sci., 53(January), 376–381, doi:10.1134/S1064229320020052, 2020.

Guenet, B., Moyano, F. E., Peylin, P., Ciais, P. and Janssens, I. A.: Towards a representation of priming on soil carbon decomposition in the global land biosphere model ORCHIDEE (version 1.9.5.2), Geosci. Model Dev., 9(2), 841–855, doi:10.5194/gmd-9-841-2016, 2016.

Hararuk, O. and Luo, Y.: Improvement of global litter turnover rate predictions using a Bayesian MCMC approach, Ecosphere, 5(12), art163, doi:10.1890/ES14-00092.1, 2014.

Hararuk, O., Xia, J. and Luo, Y.: Evaluation and improvement of a global land model against soil carbon data using a Bayesian Markov chain Monte Carlo method, J. Geophys. Res. Biogeosciences, 119(3), 403–417, doi:10.1002/2013JG002535, 2014.

Hararuk, O., Shaw, C. and Kurz, W. A.: Constraining the organic matter decay parameters in the CBM-CFS3 using Canadian National Forest Inventory data and a Bayesian inversion technique, Ecol. Modell., 364, 1–12, doi:10.1016/j.ecolmodel.2017.09.008, 2017.

Hassink, J., Whitmore, A. P. and Kubát, J.: Size and density fractionation of soil organic matter and the physical capacity of soils to protect organic matter, Dev. Crop Sci., doi:10.1016/S0378-519X(97)80025-6, 1997.

Huang, W., Hammel, K. E., Hao, J., Thompson, A., Timokhin, V. I. and Hall, S. J.: Enrichment of lignin-derived carbon in mineral-associated soil organic matter, Environ. Sci. Technol., 53(13), 7522–7531, doi:10.1021/acs.est.9b01834, 2019.

Hutengs, C., Ludwig, B., Jung, A., Eisele, A. and Vohland, M.: Comparison of Portable and Bench-Top Spectrometers for Mid-Infrared Diffuse Reflectance Measurements of Soils, Sensors, 18(4), 993, doi:10.3390/s18040993, 2018.

Jeng, W.-Y., Wang, N.-C., Lin, M.-H., Lin, C.-T., Liaw, Y.-C., Chang, W.-J., Liu, C.-I., Liang, P.-H. and Wang, A. H. J.: Structural and functional analysis of three β-glucosidases from bacterium Clostridium cellulovorans, fungus Trichoderma reesei and termite Neotermes koshunensis, J. Struct. Biol., 173(1), 46–56, doi:10.1016/j.jsb.2010.07.008, 2011.

Kallenbach, C. M., Frey, S. D. and Grandy, A. S.: Direct evidence for microbial-derived soil organic matter formation and its ecophysiological controls, Nat. Commun., 7, 1–10, doi:10.1038/ncomms13630, 2016.

Karhu, K., Hilasvuori, E., Järvenpää, M., Arppe, L., Christensen, B. T., Fritze, H., Kulmala, L., Oinonen, M., Pitkänen, J.-M., Vanhala, P., Heinonsalo, J. and Liski, J.: Similar temperature sensitivity of soil mineral-associated organic carbon regardless of age, Soil Biol. Biochem., 136(January), 107527, doi:10.1016/j.soilbio.2019.107527, 2019.

Kopittke, P. M., Hernandez-Soriano, M. C., Dalal, R. C., Finn, D., Menzies, N. W., Hoeschen, C. and Mueller, C. W.: Nitrogen-rich microbial products provide new organo-mineral associations for the stabilization of soil organic matter, Glob. Chang. Biol., 24(4), 1762–1770, doi:10.1111/gcb.14009, 2018.

Kopittke, P. M., Dalal, R. C., Hoeschen, C., Li, C., Menzies, N. W. and Mueller, C. W.: Soil organic matter is stabilized by organo-mineral associations through two key processes: The role of the carbon to nitrogen ratio, Geoderma, 357(August 2019), 113974, doi:10.1016/j.geoderma.2019.113974, 2020.

Kunlanit, B., Vityakon, P., Puttaso, A., Cadisch, G. and Rasche, F.: Mechanisms controlling soil organic carbon composition pertaining to microbial decomposition of biochemically contrasting organic residues: Evidence from midDRIFTS peak area analysis, Soil Biol. Biochem., 76, 100–108, doi:10.1016/j.soilbio.2014.05.006, 2014.

Lee, J. and Viscarra Rossel, R. A.: Soil carbon simulation confounded by different pool initialisation, Nutr. Cycl. Agroecosystems, 116(2), 245–255, doi:10.1007/s10705-019-10041-0, 2020.

Leifeld, J. and von Lützow, M.: Chemical and microbial activation energies of soil organic matter decomposition, Biol. Fertil. Soils, 50(1), 147–153, doi:10.1007/s00374-013-0822-6, 2014.

Li, X., Xie, J., Zhang, Q., Lyu, M., Xiong, X., Liu, X., Lin, T. and Yang, Y.: Substrate availability and soil microbes drive temperature sensitivity of soil organic carbon mineralization to warming along an elevation gradient in subtropical Asia, Geoderma, 364(January), 114198, doi:10.1016/j.geoderma.2020.114198, 2020.

Liu, D., Keiblinger, K. M., Leitner, S., Wegner, U., Zimmermann, M., Fuchs, S., Lassek, C., Riedel, K. and Zechmeister-Boltenstern, S.: Response of Microbial Communities and Their Metabolic Functions to Drying–Rewetting Stress in a Temperate Forest Soil, Microorganisms, 7(5), 129, doi:10.3390/microorganisms7050129, 2019.

Lu, D., Ye, M. and Hill, M. C.: Analysis of regression confidence intervals and Bayesian credible intervals for uncertainty quantification, Water Resour. Res., 48(9), 1–20, doi:10.1029/2011WR011289, 2012.

Metzler, H., Zhu, Q., Riley, W., Hoyt, A., Müller, M. and Sierra, C. A.: Mathematical Reconstruction of Land Carbon Models From Their Numerical Output: Computing Soil Radiocarbon From C Dynamics, J. Adv. Model. Earth Syst., 12(1), doi:10.1029/2019MS001776, 2020.

Michel, K. and Ludwig, B.: Prediction of model pools for a long-term experiment using near-infrared spectroscopy, J. Plant Nutr. Soil Sci., 173(1), 55–60, doi:10.1002/jpln.200800181, 2010.

Mirzaeitalarposhti, R., Demyan, M. S., Rasche, F., Cadisch, G. and Müller, T.: Overcoming carbonate interference on labile soil organic matter peaks for midDRIFTS analysis, Soil Biol. Biochem., 99, 150–157, doi:10.1016/j.soilbio.2016.05.010, 2016.

Mueller, T., Jensen, L. S. S., Magid, J. and Nielsen, N. E. E.: Temporal variation of C and N turnover in soil after oilseed rape straw incorporation in the field: simulations with the soil-plant-atmosphere model DAISY, Ecol. Modell., 99(2), 247–262, doi:http://dx.doi.org/10.1016/S0304-3800(97)01959-5, 1997.

Nkwain, F. N., Demyan, M. S., Rasche, F., Dignac, M.-F., Schulz, E., Kätterer, T., Müller, T. and Cadisch, G.: Coupling pyrolysis with mid-infrared spectroscopy (Py-MIRS) to fingerprint soil organic matter bulk chemistry, J. Anal. Appl. Pyrolysis, 133(April 2017), 176–184, doi:10.1016/j.jaap.2018.04.004, 2018.

Van Oijen, M., Rougier, J. and Smith, R.: Bayesian calibration of process-based forest models: bridging the gap between models and data, Tree Physiol., 25(7), 915–927, doi:10.1093/treephys/25.7.915, 2005.

Parolo, M. E., Savini, M. C. and Loewy, R. M.: Characterization of soil organic matter by FT-IR spectroscopy and its relationship with chlorpyrifos sorption, J. Environ. Manage., 196, 316–322, doi:10.1016/j.jenvman.2017.03.018, 2017.

Parton, W. J., Schimel, D. S., Cole, C. V. and Ojima, D. S.: Analysis of Factors Controlling Soil Organic Matter Levels in Great Plains Grasslands1, Soil Sci. Soc. Am. J., 51(5), 1173, doi:10.2136/sssaj1987.03615995005100050015x, 1987.

Piepho, H. P., Büchse, A. and Richter, C.: A Mixed Modelling Approach for Randomized Experiments with Repeated Measures, J. Agron. Crop Sci., 190(4), 230–247, doi:10.1111/j.1439-037X.2004.00097.x, 2004.

Poeplau, C., Don, A., Dondini, M., Leifeld, J., Nemo, R., Schumacher, J., Senapati, N. and Wiesmeier, M.: Reproducibility of a soil organic carbon fractionation method to derive RothC carbon pools, Eur. J. Soil Sci., 64(6), 735–746, doi:10.1111/ejss.12088, 2013.

Poeplau, C., Kätterer, T., Leblans, N. I. W. and Sigurdsson, B. D.: Sensitivity of soil carbon fractions and their specific stabilization mechanisms to extreme soil warming in a subarctic grassland, Glob. Chang. Biol., 23(3), 1316–1327, doi:10.1111/gcb.13491, 2017.

Poeter, E. P., Hill, M. C., Lu, D., Tiedeman, C. R. and Mehl, S.: UCODE_2014, with New Capabilities to Define Parameters Unique to Predictions, Calculate Weights using Simulated Values, Estimate Parameters with SVD, Evaluate Uncertainty with MCMC, and More, Integrated Groundwater Modeling Center Report Number: GWMI 2014-02., 2014.

Pullen, N. and Morris, R. J.: Bayesian Model Comparison and Parameter Inference in Systems Biology Using Nested Sampling, edited by S. Rogers, PLoS One, 9(2), e88419, doi:10.1371/journal.pone.0088419, 2014.

Qiao, Y., Wang, J., Liang, G., Du, Z., Zhou, J., Zhu, C., Huang, K., Zhou, X., Luo, Y., Yan, L. and Xia, J.: Global variation of soil microbial carbon-use efficiency in relation to growth temperature and substrate supply, Sci. Rep., 9(1), 5621, doi:10.1038/s41598-019-42145-6, 2019.

Rasche, F., Marhan, S., Berner, D., Keil, D., Kandeler, E. and Cadisch, G.: midDRIFTS-based partial least square regression analysis allows predicting microbial biomass, enzyme activities and 16S rRNA gene abundance in soils of temperate grasslands, Soil Biol. Biochem., 57, 504–512, doi:10.1016/j.soilbio.2012.09.030, 2013.

Robertson, A. D., Paustian, K., Ogle, S., Wallenstein, M. D., Lugato, E. and Cotrufo, M. F.: Unifying soil organic matter formation and persistence frameworks: the MEMS model, Biogeosciences, 16(6), 1225–1248, doi:10.5194/bg-16-1225-2019, 2019.

Schimel, J. P. and Schaeffer, S. M.: Microbial control over carbon cycling in soil, Front. Microbiol., 3(SEP), 1–11, doi:10.3389/fmicb.2012.00348, 2012.

Schöniger, A., Wöhling, T., Samaniego, L. and Nowak, W.: Model selection on solid ground: Rigorous comparison of nine ways to evaluate Bayesian model evidence, Water Resour. Res., 50(12), 9484–9513, doi:10.1002/2014WR016062, 2014.

Schweizer, S. A., Hoeschen, C., Schlüter, S., Kögel-Knabner, I. and Mueller, C. W.: Rapid soil formation after glacial retreat shaped by spatial patterns of organic matter accrual in microaggregates, Glob. Chang. Biol., 24(4), 1637–1650, doi:10.1111/gcb.14014, 2018.

Sierra, C. A., Malghani, S. and Müller, M.: Model structure and parameter identification of soil organic matter models, Soil Biol. Biochem., 90, 197–203, doi:10.1016/j.soilbio.2015.08.012, 2015.

Sinsabaugh, R. L.: Phenol oxidase, peroxidase and organic matter dynamics of soil, Soil Biol. Biochem., 42(3), 391–404, doi:10.1016/j.soilbio.2009.10.014, 2010.

Sinsabaugh, R. L., Lauber, C. L., Weintraub, M. N., Ahmed, B., Allison, S. D., Crenshaw, C., Contosta, A. R., Cusack, D., Frey, S., Gallo, M. E., Gartner, T. B., Hobbie, S. E., Holland, K., Keeler, B. L., Powers, J. S., Stursova, M., Takacs-Vesbach, C., Waldrop, M. P., Wallenstein, M. D., Zak, D. R. and Zeglin, L. H.: Stoichiometry of soil enzyme activity at global scale, Ecol. Lett., 11(11), 1252–1264, doi:10.1111/j.1461-0248.2008.01245.x, 2008.

Smith, P., Smith, J. U., Powlson, D. S., McGill, W. B., Arah, J. R. M., Chertov, O. G., Coleman, K., Franko, U., Frolking, S., Jenkinson, D. S., Jensen, L. S., Kelly, R. H., Klein-Gunnewiek, H., Komarov, A. S., Li, C., Molina, J. A. E., Mueller, T., Parton, W. J., Thornley, J. H. M. and Whitmore, A. P.: A comparison of the performance of nine soil organic matter models using datasets from seven long-term experiments, Geoderma, 81(1–2), 153–225, doi:10.1016/S0016-7061(97)00087-6, 1997.

Specka, X., Nendel, C. and Wieland, R.: Analysing the parameter sensitivity of the agro-ecosystem model MONICA for different crops, Eur. J. Agron., 71, 73–87, doi:10.1016/j.eja.2015.08.004, 2015.

Stevenson, F. J.: Humus chemistry: genesis, composition, reactions, John Wiley & Sons, New York., 1994.

Sulman, B. N., Moore, J. A. M., Abramoff, R., Averill, C., Kivlin, S., Georgiou, K., Sridhar, B., Hartman, M. D., Wang, G., Wieder, W. R., Bradford, M. A., Luo, Y., Mayes, M. A., Morrison, E., Riley, W. J., Salazar, A., Schimel, J. P., Tang, J. and Classen, A. T.: Multiple models and experiments underscore large uncertainty in soil carbon dynamics, Biogeochemistry, 141(2), 109–123, doi:10.1007/s10533-018-0509-z, 2018.

Tang, J. and Riley, W. J.: Weaker soil carbon–climate feedbacks resulting from microbial and abiotic interactions, Nat. Clim. Chang., 5(1), 56–60, doi:10.1038/nclimate2438, 2015.

Todd-Brown, K., Zheng, B. and Crowther, T. W.: Field-warmed soil carbon changes imply high 21st-century modeling uncertainty, Biogeosciences, 15(12), 3659–3671, doi:10.5194/bg-15-3659-2018, 2018.

Todd-Brown, K. E. O., Randerson, J. T., Hopkins, F., Arora, V., Hajima, T., Jones, C., Shevliakova, E., Tjiputra, J., Volodin, E., Wu, T., Zhang, Q. and Allison, S. D.: Changes in soil organic carbon storage predicted by Earth system models during the 21st century, Biogeosciences, 11(8), 2341–2356, doi:10.5194/bg-11-2341-2014, 2014.

Totsche, K. U., Amelung, W., Gerzabek, M. H., Guggenberger, G., Klumpp, E., Knief, C., Lehndorff, E., Mikutta, R., Peth, S., Prechtel, A., Ray, N. and Kögel-Knabner, I.: Microaggregates in soils, J. Plant Nutr. Soil Sci., 1–33, doi:10.1002/jpln.201600451, 2017.

Tuomi, M., Vanhala, P., Karhu, K., Fritze, H. and Liski, J.: Heterotrophic soil respiration—Comparison of different models describing its temperature dependence, Ecol. Modell., 211, 182–190, doi:10.1016/j.ecolmodel.2007.09.003, 2008.

Vaughn, L. J. S. and Torn, M. S.: 14C evidence that millennial and fast-cycling soil carbon are equally sensitive to warming, Nat. Clim. Chang., 9(6), 467–471, doi:10.1038/s41558-019-0468-y, 2019.

Wang, K., Peng, C., Zhu, Q., Zhou, X., Wang, M., Zhang, K. and Wang, G.: Modeling Global Soil Carbon and Soil Microbial Carbon by Integrating Microbial Processes into the Ecosystem Process Model TRIPLEX-GHG, J. Adv. Model. Earth Syst., 9(6), 2368–2384, doi:10.1002/2017MS000920, 2017.

Wetterstedt, J. Å. M. and Ågren, G. I.: Quality or decomposer efficiency – which is most important in the temperature response of litter decomposition? A modelling study using the GLUE methodology, Biogeosciences, 8(2), 477–487, doi:10.5194/bg-8-477-2011, 2011.

Wieder, W. R., Hartman, M. D., Sulman, B. N., Wang, Y.-P., Koven, C. D. and Bonan, G. B.: Carbon cycle confidence and uncertainty: Exploring variation among soil biogeochemical models, Glob. Chang. Biol., 24(4), 1563–1579, doi:10.1111/gcb.13979, 2018.

Wöhling, T., Schöniger, A., Gayler, S. and Nowak, W.: Bayesian model averaging to explore the worth of data for soil-plant model selection and prediction, Water Resour. Res., 51(4), 2825–2846, doi:10.1002/2014WR016292, 2015.

Woolf, D. and Lehmann, J.: Microbial models with minimal mineral protection can explain long-term soil organic carbon persistence, Sci. Rep., 9(1), 6522, doi:10.1038/s41598-019-43026-8, 2019.

Yang, X.: An extension to “Mid-infrared spectral interpretation of soils: Is it practical or accurate?,” Geoderma, 226–227(1), 415–417, doi:10.1016/j.geoderma.2014.03.022, 2014.

Yeasmin, S., Singh, B., Johnston, C. T. and Sparks, D. L.: Evaluation of pre-treatment procedures for improved interpretation of mid infrared spectra of soil organic matter, Geoderma, 304, 83–92, doi:10.1016/j.geoderma.2016.04.008, 2017.

Yeluripati, J. B., van Oijen, M., Wattenbach, M., Neftel, A., Ammann, A., Parton, W. J. and Smith, P.: Bayesian calibration as a tool for initialising the carbon pools of dynamic soil models, Soil Biol. Biochem., 41(12), 2579–2583, doi:10.1016/j.soilbio.2009.08.021, 2009.

Zhang, H., Goll, D. S., Manzoni, S., Ciais, P., Guenet, B. and Huang, Y.: Modeling the effects of litter stoichiometry and soil mineral N availability on soil organic matter formation using CENTURY-CUE (v1.0), Geosci. Model Dev., 11(12), 4779–4796, doi:10.5194/gmd-11-4779-2018, 2018.

Zimmermann, M., Leifeld, J., Schmidt, M. W. I., Smith, P. and Fuhrer, J.: Measured soil organic matter fractions can be related to pools in the RothC model, Eur. J. Soil Sci., 58(3), 658–667, doi:10.1111/j.1365-2389.2006.00855.x, 2007.

6 Supplementary material

6.1 Supplement chapter 2

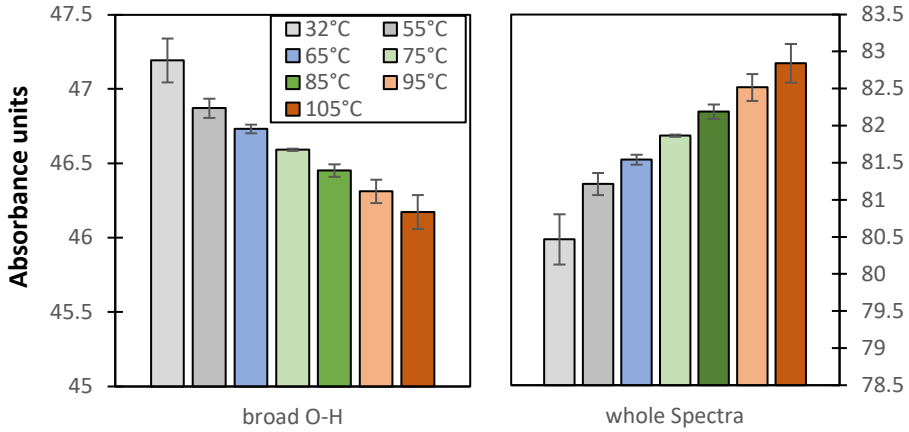

Figure S2 - 1 Least square means estimations of the broad O-H peak area (3800 to 2400 cm^{-1}) and the peak area of the whole spectra (4000 to 400 cm^{-1}) across all samples. Significant differences between all temperatures existed. Error bars indicate 95% confidence intervals of the drying temperature effect.

Table S2 - 1 Origin and selected soil properties of the samples, used in this study. The contents of TOC and TN were analyzed by dry combustion in a Variomax CN analyzer (Hanau, Germany). Texture was measured for the samples from Swabian Alb, Kraichgau and SURUMER, and from the literature for the rest.

Site	Plot location UTM Degrees Lat	UTM Degrees Long	Treatment	Year of sampling	Depth (cm)	TOC (%)	TN (%)	Sand (%)	Clay (%)	Bulk density (g/cm3)
Kraichgau	48.925723°	008.716103°	bare fallow since 09	2012	0 - 30	0.81	0.09	1.8	17.1	1.37
Swabian Alb	48.528354°	009.770306°	bare fallow since 09	2015	0 - 30	1.27	0.15	6.2	37.8	1.31
Swabian Alb	48.526689°	009.769955°	under cropping	2015	0 - 30	2.44	0.28	6.2	37.8	1.31
Kraichgau	48.927616°	008.716771°	bare fallow since 09	2015	0 - 30	0.89	0.11	1.8	17.1	1.37
Kraichgau	48.927616°	008.716771°	under cropping	2009	0 - 30	1.05	0.10	1.8	17.1	1.37
Kraichgau	48.927616°	008.716771°	under cropping	2010	60 -90	0.20	0.02	0.8	16.1	1.51
Swabian Alb	48.526689°	009.769955°	under cropping	2010	30 - 60	0.78	0.06	8.4	48.4	1.32
Swabian Alb	48.527877°	009.768333°	bare fallow since 09	2010	0 - 30	1.53	0.24	6.2	37.8	1.31
Bad Lauchstädt	51.391605°	011.877028°	no FYM, PK biannual	2008	0 - 20	1.61	0.13	11.0	21.0	NA
Bad Lauchstädt	51.391605°	011.877028°	50t/ha year FYM	2008	0 - 20	1.98	0.17	11.0	21.0	NA
Bad Lauchstädt	51.391605°	011.877028°	100t/ha year FYM	2008	0 - 20	2.55	0.22	11.0	21.0	NA
Bad Lauchstädt	51.391605°	011.877028°	200t/ha year FYM	2008	0 - 20	4.03	0.37	11.0	21.0	NA
Bad Lauchstädt	51.3901520°	011.8797610°	30 t/ha year FYM + NPK	2008	0 - 30	2.34	NA	11.0	21.0	NA
Bad Lauchstädt	51.3901520°	011.8797610°	control, no additions	2008	0 - 30	1.65	NA	11.0	21.0	NA
SURUMER	22.1703863°	100.6605682°	field survey	2014	0 - 15	1.16	0.14	19.4	35.8	1.25
SURUMER	22.1844893°	100.6627704°	field survey	2014	90 - 130	0.62	0.10	9.4	49.5	1.40
SURUMER	22.1763047°	100.5625986°	field survey	2014	0 - 30	5.05	0.45	32.7	34.5	0.56
SURUMER	22.2059529°	100.6184263°	field survey	2014	90 - 125	0.93	0.06	40.4	36.0	1.17
Ultuna Frame	59.8218790°	017.6563480°	farmyard_manure	2005	0 - 20	2.04	0.20	23.0	36.0	1.24
Ultuna Frame	59.8218790°	017.6563480°	sewage sludge	2005	0 - 20	2.47	0.26	23.0	36.0	1.02
Ultuna Frame	59.8218790°	017.6563480°	bare fallow since 56	2005	0 - 20	0.95	0.10	23.0	36.0	1.43

Table S2 - 2 DRIFTS peaks used in this study together with their integration limits

Peak name in article	Integration limits (cm^{-1})	Main assignment (Demyan 2012)	Potential other contributors
2930 cm^{-1}	3010 – 2800	Aliphatic C-H stretching	Superimposed on broad O-H peak (Stevenson, 1994)
1620 cm^{-1}	1660 – 1580	Aromatic C=C and/or –COO− stretching	C=C of alkenes (Coates, 2006), N-H of primary amides (Socrates, 2004), C=O (Stevenson, 1994)
1530 cm^{-1}	1546 – 1520	Aromatic C=C stretching	N-O (Coates, 2006),C=N , N-H (Socrates, 2004)
1159 cm^{-1}	1170 - 1148	C–O bonds of poly-alcoholic and ether groups	C-H, SO_2 (Socrates, 2004)
broad O-H peak area	3800 - 2400	O-H from water as well as clay minerals	

Table S2 - 3 Correlations between peak areas (and normalized peak areas) and total organic carbon (TOC), and total organic nitrogen (TN). Correlations > ABSOLUTE(0.444) are significant (n = 19; DF = 18). The strength of color indicates a significant positive (green) or negative (red) correlation.

correlation of	TOC	TOC	TOC	TOC	TOC	TOC	TOC	TOC
with	2930 cm^{-1}	n2930 cm^{-1}	1620 cm^{-1}	n1620 cm^{-1}	1530 cm^{-1}	n1530 cm^{-1}	1159 cm^{-1}	n1159 cm^{-1}
temperature								
32	0.77	0.85	-0.69	0.14	-0.70	-0.85	-0.60	0.18
55	0.73	0.77	-0.64	-0.01	-0.66	-0.83	-0.56	0.08
65	0.75	0.81	-0.63	0.06	-0.68	-0.84	-0.55	0.11
75	0.76	0.82	-0.62	0.12	-0.68	-0.80	-0.56	0.18
85	0.74	0.79	-0.63	0.09	-0.67	-0.81	-0.56	0.15
95	0.72	0.80	-0.63	0.19	-0.68	-0.84	-0.57	0.24
105	0.76	0.83	-0.62	0.16	-0.68	-0.81	-0.58	0.20

correlation of	TN	TN	TN	TN	TN	TN	TN	TN
with	2930 cm^{-1}	n2930 cm^{-1}	1620 cm^{-1}	n1620 cm^{-1}	1530 cm^{-1}	n1530 cm^{-1}	1159 cm^{-1}	n1159 cm^{-1}
temperature								
32	0.76	0.83	-0.62	0.06	-0.62	-0.78	-0.50	0.11
55	0.72	0.74	-0.58	-0.09	-0.58	-0.75	-0.45	0.01
65	0.74	0.77	-0.57	-0.03	-0.59	-0.76	-0.43	0.04
75	0.74	0.79	-0.57	0.04	-0.60	-0.73	-0.45	0.12
85	0.71	0.75	-0.58	0.00	-0.59	-0.73	-0.46	0.08
95	0.70	0.76	-0.58	0.11	-0.60	-0.76	-0.46	0.17
105	0.71	0.77	-0.58	0.07	-0.60	-0.73	-0.47	0.13

Table S2 - 4 Summary of Statistic models for different peak areas. Number of degrees of freedom was 125, with exception of the SI2 model (DF = 95).

Variable	Intercept	standard error (Intercept)	Slope of temperature	standard error (Slope of temperature)
2930 cm^{-1}	8.04E-03 n.s.	2.58E-02	2.83E-03 ***	2.27E-04
1620 cm^{-1}	4.58E-01 ***	2.46E-02	1.02E-03 ***	1.02E-04
1530 cm^{-1}	5.88E-02 ***	7.67E-03	1.84E-04 ***	1.39E-05
1159 cm^{-1}	8.45E-02 ***	3.20E-03	9.76E-05 ***	7.70E-06
normalized 2930 cm^{-1}	4.82E-02 n.s.	4.51E-02	3.24E-03 ***	3.78E-04
1/normalized 1620 cm^{-1}	n.s.	n.s.	n.s.	n.s.
normalized 1530 cm^{-1}	6.90E-02 ***	5.64E-03	9.17E-05 ***	1.65E-05
1/normalized 1159 cm^{-1}	9.42E+00 ***	5.29E-01	6.10E-03 ***	7.61E-04
SI = 2930 cm^{-1}/ 1620 cm^{-1}	7.89E-02 n.s.	6.33E-02	4.92E-03 ***	4.75E-04
For SI2 the samples "P1a(0-30)","UL05-15","BL791","BL779","P3(90-125)" had to be removed (outliers)				
SI2 = 2930 cm^{-1}/ 1530 cm^{-1}	7.47E-01 n.s.	6.63E-01	3.05E-02 ***	4.33E-03
relative 2930 cm^{-1}	5.02E-02 n.s.	4.50E-02	2.12E-03 ***	1.51E-04
relative 1620 cm^{-1}	7.26E-01 ***	3.38E-02	-1.62E-03 ***	1.20E-04
relative 1530 cm^{-1}	8.93E-02 ***	9.39E-03	-1.25E-04 ***	2.50E-05
relative 1159 cm^{-1}	1.35E-01 ***	6.74E-03	-3.77E-04 ***	2.50E-05
whole spectra	7.94E+01 ***	7.90E-01	3.25E-02 ***	4.18E-03
broad O-H	4.76E+01 ***	6.55E-01	-1.40E-02 ***	1.81E-03

6.2 Supplement chapter 3

6.2.1 Supplementary figures chapter 3

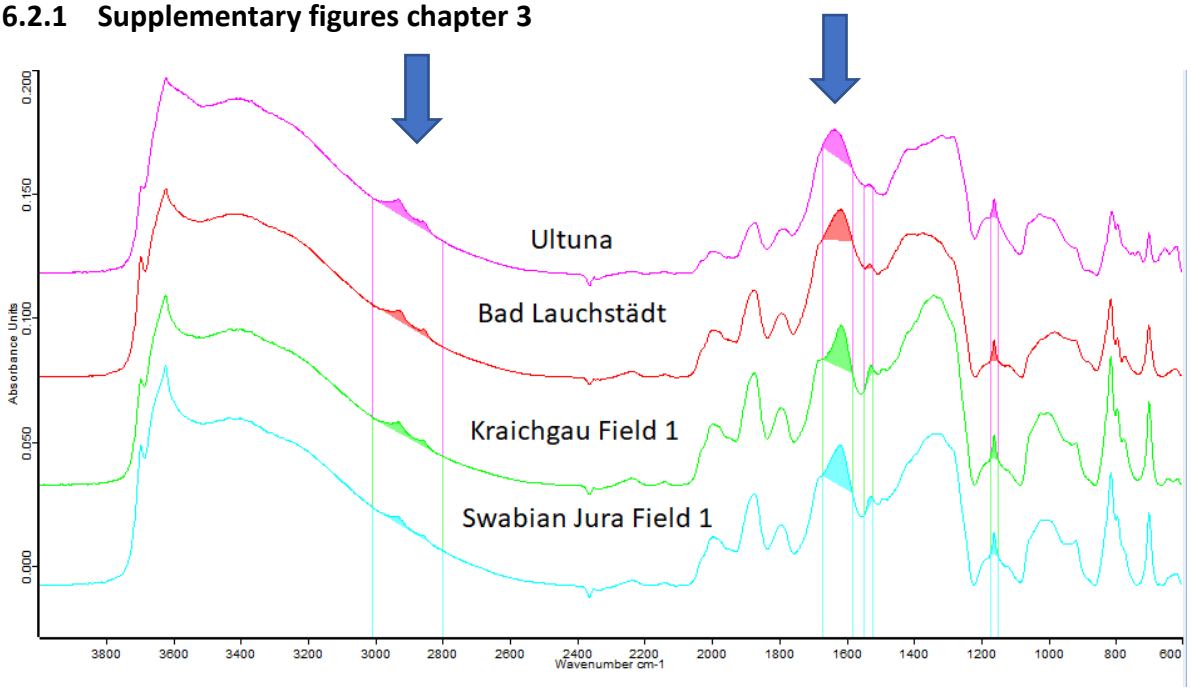

Figure S 3 - 1 Example of DRIFTS spectra with integrated specific band areas of the 2930 cm^{-1} aliphatic carbon band and the 1620 cm^{-1} aromatic-carboxylate carbon band (limits: 3010 – 2800 cm^{-1} and 1660 – 1580 cm^{-1}). The spectra were baseline corrected and vector normalized prior integration. The absorption band areas are highlighted by the blue arrows, the integrated band area is the colored area below each band, corresponding only to the top of the band.

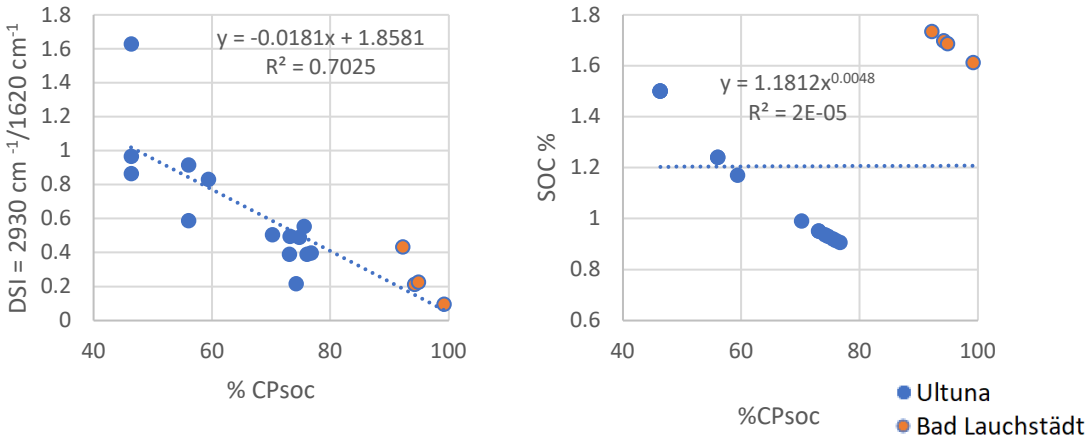

Figure S 3 - 2 Correlation between the DRIFTS stability index for the samples of this study (only Ultuna and Bad Lauchstädt) and centennially persistent SOC (CPsoc) as well as SOC and CPsoc. The CPsoc of 0.695%SOC for Ultuna and 1.6% SOC for Bad Lauchstädt were taken from Cécillon et al.(2018) and Franko and Merbach (2017).

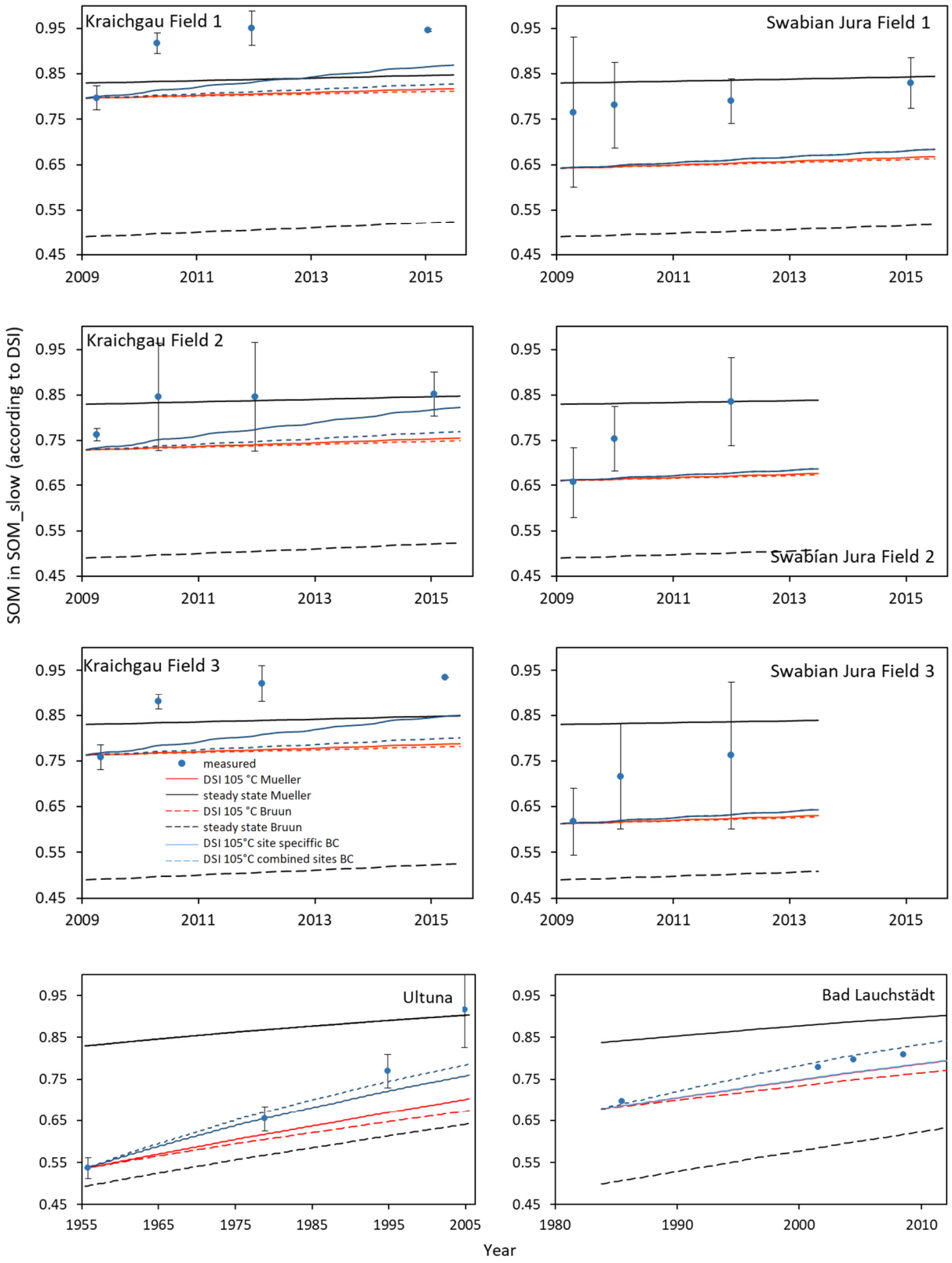

Figure S 3 - 3 Development of simulated vs observed SOM in the slow pool, according to the DSI division throughout the simulation period (for brevity only for 105 °C). Bars indicate standard deviation of all plots per field.

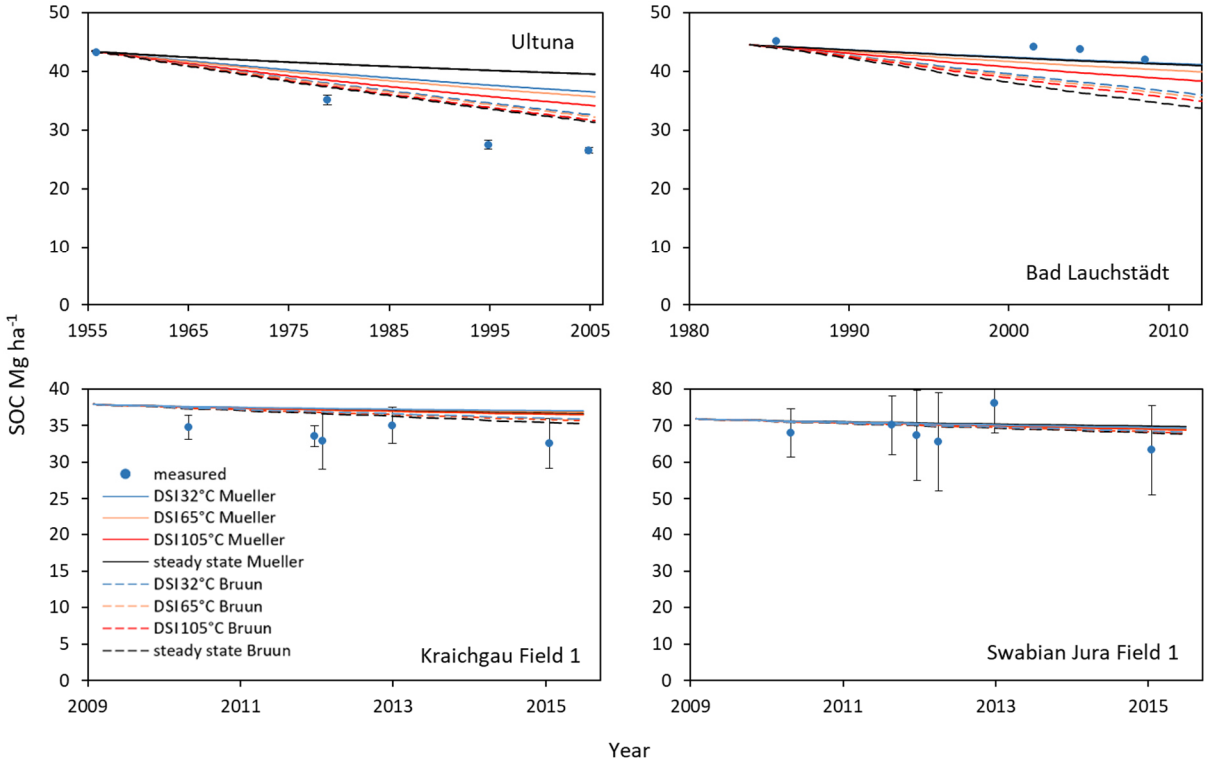

Figure S 3 - 4 Simulations for Ultuna (top left), Bad Lauchstädt (top right), Kraichgau field 1 (bottom left) and Swabian Jura Field 1 (bottom right). Initializations were done (i) assuming steady state using the formula of Bruun and Jensen (2002) with turnover rates of Mueller et al. (1997) and Bruun et al. (2003) and (ii) by the DRIFTS stability index (DSI) at different drying temperatures using both turnover rates for simulations. Bars indicate standard deviation of all plots per field.

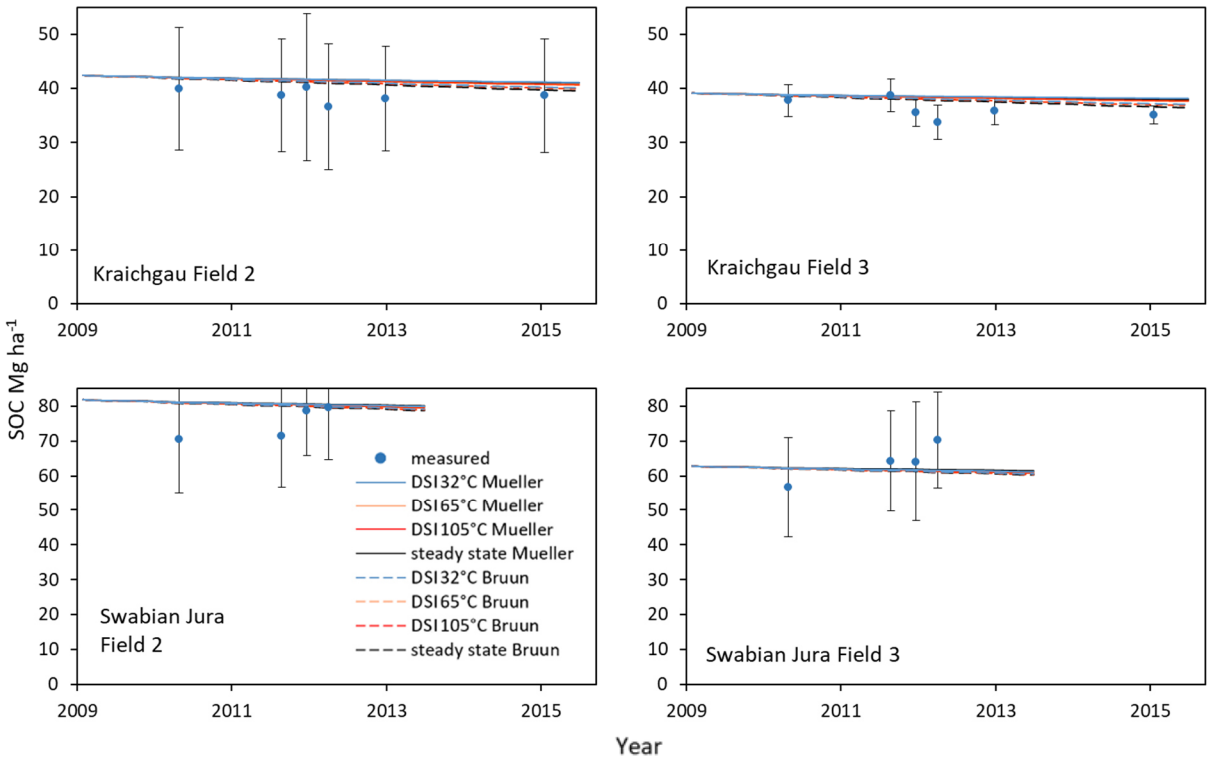

Figure S 3 - 5 SOC simulations for Kraichgau field 2 (top left) and field 3 (top right) as well as for Swabian Jura field 2 (bottom left) and field 3 (bottom right). Initializations were done (i) assuming steady state using the formula of Bruun and Jensen (2002) with turnover rates of Mueller et al. (1997) and Bruun et al. (2003) and (ii) by the DRIFTS stability index (DSI) at different drying temperatures using both turnover rates for simulations. Bars indicate standard deviation of all plots per field.

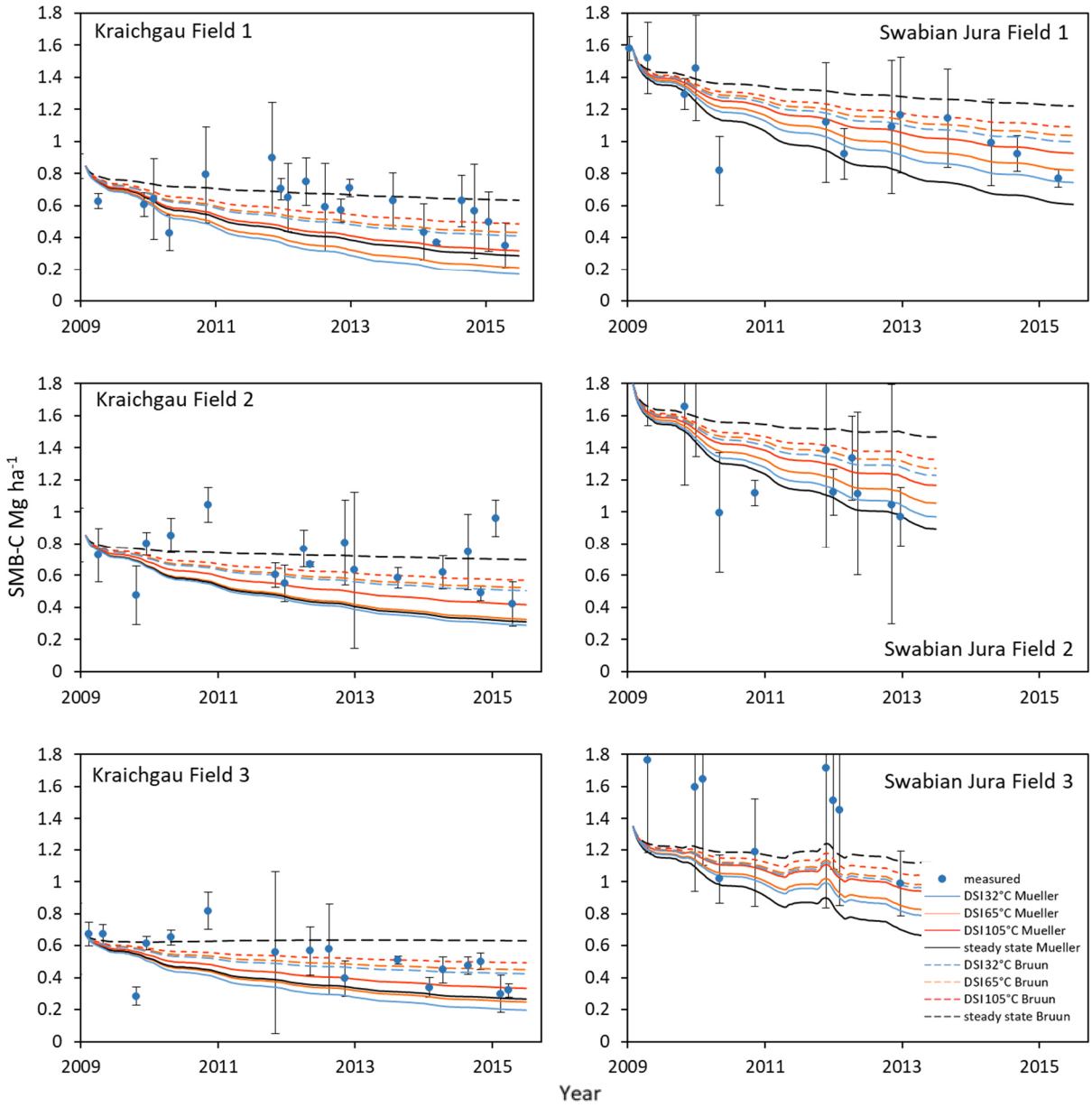

Figure S 3 - 6 SMB-C simulations for Kraichgau field 1, 2 and 3 as well as for Swabian Jura field 1, 2 and 3. Initializations were done (i) assuming steady state using the formula of Bruun and Jensen, (2002) with turnover rates of Mueller et al. (1997) and Bruun et al. (2003) and (ii) by the DRIFTS stability index (DSI) spectra at different drying temperatures using both turnover rates for simulations. Bars indicate standard deviation of all plots per field.

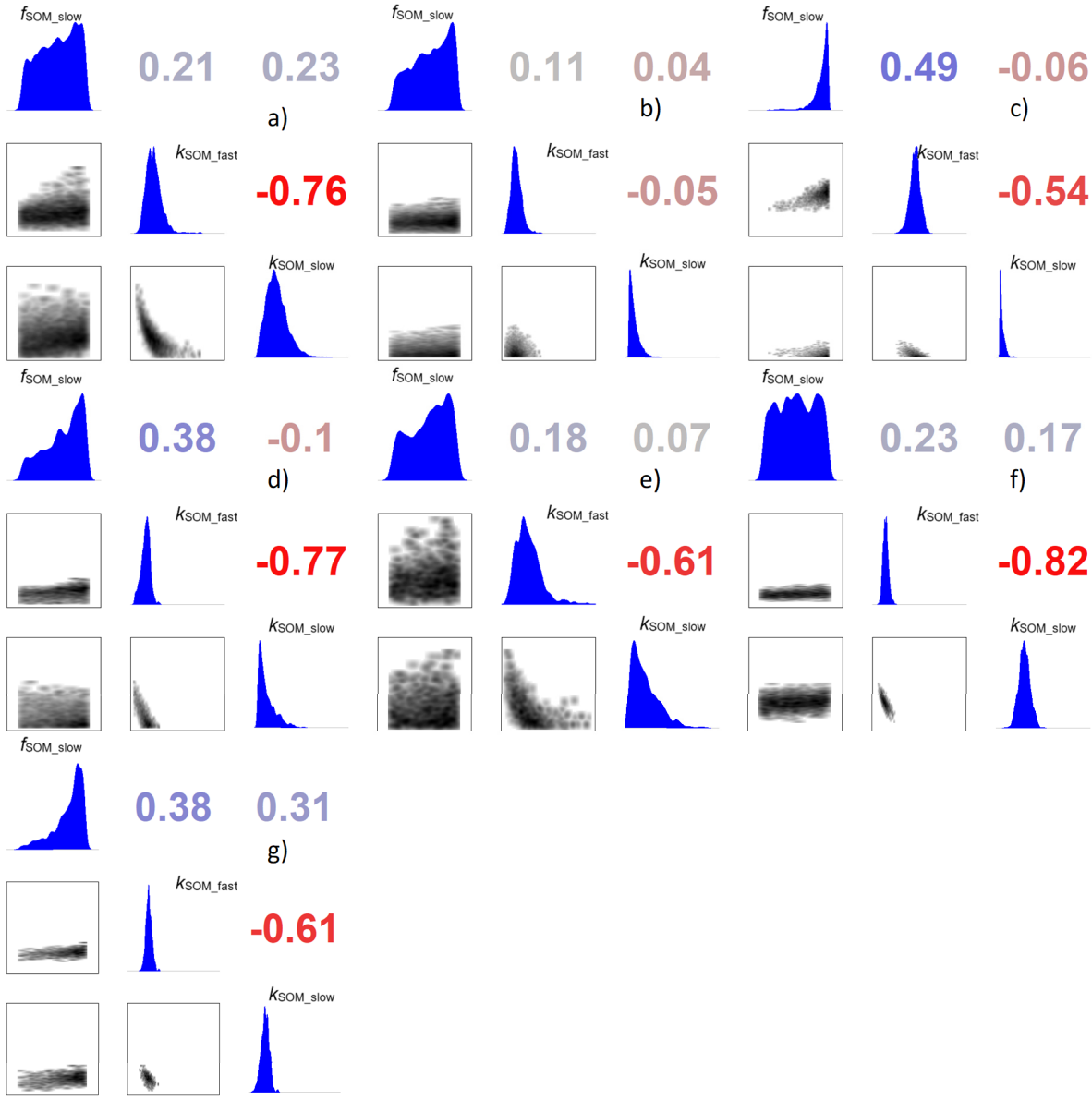

Figure S 3 - 7 Correlation matrices of the posterior distributions of different simulations from top left to bottom right: a) Ultuna (1), b) Bad Lauchstädt (2), c) Kraichgau(3), d) Swabian Jura(4), e) equal weight calibration for all sites combined using the DSI (5), f) original weight calibration for all sites combined without using the DSI (6), and g) original weight calibration for all sites combined using the DSI (7).

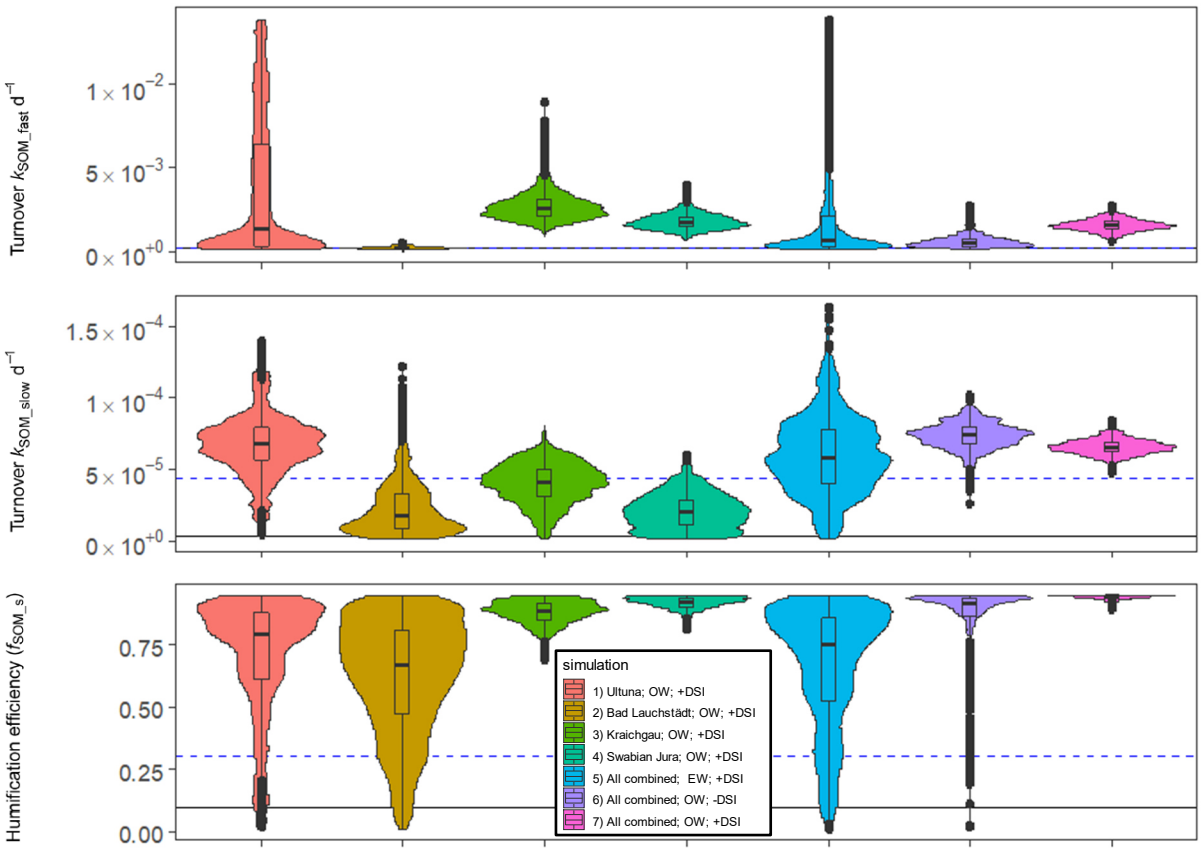

Figure S 3 - 8 Violin plots of the Daisy model parameters obtained by the Bayesian calibration when f_{SOM_slow} was constrained to 95%. Used were the individual sites (1-4) and all sites combined (5-7) with different weighing schemes (OW = original weight, EW = equal weight calibration; ± DSI indicates, whether the DSI data was used for calibration). The black line corresponds to the parameters of Mueller et al. (1997), the blue dashed line to the parameters of Bruun et al. (2003). Note that the turnover k_{SOM_fast} parameter (top of the figure) is the same in both Mueller et al. (1997) and Bruun et al. (2003).

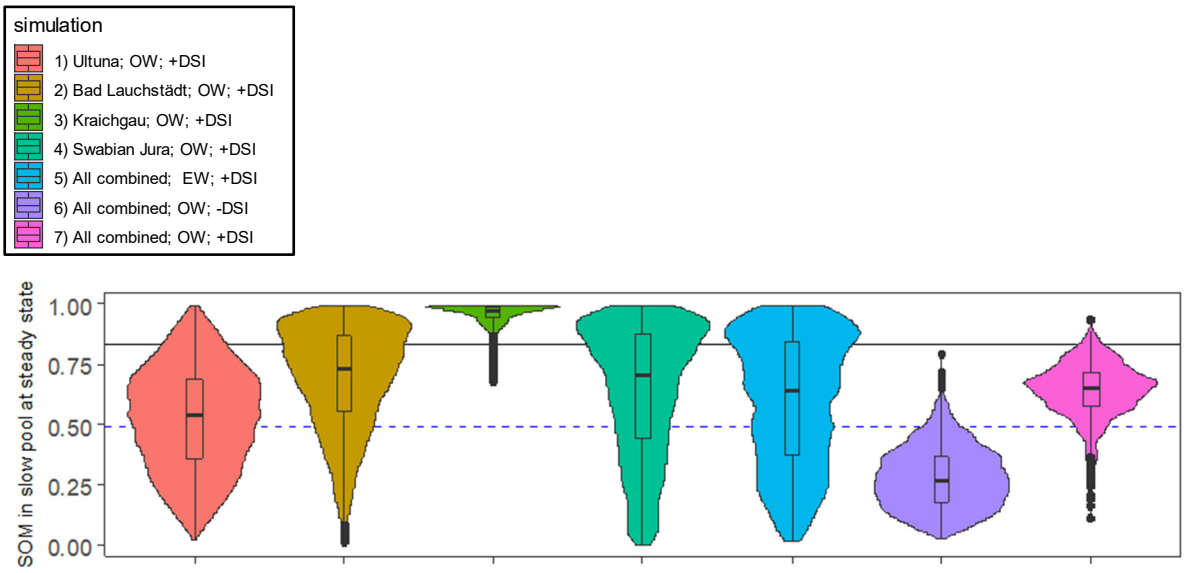

Figure S 3 - 9 Violin plots of the fraction of SOM that would be in the slow pool of the Daisy model at steady state for different Bayesian calibrations. The black line corresponds to the parameters of Mueller et al. (1997), the blue dashed line to the value of Bruun et al. (2003).

6.2.2 SAS code of models used in for analysis of the model error

```
TITLE " final TOC for KR SJ) Temporal covariance structure sph";
ods graphics on;
proc glimmix data=Errors plots=residualpanel(conditional marginal);
ods output covparms FitStatistics diffs=diffs lsmeans=lsmeans;
class initialization turnover field days_passed_class;
model E_TOC_root= initialization turnover days_passed initialization*turnover
turnover*days_passed initialization*days_passed initialization*days_passed*turnover /ddfm=KR;
random days_passed_class /sub=field type=sp(sph)(days_passed) ;
random days_passed_class /sub=field* initialization*turnover type=sp(sph)(days_passed)residual;
run;
ods graphics off;

TITLE " final full Cmic KR SJ) Temporal covariance structure POW";
ods graphics on;
proc glimmix data=Errors plots=residualpanel(conditional marginal);
ods output covparms FitStatistics diffs=diffs lsmeans=lsmeans;
class initialization turnover field days_passed_class;
model E_Cmic_abs= initialization turnover days_passed initialization*turnover
turnover*days_passed initialization*days_passed initialization*days_passed*turnover /ddfm=KR;
random days_passed_class /sub=field type=sp(pow)(days_passed) ;
random days_passed_class /sub=field* initialization*turnover type=sp(pow)(days_passed)residual;
run;
ods graphics off;

TITLE " final SOC for Ultuna) Simple random effect";
ods graphics on;
proc glimmix data=Errors plots=residualpanel(conditional marginal);
ods output covparms FitStatistics diffs=diffs lsmeans=lsmeans normal;
class initialization turnover days_passed_class;
model E_TOC_abs= initialization turnover years_passed initialization*turnover
turnover*years_passed initialization*years_passed initialization*years_passed*turnover /ddfm=KR;
random days_passed_class;
run;
ods graphics off;

TITLE " final SOC for Bad Lauchstädt) Temporal covariance structure Sph";
ods graphics on;
proc glimmix data=Errors plots=residualpanel(conditional marginal);
ods output covparms FitStatistics diffs=diffs lsmeans=lsmeans;
class initialization turnover days_passed_class;
model E_TOC_sqr= initialization turnover years_passed initialization*turnover
turnover*years_passed initialization*years_passed initialization*years_passed*turnover /ddfm=KR;
random days_passed_class /sub= initialization*turnover type=sp(Sph)(years_passed) residual;
run;
ods graphics off;
```

6.2.3 Selection of parameters subject to Bayesian calibration based on their importance within our model simulations

Here we explain, why only k_{SOM_slow}, k_{SOM_fast} and the humification efficiency (f_{SOM_slow}) were considered to be important parameters for Bayesian calibration of bare fallow plots within this study. We give a calculation example of internal recycling from SOM going to SMB and back to SOM. The fraction of remaining SOM as one part SOM cycles through SMB one time and then is stabilized as SOM again is defined as:

$$SOM_{rec} = CUE * \frac{d_m}{m_m + d_m} * f_{\mathrm{SOM\_fast}} \quad (9)$$

Where SOM_{rec} is the percentage of recycled native SOM after one cycle of microbial use, CUE is the carbon use efficiency, d_m is the microbial death rate, m_m is the microbial maintenance respiration rate, and f_{SOM_fast} is the fraction of dead microbial biomass going back to the fast SOM pool as microbes die. The results using the parameters of both parameter sets are identical here: 50% × 9% × 40% = 1.8% for the fast SOM pool, and 40% × 9% × 40% = 1.44% for the slow SOM. From this very low recycling rates, it follows that without carbon inputs, the recycling parameters are irrelevant for simulation of SOM content and only the speed of decomposition and humification determine how much is left at a certain point in time.

6.2.4 Brief test of the suggested new structure of Daisy

We briefly want to demonstrate the results of the new structure of Daisy, that was implemented to the code in the meantime. As can be seen from the figure S 3- 10 below the new structure indeed changes the turnover times of SOM slow to a minor degree (because SOM slow is no longer fed by SOM fast). What is of higher importance is that the coupling between humification efficiency and the turnover of SOM slow is eliminated with the new structure and the strong tendency of the humification efficiency to run into the upper boundary removed. It is not surprising that the new humification efficiency parameter cannot be clearly identified by the bare fallow dataset, as no new carbon comes into the system.

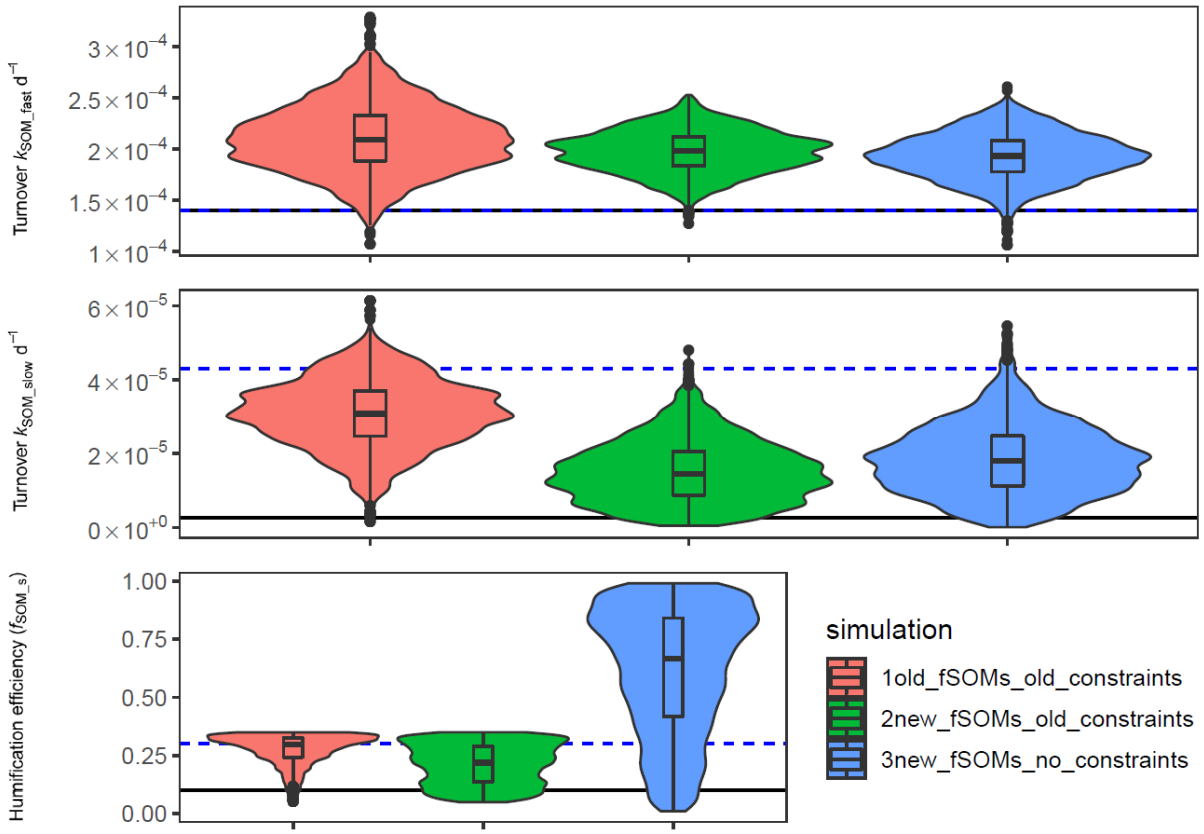

Figure S 3 - 10 Violin plots of the parameters, obtained by the Bayesian calibration using the new suggested model structure (old constraints of f_{SOM_s} are 0.05 and 0.35, no constraints means 0.01 and 0.99) for all sites combined with equal weight and using the DSI (7). The black line corresponds to the parameters of Mueller et al. (1997), the blue dashed line to the parameters of Bruun et al. (2003). Note that the turnover k_{SOM_fast} parameter (top of the figure) is the same in both Mueller et al. (1997) and Bruun et al. (2003).

6.2.5 Raw data of chapter 3 simulations

Experiment	Sampling depth	Sampling date	Subplot ID	SOC t ha^{-1}	SMB-C t ha^{-1}	Area below 2930 cm^{-1}	Area below 1620 cm^{-1}	SOM in slow pool
Ultuna	0 - 20 cm	1956-06-01	1	43.20		0.428	0.448	51.1%
Ultuna	0 - 20 cm	1956-06-01	22	43.22				
Ultuna	0 - 20 cm	1956-06-01	44	43.23		0.394	0.461	53.9%
Ultuna	0 - 20 cm	1956-06-01	55	43.25		0.369	0.471	56.0%
Ultuna	0 - 20 cm	1979-06-01	1	35.76		0.263	0.508	65.9%
Ultuna	0 - 20 cm	1979-06-01	22	35.77		0.290	0.479	62.3%
Ultuna	0 - 20 cm	1979-06-01	44	33.77		0.245	0.526	68.2%
Ultuna	0 - 20 cm	1979-06-01	55	35.22				
Ultuna	0 - 20 cm	1995-06-01	1	27.51		0.144	0.528	78.5%
Ultuna	0 - 20 cm	1995-06-01	22	28.68		0.178	0.514	74.3%
Ultuna	0 - 20 cm	1995-06-01	44	26.66		0.192	0.525	73.2%
Ultuna	0 - 20 cm	1995-06-01	55	26.96		0.115	0.516	81.8%
Ultuna	0 - 20 cm	2005-06-01	1	26.80		0.008	0.511	98.5%
Ultuna	0 - 20 cm	2005-06-01	22	27.20		0.134	0.498	78.8%
Ultuna	0 - 20 cm	2005-06-01	44	25.90		0.015	0.534	97.2%
Ultuna	0 - 20 cm	2005-06-01	55	26.15		0.046	0.516	91.9%
Bad Lauchstädt	0 - 20 cm	1985-09-01		45.08		0.226	0.522	69.8%
Bad Lauchstädt	0 - 20 cm	2001-10-01		44.12		0.149	0.515	77.6%
Bad Lauchstädt	0 - 20 cm	2004-09-01		43.83		0.127	0.501	79.8%
Bad Lauchstädt	0 - 20 cm	2008-10-01		41.91		0.129	0.490	79.2%
Kraichgau 1	0 - 30 cm	2009-05-25	1	35.23	0.944			
Kraichgau 1	0 - 30 cm	2009-05-25	2	39.75	1.080			
Kraichgau 1	0 - 30 cm	2009-05-25	3	36.32	0.943			
Kraichgau 2	0 - 30 cm	2009-05-20	6	54.32	0.330			
Kraichgau 2	0 - 30 cm	2009-05-20	7	36.70	0.466			
Kraichgau 2	0 - 30 cm	2009-05-20	8	33.80	0.301			
Kraichgau 3	0 - 30 cm	2009-06-22	11	41.12	0.890			
Kraichgau 3	0 - 30 cm	2009-06-22	12	37.93	0.462			
Kraichgau 3	0 - 30 cm	2009-06-22	13	36.46	0.570			
Swabian Jura 1	0 - 30 cm	2009-06-17	16	71.89	1.342			
Swabian Jura 1	0 - 30 cm	2009-06-17	17	56.48	0.988			
Swabian Jura 1	0 - 30 cm	2009-06-17	20	82.61	1.499			
Swabian Jura 2	0 - 30 cm	2009-06-17	22	76.66	1.495			
Swabian Jura 2	0 - 30 cm	2009-06-17	23	76.84	1.868			
Swabian Jura 2	0 - 30 cm	2009-06-17	24	83.34	2.618			
Swabian Jura 2	0 - 30 cm	2009-06-17	24	89.06	2.388			
Swabian Jura 2	0 - 30 cm	2009-06-17	24	88.17	2.311			
Swabian Jura 3	0 - 30 cm	2009-06-18	26	61.00	2.494			
Swabian Jura 3	0 - 30 cm	2009-06-18	27	59.13	1.108			
Swabian Jura 3	0 - 30 cm	2009-06-18	27	54.56	1.043			
Swabian Jura 3	0 - 30 cm	2009-06-18	27	52.35	0.887			

Experiment	Sampling depth	Sampling date	Subplot ID	SOC t ha^{-1}	SMB-C t ha^{-1}	Area below 2930 cm^{-1}	Area below 1620 cm^{-1}	SOM in slow pool
Swabian Jura 3	0 - 30 cm	2009-06-18	30	68.26	2.058			
Kraichgau 1	0 - 30 cm	2009-06-30	1		0.930			
Kraichgau 1	0 - 30 cm	2009-06-30	2		0.778			
Kraichgau 1	0 - 30 cm	2009-06-30	3		0.833			
Kraichgau 2	0 - 30 cm	2009-06-30	6		1.031			
Kraichgau 2	0 - 30 cm	2009-06-30	7		0.843			
Kraichgau 2	0 - 30 cm	2009-06-30	8		0.688			
Kraichgau 3	0 - 30 cm	2009-08-18	11		0.706			
Kraichgau 3	0 - 30 cm	2009-08-18	12		0.588			
Kraichgau 3	0 - 30 cm	2009-08-18	13		0.724			
Swabian Jura 1	0 - 30 cm	2009-07-13	16		1.655			
Swabian Jura 1	0 - 30 cm	2009-07-13	17		1.508			
Swabian Jura 1	0 - 30 cm	2009-07-13	20		1.569			
Swabian Jura 2	0 - 30 cm	2009-07-13	22		1.484			
Swabian Jura 2	0 - 30 cm	2009-07-13	23		1.849			
Swabian Jura 2	0 - 30 cm	2009-07-17	24		2.405			
Swabian Jura 2	0 - 30 cm	2009-07-17	24		1.897			
Swabian Jura 2	0 - 30 cm	2009-07-17	24		1.950			
Swabian Jura 3	0 - 30 cm	2009-07-17	26	78.14	1.378			
Swabian Jura 3	0 - 30 cm	2009-07-17	27		0.873			
Swabian Jura 3	0 - 30 cm	2009-07-17	27		0.649			
Swabian Jura 3	0 - 30 cm	2009-07-17	27		0.901			
Swabian Jura 3	0 - 30 cm	2009-07-17	30		1.865			
Kraichgau 1	0 - 30 cm	2009-10-09	1		0.574	0.146	0.695	82.7%
Kraichgau 1	0 - 30 cm	2009-10-09	2		0.667	0.182	0.690	79.1%
Kraichgau 1	0 - 30 cm	2009-10-09	3		0.638	0.209	0.716	77.4%
Kraichgau 2	0 - 30 cm	2009-10-09	6		0.896			
Kraichgau 2	0 - 30 cm	2009-10-09	7		0.561	0.207	0.704	77.3%
Kraichgau 2	0 - 30 cm	2009-10-09	8		0.721	0.236	0.720	75.3%
Kraichgau 3	0 - 30 cm	2009-10-31	11		0.629	0.261	0.697	72.8%
Kraichgau 3	0 - 30 cm	2009-10-31	12		0.643	0.201	0.702	77.8%
Kraichgau 3	0 - 30 cm	2009-10-31	13		0.742	0.208	0.700	77.1%
Swabian Jura 1	0 - 30 cm	2009-10-21	16		1.427	0.046	0.690	93.7%
Swabian Jura 1	0 - 30 cm	2009-10-21	17		1.355	0.198	0.596	75.0%
Swabian Jura 1	0 - 30 cm	2009-10-21	20		1.772	0.324	0.505	60.9%
Swabian Jura 2	0 - 30 cm	2009-10-21	22		1.493	0.206	0.600	74.5%
Swabian Jura 2	0 - 30 cm	2009-10-21	23		2.072	0.385	0.574	59.8%
Swabian Jura 2	0 - 30 cm	2009-10-21	24	87.00	2.324	0.293	0.494	62.8%
Swabian Jura 3	0 - 30 cm	2009-10-21	26	61.00	2.054	0.304	0.478	61.2%
Swabian Jura 3	0 - 30 cm	2009-10-21	27	55.35	1.092	0.272	0.615	69.3%
Swabian Jura 3	0 - 30 cm	2009-10-21	30		2.152	0.375	0.451	54.6%
Kraichgau 1	0 - 30 cm	2010-06-15	1		0.631			
Kraichgau 1	0 - 30 cm	2010-06-15	2		0.522			
Kraichgau 1	0 - 30 cm	2010-06-15	3		0.662			

Experiment	Sampling depth	Sampling date	Subplot ID	SOC t ha^{-1}	SMB-C t ha^{-1}	Area below 2930 cm^{-1}	Area below 1620 cm^{-1}	SOM in slow pool
Kraichgau 2	0 - 30 cm	2010-04-28	6		0.685			
Kraichgau 2	0 - 30 cm	2010-04-28	7		0.398			
Kraichgau 2	0 - 30 cm	2010-04-28	8		0.347			
Kraichgau 3	0 - 30 cm	2010-04-28	11		0.286			
Kraichgau 3	0 - 30 cm	2010-04-28	12		0.226			
Kraichgau 3	0 - 30 cm	2010-04-28	13		0.339			
Swabian Jura 1	0 - 30 cm	2010-05-05	16		1.254			
Swabian Jura 1	0 - 30 cm	2010-05-05	17		1.224			
Swabian Jura 1	0 - 30 cm	2010-05-05	20		1.403			
Swabian Jura 2	0 - 30 cm	2010-05-05	22		1.360			
Swabian Jura 2	0 - 30 cm	2010-05-05	23		1.388			
Swabian Jura 2	0 - 30 cm	2010-05-05	24		2.226			
Swabian Jura 3	0 - 30 cm	2010-06-28	26		1.735			
Swabian Jura 3	0 - 30 cm	2010-06-28	27		0.881			
Swabian Jura 3	0 - 30 cm	2010-06-28	30		2.173			
Kraichgau 1	0 - 30 cm	2010-08-06	1		0.548			
Kraichgau 1	0 - 30 cm	2010-08-06	2		0.925			
Kraichgau 1	0 - 30 cm	2010-08-06	3		0.445			
Kraichgau 2	0 - 30 cm	2010-06-21	6		0.878			
Kraichgau 2	0 - 30 cm	2010-06-21	7		0.736			
Kraichgau 2	0 - 30 cm	2010-06-21	8		0.786			
Kraichgau 3	0 - 30 cm	2010-06-21	11		0.659			
Kraichgau 3	0 - 30 cm	2010-06-21	12		0.577			
Kraichgau 3	0 - 30 cm	2010-06-21	13		0.604			
Swabian Jura 1	0 - 30 cm	2010-07-05	16		1.810	0.225	0.533	70.3%
Swabian Jura 1	0 - 30 cm	2010-07-05	17		1.155	0.069	0.535	88.6%
Swabian Jura 1	0 - 30 cm	2010-07-05	20		1.407	0.146	0.446	75.3%
Swabian Jura 2	0 - 30 cm	2010-07-05	22		1.570	0.129	0.541	80.8%
Swabian Jura 2	0 - 30 cm	2010-07-05	23		1.506	0.147	0.523	78.1%
Swabian Jura 2	0 - 30 cm	2010-07-05	24		2.328	0.230	0.471	67.2%
Swabian Jura 3	0 - 30 cm	2010-08-10	26		2.114	0.238	0.445	65.2%
Swabian Jura 3	0 - 30 cm	2010-08-10	27		1.049	0.095	0.538	85.1%
Swabian Jura 3	0 - 30 cm	2010-08-10	30		1.768	0.223	0.409	64.7%
Kraichgau 1	0 - 30 cm	2010-10-30	1	35.13	0.351	0.066	0.673	91.1%
Kraichgau 1	0 - 30 cm	2010-10-30	2	36.23	0.384	0.037	0.618	94.3%
Kraichgau 1	0 - 30 cm	2010-10-30	3	32.99	0.554	0.079	0.691	89.8%
Kraichgau 2	0 - 30 cm	2010-10-30	6	52.79	0.877	0.239	0.631	72.5%
Kraichgau 2	0 - 30 cm	2010-10-30	7	31.60	0.944	0.028	0.661	95.9%
Kraichgau 2	0 - 30 cm	2010-10-30	8	35.44	0.735	0.119	0.697	85.4%
Kraichgau 3	0 - 30 cm	2010-10-30	11	41.02	0.704	0.110	0.709	86.6%
Kraichgau 3	0 - 30 cm	2010-10-30	12	36.90	0.634	0.078	0.693	89.9%
Kraichgau 3	0 - 30 cm	2010-10-30	13	35.33	0.614	0.098	0.700	87.7%
Swabian Jura 1	0 - 30 cm	2010-11-06	16	70.75	0.782			
Swabian Jura 1	0 - 30 cm	2010-11-06	17	60.44	0.623			

Experiment	Sampling depth	Sampling date	Subplot ID	SOC t ha^{-1}	SMB-C t ha^{-1}	Area below 2930 cm^{-1}	Area below 1620 cm^{-1}	SOM in slow pool
Swabian Jura 1	0 - 30 cm	2010-11-06	20	72.89	1.047			
Swabian Jura 2	0 - 30 cm	2010-11-06	22	70.82	0.832			
Swabian Jura 2	0 - 30 cm	2010-11-06	23	56.81	0.729			
Swabian Jura 2	0 - 30 cm	2010-11-06	24	87.22	1.425			
Swabian Jura 3	0 - 30 cm	2010-11-06	26	50.15	0.958			
Swabian Jura 3	0 - 30 cm	2010-11-06	27	57.69	0.903			
Swabian Jura 3	0 - 30 cm	2010-11-06	30	76.54	1.188			
Kraichgau 1	0 - 30 cm	2011-05-15	1		1.070			
Kraichgau 1	0 - 30 cm	2011-05-15	2		0.479			
Kraichgau 1	0 - 30 cm	2011-05-15	3		0.824			
Kraichgau 2	0 - 30 cm	2011-05-15	6		1.166			
Kraichgau 2	0 - 30 cm	2011-05-15	7		0.963			
Kraichgau 2	0 - 30 cm	2011-05-15	8		1.000			
Kraichgau 3	0 - 30 cm	2011-05-15	11		0.927			
Kraichgau 3	0 - 30 cm	2011-05-15	12		0.829			
Kraichgau 3	0 - 30 cm	2011-05-15	13		0.695			
Swabian Jura 1	0 - 30 cm	2011-05-13	16		0.962			
Swabian Jura 1	0 - 30 cm	2011-05-13	17		1.379			
Swabian Jura 1	0 - 30 cm	2011-05-13	20		1.950			
Swabian Jura 2	0 - 30 cm	2011-05-13	22		1.195			
Swabian Jura 2	0 - 30 cm	2011-05-13	23		1.039			
Swabian Jura 2	0 - 30 cm	2011-05-13	24		1.120			
Swabian Jura 3	0 - 30 cm	2011-05-13	26		1.345			
Swabian Jura 3	0 - 30 cm	2011-05-13	27		0.795			
Swabian Jura 3	0 - 30 cm	2011-05-13	30		1.413			
Kraichgau 1	0 - 30 cm	2012-02-26	1	32.80				
Kraichgau 1	0 - 30 cm	2012-02-26	2	32.35				
Kraichgau 2	0 - 30 cm	2012-02-26	6	50.39				
Kraichgau 2	0 - 30 cm	2012-02-26	7	30.20				
Kraichgau 2	0 - 30 cm	2012-02-26	8	35.55				
Kraichgau 3	0 - 30 cm	2012-02-26	11	42.13				
Kraichgau 3	0 - 30 cm	2012-02-26	12	37.07				
Kraichgau 3	0 - 30 cm	2012-02-26	13	36.95				
Swabian Jura 1	0 - 30 cm	2012-03-15	16	72.06				
Swabian Jura 1	0 - 30 cm	2012-03-15	17	61.29				
Swabian Jura 1	0 - 30 cm	2012-03-15	20	77.04				
Swabian Jura 2	0 - 30 cm	2012-03-15	22	67.32				
Swabian Jura 2	0 - 30 cm	2012-03-15	23	57.01				
Swabian Jura 2	0 - 30 cm	2012-03-15	24	87.15				
Swabian Jura 3	0 - 30 cm	2012-02-27	26	46.05				
Swabian Jura 3	0 - 30 cm	2012-02-27	27	50.87				
Swabian Jura 3	0 - 30 cm	2012-02-27	30	73.01				
Kraichgau 1	0 - 30 cm	2012-05-07	1		1.117			
Kraichgau 1	0 - 30 cm	2012-05-07	2		1.072			

Experiment	Sampling depth	Sampling date	Subplot ID	SOC t ha^{-1}	SMB-C t ha^{-1}	Area below 2930 cm^{-1}	Area below 1620 cm^{-1}	SOM in slow pool
Kraichgau 1	0 - 30 cm	2012-05-07	3		0.499			
Kraichgau 2	0 - 30 cm	2012-05-07	6		0.649			
Kraichgau 2	0 - 30 cm	2012-05-07	7		0.512			
Kraichgau 2	0 - 30 cm	2012-05-07	8		0.645			
Kraichgau 3	0 - 30 cm	2012-05-07	11		0.680			
Kraichgau 3	0 - 30 cm	2012-05-07	12		0.989			
Kraichgau 3	0 - 30 cm	2012-05-07	13					
Swabian Jura 1	0 - 30 cm	2012-05-25	16		1.172			
Swabian Jura 1	0 - 30 cm	2012-05-25	17		0.720			
Swabian Jura 1	0 - 30 cm	2012-05-25	20		1.459			
Swabian Jura 2	0 - 30 cm	2012-05-25	22		0.806			
Swabian Jura 2	0 - 30 cm	2012-05-25	23		1.330			
Swabian Jura 2	0 - 30 cm	2012-05-25	24		2.015			
Swabian Jura 3	0 - 30 cm	2012-05-25	26		1.602			
Swabian Jura 3	0 - 30 cm	2012-05-25	27		0.897			
Swabian Jura 3	0 - 30 cm	2012-05-25	30		2.644			
Kraichgau 1	0 - 30 cm	2012-06-24	1	33.58	0.629	0.017	0.708	97.7%
Kraichgau 1	0 - 30 cm	2012-06-24	2	34.98	0.758	-0.078	0.660	113.4%
Kraichgau 1	0 - 30 cm	2012-06-24	3	32.18	0.720	0.057	0.696	92.4%
Kraichgau 2	0 - 30 cm	2012-06-24	6	55.58	0.659	0.200	0.618	75.5%
Kraichgau 2	0 - 30 cm	2012-06-24	7	29.49	0.555	0.013	0.680	98.1%
Kraichgau 2	0 - 30 cm	2012-06-24	8	35.67	0.436	0.176	0.713	80.2%
Kraichgau 3	0 - 30 cm	2012-06-24	11	38.14	0.548			
Kraichgau 3	0 - 30 cm	2012-06-24	12	33.21	0.368			
Kraichgau 3	0 - 30 cm	2012-06-24	13	35.22	0.486			
Swabian Jura 1	0 - 30 cm	2012-07-05	16	65.69	1.057	0.135	0.529	79.7%
Swabian Jura 1	0 - 30 cm	2012-07-05	17	55.79	1.038	0.112	0.565	83.5%
Swabian Jura 1	0 - 30 cm	2012-07-05	20	80.25	1.244	0.170	0.477	73.8%
Swabian Jura 2	0 - 30 cm	2012-07-05	22	64.21	1.056	0.041	0.525	92.7%
Swabian Jura 2	0 - 30 cm	2012-07-05	23	61.81	1.026	0.100	0.544	84.4%
Swabian Jura 2	0 - 30 cm	2012-07-05	24	88.51	1.290	0.164	0.454	73.5%
Swabian Jura 3	0 - 30 cm	2012-07-05	26	55.69	1.822	0.190	0.448	70.3%
Swabian Jura 3	0 - 30 cm	2012-07-05	27	56.16	1.018	0.032	0.559	94.5%
Swabian Jura 3	0 - 30 cm	2012-07-05	30	80.93	1.694	0.248	0.441	64.0%
Kraichgau 1	0 - 30 cm	2012-07-31	1	32.14	0.535			
Kraichgau 1	0 - 30 cm	2012-07-31	2	37.07	0.897			
Kraichgau 1	0 - 30 cm	2012-07-31	3	29.51	0.523			
Kraichgau 2	0 - 30 cm	2012-10-05	6	49.95	0.861			
Kraichgau 2	0 - 30 cm	2012-10-05	7	28.65	0.637			
Kraichgau 2	0 - 30 cm	2012-10-05	8	31.28	0.806			
Kraichgau 3	0 - 30 cm	2012-08-07	11	36.25	0.590	0.078	0.704	90.0%
Kraichgau 3	0 - 30 cm	2012-08-07	12	30.25	0.470	0.024	0.707	96.7%
Kraichgau 3	0 - 30 cm	2012-08-07	13	34.77	0.654	0.084	0.713	89.5%
Swabian Jura 1	0 - 30 cm	2012-08-30	16	61.61	0.780			

Experiment	Sampling depth	Sampling date	Subplot ID	SOC t ha^{-1}	SMB-C t ha^{-1}	Area below 2930 cm^{-1}	Area below 1620 cm^{-1}	SOM in slow pool
Swabian Jura 1	0 - 30 cm	2012-08-30	17	54.65	0.899			
Swabian Jura 1	0 - 30 cm	2012-08-30	20	80.41	1.093			
Swabian Jura 2	0 - 30 cm	2012-10-11	22	74.15	1.068			
Swabian Jura 2	0 - 30 cm	2012-10-11	23	68.64	1.349			
Swabian Jura 2	0 - 30 cm	2012-10-11	24	93.19	1.592			
Swabian Jura 3	0 - 30 cm	2012-08-06	26	57.19	1.620			
Swabian Jura 3	0 - 30 cm	2012-08-06	27	51.44	0.785			
Swabian Jura 3	0 - 30 cm	2012-08-06	30	83.65	1.955			
Kraichgau 1	0 - 30 cm	2012-11-07	1		0.829			
Kraichgau 1	0 - 30 cm	2012-11-07	2	39.66	0.835			
Kraichgau 1	0 - 30 cm	2012-11-07	3		0.576			
Kraichgau 2	0 - 30 cm	2012-11-07	6		0.652			
Kraichgau 2	0 - 30 cm	2012-11-07	7		0.680			
Kraichgau 2	0 - 30 cm	2012-11-07	8		0.668			
Kraichgau 3	0 - 30 cm	2012-11-07	11		0.701			
Kraichgau 3	0 - 30 cm	2012-11-07	12		0.596			
Kraichgau 3	0 - 30 cm	2012-11-07	13		0.404			
Swabian Jura 1	0 - 30 cm	2012-11-10	16		0.739			
Swabian Jura 1	0 - 30 cm	2012-11-10	17		0.649			
Swabian Jura 1	0 - 30 cm	2012-11-10	20		0.523			
Swabian Jura 2	0 - 30 cm	2012-11-10	22		1.695			
Swabian Jura 2	0 - 30 cm	2012-11-10	23		0.755			
Swabian Jura 2	0 - 30 cm	2012-11-10	24		0.888			
Swabian Jura 3	0 - 30 cm	2012-11-10	26		0.861			
Swabian Jura 3	0 - 30 cm	2012-11-10	27		0.585			
Swabian Jura 3	0 - 30 cm	2012-11-10	30		1.864			
Kraichgau 1	0 - 30 cm	2013-02-18	1		0.831			
Kraichgau 1	0 - 30 cm	2013-02-18	2		0.291			
Kraichgau 1	0 - 30 cm	2013-02-18	3		0.646			
Kraichgau 2	0 - 30 cm	2013-02-18	6		0.773			
Kraichgau 2	0 - 30 cm	2013-02-18	7		0.881			
Kraichgau 2	0 - 30 cm	2013-02-18	8		0.713			
Kraichgau 3	0 - 30 cm	2013-02-18	11		0.772			
Kraichgau 3	0 - 30 cm	2013-02-18	12		0.251			
Kraichgau 3	0 - 30 cm	2013-02-18	13		0.710			
Swabian Jura 1	0 - 30 cm	2013-05-10	16		0.695			
Swabian Jura 1	0 - 30 cm	2013-05-10	17		1.523			
Swabian Jura 1	0 - 30 cm	2013-05-10	20		1.054			
Swabian Jura 2	0 - 30 cm	2013-05-10	22		1.488			
Swabian Jura 2	0 - 30 cm	2013-05-10	23		0.183			
Swabian Jura 2	0 - 30 cm	2013-05-10	24		1.466			
Swabian Jura 3	0 - 30 cm	2013-05-10	26		0.621			
Kraichgau 1	0 - 30 cm	2013-05-13	1		0.546			
Kraichgau 1	0 - 30 cm	2013-05-13	2		0.648			

Experiment	Sampling depth	Sampling date	Subplot ID	SOC t ha^{-1}	SMB-C t ha^{-1}	Area below 2930 cm^{-1}	Area below 1620 cm^{-1}	SOM in slow pool
Kraichgau 1	0 - 30 cm	2013-05-13	3		0.514			
Kraichgau 2	0 - 30 cm	2013-05-13	6		1.065			
Kraichgau 2	0 - 30 cm	2013-05-13	7		0.825			
Kraichgau 2	0 - 30 cm	2013-05-13	8		0.531			
Kraichgau 3	0 - 30 cm	2013-05-13	11		0.395			
Kraichgau 3	0 - 30 cm	2013-05-13	12		0.506			
Kraichgau 3	0 - 30 cm	2013-05-13	13		0.281			
Swabian Jura 1	0 - 30 cm	2013-06-27	16	72.81	0.887			
Swabian Jura 1	0 - 30 cm	2013-06-27	17	70.08	1.031			
Swabian Jura 1	0 - 30 cm	2013-06-27	20	85.15	1.569			
Swabian Jura 2	0 - 30 cm	2013-06-27	22	77.54	0.871			
Swabian Jura 2	0 - 30 cm	2013-06-27	23	65.91	0.857			
Swabian Jura 2	0 - 30 cm	2013-06-27	24	95.39	1.179			
Swabian Jura 3	0 - 30 cm	2013-06-27	26	67.44	1.165			
Swabian Jura 3	0 - 30 cm	2013-06-27	27	58.08	0.769			
Swabian Jura 3	0 - 30 cm	2013-06-27	30	85.36	1.038			
Kraichgau 1	0 - 30 cm	2013-07-01	1	34.77	0.652			
Kraichgau 1	0 - 30 cm	2013-07-01	2	37.57	0.761			
Kraichgau 1	0 - 30 cm	2013-07-01	3	32.67	0.716			
Kraichgau 2	0 - 30 cm	2013-07-01	6	49.28	1.136			
Kraichgau 2	0 - 30 cm	2013-07-01	7	32.76	0.156			
Kraichgau 2	0 - 30 cm	2013-07-01	8	32.44	0.611			
Kraichgau 3	0 - 30 cm	2013-07-01	11	38.63	3.182			
Kraichgau 3	0 - 30 cm	2013-07-01	12	33.87	0.470			
Kraichgau 3	0 - 30 cm	2013-07-01	13	34.94	0.713			
Kraichgau 1	0 - 30 cm	2014-02-19	1		0.555			
Kraichgau 1	0 - 30 cm	2014-02-19	2		0.829			
Kraichgau 1	0 - 30 cm	2014-02-19	3		0.503			
Kraichgau 2	0 - 30 cm	2014-02-19	6		0.660			
Kraichgau 2	0 - 30 cm	2014-02-19	7		0.539			
Kraichgau 2	0 - 30 cm	2014-02-19	8		0.554			
Kraichgau 3	0 - 30 cm	2014-02-19	11		0.501			
Kraichgau 3	0 - 30 cm	2014-02-19	12		0.490			
Kraichgau 3	0 - 30 cm	2014-02-19	13		0.537			
Swabian Jura 1	0 - 30 cm	2014-03-04	16		1.127			
Swabian Jura 1	0 - 30 cm	2014-03-04	17		0.848			
Swabian Jura 1	0 - 30 cm	2014-03-04	20		1.457			
Kraichgau 1	0 - 30 cm	2014-08-04	1		0.339			
Kraichgau 1	0 - 30 cm	2014-08-04	2		0.638			
Kraichgau 1	0 - 30 cm	2014-08-04	3		0.327			
Kraichgau 3	0 - 30 cm	2014-08-04	11		0.320			
Kraichgau 3	0 - 30 cm	2014-08-04	12		0.291			
Kraichgau 3	0 - 30 cm	2014-08-04	13		0.405			
Kraichgau 1	0 - 30 cm	2014-10-15	1		0.376			

Experiment	Sampling depth	Sampling date	Subplot ID	SOC t ha^{-1}	SMB-C t ha^{-1}	Area below 2930 cm^{-1}	Area below 1620 cm^{-1}	SOM in slow pool
Kraichgau 1	0 - 30 cm	2014-10-15	2		0.351			
Kraichgau 1	0 - 30 cm	2014-10-15	3		0.372			
Kraichgau 2	0 - 30 cm	2014-10-15	6		0.738			
Kraichgau 2	0 - 30 cm	2014-10-15	7		0.561			
Kraichgau 2	0 - 30 cm	2014-10-15	8		0.553			
Kraichgau 3	0 - 30 cm	2014-10-15	11		0.385			
Kraichgau 3	0 - 30 cm	2014-10-15	12		0.419			
Kraichgau 3	0 - 30 cm	2014-10-15	13		0.539			
Swabian Jura 1	0 - 30 cm	2014-10-21	16		1.226			
Swabian Jura 1	0 - 30 cm	2014-10-21	17		0.699			
Swabian Jura 1	0 - 30 cm	2014-10-21	20		1.051			
Kraichgau 1	0 - 30 cm	2015-02-25	1		0.702			
Kraichgau 1	0 - 30 cm	2015-02-25	2		0.739			
Kraichgau 1	0 - 30 cm	2015-02-25	3		0.445			
Kraichgau 2	0 - 30 cm	2015-02-25	6		0.990			
Kraichgau 2	0 - 30 cm	2015-02-25	7		0.513			
Kraichgau 2	0 - 30 cm	2015-02-25	8		0.739			
Kraichgau 3	0 - 30 cm	2015-02-25	11		0.533			
Kraichgau 3	0 - 30 cm	2015-02-25	12		0.458			
Kraichgau 3	0 - 30 cm	2015-02-25	13		0.429			
Swabian Jura 1	0 - 30 cm	2015-03-09	16		0.942			
Swabian Jura 1	0 - 30 cm	2015-03-09	17		0.805			
Swabian Jura 1	0 - 30 cm	2015-03-09	20		1.022			
Kraichgau 1	0 - 30 cm	2015-05-04	1		0.654			
Kraichgau 1	0 - 30 cm	2015-05-04	2		0.802			
Kraichgau 1	0 - 30 cm	2015-05-04	3		0.235			
Kraichgau 2	0 - 30 cm	2015-05-04	6		0.500			
Kraichgau 2	0 - 30 cm	2015-05-04	7		0.438			
Kraichgau 2	0 - 30 cm	2015-05-04	8		0.531			
Kraichgau 3	0 - 30 cm	2015-05-04	11		0.560			
Kraichgau 3	0 - 30 cm	2015-05-04	12		0.480			
Kraichgau 3	0 - 30 cm	2015-05-04	13		0.465			
Kraichgau 1	0 - 30 cm	2015-07-22	1	30.93	0.447	-0.024	0.699	103.6%
Kraichgau 1	0 - 30 cm	2015-07-22	2	36.48	0.705	0.037	0.671	94.8%
Kraichgau 1	0 - 30 cm	2015-07-22	3	30.37	0.343	0.043	0.720	94.4%
Kraichgau 2	0 - 30 cm	2015-07-22	6	50.67	1.047	0.151	0.675	81.8%
Kraichgau 2	0 - 30 cm	2015-07-22	7	31.45	0.830	-0.051	0.673	108.1%
Kraichgau 2	0 - 30 cm	2015-07-22	8	33.85	1.001	0.093	0.726	88.6%
Kraichgau 3	0 - 30 cm	2015-08-20	11		0.357			
Kraichgau 3	0 - 30 cm	2015-08-20	12		0.164			
Kraichgau 3	0 - 30 cm	2015-08-20	13		0.371			
Swabian Jura 1	0 - 30 cm	2015-08-05	16	65.29		0.163	0.605	78.7%
Swabian Jura 1	0 - 30 cm	2015-08-05	17	50.20		0.068	0.572	89.4%
Swabian Jura 1	0 - 30 cm	2015-08-05	20	74.39		0.115	0.488	80.9%

Experiment	Sampling depth	Sampling date	Subplot ID	SOC t ha^{-1}	SMB-C t ha^{-1}	Area below 2930 cm^{-1}	Area below 1620 cm^{-1}	SOM in slow pool
Kraichgau 3	0 - 30 cm	2015-09-30	11	36.70	0.298	-0.001	0.697	100.2%
Kraichgau 3	0 - 30 cm	2015-09-30	12	35.05	0.369	-0.016	0.703	102.4%
Kraichgau 3	0 - 30 cm	2015-09-30	13	33.43	0.293	0.045	0.648	93.5%
Kraichgau 1	0 - 30 cm	2015-10-21	1		0.508			
Kraichgau 1	0 - 30 cm	2015-10-21	2		0.245			
Kraichgau 1	0 - 30 cm	2015-10-21	3		0.300			
Kraichgau 2	0 - 30 cm	2015-10-21	6		0.402			
Kraichgau 2	0 - 30 cm	2015-10-21	7		0.568			
Kraichgau 2	0 - 30 cm	2015-10-21	8		0.296			
Swabian Jura 1	0 - 30 cm	2015-10-14	16		0.707			
Swabian Jura 1	0 - 30 cm	2015-10-14	17		0.805			
Swabian Jura 1	0 - 30 cm	2015-10-14	20		0.795			
Kraichgau 2	0 - 30 cm	2016-05-09	6		0.559			
Kraichgau 2	0 - 30 cm	2016-05-09	7		0.490			
Kraichgau 2	0 - 30 cm	2016-05-09	8		0.532			
Kraichgau 3	0 - 30 cm	2016-05-09	11		0.412			
Kraichgau 3	0 - 30 cm	2016-05-09	12		0.339			
Kraichgau 3	0 - 30 cm	2016-05-09	13		0.685			
Swabian Jura 1	0 - 30 cm	2016-05-17	16		0.861			
Swabian Jura 1	0 - 30 cm	2016-05-17	17		0.875			
Swabian Jura 1	0 - 30 cm	2016-05-17	20		0.586			
Kraichgau 1	0 - 30 cm	2016-07-06	1		0.462			
Kraichgau 1	0 - 30 cm	2016-07-06	2		0.339			
Kraichgau 1	0 - 30 cm	2016-07-06	3		0.424			
Kraichgau 2	0 - 30 cm	2016-07-06	6		0.344			
Kraichgau 2	0 - 30 cm	2016-07-06	7		0.319			
Kraichgau 2	0 - 30 cm	2016-07-06	8		0.282			
Kraichgau 3	0 - 30 cm	2016-07-06	11		0.215			
Kraichgau 3	0 - 30 cm	2016-07-06	12		0.286			
Kraichgau 3	0 - 30 cm	2016-07-06	13		0.283			
Swabian Jura 1	0 - 30 cm	2016-07-20	16		0.509			
Swabian Jura 1	0 - 30 cm	2016-07-20	17		0.551			
Swabian Jura 1	0 - 30 cm	2016-07-20	20		0.904			

6.3 Supplement chapter 4

6.3.1 Temperature sensitivities of enzymatic activities

Temperature sensitivities of enzymes β-glucosidase, xylanase and phenol/peroxidase were measured from April 2012 to April 2013 by substrate additions to field moist soil samples from Exp. 1 and 2, which had been stored at -24 °C (for details see Ali et al., 2015). In the present study, the TS, i.e., the Q_{10} values of β-glucosidase and xylanase data were taken directly from the supplement of Ali et al. (2015), while phenol/peroxidase measurements were redone using an optimized method and an alternative substrate which led to substantially improved modelling efficiencies of Q_{10} values compared to the values published by Ali et al. (2015). Briefly, for phenol/peroxidase activity measurements suspensions of soil in sterilized water were placed in a microplate amended with buffer solutions and substrate (2,2'-azinobis-(-3-ethylbenzothiazoline-6-sulfononic acid) diammonium salt (ABTS)). At different time intervals, substrate turnover was measured at 630 nm by a microplate reader. The measurements were done with incubations at 5, 10, 17, 24 and 30 °C. As in Ali et al. (2015), the temperature response of phenol/peroxidase activities (*k*) was modelled by an exponential equation as follows:

$$k(T) = k_0 e^{aT} \quad \text{(S4-1)}$$

T being the incubation temperature (°C), k_0 the intercept and *a* being the fitted exponential coefficient. Temperature sensitivity was calculated as a Q_{10} value, representing the activity increase with + 10 °C:

$$Q_{10} = e^{(a\ x\ 10)} \quad \text{(S4-2)}$$

Calculated Q_{10} of remeasured phenol/peroxidase activities are presented in supplement (Table S4 - 4).

6.3.2 Details on the specification of Expert-N 5.0

Further sub-models used for the simulation of Daisy driving factors were the following: i) soil temperature, net radiation and emissivity were simulated by the Daisy heat module (Hansen et al., 1993); ii) evaporation by the Penman Monteith equation (Monteith, 1976); and iii) water flow by Hydrus-1D (van Genuchten, 1982) using the hydraulic function of Mualem (1976). Parameters of the hydraulic conductivity curve were estimated based on texture and bulk density using Rosetta (Schaap et al., 2001). The crop model for Exp. 2 was GECROS (Biernath et al., 2013; Yin and van Laar, 2005), which was calibrated to local conditions (supplement section S4). Nitrification, denitrification and nitrogen leaching were simulated with LEACHN (Hutson and Wagenet., 1992). The selected Expert-N 5.0 timestep was 0.09 days (largest timestep with unaltered model outputs).

6.3.3 Calibration of the crop growth model

GECROS parameters were estimated for all main crops, namely winter wheat, silage maize, winter rapeseed, winter barley, spring barley and cover crops with 11, 7, 6, 3, 4 and 5 site-years used for calibration, respectively. As spring barley was only grown in one site-year during the study period, additional BBCH and crop yield data obtained by the "Landestechnologiezentrum Augustenberg" for the years 2009, 2010 and 2011 were included in the dataset. For cover crops, no information on BBCH stages was available and the phenology parameters of winter rapeseed were used. A brief description of GECROS and modifications on the original version, similarly used in this study, are given by Ingwersen et al. (2018). Parameter optimization based on a seven-year dataset (2010-2016) of plant measurements from the six study sites of experiment 2 was executed using the software UCODE_2014 (Poeter et al., 2014). The parameter set was obtained by intensive monitoring of all crops roughly every two weeks during the growing season. Sampling was conducted on the three soil plots and two additional plots, resulting in five permanent plots, evenly distributed across each field. Canopy height and phenological development stage were measured with ten replicates at each sampling time. Aboveground samples of plant biomass were obtained at the beginning of shoot development, full flowering and maturity, measuring dry matter by oven drying at 60 °C. The samples from maturity were further divided into vegetative and generative organs and their C and N content was measured with an elemental analyzer (Vario EL, Elementar Analysensysteme, Hanau, Germany). The software estimates parameter values that minimize a weighted least-square objective function. For the calibration procedure, soil properties and state variables were initialized at the beginning of the simulation period (August 2010) and the crop rotations of the six sites were continuously simulated. This approach ensures a better representation of soil-crop interactions and pre-crop effects compared to a re-initialization of every cropping year. The optimization of GECROS parameters was performed for one crop at a time. Thus, parameters were varied for those years where that specific crop was grown while the parameters of other crops were kept constant. The calibration followed a two-step approach. Phenology parameters based on measured development stages in BBCH-scale (Meier, 2001) were optimized first. Then optimized phenology parameters were fixed while remaining parameters (e.g., N partitioning between plant organs, specific leaf area and photosynthetic efficiency) were optimized. Data used for this step included leaf area index (LAI), vegetative and generative biomass at three BBCH stages, corresponding N contents and actual evapotranspiration measured by eddy covariance (data presented by Eshonkulov et al., 2019). Data of the different groups were normalized to the respective maximum value and weighted according to the number of measurements within each group. Based on a sensitivity analysis, a step-wise optimization procedure, similar to that described by Ingwersen et al. (2018), was applied. Initial and optimized GECROS parameter values can be found in Table S4 - 1 with an explanation of parameters in Table S4 - 2.

Table S4 - 1 Default (Def.) and optimized (Opt.) GECROS parameter values for the specific crops. For cover crops, default values of winter rapeseed were used. Default parameter values were taken from Yin and van Laar (2005). If information on default values was missing, initial parameter values were defined based on measurements or expert guess. The parameters and their unit are defined in Table S4 - 2.

Parameter	Winter wheat		Silage maize		Winter rapeseed		Winter barley		Spring barley		Cover crops	
	Def.	Opt.	Def.	Opt.	Def.	Opt.	Def.	Opt.	Def.	Opt.	Def.	Opt.
EG	0.25	0.75	0.25	0.75	0.45	0.99	0.25	0.95	0.25	0.95	n.a.	0.99
CDMHT	460	460	570	570	285	285	450	460	450	450	n.a.	285
TOD	25	23.93	30	25/ 21.26*	25	24	25	25	25	25	n.a.	27.2
TCD	37	44.88	42	37.79/42*	37	37	37	37	37	37	n.a.	39.74
NUPTX	0.5	0.5522	0.5	0.5	0.5	0.5	0.5	0.55	0.5	0.5	n.a.	0.5
RNCMIN	0.005	0.005	0.005	0.005	0.005	0.004	0.005	0.003	0.005	0.005	n.a.	0.004
STEMNC	0.01	0.005	0.008	0.0035	0.01	0.003	0.01	0.003	0.01	0.005	n.a.	0.003
SLNMIN	0.35	0.45	0.25	0.25	0.3	0.12	0.3	0.15	0.3	0.3	n.a.	0.12
LNCI	0.05	0.0587	0.05	0.0267	0.05	0.0568	0.05	0.0321	0.05	0.0274	n.a.	0.0534
SLA0	0.028	0.015	0.022	0.017	0.03	0.04	0.031	0.025	0.031	0.02	n.a.	0.04
EAJMAX	48270	47000	70890	72280	n.a.	62200	30200	30200	30200	30200	n.a.	53440
XVN	60	28.38	60	39.15	60	79.2	60	29.23	60	60.1	n.a.	42.46
XJN	120	56.76	120	78.3	120	158.4	120	58.46	120	120.2	n.a.	84.92
SEEDW	n.a.	0.0475	n.a.	0.3	n.a.	0.0045	n.a.	0.045	n.a.	0.045	n.a.	0.0045
SEEDNC	n.a.	0.0263	n.a.	0.013	n.a.	0.027	n.a.	0.02	n.a.	0.015	n.a.	0.027
MTDV	n.a.	45.39	n.a.	50.57/ 58.66*	n.a.	27.53	n.a.	24.24	n.a.	29.11	n.a.	15.41
MTDR	n.a.	52.24	n.a.	42.73/ 53.46*	n.a.	89.02	n.a.	30.32	n.a.	27.43	n.a.	53.24
PSEN	n.a.	-0.103	n.a.	0	n.a.	-0.082	n.a.	-0.098	n.a.	0	n.a.	0
PMEH	0.8	0.5	0.8	0.8	0.8	0.8	0.8	0.5	0.8	0.8828	n.a.	0.8
FCRSH	0.5	0.5906	0.5	0.6766	0.5	0.5542	0.5	0.5	0.5	0.5	n.a.	0.7123
FNRSH	0.62	0.555	0.62	0.68	0.62	0.4983	0.62	0.6	0.62	0.62	n.a.	0.5151
CB	n.a.	0.8	n.a.	1	n.a.	3	n.a.	0.8	n.a.	0.75	n.a.	0.75
CX	n.a.	1.067	n.a.	1.4	n.a.	4	n.a.	1.1	n.a.	1	n.a.	1

n.a.: not applicable.

*Different values for Kraichgau/Swabian Jura.

Table S4 - 2 Definition of adjusted GECROS parameters.

Parameter	Unit	Definition
EG	1	Efficiency of germination
CDMHT	g m^{-2} m^{-1}	Stem dry weight per unit of plant height
TOD	°C	Optimum temperature for phenology
TCD	°C	Ceiling temperature for phenology
NUPTX	g N m^{-2} d^{-1}	Maximum crop nitrogen uptake
RNCMIN	g N g^{-1}	Minimum N concentration in the roots
STEMNC	g N g^{-1}	Nitrogen concentration in the stem
SLNMIN	g N m^{-2}	Minimum or base specific leaf nitrogen content for photosynthesis
LNCI	g N g^{-1}	Initial nitrogen concentration in living leaves
SLA0	m^2 g^{-1}	Specific leaf area constant
EAJMAX	J mol^{-1}	Activation energy for maximum rate of electron transport through photosystem II
XVN	µmol s^{-1} g^{-1} N	Slope of linear relationship between maximum rate of Rubisco-limited carboxylation and leaf nitrogen
XJN	µmol s^{-1} g^{-1} N	Slope of linear relationship between maximum rate of electron transport through photosystem II and leaf nitrogen
SEEDW	g $seed^{-1}$	Seed weight
SEEDNC	g N g^{-1}	Standard seed (storage organ) N concentration
MTDV	d	Minimum thermal days for vegetative growth phase
MTDR	d	Minimum thermal days for reproductive (seed fill) phase
PSEN	h^{-1}	Photoperiod sensitivity of phenological development
PMEH	-	Fraction of sigmoid curve inflexion in entire plant height growth period
FCRSH	g C g^{-1} C	Initial fraction of carbon in the shoot
FNRSH	g N g^{-1} N	Initial fraction of nitrogen in the shoot
CB	-	Factor for initial nitrogen concentration of seed fill
CX	-	Factor for final nitrogen concentration of seed fill

6.3.4 Statistical weight derivation

The objective function used for the Bayesian calibration in UCODE_2014 is the sum of weighted squared model errors (SWSME; Poeter et al., 2005):

$$SWSME = \sum_1^x \sum_1^y \sum_1^z \frac{(O_{xyz} - P_{xyz})^2}{\sigma^2{}_{xy}} \quad \text{(S4-3)}$$

Here, O_{xyz} is the *z-th* observed value of *y-th* type of measurement in the *x-th* experiment, P_{xyz} is the respective predicted value of O_{xyz} and $\sigma^2{}_{xy}$ is the error variance of the y-*th* type of measurement of the *x-th* experiment. This error variance $\sigma^2{}_{xy}$ was estimated for each type of measurement at each field from the raw data using a mixed linear model. By this, each squared model error should be divided by the typical unexplained variance of each type of measurement at each experiment. The model reads as follows:

$$y_{kl} = \phi_0 + \phi_1 t_k + u_l + u_k + u_{kl} \quad \text{(S4-4)}$$

Here, y_{kl} is the measurement at time k in the plot or repetition l, ϕ_0 the intercept, ϕ_1 the slope of time t_k, u_l the intercept (random), u_k is the autocorrelated random deviation of the slope and u_{kl} is the autocorrelated residual error term corresponding to y_{kl}. From this statistical model, the error variance of each type of measurement ${\sigma_{fM}}^2 = \sigma_{u_k}^2 + \sigma_{u_{kl}}^2$ was used for weighting of obsevations, thus excluding the variance $\sigma_{u_l}^2$ of non-random effects from the weighting scheme. By this procedure, the error variance used for weighting each type of measurement represents the measurement uncertainty, but not the variance components, that can be attributed to the experimental design.

6.3.5 Statistical evaluation of enzyme TS allocations

Model error statistics as defined by Loague and Green, (1991) were used:

$$MSD = \frac{1}{n}\sum_{z=1}^{n}(O_{yz} - P_{yz})^2 \quad \text{(S4-5)}$$

$$RMSD = \sqrt{MSD} \quad \text{(S4-6)}$$

$$EF = \frac{(\sum_{z=1}^{n}(O_{yz} - \bar{O}_y)^2 - \sum_{z=1}^{n}(O_{yz} - P_{yz})^2)}{\sum_{z=1}^{n}(O_{yz} - \bar{O}_y)^2} \quad \text{(S4-7)}$$

Here, MSD and RMSD are the mean-squared-deviation and its root, EF stands for the modelling efficiency, O_{yz} denotes the measured value of the *z-th* measurement in the *y-th* subunit of the experiment, $\bar{O}_y$ is the mean of measured values of the *y-th* subunit and P_{yz} stands for the model-predicted value corresponding to O_{yz}. The subunit in this respect was the individual field for Exp. 1 and 2, the individual crop-litter at each site for Exp. 3, the individual crop-litter at each temperature for Exp. 4 and the individual fallow soil at each temperature for Exp. 5.

According to Gauch et al. (2003), the MSD can be further divided into the squared bias (SB), nonunity slope (NU) and lack of correlation (LC), giving further insight into the origin of model error.

$$SB = (\bar{O} - \bar{P})^2 \quad \text{(S4-8)}$$

$$NU = (1 - b)^2 * (\sum O_n^2/N) \quad \text{(S4-9)}$$

$$LC = (1 - r^2) * (\sum P_n^2/N) \quad \text{(S4-10)}$$

Here, $\bar{P}$ is the mean of all predicted values, *b* is the slope of the least-squares regression of *P* on *O* and *r* is the correlation between *O* and *P*. The SB and NU provide information on systematic biases between observations and predictions and can be interpreted as the intercept and slope of a regression between predictions and observations. In this study, they are displayed as percent of the MSD because:

$$MSD = SB + NU + LC \quad \text{(S4-11)}$$

Finally, to compare performance of models, which have different number of parameters (enzyme Q_{10}), Akaike information criterion (AIC) as defined by Del Grosso et al. (2005) was used:

$$AIC = -2\ln(L(\theta)) + 2k \quad \text{(S4-12)}$$

Here, $\ln(L(\theta))$ is the log-likelihood, and k stands for the number of Q_{10} parameters used. The loglikelihood was derived from a linear regression of predicted values on observed values with a forced slope of 1 and intercept of 0, using the logLik() function of R software 3.4.3 (R Core Team, 2017).

6.3.6 General goodness-of-fit

The simulation bias for incubation experiments (Exp. 4-5) indicated that besides Q_{10}, other parameters should be optimized by Bayesian calibration as well. For field simulations, the predetermined parameter set showed systematic biases for CO_2 evolution, but mostly random errors for SMB and litter decomposition. The analysis of model performance in terms of SB, NU and LC could provide deeper insight than EF alone (Table 4 - 3). For example, while the SMB-C of experiment 1 and 2 had low EF, the errors were mostly LC and visual inspection of predicted versus simulated SMB-C suggested that the reason for the low EF was the high measurement variability and that SMB-C only changed slowly, even after bare fallow establishment (Figure S4 - 1). Contrasting that, the higher SB and NU for incubation experiments 4 and 5 showed their systematic bias. For experiment 4, a reduction of carbon use efficiency due to higher temperatures (Frey et al., 2013) seemingly occurred, which was not a feature of the current model version. This is likely the reason why simulations could capture cumulative CO_2 evolution and therefore the litter decomposition, but overestimated the resulting SMB-C, especially at 25 °C (Figure S4 - 3). Underestimation of SOC loss in experiment 5 could be a result of soil disturbance by sieving prior incubation (Lefèvre et al., 2014), destroying physical protection of SOC. The calibration of the parameter set (Table S4 - 5) included the Ultuna fallow fields (Laub et al., 2020), so both the higher turnover the high assigned Q_{10} by Bayesian calibration (~3) for both SOM pools point to protection loss. The reason is, that unprotected SOM is associated with higher TS (Benbi et al., 2014; Karhu et al., 2019) and turnover. This would also be in alignment with Vaughn and Torn (2019), who only found a Q_{10} of 2 for laboratory incubation experiments of intact soil columns. The simulation of SMB-C and litter decomposition in the field experiments showed no evidence of systematic bias (Figure S4 - 1 and S 2). The high SB of field CO_2 measurements could therefore represent measurement uncertainty as the parameter set was calibrated with SOC data of experiment 1 (Laub et al., 2020) giving confidence in the longer-term carbon budget. The mismatch between field CO_2 evolutions and overall carbon budgets is a known issue (Smith et al., 2010). Field chamber CO_2 data are influenced by small scale heterogeneity (Del Grosso et al., 2005) and only represent snapshots in time.

6.3.7 Considerations about the temperature function

The temperature function of Daisy seems to be adequate to infer Q_{10} by Bayesian calibration and test enzyme TS hypothesis within the temperature range analyzed in this study. The high EF of experiment 3 simulations (Figure S4 - 2), which up to the last two months had hardly any temperatures > 10 °C, suggested a decent fit for temperatures below 10 °C. The well-captured differences in CO_2 evolution between 15 and 25 °C in experiment 4 (Figure S4 - 3) supported the correctness of exponential increase above 10 °C in the model. While the linear function below 10 °C represents a simplification, for temperatures in the 0 to 10 °C range no advantage of an exponential model over a linear model is found (Del Grosso et al., 2005), and the departure from linearity above 10 °C is represented in Daisy. Exponential models are a poor representation of the observed temperature response below 5 °C (Kätterer et al., 1998) and more complex temperature functions such as Gaussian functions, which have no consistent Q_{10}, are more suitable if one temperature function represents all SOM pools (Tuomi et al., 2008). However, they have more parameters and such a complex function for each individual pool may lead to model equifinality or overfitting (Sierra et al., 2015a). As the difference between different temperature functions only becomes evident above 30 °C (Tuomi et al., 2008), the combined linear and exponential functions used in Daisy seem to be adequate for this study.

6.3.8 Other supplementary tables chapter 4

Table S4 - 3 Locations and soil texture of the regional crop-litter incubation experiments used in this study. Additionally, parameters of Van Genuchten type soil water retention curves, calculated by Rosetta (Schaap et al., 2001) are displayed.

Station	Region	UTM Degrees Latitude	UTM Degrees Longitude	Clay (%)	Sand (%)	Silt (%)	Bulk density (g cm^{-3})	θr	θs	α	*n*	Ks
X.1-1	Kraichgau	49.19896437	8.859489457	26.2	3.54	70.3	1.47	8.07	43.9	0.007	1.569	77
X.1-2	Kraichgau	49.18539348	8.865069735	23.6	2.41	79.3	1.32	7.68	47.3	0.006	1.637	218.7
X.1-5	Kraichgau	49.17972106	8.851533824	14.6	3.61	82.3	1.51	6.49	42.2	0.006	1.619	139.8
X.6	Kraichgau	49.16207207	8.904387789	25.2	1.76	75.4	1.43	7.91	45.1	0.006	1.596	103.2
X.8	Kraichgau	49.15351206	8.821247403	22.5	3.13	75.9	1.57	7.5	43.4	0.006	1.603	97.7
X.14	Kraichgau	49.10599329	8.992065054	23.6	7.17	71	1.51	7.1	40.2	0.006	1.581	67.9
X.18-3	Swabian Jura	48.42873387	9.447100675	50	2.45	49.1	1.23	10.3	53.4	0.015	1.353	184.2
X.18-5	Swabian Jura	48.41580425	9.432383778	50.1	11	37.4	1.16	10.5	55	0.018	1.323	336.8
X.20	Swabian Jura	48.4565953	9.460459771	50.1	2.55	50.7	0.78	10.6	57.9	0.016	1.35	413.2
X.22	Swabian Jura	48.42366173	9.484874423	53.9	1.5	44	0.96	12	69.4	0.032	1.259	1462
X.26	Swabian Jura	48.42570707	9.38106863	66.2	10.7	43.4	1.28	10.5	56.9	0.016	1.358	536.7
X.27	Swabian Jura	48.5038541	9.325859188	37.5	3.91	57.8	1.23	10.4	60.3	0.013	1.406	748.9
X.33	Swabian Jura	48.342064	9.325042321	38.2	6.09	57.6	1.08	9.38	49.8	0.009	1.473	162.6

UTM = Universal Transverse Mercator reference system

Table S4 - 4 Q_{10} of individual plots (fallow and cropped) from Kraichgau and Swabian Jura with coefficient of exponential model applied (a), k0 as well as R^2 and model efficiencies (EF).

Date (M.Y)	Plot	Site	k0	a	Q10	R^2	EF
5.2012	fallow 1	Kraichgau	1.77	0.0225	1.25	0.47	0.59
5.2012	fallow 2	Kraichgau	1.56	0.0295	1.34	0.97	0.98
5.2012	fallow 3	Kraichgau	1.67	0.0152	1.16	0.65	0.65
5.2012	cropped 1	Kraichgau	1.80	0.0118	1.13	0.28	0.34
5.2012	cropped 2	Kraichgau	1.49	0.0287	1.33	0.77	0.64
5.2012	cropped 3	Kraichgau	1.07	0.0373	1.45	0.56	0.71
5.2012	fallow 1	Swabian Jura	1.72	0.0178	1.19	0.59	0.67
5.2012	fallow 2	Swabian Jura	1.60	0.0290	1.34	0.58	0.55
5.2012	fallow 3	Swabian Jura	2.25	0.0182	1.20	0.42	0.52
5.2012	cropped 1	Swabian Jura	1.96	0.0123	1.13	0.53	0.60
5.2012	cropped 2	Swabian Jura	1.44	0.0328	1.39	0.90	0.90
5.2012	cropped 3	Swabian Jura	2.07	0.0130	1.14	0.29	0.36
6.2012	fallow 1	Kraichgau	1.92	- 0.0109	0.90	0.32	0.28
6.2012	fallow 2	Kraichgau	1.70	0.0077	1.08	0.18	0.15
6.2012	fallow 3	Kraichgau	1.05	0.0331	1.39	0.43	0.24
6.2012	cropped 1	Kraichgau	1.37	0.0284	1.33	0.76	0.65
6.2012	cropped 2	Kraichgau	1.99	- 0.0059	0.94	0.18	0.13
6.2012	cropped 3	Kraichgau	1.35	0.0243	1.28	0.79	0.82
6.2012	fallow 1	Swabian Jura	1.91	0.0056	1.06	0.09	0.12
6.2012	fallow 2	Swabian Jura	1.50	0.0383	1.47	0.69	0.78
6.2012	fallow 3	Swabian Jura	1.95	0.0318	1.37	0.90	0.92
6.2012	cropped 1	Swabian Jura	2.05	0.0162	1.18	0.69	0.74
6.2012	cropped 2	Swabian Jura	1.58	0.0148	1.16	0.71	0.73
6.2012	cropped 3	Swabian Jura	1.94	0.0232	1.26	0.77	0.81
6.2012	fallow 1	Kraichgau	1.25	0.0330	1.39	0.38	0.33
6.2012	fallow 2	Kraichgau	0.81	0.0422	1.52	0.55	0.54
6.2012	fallow 3	Kraichgau	0.92	0.0342	1.41	0.46	0.49
6.2012	cropped 1	Kraichgau	1.35	0.0176	1.19	0.23	0.18
6.2012	cropped 2	Kraichgau	0.60	0.0311	1.37	0.73	0.72
6.2012	cropped 3	Kraichgau	0.65	0.0410	1.51	0.50	0.41
6.2012	fallow 1	Swabian Jura	1.25	0.0231	1.26	0.79	0.78
6.2012	fallow 2	Swabian Jura	1.41	0.0270	1.31	0.96	0.97
6.2012	fallow 3	Swabian Jura	1.27	0.0435	1.54	0.68	0.69
6.2012	cropped 1	Swabian Jura	1.39	0.0378	1.46	1.00	1.00

Date (M.Y)	Plot	Site	k0	a	Q10	R^2	EF
6.2012	cropped 2	Swabian Jura	0.78	0.0591	1.81	0.71	0.59
6.2012	cropped 3	Swabian Jura	1.00	0.0330	1.39	0.76	0.81
8.2012	fallow 1	Kraichgau	0.09	0.0824	2.28	0.67	0.53
8.2012	fallow 2	Kraichgau	0.51	0.0620	1.86	0.66	0.41
8.2012	fallow 3	Kraichgau	- 0.22	0.0903	2.47	0.72	0.44
8.2012	cropped 1	Kraichgau	0.01	0.0768	2.16	0.81	0.88
8.2012	cropped 2	Kraichgau	0.21	0.0602	1.83	0.51	0.37
8.2012	cropped 3	Kraichgau	0.24	0.0572	1.77	0.59	0.42
8.2012	fallow 1	Swabian Jura	0.11	0.0757	2.13	0.68	0.64
8.2012	fallow 2	Swabian Jura	1.25	0.0431	1.54	0.99	1.00
8.2012	fallow 3	Swabian Jura	0.45	0.0717	2.05	0.94	0.82
8.2012	cropped 1	Swabian Jura	1.72	0.0174	1.19	0.39	0.46
8.2012	cropped 2	Swabian Jura	0.81	0.0431	1.54	0.49	0.69
8.2012	cropped 3	Swabian Jura	1.25	0.0414	1.51	0.95	0.97
10.2012	fallow 1	Kraichgau	0.75	0.0528	1.70	0.83	0.83
10.2012	fallow 2	Kraichgau	0.27	0.0526	1.69	0.98	0.98
10.2012	fallow 3	Kraichgau	0.95	0.0298	1.35	0.91	0.94
10.2012	cropped 1	Kraichgau	1.22	0.0182	1.20	0.66	0.67
10.2012	cropped 2	Kraichgau	0.69	0.0312	1.37	0.49	0.62
10.2012	cropped 3	Kraichgau	0.94	0.0264	1.30	0.47	0.53
10.2012	fallow 1	Swabian Jura	0.55	0.0407	1.50	0.74	0.55
10.2012	fallow 2	Swabian Jura	1.32	0.0235	1.26	0.52	0.43
10.2012	fallow 3	Swabian Jura	1.34	0.0352	1.42	0.75	0.87
10.2012	cropped 1	Swabian Jura	1.01	0.0468	1.60	0.87	0.86
10.2012	cropped 2	Swabian Jura	1.32	0.0252	1.29	0.64	0.74
10.2012	cropped 3	Swabian Jura	0.92	0.0514	1.67	0.78	0.85
12.2012	fallow 1	Kraichgau	1.82	0.0207	1.23	0.66	0.67
12.2012	fallow 2	Kraichgau	1.58	0.0140	1.15	0.20	0.31
12.2012	fallow 3	Kraichgau	1.29	0.0178	1.20	0.49	0.52
12.2012	cropped 1	Kraichgau	1.41	0.0173	1.19	0.55	0.62
12.2012	cropped 2	Kraichgau	1.58	0.0006	1.01	0.00	- 0.01
12.2012	cropped 3	Kraichgau	1.60	0.0076	1.08	0.46	0.49
12.2012	fallow 1	Swabian Jura	1.63	0.0189	1.21	0.90	0.93
12.2012	fallow 2	Swabian Jura	1.64	0.0296	1.34	0.81	0.83
12.2012	fallow 3	Swabian Jura	1.84	0.0274	1.32	0.75	0.75
12.2012	cropped 1	Swabian Jura	1.42	0.0367	1.44	0.60	0.58

Date (M.Y)	Plot	Site	k0	a	Q10	R^2	EF
12.2012	cropped 2	Swabian Jura	1.62	0.0187	1.21	0.91	0.89
12.2012	cropped 3	Swabian Jura	1.91	0.0242	1.27	0.83	0.79
2.2013	fallow 1	Kraichgau	2.09	0.0179	1.20	0.75	0.75
2.2013	fallow 2	Kraichgau	1.85	0.0167	1.18	0.72	0.78
2.2013	fallow 3	Kraichgau	1.97	0.0177	1.19	0.88	0.90
2.2013	cropped 1	Kraichgau	2.11	0.0134	1.14	0.98	0.98
2.2013	cropped 2	Kraichgau	1.81	0.0187	1.21	0.85	0.88
2.2013	cropped 3	Kraichgau	2.17	0.0010	1.01	0.04	0.05
2.2013	fallow 1	Swabian Jura	1.42	0.0416	1.52	0.98	0.98
2.2013	fallow 2	Swabian Jura	1.87	0.0292	1.34	0.74	0.62
2.2013	fallow 3	Swabian Jura	2.32	0.0243	1.28	0.96	0.95
2.2013	cropped 1	Swabian Jura	2.24	0.0213	1.24	0.90	0.88
2.2013	cropped 2	Swabian Jura	2.04	0.0211	1.24	0.99	0.99
2.2013	cropped 3	Swabian Jura	2.09	0.0265	1.30	0.92	0.88
4.2013	fallow 1	Kraichgau	1.10	0.0232	1.26	0.21	0.21
4.2013	fallow 2	Kraichgau	1.36	0.0210	1.23	0.76	0.76
4.2013	fallow 3	Kraichgau	1.21	0.0299	1.35	0.57	0.50
4.2013	cropped 1	Kraichgau	1.10	0.0432	1.54	0.79	0.78
4.2013	cropped 2	Kraichgau	0.91	0.0363	1.44	0.68	0.73
4.2013	cropped 3	Kraichgau	1.24	0.0285	1.33	0.60	0.62
4.2013	fallow 1	Swabian Jura	1.29	0.0264	1.30	0.69	0.70
4.2013	fallow 2	Swabian Jura	0.88	0.0553	1.74	0.99	0.98
4.2013	fallow 3	Swabian Jura	1.48	0.0430	1.54	0.89	0.93
4.2013	cropped 1	Swabian Jura	1.12	0.0434	1.54	0.90	0.89
4.2013	cropped 2	Swabian Jura	0.79	0.0452	1.57	0.74	0.82
4.2013	cropped 3	Swabian Jura	1.55	0.0268	1.31	0.98	0.97

Table S4 - 5 Standard parameters of the Daisy model (see also Figure 4 -2), used in this study and for running the simulations, subject to statistical analysis. Additionally, the form, constraints and standard deviation (where applicable) of the prior are displayed.

Parameter Name	Probability distribution function	Lower constraint	Upper constraint	Standard parameter value used for testing enzyme allocations	Standard deviation in Bayesian calibration	Unit	Reference of standard value
AOM_s_Q10	uniform	1	3	2			
AOM_f_Q10	uniform	1	3	2			
SMB_Q10	uniform	1	3	2			
SOM_s_Q10	uniform	1	3	2			
SOM_f_Q10	uniform	1	3	2			
fSOM_s	normal	0.01	0.99	0.3	0.15		Bruun
CUE_AOM_s	normal	0.01	0.45	0.13	0.07		Mueller
CUE_AOM_f	normal	0.2	0.8	0.45	0.15		Parton
CUE_SMB	normal	0.2	0.9	0.6	0.15		Mueller
CUE_SOM_s	normal	0.1	0.7	0.4	0.15		Mueller
CUE_SOM_f	normal	0.1	0.8	0.5	0.15		Mueller
k_AOM_s	normal	1.35×10^{-4}	5.40×10^{-2}	2.70×10^{-3}	1.00×10^{-2}	d^{-1}	Parton
k_AOM_f	normal	5.05×10^{-4}	2.02×10^{-1}	1.01×10^{-2}	5.00×10^{-2}	d^{-1}	Parton
k_SMB_s	normal	9.95×10^{-5}	3.98×10^{-2}	1.99×10^{-3}	2.00×10^{-3}	d^{-1}	Mueller
k_SMB_f	normal	1.00×10^{-3}	4.00×10^{-1}	2.00×10^{-2}	1.50×10^{-2}	d^{-1}	Mueller
k_SOM_s	normal	3.80×10^{-8}	9.50×10^{-4}	1.90×10^{-5}	1.00×10^{-5}	d^{-1}	Laub
k_SOM_f	normal	4.20×10^{-6}	1.05×10^{-2}	2.10×10^{-4}	2.50×10^{-5}	d^{-1}	Laub
maint_SMB_s	not altered			0.0018		d^{-1}	Mueller
maint_SMB_f	not altered			0.01		d^{-1}	Mueller
fSOM_f	not altered			0.4		d^{-1}	Mueller
$S_{L/N}$ (EQ3)	not altered			0.018			Parton
M_0 (EQ3)	not altered			0.85			Parton

References: (Bruun et al., 2003), (Mueller et al., 1997), (Parton et al., 1987) – normalized to daily and 10 °C, (Laub et al., 2020)*, CUE = carbon use efficiency*

Table S4 - 6 Summary of lignin contents from the literature with sources and in bold italics the final estimated lignin contents that were used as lignin content for plants, simulated by GECROS. The method by Van Soest and Wine (1968) was used as standard. Lignin contents measured by the Klason method (Theander et al., 1995) were converted to Van Soest equivalents by the formula of Van Soest et al. (2018).

Plant	Plant_Part	Lignin%	method	VS_lig	source:
Maize	leaf	5	*unclear*		https://doi.org/10.1007/s11104-011-0725-y
Maize	stem	15	*unclear*		https://doi.org/10.1007/s11104-011-0725-y
Maize	root	20	*unclear*		https://doi.org/10.1007/s11104-011-0725-y
Maize	stem+leaves	3.905	VS	3.9	Measurements Petra Högy, 2016
Maize	stover(stem+root)	18	Klason	10.25	https://doi.org/10.1016/j.indcrop.2008.03.008
Maize	stalk	15.3	Klason	7.89	https://doi.org/10.1016/j.indcrop.2016.07.032
Maize	root	19.8	Klason	11.82	https://doi.org/10.1016/j.indcrop.2016.07.032
Maize	root	17	Klason	9.37	https://doi.org/10.1016/j.soilbio.2011.04.002
Maize	root	8	VS	8	https://doi.org/10.1016/j.soilbio.2011.04.002
Maize	leaf	12.84	Klason	5.74	https://doi.org/10.1007/s10533-013-9856-y
Maize	root	17.52	Klason	9.83	https://doi.org/10.1007/s10533-013-9856-y
Maize	***leaf***			***2***	***Estimated to be lower ~ 25% of stem as in*** https://doi.org/10.1007/s10533-013-9856-y
Maize	***stem***			***8***	***Estimated from stem and leaf mean values***
Maize	***root***			***11***	***Estimated to be stem +3***
Wheat	leaf	2.5	*unclear*		https://doi.org/10.1007/s10533-013-9856-y
Wheat	stem	10	*unclear*		https://doi.org/10.1007/s10533-013-9856-y
Wheat	root	13	*unclear*		https://doi.org/10.1007/s10533-013-9856-y
Wheat	straw	15	Klason	7.63	https://doi.org/10.1186/s13068-014-0121-y
Wheat	stem+leaves	6.677	VS	6.68	Measurements Petra Högy
Wheat	straw	15.5	Klason	8.06	https://doi.org/10.1021/jf1036678
Wheat	straw	15	Klason	7.63	https://doi.org/10.1016/j.biombioe.2013.07.015
Wheat	straw	11	Klason	4.13	https://doi.org/10.1016/j.indcrop.2008.03.008
Triticale	straw	15.5	Klason	8.06	https://doi.org/10.1021/jf1036678
Wheat	straw	15	Klason	7.63	https://doi.org/10.1016/j.biosystemseng.2009.06.022
Wheat	straw	17	Klason	9.37	https://doi.org/10.15376/biores.10.4.8039-8047
Barley	root	23.1	Klason	14.7	https://doi.org/10.1016/j.soilbio.2006.06.013
Barley	straw	6.8	VS	6.8	https://doi.org/10.1016/S0304-3800(03)00114-5
Barley	stem+leaves	7.205	VS	7.21	Measurements Petra Högy, 2016
Barley	stem	18.9	Klason	11.03	https://doi.org/10.1016/S0031-9422(98)00103-4
Barley	leaves	9	Klason	2.38	https://doi.org/10.1016/S0031-9422(98)00103-4
Cereals	***leaf***			***2***	***Estimated to be lower ~ 25% of stem as in*** https://doi.org/10.1007/s11104-011-0725-y
Cereals	***stem***			***9***	***Estimated from stem and leaf mean values***

Plant	Plant_Part	Lignin%	method	VS_lig	source:
Cereals	***root***			***12***	***Estimated to be stem +3***
Rapeseed	straw	25	Klason	16.36	https://doi.org/10.1016/j.indcrop.2016.11.033
Rapeseed	straw	14.1	VS	14.1	https://doi.org/10.1016/S0304-3800(03)00114-5
Rapeseed	stem+leaves	10.668	VS	10.67	Measurements Petra Högy, 2016
Rapeseed	stem	11	VS	11	https://doi.org/10.1016/j.fcr.2016.09.025
Rapeseed	stem+leaves	19	Klason	11.12	https://doi.org/10.1016/j.indcrop.2016.10.038
Rapeseed	straw	14.15	VS	14.15	https://doi.org/10.1016/j.biosystemseng.2009.06.022
Rapeseed	***leaf***			***2***	***Estimated to be lower ~ 25% of stem as in*** https://doi.org/10.1007/s11104-011-0725-y
Rapeseed	***stem***			***13***	***Estimated from stem and leaf mean values***
Rapeseed	***root***			***16***	***Estimated to be stem +3***
Oil radish	stem+leaves	8.1	VS	8.1	https://doi.org/10.1016/j.ecolmodel.2005.05.026
Oil radish	***leaf***			***2***	***Estimated to be lower ~ 25% of stem as in*** https://doi.org/10.1007/s11104-011-0725-y
Oil radish	***stem***			***8***	***Value from Mueller*** https://doi.org/10.1016/j.ecolmodel.2005.05.026
Oil radish	***root***			***11***	***Estimated to be stem +3***

Formula to convert between Van Soest (VS) and Klason (KL) lignin:

https://hdl.handle.net/1813/59852

*KL = 1.15*VS+6.3*

*VS = 0.87*KL-5.48*

6.3.9 Supplementary figures chapter 4

Experiment 1- bare soil

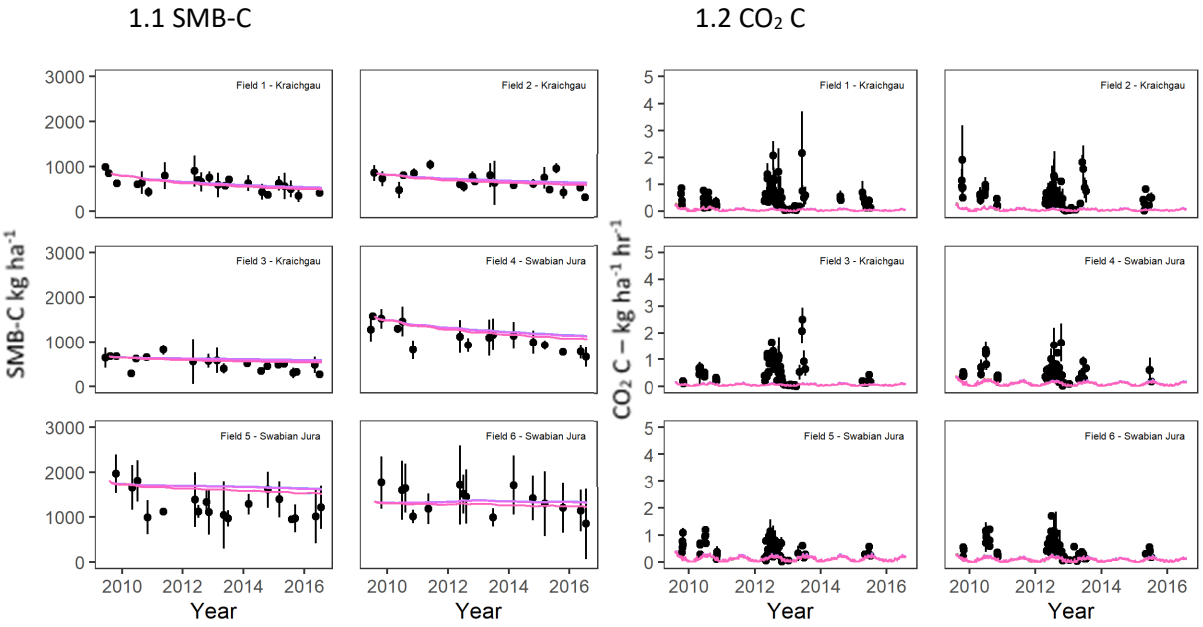

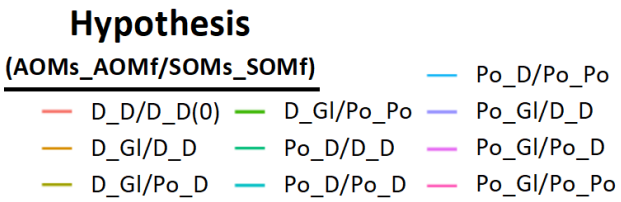

Experiment 2 - cropped plots

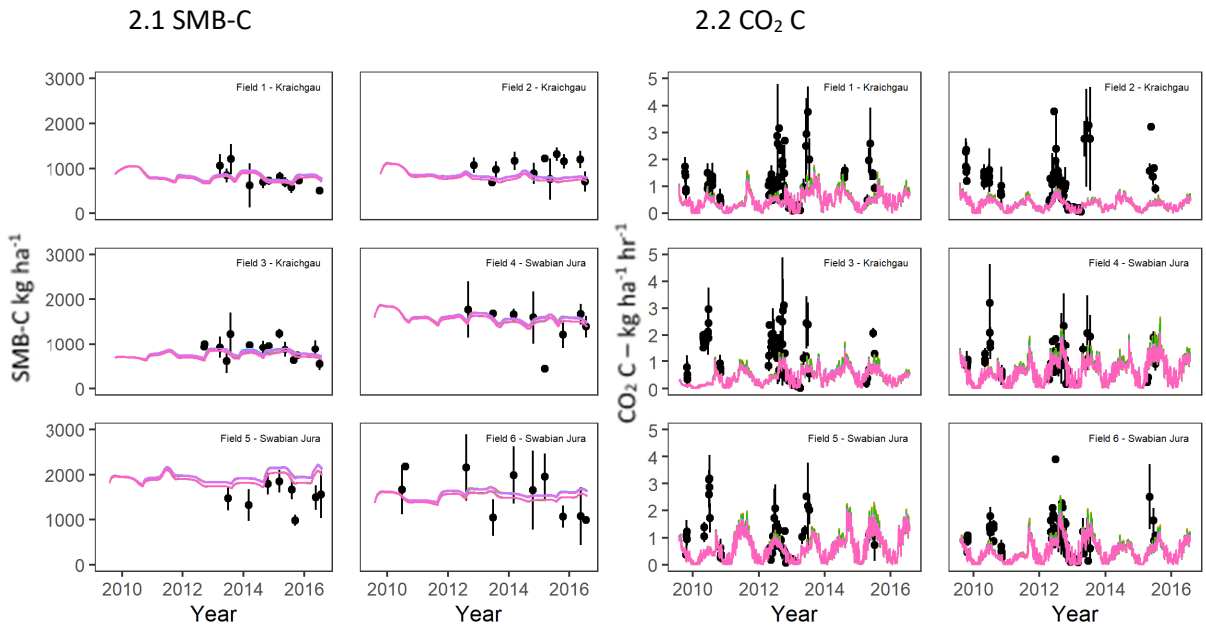

Figure S4 - 1 Simulations of SMB-C (left) and CO_2 (right) for experiment 1 (top) and experiment 2 (bottom) for all hypotheses regarding allocations of measured enzyme TS allocation compared to the 0 hypothesis (all Q_{10} equal 2). Dots represent the average and error bars the standard deviation of the three replicates per field. For SMB, there were 20 (fallow) and 10 (cropped plots) measurements throughout the simulation period, for CO_2 there were 70 measurements for both.

Experiment 3 - regional litterbag incubation:

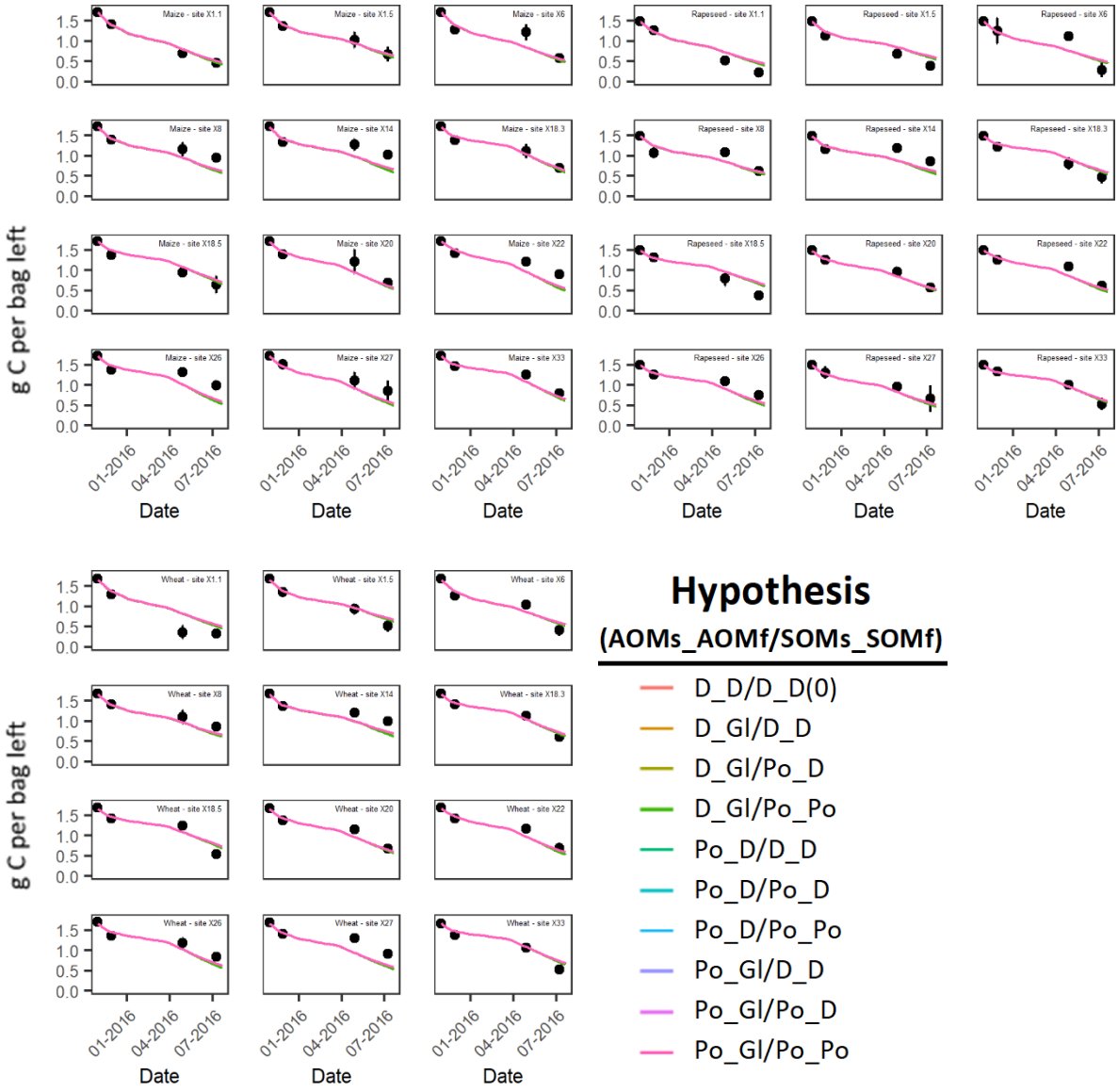

Figure S4 - 2 Simulations of remaining C in litterbags of experiment 3 for all hypotheses regarding allocations of measured enzyme TS allocation compared to the 0 hypothesis (all Q_{10} equal 2). Dots represent the average and error bars the standard deviation of the three replicates.

Experiment 4 - crop-litter incubation

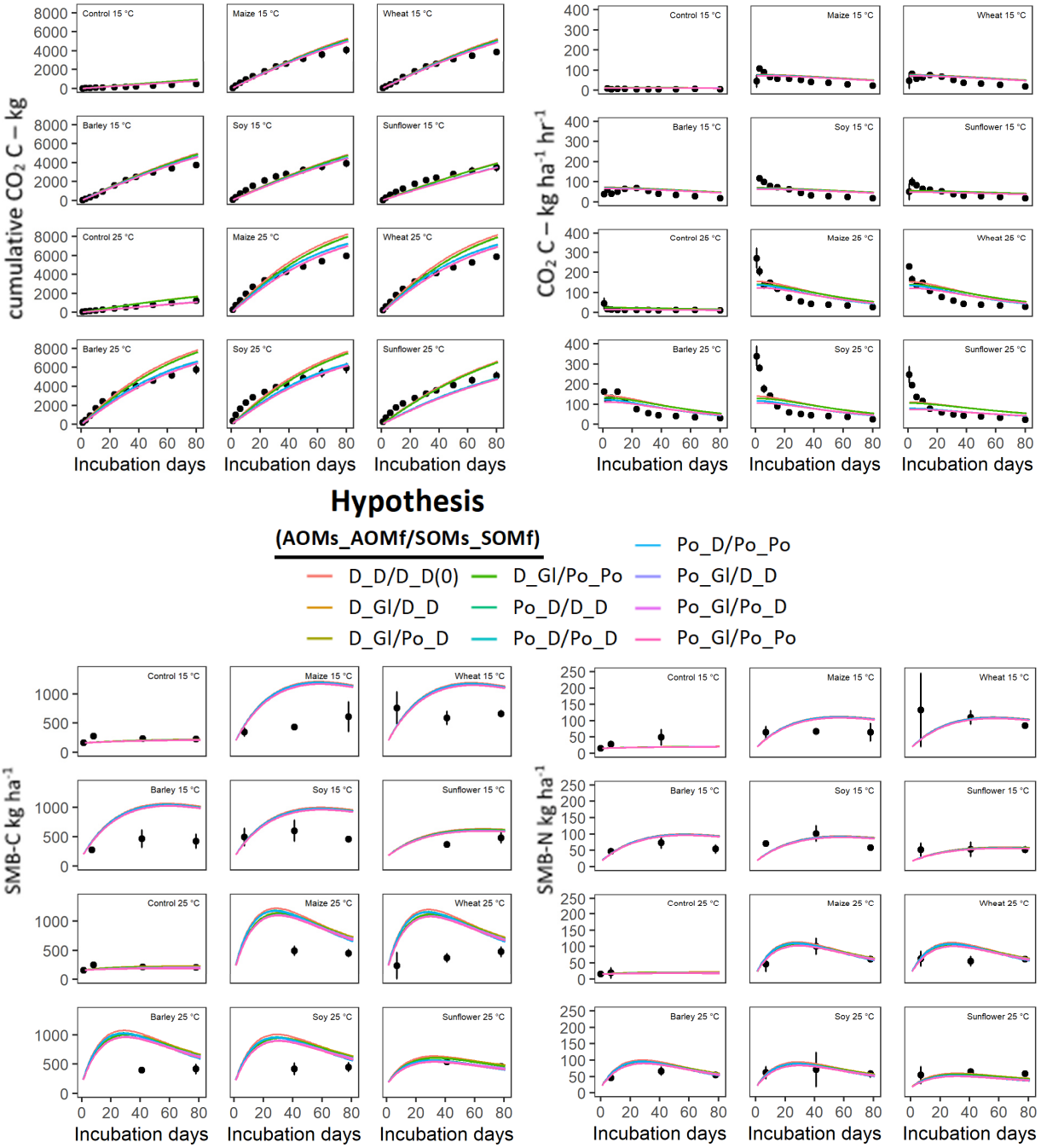

Figure S4 - 3 Simulations of experiment 4. Displayed are cumulative CO_2 evolution (top-left), rate of CO_2 evolution (top-right), SMB-C (bottom-left) and SMB-N (bottom right) for all hypotheses regarding allocations of measured enzyme TS allocation compared to the 0 hypothesis (all Q_{10} equal 2). Dots represent the average and error bars the standard deviation of the three replicates.

Experiment 5 - Ultuna fallow soil incubation

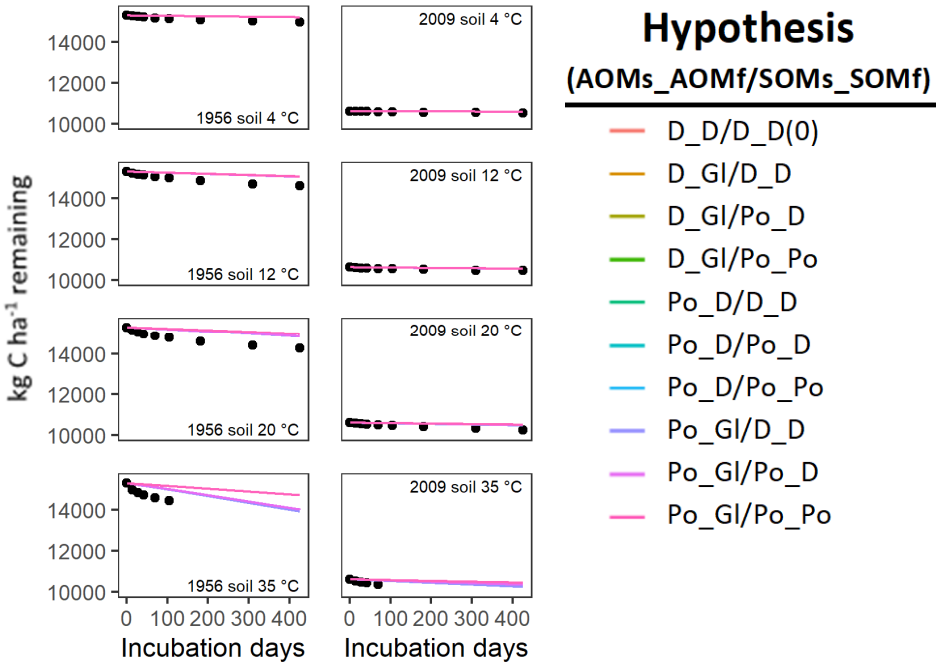

Figure S4 - 4 Simulations of remaining C of experiment 5 for all hypotheses regarding allocations of measured enzyme TS allocation compared to the 0 hypothesis (all Q_{10} equal 2).

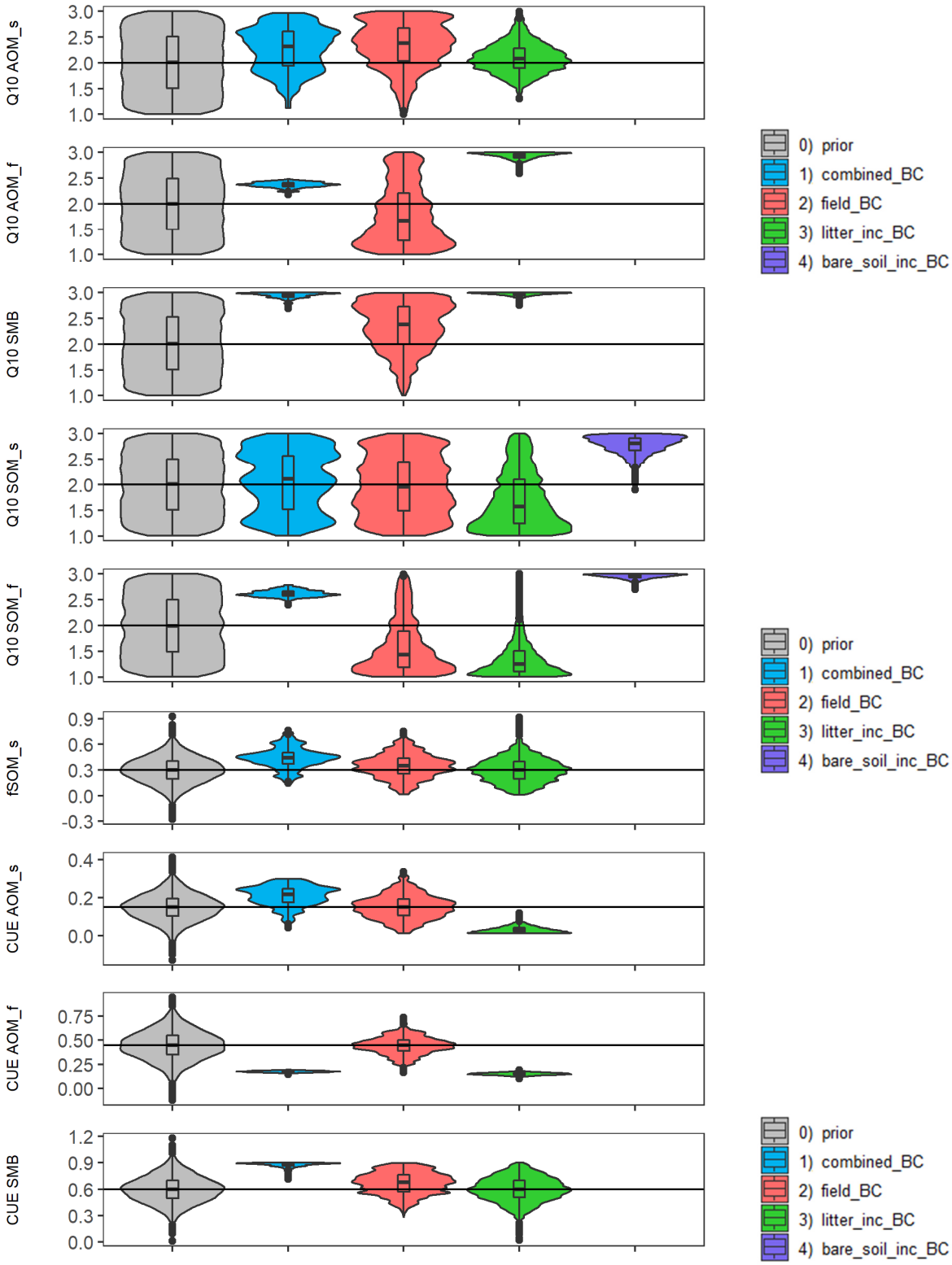

Figure S4 – 5 Prior and posterior distributions of all parameters (Table S4 - 5) optimized by the combined and individual Bayesian calibrations explained in section 4.4. Horizontal lines on graphs show the prior values. All priors, except Q_{10} value were normally distributed, but were trimmed for k_AOMs, k_AOM_f and k_SMB_f so that posteriors would be properly visible.

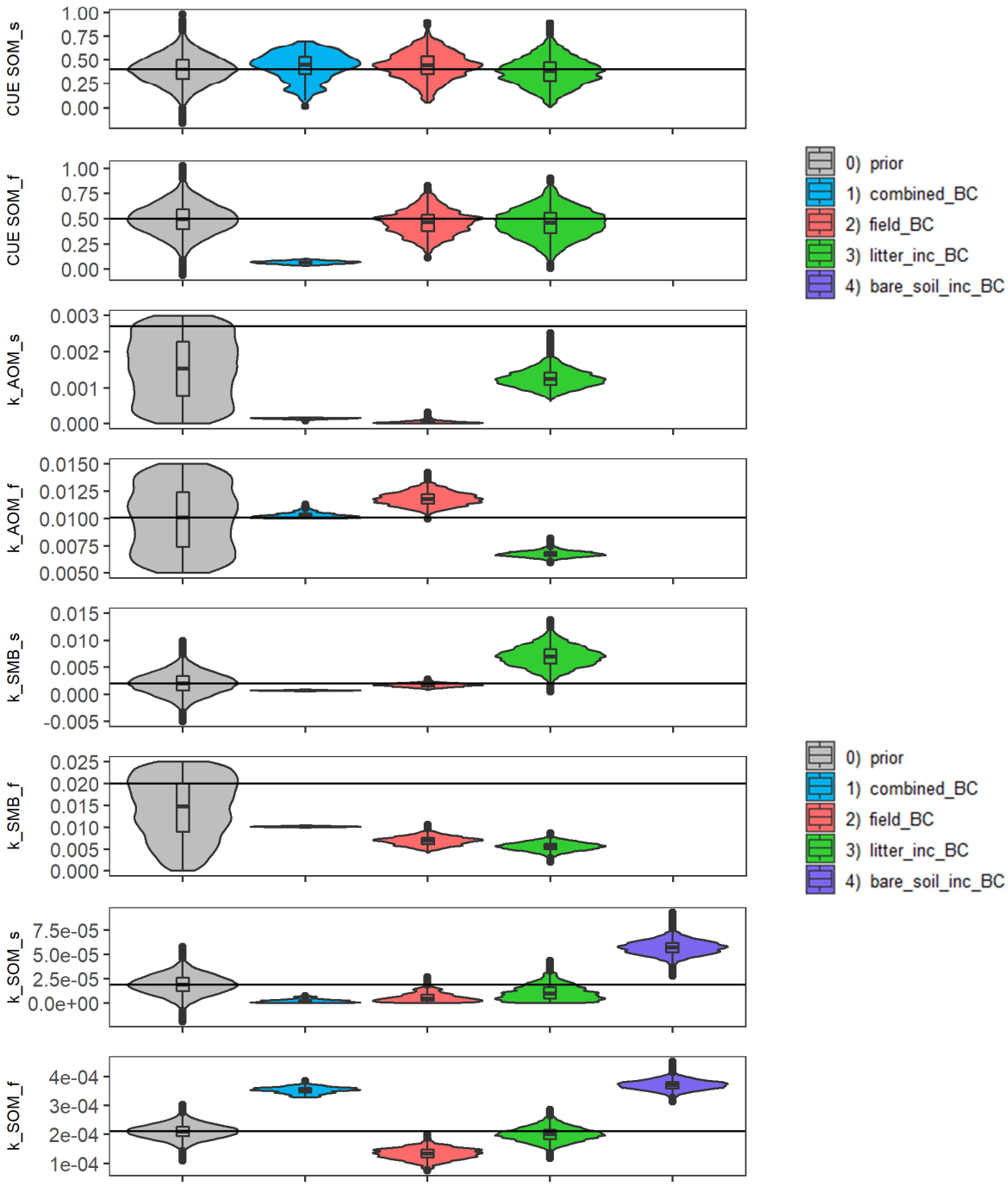

Figure S4 - 5 Prior and posterior distributions of all parameters (Table S4 - 5) optimized by the combined and individual Bayesian calibrations explained in section 4.4. Horizontal lines on graphs show the prior values. All priors, except Q_{10} value were normally distributed, but were trimmed for k_AOMs, k_AOM_f and k_SMB_f so that posteriors would be properly visible.

a) field_BC

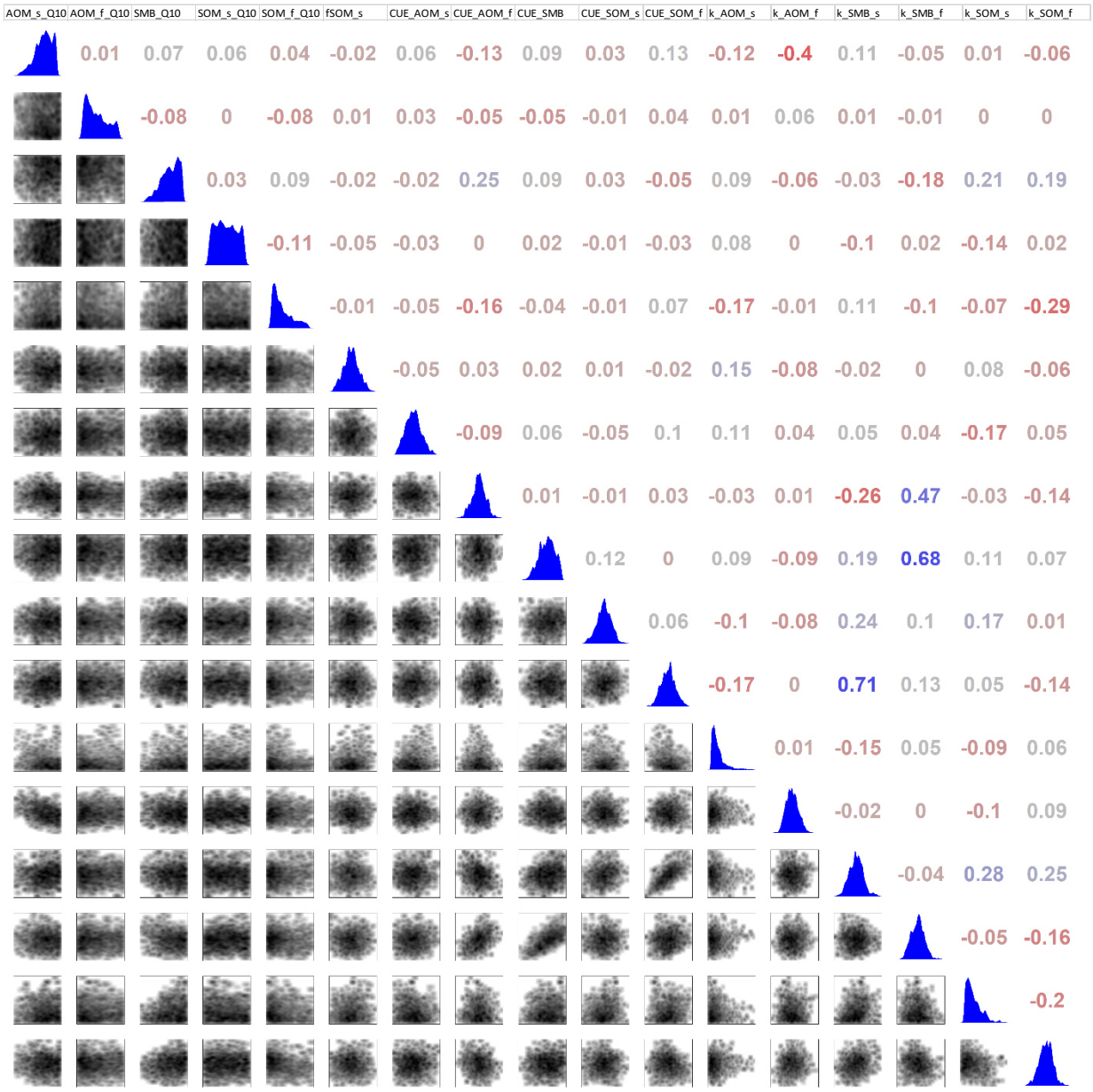

Figure S4 – 6 Correlation plots for the Bayesian calibrations for individual experiments (a = field_BC, b = litter_inc_BC, c = bare_soil_inc_BC). Displayed are a graphical plot of parameters against each other (bottom left), density plots of parameter distribution (diagonal) and Pearson's correlation coefficient (top right).

b) litter_inc_BC

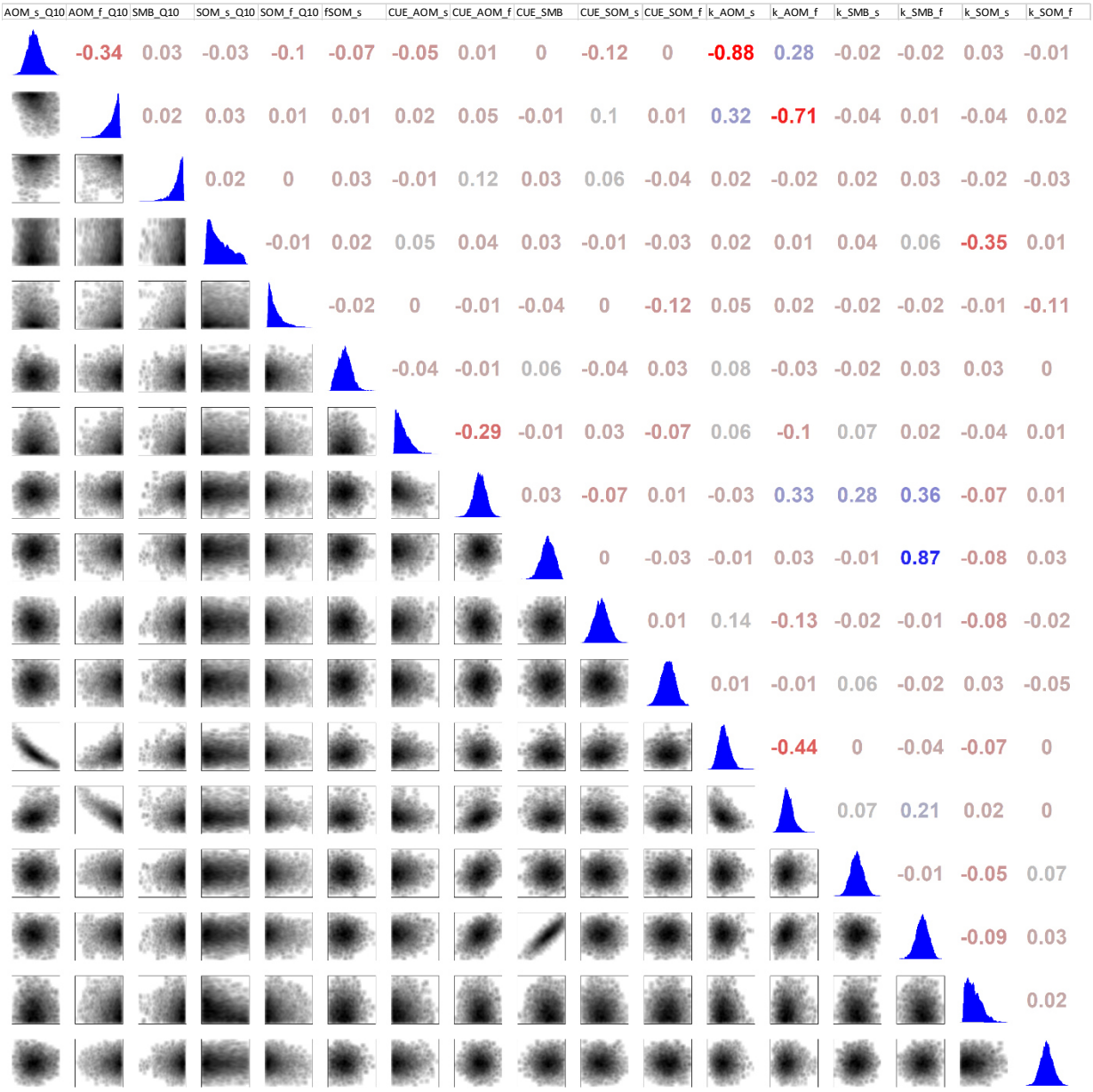

Figure S4 – 6 Correlation plots for the Bayesian calibrations for individual experiments (a = field_BC, b = litter_inc_BC, c = bare_soil_inc_BC). Displayed are a graphical plot of parameters against each other (bottom left), density plots of parameter distribution (diagonal) and Pearson's correlation coefficient (top right).

c) bare_soil_inc_BC

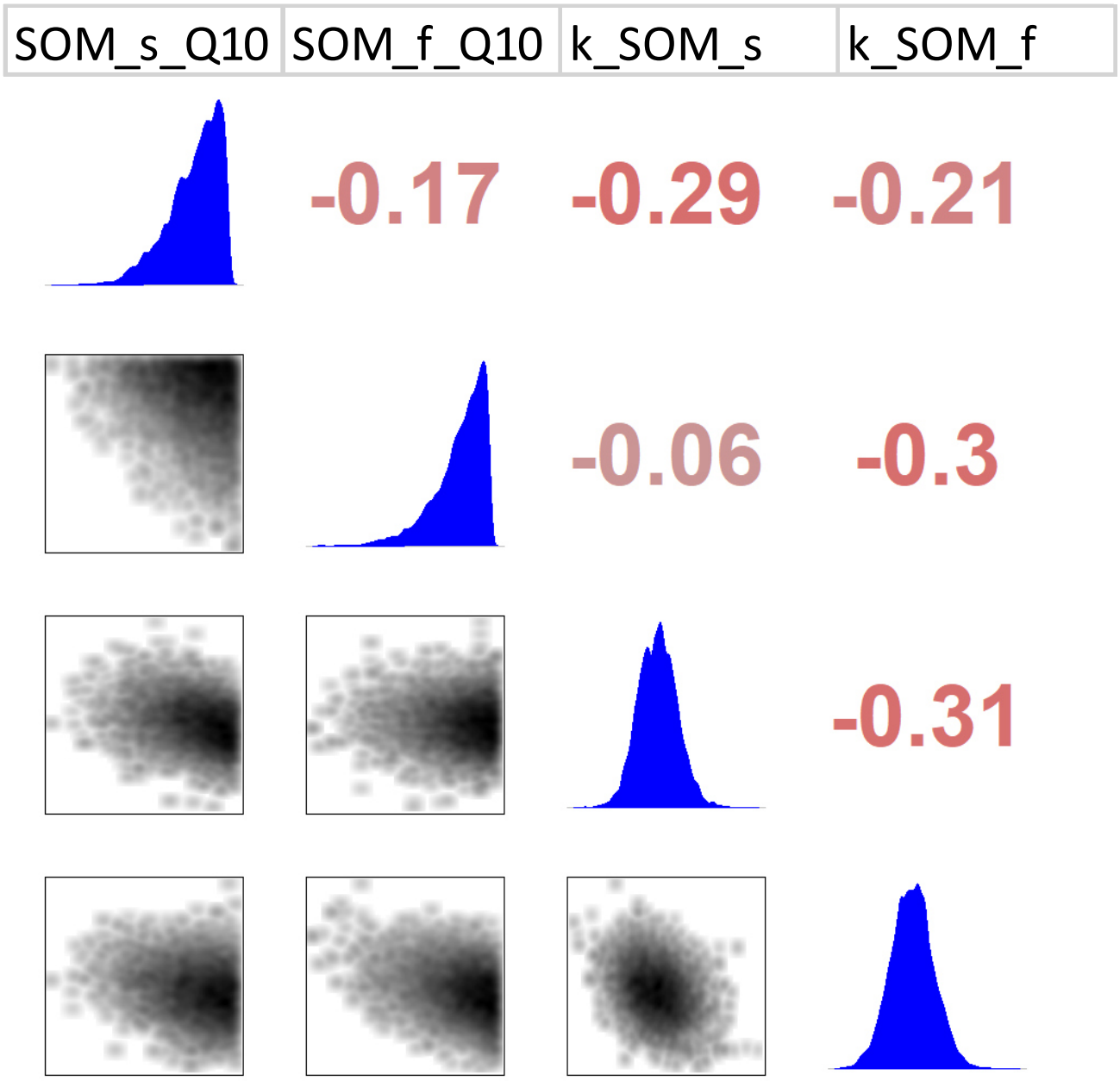

Figure S4 - 6 Correlation plots for the Bayesian calibrations for individual experiments (a = field_BC, b = litter_inc_BC, c = bare_soil_inc_BC). Displayed are a graphical plot of parameters against each other (bottom left), density plots of parameter distribution (diagonal) and Pearson's correlation coefficient (top right).

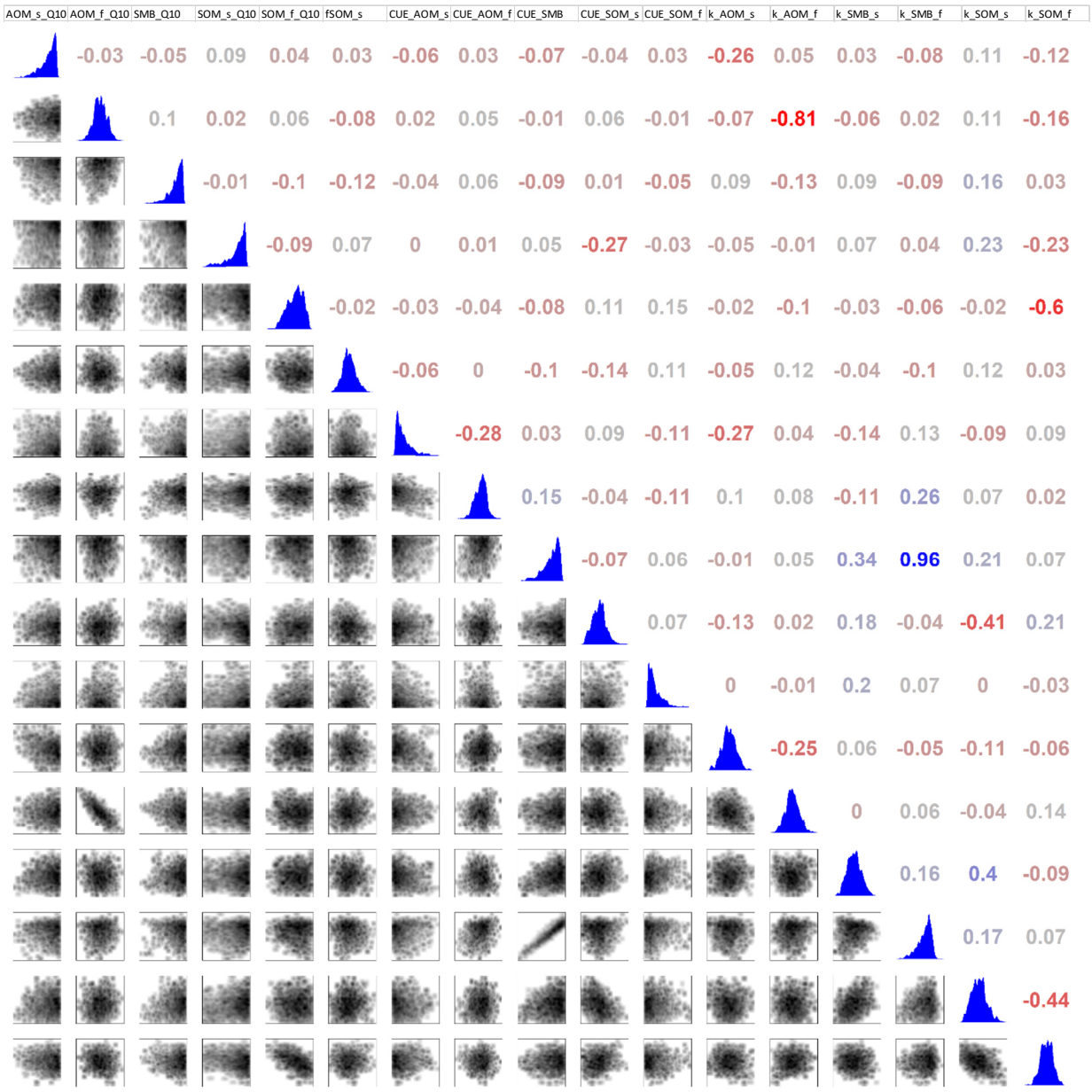

Figure S4 - 7 Correlation plots for the Bayesian calibration of all simulations combined (combined_BC). Displayed are a graphical plot of parameters against each other (bottom left), density plots of parameter distribution (diagonal) and Pearson's correlation coefficient (top right).

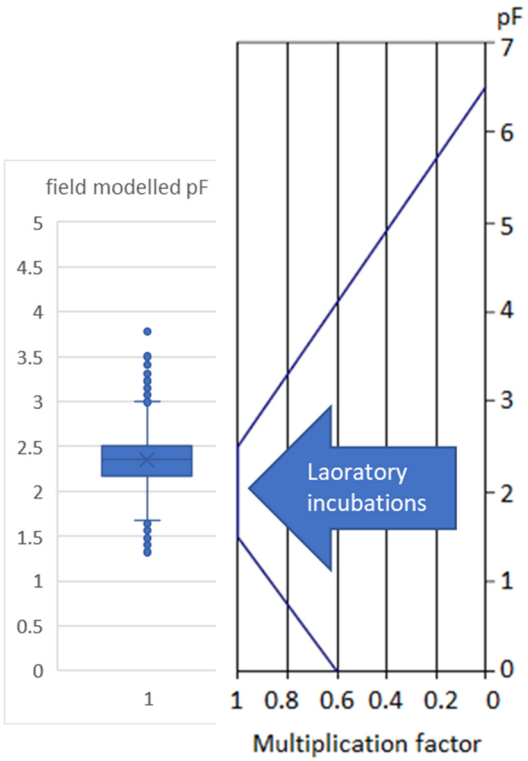

Figure S4 - 8 Boxplot of simulated moisture of all fields of experiment 2, compared to the multiplication factor that Daisy multiplies turnover with as result of simulated soil moisture. Both are displayed as pressure potential in the form of a pF value. Laboratory incubation experiments 4 and 5 were under optimal conditions and not subject to any constraints due to soil moisture.

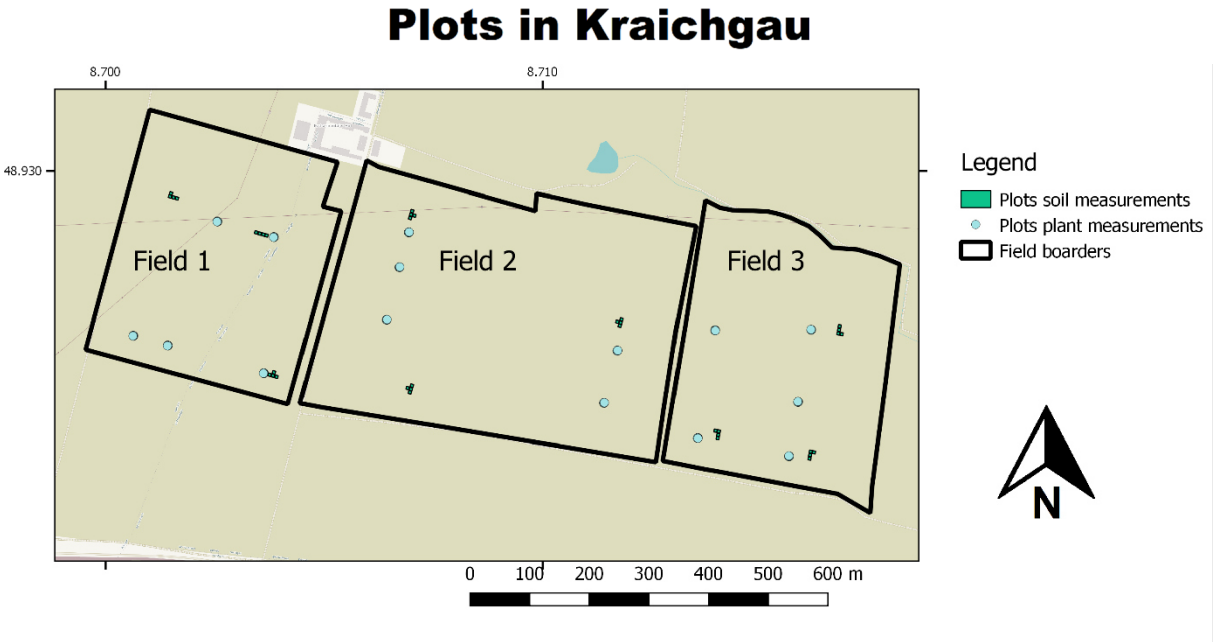

Figure S4 - 9 Map of plot locations of experiment 1 and 2 within the fields in Kraichgau with coordinates according to the World Geodetic System.

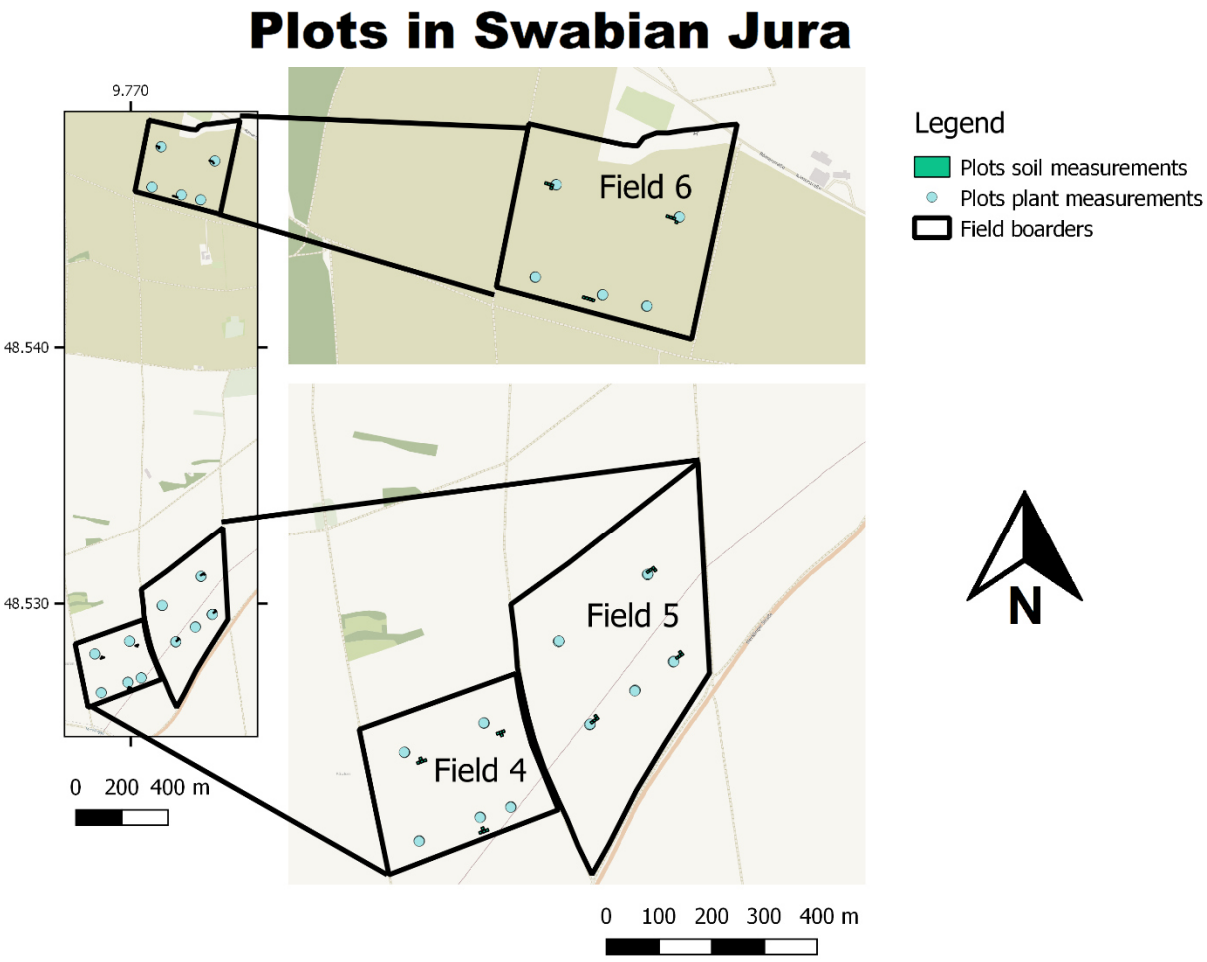

Figure S4 - 10 Map of plot locations of experiment 1 and 2 within the fields in Swabian Jura with coordinates according to the World Geodetic System.

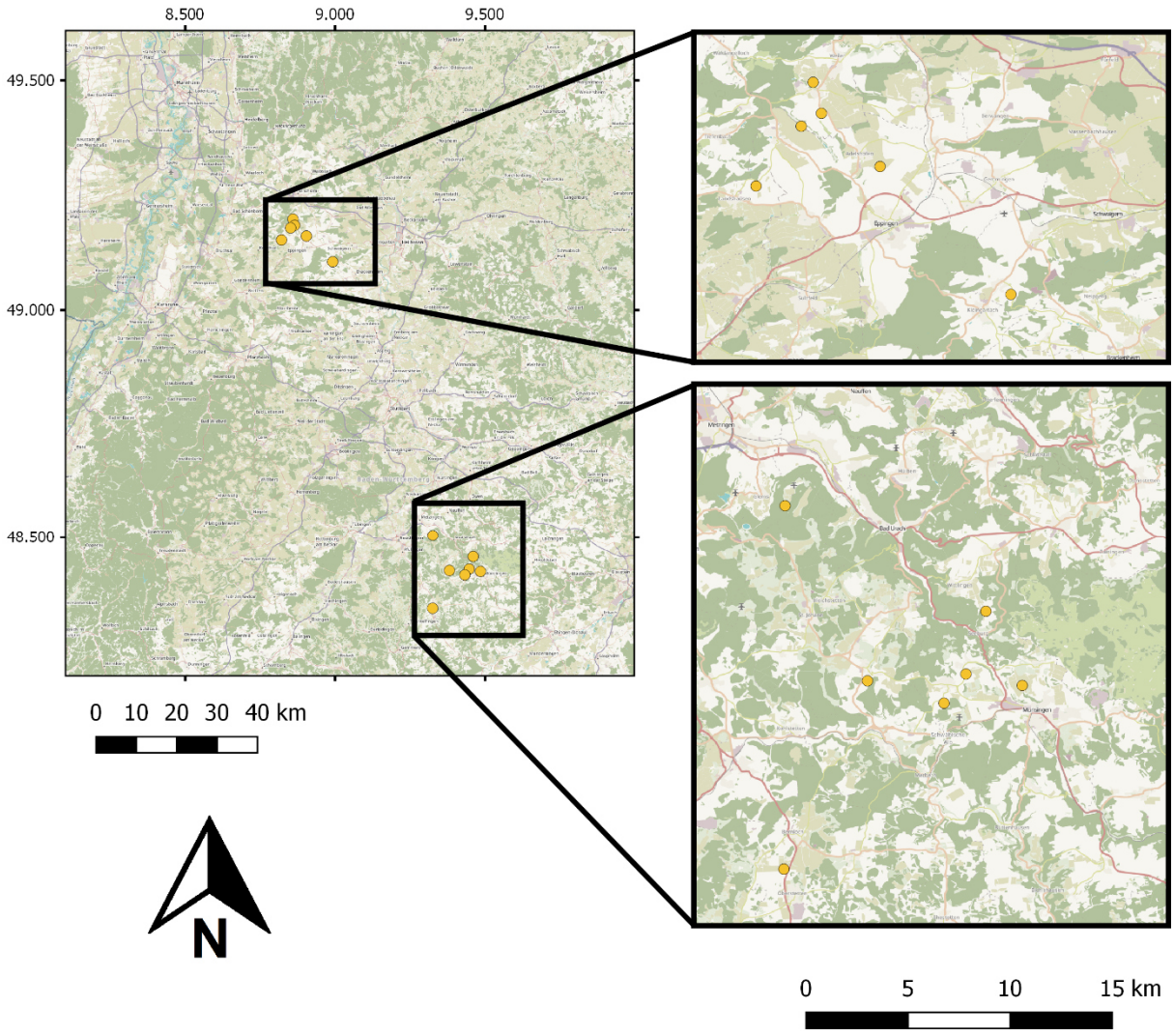

Figure S4 - 11 Map of regional plot locations of the litter bag burials of experiment 3 with coordinates according to the World Geodetic System.

6.3.10 References for supplementary chapter 4

Ali, R.S., Ingwersen, J., Demyan, M.S., Funkuin, Y.N., Wizemann, H.-D., Kandeler, E., Poll, C., 2015. Modelling in situ activities of enzymes as a tool to explain seasonal variation of soil respiration from agro-ecosystems. Soil Biology & Biochemistry 81, 291–303. doi:10.1016/j.soilbio.2014.12.001

Benbi, D.K., Boparai, A.K., Brar, K., 2014. Decomposition of particulate organic matter is more sensitive to temperature than the mineral associated organic matter. Soil Biology & Biochemistry 70, 183–192. doi:10.1016/j.soilbio.2013.12.032

Biernath, C., Bittner, S., Klein, C., Gayler, S., Hentschel, R., Hoffmann, P., Högy, P., Fangmeier, A., Priesack, E., 2013. Modeling acclimation of leaf photosynthesis to atmospheric CO2 enrichment. European Journal of Agronomy 48, 74–87. doi:10.1016/j.eja.2013.02.008

Bruun, S., Christensen, B.T., Hansen, E.M., Magid, J., Jensen, L.S., 2003. Calibration and validation of the soil organic matter dynamics of the Daisy model with data from the Askov long-term experiments. Soil Biology & Biochemistry 35, 67–76. doi:10.1016/S0038-0717(02)00237-7

Del Grosso, S.J., Parton, W.J., Mosier, A.R., Holland, E.A., Pendall, E., Schimel, D.S., Ojima, D.S., 2005. Modeling soil CO2 emissions from ecosystems. Biogeochemistry 73, 71–91. doi:10.1007/s10533-004-0898-z

Eshonkulov, R., Poyda, A., Ingwersen, J., Wizemann, H.-D., Weber, T.K.D., Kremer, P., Högy, P., Pulatov, A., Streck, T., 2019. Evaluating multi-year, multi-site data on the energy balance closure of eddy-covariance flux measurements at cropland sites in southwestern Germany. Biogeosciences 16, 521–540. doi:10.5194/bg-16-521-2019

Frey, S.D., Lee, J., Melillo, J.M., Six, J., 2013. The temperature response of soil microbial efficiency and its feedback to climate. Nature Climate Change 3, 395–398. doi:10.1038/nclimate1796

Gauch, H.G., Hwang, J.T.G., Fick, G.W., 2003. Model Evaluation by Comparison of Model-Based Predictions and Measured Values. Agronomy Journal 95, 1442. doi:10.2134/agronj2003.1442

Hansen, S., Jensen, L.S., Nielsen, N.E., Svendsen, H., 1993. The Soil Plant System Model Daisy - Basic Principles and Modelling Approach. Copenhagen: The Royal Veterinary and Agricultural University.

Hutson, J.L., Wagenet., R.J., 1992. LEACHM (Leaching Estimation and Chemistry Model): A Process-Based Model of Water and Solute Movement, Transformations, Plant Uptake and Chemical Reactions in the Unsaturated Zone, Version 3.0. Department of Soil, Crop and Atmospheric Sciences, Cornell University, Ithaca.

Ingwersen, J., Högy, P., Wizemann, H.D., Warrach-Sagi, K., Streck, T., 2018. Coupling the land surface model Noah-MP with the generic crop growth model Gecros: Model description, calibration and validation. Agricultural and Forest Meteorology 262, 322–339. doi:10.1016/j.agrformet.2018.06.023

Karhu, K., Hilasvuori, E., Järvenpää, M., Arppe, L., Christensen, B.T., Fritze, H., Kulmala, L., Oinonen, M., Pitkänen, J.-M., Vanhala, P., Heinonsalo, J., Liski, J., 2019. Similar temperature sensitivity of soil mineral-associated organic carbon regardless of age. Soil Biology & Biochemistry 136, 107527. doi:10.1016/j.soilbio.2019.107527

Kätterer, T., Reichstein, M., Andrén, O., Lomander, A., 1998. Temperature dependence of organic matter decomposition: a critical review using literature data analyzed with different models. Biology and Fertility of Soils 27, 258–262. doi:10.1007/s003740050430

Laub, M., Demyan, M.S., Nkwain, Y.F., Blagodatsky, S., Kätterer, T., Piepho, H., Cadisch, G., 2020. DRIFTS band areas as measured pool size proxy to reduce parameter uncertainty in soil organic matter models. Biogeosciences 17, 1393–1413. doi:10.5194/bg-17-1393-2020

Lefèvre, R., Barré, P., Moyano, F.E., Christensen, B.T., Bardoux, G., Eglin, T., Girardin, C., Houot, S., Kätterer, T., van Oort, F., Chenu, C., 2014. Higher temperature sensitivity for stable than for labile soil

organic carbon - Evidence from incubations of long-term bare fallow soils. Global Change Biology 20, 633–640. doi:10.1111/gcb.12402

Loague, K., Green, R.E., 1991. Statistical and graphical methods for evaluating solute transport models: Overview and application. Journal of Contaminant Hydrology 7, 51–73. doi:10.1016/0169-7722(91)90038-3

Meier, U., 2001. Growth stages of mono-and dicotyledonous plants BBCH Monograph,. Blackwell Publishing Ltd, Oxford, UK, pp. 29–34.

Monteith, J.L., 1976. Evaporation and surface temperature. Quarterly Journal of the Royal Meteorological Society 12, 513–522. doi:10.1002/qj.49710745102

Mualem, Y., 1976. A new model for predicting the hydraulic conductivity of unsaturated porous media. Water Resources Research 12, 513–522. doi:10.1029/WR012i003p00513

Mueller, T., Jensen, L.S.S., Magid, J., Nielsen, N.E.E., 1997. Temporal variation of C and N turnover in soil after oilseed rape straw incorporation in the field: simulations with the soil-plant-atmosphere model DAISY. Ecological Modelling 99, 247–262. doi:http://dx.doi.org/10.1016/S0304-3800(97)01959-5

Parton, W.J., Schimel, D.S., Cole, C. V., Ojima, D.S., 1987. Analysis of Factors Controlling Soil Organic Matter Levels in Great Plains Grasslands. Soil Science Society of America Journal 51, 1173–1179. doi:10.2136/sssaj1987.03615995005100050015x

Poeter, E.P., Hill, M.C., Banta, E.R., Mehl, S., Christensen, S., 2005. UCODE_2005 and six other computer codes for universal sensitivity analysis, inverse modeling, and uncertainty evaluation. U.S. Geological Survey Techniques and Methods 6-A11, 283p. (As updated in Feb 2008). doi:10.3133/TM6A11

Poeter, E.P., Hill, M.C., Lu, D., Tiedeman, C.R., Mehl, S., 2014. UCODE_2014, with New Capabilities to Define Parameters Unique to Predictions, Calculate Weights using Simulated Values, Estimate Parameters with SVD, Evaluate Uncertainty with MCMC, and More. Integrated Groundwater Modeling Center Report Number: GWMI 2014-02.

R Core Team, 2017. R: A Language and Environment for Statistical Computing.

Schaap, M.G., Leij, F.J., van Genuchten, M.T., 2001. ROSETTA: a computer program for estimating soil hydraulic parameters with hierarchical pedotransfer functions. Journal of Hydrology 251, 163–176. doi:10.1016/S0022-1694(01)00466-8

Sierra, C.A., Malghani, S., Müller, M., 2015. Model structure and parameter identification of soil organic matter models. Soil Biology & Biochemistry 90, 197–203. doi:10.1016/j.soilbio.2015.08.012

Smith, P., Lanigan, G., Kutsch, W.L., Buchmann, N., Eugster, W., Aubinet, M., Ceschia, E., Béziat, P., Yeluripati, J.B., Osborne, B., Moors, E.J., Brut, A., Wattenbach, M., Saunders, M., Jones, M., 2010. Measurements necessary for assessing the net ecosystem carbon budget of croplands. Agriculture, Ecosystems and Environment 139, 302–315. doi:10.1016/j.agee.2010.04.004

Theander, O., Åman, P., Westerlund, E., Andersson, R., Pettersson, D., 1995. Total Dietary Fiber Determined as Neutral Sugar Residues, Uronic Acid Residues, and Klason Lignin (The Uppsala Method): Collaborative Study. Journal of AOAC INTERNATIONAL 78, 1030–1044. doi:10.1093/jaoac/78.4.1030

Tuomi, M., Vanhala, P., Karhu, K., Fritze, H., Liski, J., 2008. Heterotrophic soil respiration—Comparison of different models describing its temperature dependence. Ecological Modelling 211, 182–190. doi:10.1016/j.ecolmodel.2007.09.003

van Genuchten, M.T., 1982. A comparison of numerical solutions of the one-dimensional unsaturated—saturated flow and mass transport equations. Advances in Water Resources 5, 47–55. doi:10.1016/0309-1708(82)90028-8

Van Soest, P.J., Robertson, J.B., Barry, M.C., 2018. Soluble lignin and its relation to Klason lignin , acid - detergent lignin and digestibility of NDF, in: Cornell Nutrition Conference. Cornell University Ithaca, NY, available online at https://hdl.handle.net/1813/59852.

Van Soest, P.J., Wine, R.H., 1968. Determination of Lignin and Cellulose in Acid-Detergent Fiber with Permanganate. Journal of AOAC INTERNATIONAL 51, 780–785. doi:10.1093/jaoac/51.4.780

Vaughn, L.J.S., Torn, M.S., 2019. 14C evidence that millennial and fast-cycling soil carbon are equally sensitive to warming. Nature Climate Change 9, 467–471. doi:10.1038/s41558-019-0468-y

Yin, X., van Laar, H.H., 2005. Crop Systems Dynamics:An Ecophysiological Simulation Model for Genotype-by-Environment Interactions. Wageningen Academic Publishers, The Netherlands. doi:10.3920/978-90-8686-539-0

Curriculum vitae

Moritz Laub

Born 31.03.1989 in Filderstadt,

email: moritz.laub@uni-hohenheim.de, Phone: +49 (0)711 – 459 - 23473

Education

Jan. 2017 – Jan. 2021	PhD candidate. Institute of Agronomy in the Tropics and Subtropics, University of Hohenheim, Stuttgart, Germany. Dissertation Title: Mid-infrared spectroscopy and enzyme activity temperature sensitivities as experimental proxies to reduce parameter uncertainty of soil carbon models.
Oct. 2013 – May 2016	M.Sc. in Agricultural Science in the Tropics and Subtropics, University of Hohenheim, Stuttgart, Germany. Thesis: Digital Mapping of Soil Organic Carbon Stocks and Soil Properties in the Naban River Watershed National Nature Reserve in Southwest China.
Oct. 2009 – Sept. 2013	B.Sc. in Renewable Resources and Bioenergy, University of Hohenheim, Stuttgart, Germany.
Jun. 2008	Allgemeines Abitur (equivalent to A level), Gymnasium Hechingen, Hechingen, Germany.

Work experience

Jan. 2017 – Jan. 2021	Scientific staff, University of Hohenheim, Stuttgart, Germany, Institute of Agronomy in the Tropics and Subtropics. DFG Research Unit 1695 'Regional Climate Change' in Subproject P3, Soil Carbon Dynamics.
Jun. 2016 – Dec. 2016	Certified graduate research assistant at the Institute of Agronomy in the Tropics and Subtropics, University of Hohenheim, Stuttgart, Germany (part time).
2012 - 2014	Student assistant for soil surveying at SakostaCAU GmbH., construction engineering, Stuttgart, Germany (part time).

Publications included in the dissertation

Laub, M., Ali, R.S., Demyan, M.S., Nkwain, Y.F., Poll, C., Högy, P., Poyda, A., Ingwersen, J., Blagodatsky, S., Kandeler, E., Cadisch, G., (2021). Modeling temperature sensitivity of soil organic matter decomposition: Splitting the pools. Soil Biol. Biochem. 153, 108108. doi: 10.1016/j.soilbio.2020.108108

Laub, M., Demyan, M.S., Nkwain, Y.F., Blagodatsky, S., Kätterer, T., Piepho, H., Cadisch, G., (2020). DRIFTS band areas as measured pool size proxy to reduce parameter uncertainty in soil organic matter models, Biogeosciences, 17(6), 1393–1413, doi:10.5194/bg-17-1393-2020, 2020.

Laub, M., Blagodatsky, S., Nkwain, Y.F., Cadisch, G., (2019). Soil sample drying temperature affects specific organic mid-DRIFTS peaks and quality indices. Geoderma 355, 113897. doi:10.1016/j.geoderma.2019.113897

Publications not included in the dissertation

Laub, M., Blagodatsky, S., Lang, R., Yang, X., & Cadisch, G. (2018). A mixed model for landscape soil organic carbon prediction across continuous profile depth in the mountainous subtropics. Geoderma, 330, 177–192. doi:10.1016/j.geoderma.2018.05.020

Gauder, M., Billen, N., Zikeli, S., Laub, M., Graeff-Hönninger, S., Claupein, W., (2016). Soil carbon stocks in different bioenergy cropping systems including subsoil. Soil Tillage Res. 155, 308 – 317. doi:10.1016/j.still.2015.09.005

Conference contributions

Laub, M., Ali, R.S., Demyan, M.S., Nkwain, Y.F., Poll, C., Högy, P., Poyda, A., Ingwersen, J., Blagodatsky, S., Kandeler, E., Cadisch, G. Linking temperature sensitivities of soil enzymes to temperature responses of different organic matter pools in the DAISY model. EGU General Assembly 2020. 4. – 8. May 2020. Online presentation.

Laub, M., Nkwain, Y.F., Ali, R.S., Demyan, M.S., Rache, F., Blagodatsky, S., Poll, C., Kandeler, E., Cadisch, G. Using proxies from mid-DRIFTS Spectroscopy and enzyme temperature sensitivities to improve soil organic matter modelling. Final Conference of the DFG Research Unit 1695 Regional Climate Change. 24.-26. April 2019. University of Hohenheim, Stuttgart, Germany. Oral presentation.

Laub, M., Nkwain, Y.F., Demyan, M.S., Rache, F., Blagodatsky, S., Schulz, E., Kätterer, T., Cadisch, G. Advantages of mid-DRIFTS Spectroscopy to initialize soil organic matter models. EGU General Assembly. 7.–12. April 2019. Vienna, Austria. Poster presentation.

Laub, M. Soil Organic Carbon Stocks Mapping In Mountainous Subtropics Using A 3D Mixed Model With Upscaling Capabilities. AG Digital Soil Mapping Workshop 2019. 04.-05. April 2019. Tübingen, Germany. Oral presentation.

Laub, M., Blagodatsky, S., Lang, R., Yang, X., & Cadisch, G. A 3D Mixed Model for Soil Organic Carbon Mapping in Mountainous Subtropics. Tropentag. September 17-19, 2018. Ghent, Belgium. Poster presentation.

Laub, M., Nkwain, Y.F., Ali, R.S., Demyan, M.S., Rasche, F., Cadisch, G. Advancing SOM modeling by the use of measurable proxies for different soil organic matter pools. Soil organic matter management in agriculture – International Symposium. 29.-30. May 2018. Braunschweig, Germany. Oral presentation.

International experiences

Nov. 2019 – Dec. 2019	Research visit, SOM research group of Prof. Patma Vityakon, Khon Khaen University, Khon Khaen, Thailand.
Jun. 2017 – Aug. 2017	Research visit, SOM group, Khon Khaen University, Khon Khaen, Thailand.
Mar. 2015 – May 2015	Field work for Msc. Thesis in Jinghong, China.
Sept. 2014 – Feb. 2015	Exchange semester, Chiang Mai University, Chiang Mai, Thailand.
Aug. 2011 – Feb. 2012	Exchange semester, Universidad Autónoma Chapingo, Texcoco, Mexico.

Stuttgart, 10.01.2021